THREE-DIMENSIONAL (3D) SYSTEMS IN COMBINATION WITH MULTIPOTENT STROMAL CELLS (MSCs) AS A CLINICAL OPTION FOR TISSUE ENGINEERING

A Dissertation

by

ROBERT NORRIS BEARDEN

Submitted to the Office of Graduate and Professional Studies of
Texas A&M University
in partial fulfillment of the requirements for the degree of

DOCTOR OF PHILOSOPHY

Chair of Committee,	W. Brian Saunders
Committee Members,	Kayla Bayless
	Carl Gregory
	Melissa Grunlan
	Gonzalo Rivera
Head of Department,	Jonathan Levine

August 2016

Major Subject: Biomedical Sciences

ABSTRACT

Tissue engineering is a promising treatment strategy for osteochondrosis and osteoarthritis induced articular cartilage injuries, with the goal of restoring structure and function, reducing/eliminating clinical signs, and preventing major surgical treatment. The objective of the work presented herein describes the manipulation of 3D scaffolds and progenitor cells known as multipotent stromal cells (MSCs) as a potential combination treatment for articular cartilage injuries. First, a three-dimensional (3D), serum-free collagen system was used as a model to demonstrate the importance of growth factors and cell-matrix interactions in 3D environments. Results demonstrated PDGF-BB induced dose- and time-dependent invasion of MG-63 cells into 3D collagen type I matrices. To examine the specific MT-MMP responsible, siRNA knockdown experiments were performed. Significant reduction of invasion was exhibited in MT1-MMP siRNA cultures, but not MT2- or MT3-MMP siRNAs. This work demonstrates that PDGF-BB is an important growth factor in MG-63 osteosarcoma cell invasion, and that MT1-MMP is required for this process. Second, canine multipotent stromal cells (cMSCs) were isolated from synovium, marrow, and adipose tissue and comprehensively characterized using a donor-matched study and assays optimized for the canine species. Tissues were isolated from five client owned dogs with cranial cruciate ligament rupture. All tissues produced plastic adherent, spindle shaped cMSCs. Each cell preparation was assessed for MSC criteria using flow cytometry, colony forming unit (CFU) potential, tri-lineage differentiation, and immunomodulation assays. There were significant differences between cMSCs as assessed by growth parameters,

CFU potential, tri-lineage differentiation, and immunomodulatory response when comparing donor and tissue source. Synovial and marrow cMSCs exhibited superior short-term osteogenesis while synovium and adipose proliferated more rapidly, displayed higher CFU potential, and formed larger chondrogenic pellets. All cMSCs reduced concentration of murine TNF-α in LPS-stimulated mouse macrophage co-culture assays, a novel finding for cMSCs. In summary, as described in humans, significant differences in cMSCs exist due to both tissue source and donor variability. Lastly, fabrication method for incorporation of cMSCs with polyethylene glycol-diacrylate (PEG-DA) based hydrogels for *in vitro* and *in vivo* studies was optimized. PEG-DA hydrogels fabricated with "conventional" photoinitiators were compared to a novel solvent induced phase separation via solvent-casted particulate leaching (SIPS/SCPL) hydrogel system. Using a 21-day time course, marrow cMSCs cultured on SIPS/SCPL-PEG-DA hydrogels exhibited significantly greater attachment, spreading, and proliferation while limiting cytotoxicity when compared to cMSCs photoencapsulated within conventional hydrogels. Furthermore, using the rat subcutaneous and intra-articular implant models, SIPS/SCPL-PEG-DA hydrogels were biocompatible, as determined by an appropriate vascular, cellular, and fibrous tissue response 21 days post-implantation. In summary, PEG-DA hydrogels fabricated via SIPS/SCPL may be preferential to conventional PEG-DA hydrogels for articular cartilage tissue-engineering scaffolds. Collectively, the work presented herein describes manipulation of 3D scaffolds in combination with cMSCs and represents advancement in the field of canine tissue engineering for focal articular cartilage injuries.

ACKNOWLEDGEMENTS

This thesis becomes a reality with the support and help of many individuals. I would like to extend my sincere gratitude to all of them.

First and foremost, I am thankful for my Lord and Savior. This endeavor was accomplished with the wisdom He bestowed upon me, the knowledge and peace of mind in order to pursue this research.

I must thank my wife for being a pillar of support. The words of encouragement, acts of support, and reassurance have given me the strength and belief that I could accomplish any task. My gratitude cannot be fully expressed for her selflessness and support in allowing me to pursue my calling, even during the struggles.

There are so many people who have contributed to this dissertation. First, I would like to express my sincere thanks to my committee chair, Dr. Brian Saunders, for the opportunity to complete this work in his lab. I am grateful for experience gained, enabling me to build my skills scientifically, professionally, and personally. In addition, I would like to thank my committee members, Dr. Kayla Bayless, Dr. Carl Gregory, Dr. Melissa Grunlan, and Dr. Gonzalo Rivera, for their guidance and support throughout the course of this research. The contributions made by the committee members have helped me to advance my research and develop my academic training.

Special thanks to Shannon Huggins for the support through success and obstacles encountered in the lab. I am indebted to her for her guidance and ability to help in situations where I was struggling to find solutions. I am grateful for our time and

friendship we have shared over the past four years. I don't think I would have had near the experience or success without her.

My thanks and appreciations also go to my friends, colleagues, and department faculty and staff for making my time at Texas A&M University a great experience.

NOMENCLATURE

2D	Two-dimensional
3D	Three-dimensional
ACI	Autologous chondrocyte implantation
ALP	Alkaline phosphatase
ANOVA	Analysis of variance
ARS	Alizarin red stain
ATCC	American Type Culture Collection
AUP	Animal use protocol
β–GP	Beta-glycerol phosphate
BMP-2	Bone morphogenic protein-2
CCM	Complete culture medium
cDNA	Complementary DNA
CFU	Colony forming unit
cMSC	Canine MSC
DCM	Dichloromethane
DI	Deionized water
DMA	Dynamic mechanical analysis
DMEM	Dulbecco's Modified Eagle Medium
DMSO	Dimethyl sulfoxide
ECM	Extracellular matrix
ELISA	Enzyme-linked immunosorbent assay

FBS	Fetal bovine serum
GAGs	Glycosaminoglycans
HA	Hyaluronic acid
H&E	Hematoxylin and eosin
IA	Intra-articular
IACUC	Institutional Animal Care and Use Committee
Igracure 651	2,2-dimethyl-2-phenyl-acetophenone 1-vinyl-2-pyrrolidinone
Igracure 2959	2-hydroxy-4'-(2-hydroxyethoxy)-2-methylpropiophenone
IL-6	Interleukin 6
LDH	Lactate dehydrogenase
MMP	Matrix metalloproteinase
MT-MMP	Membrane-type matrix metalloproteinase
MSC	Mesenchymal stem cell, multipotent stromal cell
NSAIDS	Non-steroidal anti-inflammatory drugs
OA	Osteoarthritis
OAT	Osteochondral autologous transplant
OBM	Osteogenic basal media
OC	Osteochondrosis
ODM	Osteogenic differentiation media
OSA	Osteosarcoma
PBS	Phosphate buffered saline
PD	Population doubling

PDGF	Platelet derived growth factor
PEG	Polyethylene glycol
PEG-DA	Polyethylene glycol diacrylate
PDMS	Polydimethylsiloxane$_{star}$
P-NPP	p-nitrophenyl phosphate
PS-FBS	Premium select FBS
PTEN	Phosphatase and tensin homolog
RB1	Retinoblastoma protein
rER	Rough endoplasmic reticulum
ROP	Regenerative osteochondral plug
RSII	Reduced serum supplement
SD	Standard deviation
SEM	Scanning electron microscopy
SIPS	Solvent induced phase separation
SCPL	Solvent-casted particulate leaching
TIMP	Tissue inhibitor of metalloproteinase
TLR	Toll-like receptor
TNF-α	Tumor necrosis factor alpha
UV	Ultra-violet
VEGF	Vascular endothelial growth factor

TABLE OF CONTENTS

Page

ABSTRACT ii

ACKNOWLEDGEMENTS iv

NOMENCLATURE vi

TABLE OF CONTENTS ix

LIST OF FIGURES xi

LIST OF TABLES xiii

CHAPTER

I INTRODUCTION 1

Articular (hyaline) cartilage 1
Osteoarthritis 2
Regenerative medicine and tissue engineering 5
Multipotent stromal cells (MSCs) 6
MSC differentiation capacity 7
MSC characterization 8
Canine MSCs (cMSCs) 10
Hydrogel scaffolds for osteochondral tissue repair 12
Polyethylene glycol (PEG) 14
Combining MSCs with 3D scaffolds for tissue engineering 15
Summary and outline 16

II PLATELET-DERIVED GROWTH FACTOR-BB (PDGF-BB) STIMULATES MG-63 OSTEOSARCOMA CELL INVASION OF THREE-DIMENSIONAL COLLAGEN MATRICES IN A MEMBRANE-TYPE MMP DEPENDENT MANNER 18

Summary 18
Introduction 19
Materials and methods 31
Results 36
Discussion 50

III CHARACTERIZATION OF CANINE MULTIPOTENT STROMAL CELLS ISOLATED FROM SYNOVIUM, BONE MARROW, OR ADIPOSE TISSUE: A SUBJECT-MATCHED COMPARISON USING ASSAYS OPTIMIZED FOR THE DOG 59

Summary 59
Introduction 60
Materials and methods 63
Results 73
Discussion 95

IV COMPARISON OF CONVENTIONAL AND NOVEL FABRICATION METHODS FOR POLYETHYLENE GLYCOL DIACRYLATE (PEG-DA) HYDROGELS AS THREE-DIMENSIONAL (3D) SCAFFOLDS FOR CANINE ARTICULAR CARTILAGE TISSUE ENGINEERING 107

Summary 107
Introduction 109
Materials and methods 115
Results 126
Discussion 145

V CONCLUSIONS AND FUTURE DIRECTIONS 153

REFERENCES 162

APPENDIX 188

LIST OF FIGURES

Page

Fig. 2.1. PDGF receptor identification in normal and neoplastic cell types 37

Fig. 2.2. MG-63 cells migrate in response to PDGF-BB 39

Fig. 2.3. PDGF-BB meditated MG-63 invasion in collagen type I matrices 40

Fig. 2.4. Time course analysis of MG-63 invasion in response to PDGF-BB 42

Fig. 2.5. Effect of PDGF receptor tyrosine kinase inhibitor on MG-63 cell invasion in collagen type I matrices 44

Fig. 2.6. MT-MMPs are required for MG-63 invasion of 3D collagen type I matrices 48

Fig. 2.7. MT-MMP gene expression in MG-63 cells 49

Fig. 2.8. PDGF-BB mediated MG-63 invasion of collagen type I requires MT1-MMP 51

Fig. 3.1. Nucleated cell isolation and CFU potential of synovium, marrow, and adipose cMSCs 75

Fig. 3.2. Flow cytometry analysis of synovium, marrow, and adipose cMSCs 77

Fig. 3.3. Expression of plasticity-associated genes in synovium, marrow, and adipose cMSCs 79

Fig. 3.4. Short- and long-term proliferation of synovium, marrow, and adipose cMSCs 81

Fig. 3.5. Adipogenesis of synovium, marrow, and adipose cMSCs 85

Fig. 3.6. Short-term osteogenesis of synovium, marrow, and adipose cMSCs 86

Fig. 3.7. Long-term osteogenesis of synovium, marrow, and adipose cMSCs 88

Fig. 3.8. Chondrogenesis of synovium, marrow, and adipose cMSCs 90

Fig. 3.9. Immunomodulation of murine TNF-α by synovium, marrow, and adipose cMSCs 93

Fig. 3.10. Immunomodulation of murine IL-6 by synovium, marrow, and adipose cMSCs 94

Fig. 4.1. Characterization of canine bone marrow MSCs..... 127

Fig. 4.2. Varying PEG-DA hydrogel fabrication methods 129

Fig. 4.3. cMSC morphology and viability when seeded in varying fabrication methods of PEG-DA hydrogels 131

Fig. 4.4. Effect of SIPS/SCPL pore size on cMSC cell morphology and viability..... 132

Fig. 4.5. Assessment of cMSC cytotoxicity and proliferation in varying fabrication methods of PEG-DA hydrogels 134

Fig. 4.6. SEM and DMA of cMSC seeded SIPS/SCPL fabricated hydrogels 136

Fig. 4.7. Subcutaneous SIPS/SCPL hydrogel implant biocompatibility 139

Fig. 4.8. SIPS/SCPL hydrogel intra-femoral biocompatibility..... 140

Fig. 4.9. Intra-articular hydrogel displacement 142

Fig. 4.10. Conventional hydrogel intra-femoral biocompatibility..... 143

Fig. 4.11. Intra-articular SIPS/SCPL hydrogel implant biocompatibility 144

LIST OF TABLES

Page

Table 3.1. Nucleated cell isolation and CFU potential of synovium, marrow, and adipose cMSCs 74

Table 3.2. Flow cytometry analysis of synovium, marrow, and adipose cMSCs 78

CHAPTER I

INTRODUCTION

ARTICULAR (HYALINE) CARTILAGE

Articular cartilage is connective tissue lining the subchondral bone of articulating surfaces of joints primarily composed of extracellular matrix (ECM) components, collagen type II and proteoglycans. Collagen type II is the principal component (90-95%) of the microfibrillar network and is composed of three α_1 chains in a triple-helical structure organized into multi-fibril structures. The collagen fibril network is cross-linked and thought to provide stability and stiffness while being resistant to swelling and tensile strains (Wilson et al., 2005). Interwoven within the collagen fibril network are protein polysaccharide molecules, proteoglycans. Proteoglycans provide a backbone structure for subunits binding of glycosaminoglycans (GAGs). GAGs are negatively charged disaccharides involved in attraction of positively charged molecules to maintain osmolarity. In turn, fluid and electrolyte balance is maintained. This balance of fluid (water) is responsible for the tensile and shear properties of cartilage. Water allows for the load-dependent deformation as a shock absorber, minimizing peak pressures; in addition, water also assists in providing a low-friction gliding surface for pain free movement. When the microfibrillar collagen network or proteoglycans incur acute trauma or damage, normal wound healing mechanisms are limited due to the avascular and aneural properties of this specialized tissue. Thus damage is minimally repaired. Damage to the macrostructure of cartilage alters the intrinsic tissue properties allowing increased permeability, leading to an increase in water content. This increase in water

reduces the elasticity modulus thereby decreasing the load bearing capacity. In osteoarthritis, water content can exceed >90% of tissue weight, allowing for increased damage and progression across the joint surface (Martin and Buckwalter, 2000).

OSTEOARTHRITIS

Developmental and degenerative joint diseases such as OC and OA are debilitating conditions that affect the quality of life, economic productivity, and life expectancy of humans and domestic animals (Woolf and Pfleger, 2003; Ytrehus et al., 2007). Osteochondrosis is characterized by a genetic or developmental disorder of abnormal endochondral ossification of articular cartilage leading to focally thickened cartilage, tissue necrosis, detachment, synovitis, and pain. OC has been hypothesized to occur in a focal region of subcondral bone with the overlying cartilage incurring secondary lesions and necrosis (Robertson et al., 2003). Deformation to cartilage surrounding OC lesions often results in joint effusion, arthralgia, lameness, and eventual progression to OA (Breur and Lambrechts, 2011). In contrast to OC where the articular cartilage is developmentally abnormal, normal cartilage can be affected by traumatic, high-impact injuries during athletic events. These focal traumatic injuries result in cartilage fibrillation, fragmentation, and subsequent OA. Approximately 52.5 million adults in the United States are currently affected by OA. Due to the aging population and increased obesity rates, this number is expected to grow to 67 million by 2030 (Barbour et al., 2013). Furthermore, the economic impact of OA approaches 60 billion dollars per year in humans (Buckwalter et al., 2004).

From a biomechanical perspective, the canine skeleton undergoes loading in a manner that approximates that of the human skeleton (Bergmann et al., 1984; Liebschner, 2004). For this reason, canine models of osteoarthritis, anterior cruciate ligament repair, meniscal injury, and non-union fractures are acceptable models for translational into human clinical trials. As a model species, approximately 25% of dogs over 2 years of age are affected by OA with increasing prevalence as age progresses (Johnston, 1997); while knee OA associated with rupture of the cranial cruciate ligament (a ligament in the knee of dogs analogous to the ACL in humans) in dogs was estimated at 1.32 billion dollars in 2005 (Wilke et al., 2005). Longitudinal studies, in which healthy dogs are followed to the end of life, demonstrate that between 50% and 87% of dogs develop OA of the elbow, hip, and shoulder (Huck et al., 2009; Runge et al., 2008; Smith et al., 2006).

Broadly, two strategies are currently used for the treatment of joint disorders: medical and surgical. Medical approach involves the management of symptoms through the use of non-steroidal anti-inflammatory drugs (NSAIDs) or corticosteroids, initiation of weight loss, diet modifications, maintenance of regular low-impact activity, and occasional use of joint lubricants such as Hyaluronic Acid (HA) administered into the joint to control pain. Clinical signs are likely to progress despite escalation of medical treatments (Moran et al., 2003). Not only does medical management require life-long treatment, long-term administration of some of these medications carry a risk of major complications such as bleeding disorders, gastrointestinal ulceration, and kidney or liver damage. Alternative options for relief can be explored for patients in whom medical

treatments do not provide quality pain management or improved function. These options include: surgical debridement of damaged joint surfaces using arthroscopy, microfracture to stimulate fibrocartilage ingrowth, osteochondral autograft transplant (OAT), and autologous cartilage implantation (ACI). While some of these treatments provide short-term alleviation of pain, they often do not provide long-term relief (Al-Shaikh et al., 2002; Clair et al., 2009; Gobbi et al., 2006; Harris et al., 2011; Peterson et al., 2000). When these options have been exhausted, major surgical intervention becomes necessary. While surgical treatments such as joint replacement are highly effective, joint replacement is costly and not without its own complications such as implant loosening, infection, luxation, or fracture (Clohisy et al., 2004; Ranawat, 1986). For these reasons, joint replacement is considered by many to be a procedure intended only for patients with end-stage OA.

There are currently few viable treatment options for patients with early-stage OA intended to bridge the gap between medical management and major surgical interventions such as total joint replacement. These treatments include the aforementioned: ACI, OAT, microfracture, and abrasion arthroplasty procedures. While microfacture and abrasion arthroplasty have proven effective in fibrocartilage production, the mechanical properties of this tissue do not approach that of normal articular cartilage (Ochi et al., 2001). On the other hand, while ACI and OAT procedures have demonstrated promising early results, long-term effects are questionable due to poor integration with surrounding tissue, donor site morbidity, fibrocartilage formation,

and cell phenotype changes (Constantinou et al., 2014; Madry et al., 2011; Pacifici et al., 1991).

REGENERATIVE MEDICINE AND TISSUE ENGINEERING

Due to costs, limitations, and risks associated with treatments described above, regenerative medicine using novel tissue engineering scaffolds holds much promise in the treatment of OA and other focal cartilage defects. Ideally, a successful treatment would reduce clinical signs, improve quality of life, reduce the frequency of medical management, and delay or eliminate the need for total joint replacement. In fact, regenerative medicine and tissue engineering approaches are well suited to serve as a bridge between medical and surgical treatments. In 2006, Greenwood defined *regenerative medicine* as an emerging interdisciplinary field of research and clinical application focused on the repair, replacement, or regeneration of cells, tissues, or organs to restore impaired function resulting from any cause, including congenital defects, disease, and trauma (Greenwood et al., 2006). *Tissue engineering* is considered a subspecialty within regenerative medicine in which 3D scaffolds, either alone or in conjunction with cells, are used to repair and improve the function of injured tissues (Daar and Greenwood, 2007; Greenwood et al., 2006). Regenerative medicine and tissue engineering may provide treatment options for a number of traumatic injuries, spontaneous diseases, or genetic mutations (Horwitz et al., 1999; Tsubota et al., 1999).

The objective of tissue engineering in the context of focal cartilage injury is to re-create a tissue interface capable of restoring function, eliminating pain, and limiting

the progression of focal cartilage injury to widespread OA. There have been numerous attempts to engineer articular (hyaline) cartilage using cell-free tissue-engineering systems. To date, previous tissue engineering strategies have not proven effective due to limitations of tissue engineering constructs to duplicate the unique structure, function, and biomechanical properties of the specialized zones of articular cartilage (Gao et al., 2001; Niederauer et al., 2000). For these reasons, the addition of multipotent stromal cells to tailored 3D scaffolds may improve the ability to generate a tissue-engineering device capable of restoring the structure and function of the osteochondral interface.

MULTIPOTENT STROMAL CELLS (MSCS)

Multipotent stromal cells, also known as mesenchymal stem cells or marrow stromal cells, are spindle-shaped progenitor cells of mesenchymal origin capable of differentiating into a variety of cells within the mesenchymal lineage including bone, fat, and cartilage (Caplan, 1991; Dominici et al., 2006). Recent work has suggested that MSCs also function in a similar manner as specialized perivascular smooth muscle cells known as pericytes and have been shown to exist in a variety of tissues such as bone marrow, adipose tissue, dermis, synovium, and umbilical cord (Erices et al., 2000; Fraser et al., 2008; Friedenstein et al., 1987; Sakaguchi et al., 2005; Toma et al., 2001). It is known that MSCs play a central role in both development and tissue repair; however, the existence of MSCs was not recognized until Alexander Friedenstein identified fibroblastic colony-forming cells from the non-hematopoietic fraction of bone marrow in the early 1970's (Friedenstein et al., 1970; Owen and Friedenstein, 1988). Friedenstein's

groundbreaking work described the morphology, colony forming potential, and differentiation of MSCs into osteogenic and cartilaginous lineage. Subsequent studies proved differentiation into various cell types such as osteoblasts, adipocytes, chondrocytes, and fibrous tissue (Prockop, 1997). Friedenstein's pioneering work also demonstrated that when transplanted *in vivo* to the renal capsule or peritoneal cavity, these cells would lead to *de novo* formation of bone-like tissue (Friedenstein et al., 1987; Owen and Friedenstein, 1988).

MSC DIFFERENTIATION CAPACITY

Stem cells (mesenchymal or other) are classified based on differentiation potential. Differentiation potential is typically categorized by three levels: totipotent, pluripotent, and multipotent. These levels of differentiation potential are best described in the context of human development. The term "totipotent" refers to a stem cells' ability to differentiate into all three embryonic germ layers (ectoderm, endoderm, mesoderm), placenta, and supporting tissues required for development. Totipotent stem cells are present only during the early stages of embryonic development. Cell division occurs over 2-3 days, forming a morula (mass consisting of eight cells). At this point the cells are totipotent, as defined by the cells' capacity to differentiate into any cell type. After approximately five days the morula develops into a blastocyst, consisting of two distinct cell types: the inner cell mass and the trophectoderm. The trophectoderm forms the outer layer of the blastocyst and is responsible for the placenta while the inner cell mass continues cellular division as a developing embryo. Prior to gastrulation embryonic cells

are capable of differentiating into any of the three primary germ layers (ectoderm, mesoderm, endoderm), making these cells pluripotent. This state of pluripotency is present until the mid-gestation period. As the embryo continues to form, stem cells continue to divide, creating daughter cells. Daughter cells are replicas of stem cells but undergo further specialization due to subsequent division and changing environmental cues. Stem cells present during this period of development are referred to as multipotent cells, as they have the ability to differentiate into various cell types, but this differentiation is limited to cells within their specific lineage of origin. In summary, totipotent stem cells have the capacity to differentiate into all three germ layers, placenta, and supporting tissue during embryonic development; pluripotent stem cells have the capacity to differentiate in the any of the primary germ layers (ectoderm, mesoderm, endoderm); multipotent stem cells have the capacity to differentiate into specialized cells within their respective germ layer.

MSC CHARACTERIZATION

Although the use of MSCs as regenerative medicine agents holds much promise, the ability to precisely define what constitutes an MSC remains a challenge in the field. Differences in isolation and culture techniques make it difficult to use potency as a classification criterion for stem cells. Due to the disparate characteristics of MSCs reported, a working group convened in 2006 to establish more rigorously and generally accepted criteria for MSCs (Dominici et al., 2006). Accordingly, MSCs are cells that: 1) adhere to tissue culture plastic and exhibit a spindle-shaped or “mesenchymal”

appearance; 2) form colonies of cells from single parent cells when cultured in low-density "clonal" cultures without media exchange; 3) express specific surface epitopes negative for hematopoietic lineages; and 4) possess the ability to differentiate into osteoblasts, adipocytes, and chondrocytes (tri-lineage differentiation) using defined in vitro differentiation assays (Dominici et al., 2006). More recently, immunomodulation has been suggested as an additional criterion (Nauta and Fibbe, 2007; Rasmusson, 2006; Uccelli et al., 2006)

Although MSCs have been used in regenerative medicine and tissue-engineering approaches to repair or replace diseased tissues in humans and several animal species (Granero-Moltó et al., 2009; Greenwood et al., 2006; Horie et al., 2012a; Nishida et al., 2004), a better understanding of interactions between micro environmental cues and cellular responses such as proliferation potential, differentiation capacity, and immunomodulation will expand their therapeutic use. MSCs are most commonly isolated from bone marrow and adipose tissue but it is now well documented that MSCs can be isolated from a variety of tissues; including synovium (De Bari et al., 2001), periosteum (De Bari et al., 2006), muscle (Danišovič et al., 2013), dental pulp (Pierdomenico et al., 2005), and others (Sakaguchi et al., 2005). During their initial discovery, MSCs from these alternate tissues were assumed to be similar to marrow and adipose derived MSCs due to their common ability to self-renew, expression of similar surface epitopes, and their ability to undergo tri-lineage differentiation in vitro. Although cells isolated from each of these tissues have been shown to meet established criteria that define MSCs, more recent donor-matched studies have revealed that the ability of MSCs

to proliferate and undergo lineage specific differentiation varies widely based on the tissue of origin and donor (Bruder et al., 1994; Reger et al., 2008; Sakaguchi et al., 2005; Sekiya et al., 2002; Volk et al., 2005; Volk et al., 2012). As previously discussed, MSC properties are affected by isolation and culture techniques, which have not been accounted for in some studies. In summary, drawing distinctions between canine MSCs based on existing literature is difficult due to donor variation and differences in the isolation and culture techniques used in each study.

CANINE MSCS (cMSCS)

Translation of promising findings from rodent models to humans represents a significant hurdle for cell-based therapies due to variances in size and biomechanics. Therefore, a number of large animal species have been used to bridge the gap from rodents to humans (Hatsushika et al., 2014; Horie et al., 2012b; Horie et al., 2009; Kon et al., 2000; Murphy et al., 2003). The dog is a compelling model species for these types of cell-based translational studies. When compared to rodents, dogs are large, long-lived, genetically diverse, and share many biochemical and physiological similarities with humans. Canine models have been used successfully for adult bone marrow transplantation, gene therapy, and development of protocols to overcome allograft rejection (Prentice et al., 1984; Socie and Blazar, 2009; Storb et al., 1970). Due to their response to learned behaviors such as treadmill exercise, dogs have been used to develop new therapies for cardiovascular and orthopedic diseases (Bockstahler et al., 2007; Kiviranta et al., 1988). From a biomechanical perspective, the canine skeleton undergoes

loading in a manner that approximates that of the human skeleton (Bergmann et al., 1984; Liebschner, 2004). For these reasons, canine models of osteoarthritis, anterior cruciate ligament repair, meniscal injury, and non-union fractures are well suited (Arnoczky and Warren, 1983; Johnson et al., 1989; Liu et al., 2006; Nelson et al., 1988; Pond and Nuki, 1973; Shortkroff et al., 1996) for the development of new treatments for focal or diffuse OA, including the optimization of tissue engineering strategies. Many of these studies require the use of MSCs or other progenitor cells; however, currently only a modest number of reports exist describing the isolation and differentiation of cMSCs from bone marrow, adipose tissue, and other tissues (Kisiel et al., 2012; Neupane et al., 2008; Sakaguchi et al., 2005; Volk et al., 2005; Volk et al., 2012). Kadiyala's initial cMSC report in 1997 exhibited an ability to identify and isolate cMSCs from canine bone marrow (Kadiyala et al., 1997). Moreover, this study was seminal in displaying the ability of cMSCs to regenerate bone in a critical gap defect model. Subsequently, in 2005, Volk et al. described the necessity of supplementation of bone morphogenic protein- 2 (BMP-2) when culturing cMSCs towards an osteogenic lineage (Volk et al., 2005). In 2008, Neupane et al. detailed the first isolation and characterization of adipose derived canine MSCs, showing expression of genes commonly associated with developmental plasticity (Neupane et al., 2008). In 2012, Kisiel et al. evaluated MSCs from a variety of tissues, demonstrating that cMSCs could be successfully isolated from a multiple tissues and that key differences are present when comparing MSC characteristics between different tissue sources (Kisiel et al., 2012). While these aforementioned publications are important to the cMSC field, it is not possible to make

direct comparisons between studies due to donor variation, isolation techniques, and culture inconsistencies utilized by individual laboratories. For these reasons, in conjunction with the scarcity of canine literature, a comprehensive report describing the characteristics of subject-matched cMSCs isolated from bone marrow, synovium, and adipose tissues using identical isolation and characterization methods is of the utmost importance in order to facilitate the selection of cMSCs for cell-based translational studies.

HYDROGEL SCAFFOLDS FOR OSTEOCHONDRAL TISSUE REPAIR

Many techniques have been used to improve differentiation of MSCs with the goal to repair articular cartilage. Examples include the use of lineage specific media, supplementation with growth factors, and use of pelleted cell aggregates to alter cellular arrangement (Lee and Shin, 2007; Martin et al., 2007; Nooeaid et al., 2012; Sherwood et al., 2002). While these techniques may prove useful, they are not without restrictions such as limitations on size alterations for appropriate translation to clinical-sized defects, time required to induce chondrogenesis through traditional methods, cost prohibitions in regards to the use of recombinant growth factors, safety concerns in regards to use of growth factors such as BMP-2, and the inability of these techniques to produce biologically and biomechanically consistent, reproducible tissue engineering constructs (Garrison et al., 2007; Jin et al., 2001; Shields et al., 2006). Due to these limitations, recent emphasis has been placed on alternative methods to enhance differentiation. Use of 3D scaffolds hold much promise for tissue engineering approaches as treatments for

bone and joint defects (Bailey et al., 2013; Brandl et al., 2007; Gunatillake and Adhikari, 2003; Hou et al., 2010; Kirschner and Anseth, 2013; Munoz-Pinto et al., 2012; Park et al., 2005). Scaffolds constructed of biologic (collagen, hydroxyapatite, gelatin, silk, and alginate) and synthetic polymers (polyurethane, polyanhydride, polyphosphazene, and polyethylene glycol) (Gunatillake and Adhikari, 2003; Guo and Ma, 2014; Park et al., 2005) have been successfully used in animal models to treat small, experimentally-induced osteochondral defects (de Girolamo et al., 2015). Additionally, many of these biologic and synthetic scaffolds are currently being commercially used for healthcare treatment (Park et al., 2007). Implementation of 3D scaffolds offer a means to deliver drugs or growth factors to a specific site as well as to enhance local cell retention, provide structural support, and facilitate tissue repair (Gunatillake and Adhikari, 2003; Park et al., 2005). The ideal 3D scaffold for tissue engineering of articular cartilage should possess the following properties:

1. Biocompatible- referring to the ability of the material to interact with the host tissue without inducing toxicity, inflammation, or immune response.
2. Tunable- referring to the ability of the material to be custom modulated for overall size and gradient transition (from cancellous bone, to subchondral bone, to articular cartilage).
3. Tetherable- referring to the ability to incorporate growth factors, cytokines, and cell binding domains- amplifying properties for facilitating cell adhesion and response to local environmental cues.

4. Biomechanically similar to native tissue - referring to the ability to mimic normal articular cartilage biomechanics.
5. Cost efficient
6. Reproducible - referring to the manufacturing consistency of the implant
7. Readily implantable- referring to the ability of the material/device to be implanted using minimally invasive procedures and standard surgical instruments.
8. Bondable to adjacent host tissue- referring to ability to be incorporated and respond with surrounding local environment over time.
9. Biodegradable- referring to the ability of material to be degraded or broken down under normal biologic conditions. Furthermore, allowing the physiologic process of the body to permanently remodel and replace the temporary implant.

POLYETHYLENE GLYCOL (PEG)

Polyethylene glycol (PEG) is a synthetic, biodegradable compound that has been extensively studied as a polymer for hydrogel fabrication because it has been shown to inhibit protein aggregation and to be inherently biocompatible (Bailey et al., 2013; Guo and Ma, 2014; Ma and Elisseeff, 2005; Munoz-Pinto et al., 2012). PEG is a common component of surgical implants and other medical devices, including contact lenses, catheters, cell delivery scaffolds, orthopedic implants (Park et al., 2007). PEG has been evaluated extensively as a 3D scaffold for tissue engineering. It has been described as a "gold standard" in synthetic biopolymers due to its ability to be incorporated without

increased negative complications (Pasut, 2014; Ulbricht et al., 2014). PEG based hydrogels have been shown to be hydrophilic, tissue compatible, and tunable to necessary specifications. In particular, PEG based hydrogels are especially popular because they are immunologically inert, preventing non-specific protein adhesion that would induce immune and/or inflammatory responses (Bailey et al., 2012; Pasut, 2014). This "biologic blank slate" also allows for control of cellular behavior through incorporation of specific cytokines, growth factors, and cell adhesion ligands tailored to the scaffold and specific need of the tissue-engineering device. In addition, modulation of polymer size and crosslinking can contribute to mechanical changes in an attempt to mimic surrounding tissue biomechanics. While these properties have made PEG hydrogels attractive for cartilage tissue engineering, current hydrogel fabrication techniques have limited the translation of PEG hydrogels into the clinical setting. To date, prior *in vivo* studies attempting to restore osteochondral defects using 3D tissue engineering constructs composed of PEG have been limited due to poor integration with adjacent tissue and an inability to reconstruct normal tissue architecture (de Girolamo et al., 2015; Duan et al., 2013).

COMBINING MSCS WITH 3D SCAFFOLDS FOR TISSUE ENGINEERING

Differentiation of MSC can be influenced by mechanical and structural properties of scaffolds and the inclusion of growth factors. It has been shown that a cell's ability to convert extracellular mechanical stimulus into a phenotypic response, known as mechanotransduction, is enhanced in 3D environments (Engler et al., 2006;

Tibbitt and Anseth, 2009). Mechanotransduction in 3D environments is known to affect cell proliferation, migration, invasion, and differentiation through integrin signaling and cytoskeletal tensegrity (Brandl et al., 2007; Grinnell and Petroll, 2010; Miyamoto et al., 1995; van der Flier and Sonnenberg, 2001). Thus, 3D scaffolds designed for osteochondral tissue repair or replacement may provide an environment that allows creation of focal adhesions, development of unique cellular functions, and differentiation into tissue specific progenitors. Due to these effects, it has been proposed that induction of MSC differentiation via the osteoinductive and bioactive properties of PEG hydrogel scaffolds is possible, without inducing cytotoxicity or apoptosis. These bioactive, gradient systems composed of PEG and MSCs have previously been termed as Regenerative Osteochondral Plugs (ROPs) (Gacasan et al., 2016). Prior studies and our own preliminary data have demonstrated that structural properties of ROPs are critically important for integration with surrounding tissues. Upon successful integration with adjacent host tissue, PEG hydrogel scaffolds may direct MSC differentiation so that in the future, zone-specific tissues can be created to potential replicate the specialized zones of articular (hyaline) cartilage.

SUMMARY AND OUTLINE

In summary, this chapter outlines the unique properties of articular cartilage, clinical and economic impact of cartilage injury and subsequent OA, and limitations of current treatment strategies. While a number of treatments exist in both humans and veterinary species, none are without limitations. The ideal treatment for injured joint

tissue has yet to be determined. The use of regenerative medicine, specifically tissue engineering, as a potential treatment for articular cartilage injuries is discussed in detail above. Tissue engineering is a promising treatment strategy for these injuries, with the goal of restoring structure and function, reducing/eliminating clinical signs, and delaying or preventing major surgical treatment. In subsequent chapters of this dissertation, important components of tissue engineering will be detailed. First, in Chapter II, a well-described, 3D, serum-free collagen system was used as a model system in the study of human MG-63 osteosarcoma cell invasion. This system will elucidate the role of platelet derived growth factor-BB and cell-matrix interactions during osteosarcoma cell invasion in 3D environments. In Chapter III, cMSCs were isolated from synovium, bone marrow, and adipose tissue and comprehensively characterize using a donor-matched study and assays optimized for the canine species. In Chapter IV, the optimal fabrication method for incorporation of cMSCs with PEG based hydrogels for *in vitro* studies and eventual transition into a clinical setting was determined. Lastly, Chapter V contains concluding comments, future directions/perspectives, and establishes long-term goals for success.

CHAPTER II

PLATELET-DERIVED GROWTH FACTOR-BB (PDGF-BB) STIMULATES MG-63 OSTEOSARCOMA CELL INVASION OF THREE-DIMENSIONAL COLLAGEN MATRICES IN A MEMBRANE-TYPE MMP DEPENDENT MANNER

SUMMARY

Invasion of the extracellular matrix is essential for many physiological and pathological processes. Invasion of 3D matrices requires an invasion stimulus, integrins, proteinases such as matrix metalloproteinases (MMPs), and cytoskeletal rearrangement. Previous work has linked soluble MMPs to tumor invasion and metastasis while recent studies suggest that membrane-type MMPs (MT-MMPs) are required for focused pericellular proteolysis that occurs during tumor invasion. The objective of this study was to evaluate the role of MMPs in osteosarcoma cell invasion in response to platelet-derived growth factor-BB (PDGF-BB). We hypothesized that PDGF-BB would induce invasion of 3D collagen type I matrices by MG-63 osteosarcoma cells in an MT-MMP dependent manner and that soluble MMPs would be less critical in these events. MG-63 cells were seeded on 3.75mg/mL collagen type I gels in a serum-free environment and allowed to invade for 24-72 hours. Cell invasion was determined and analysis of conditioned media and cell lysates via western blot and gelatin zymography was performed. PDGF-BB induced a dose- and time-dependent invasion of MG-63 cells into 3D collagen type I matrices. In addition, PDGF-BB resulted in increased expression of soluble interstitial collagenase MMP-1 as well as an increased activation of MMP-2. The addition of the PDGF receptor tyrosine kinase inhibitor AG1296 resulted in a significant

reduction in invasion; thus, suggesting a connection between MG-63 invasion and PDGF-BB receptor signaling. Furthermore, disruption of MMP activity through broad-spectrum MMP inhibitors (GM6001 and TAPI-0) significantly inhibited MG-63 invasion in response to PDGF-BB. On the other hand, cultures containing tissue inhibitor of metalloproteinase-1 (TIMP-1), which inhibits soluble MMPs, or the serine proteinase inhibitor aprotinin, had a substantial invasion response. To examine the specific MT-MMP responsible for MG-63 invasion, siRNA knockdown experiments were performed. There was a significantly reduced invasion after treatment with MT1-MMP siRNA, but not MT2- or MT3-MMP siRNAs. This work suggests that PDGF-BB is an important growth factor in MG-63 osteosarcoma cell invasion, and that MT1-MMP is required for this process.

INTRODUCTION

Osteosarcoma

Osteosarcoma (OSA) is the most common form of malignant bone cancer in children and dogs in which very few effective therapeutic options are currently available (Fenger et al., 2014). In 2014, approximately one thousand adolescents were diagnosed with OSA, occurring in the appendicular skeleton with the long bones affected 90% of the time (Jaffe et al., 2010). Currently, chemotherapy followed by either tumor excision surgery or complete amputation of the affected limb is the only treatment option available. The ability to actively pursue advancement in new medical care of human OSA is difficult because of its high occurrence in the pubescent years, typically spanning between 10 to 14 years of age. The fact that OSA is often initiated during this

stage of human development creates major challenges for novel drug therapies due to the anatomical, hormonal, and physiologic changes occurring within the body during this time. These challenges, along with the low incidence of OSA as compared to other neoplasms, make therapeutic advancement difficult. Therefore new strategies need to be developed if improved treatment options are to be developed.

While the cause and progression of OSA is widely unknown, determining genetic and environmental influences of OSA are likely key to understanding incidence and progression. In an environmental setting, recent studies displayed increased plutonium induced axial skeleton OSA in beagles similar to that of humans whom had prolonged plutonium exposure (Miller et al., 2003). In addition, increased incidence of OSA is prevalent in both humans and canines that have previously been treated for non-OSA associated diseases using radiotherapy. Exposure to radiotherapy in these cases was shown to increase incidence of OSA. Additionally, OSA can also be linked to other bone conditions such as Paget's disease in humans, bone infarcts in dogs, and osteomyelitis (Thomas et al., 2009). While the cause is unknown, the susceptibility of the rapidly proliferating cells for healing, carcinogenic agents, and cytokinesis mutations has been proposed (Fenger et al., 2014; Sandberg and Bridge, 2003). Collectively, these studies demonstrate that an environmental influence likely exists as a direct cause of OSA; likely in addition to the purely spontaneous manner by which neoplastic transformation occurs in the absence of environmental stimuli.

Although development of human and canine OSA can be influenced by environmental factors, there is a growing body of evidence supporting genetic

predisposition to inheritance of OSA risk factors. In some cases gene mutation or deletion inheritance is correlated to specific breeds of dogs but in large part retinoblastoma protein (RB1), p53, and phosphatase and tensin homolog (PTEN) are the most extensively implicated with inherited predisposition to OSA in humans and canines (Hu et al., 2010; Miller et al., 1996; Park et al., 2001; Sandberg and Bridge, 2003; Thomas et al., 2009; Walkley et al., 2008). The most thoroughly described genetic alteration in human OSA is a mutation to the p53 and retinoblastoma genes.

The tumor suppressor gene, p53, helps regulate proliferation, DNA repair, and programed cell death through cell-cycle arrest. Mutations of p53 gene are present in 50% of all cancers and 22% in osteosarcomas (Miller et al., 1996). Miller et al. in 1996 described DNA damage resulting in the phosphorylation of p53, allowing for dissociation of MDM2 (Miller et al., 1996). In these cases, the MDM2 protein is unable to act as a negative regulator for p53; thus, p53 becomes a proto-oncogene in cases where regulation is lost allowing for continued transcription. When p53 is mutated, cancer cells are able to survive and proliferate without restraint. The checks and balance system of delinquent DNA is lost and leads to further malignancy in some cases. Li-Fraumeni syndrome is linked to an autosomal dominant mutation of p53, a direct link to cancer malignancies, including OSA (Walkley et al., 2008). While a correlation may exist, it is unclear whether p53 is the primary cause of OSA. Studies provide conflicting evidence of the role of p53 in OSA. One study claims that p53 has potential to influence the degree of severity of OSA (Park et al., 2001) while another states that p53 may in fact reduce metastasis and increase survival (Hu et al., 2010).

In addition to mutations of the p53 gene, frequency of the tumor suppressor RB1 gene has been shown to be involved in tumorigenesis of OSA (Walkley et al., 2008). The inheritance of a mutation in RB1 gene causes retinoblastoma syndrome and is consistent with multiple malignancies, 40% of which are OSA (Gorlick, 2009). RB1 regulates the cell cycle between the G1 and S phases; binding transcription factors to prevent DNA duplication. When RB1 is deleted, mutated, or phosphorylated, DNA can be transcribed and the cell cycle operates unabated. Loss of the RB1 associated gene may explain genetic inheritance risk, but somatic mutations are still poorly understood.

Lastly, PTEN abnormalities are documented more commonly in canine OSA than humans. PTEN is a tumor suppressor gene participating through negative regulation of the AKT pathway. Regulation occurs through dephosphorylation of the inositol ring of phosphatidylinositol triphosphate. PTEN can also influence p53 pathway by blocking signaling to the proteasome. These influences allow the cell to transcribe and proliferate without regulation. Deletion or decrease in PTEN expression is found in OSA and more prevalent in canines as compared to humans with copy number loss present in 30%-42% of tumors analyzed (Thomas et al., 2009).

While traditional experimental models using rodent and non-human primates to study OSA *in vivo* have been described, they do not come without inherent disadvantages. Promising results obtained in rodent models of OSA have not translated to the clinical setting. The genetic modifications required to generate mouse models of OSA have resulted in tumors occurring more frequently in the flat bones as opposed to long bones predominately seen in humans and other species (Walkley et al., 2008). Due

to the potential risk of zoonotic disease transmission, non-human primate research is tightly regulated in regards to housing conditions, colony maintenance, and euthanasia procedures. These factors often create a financial and regulatory burden that proves insurmountable for many investigators. Due to these limitations, it is important to consider other *in vivo* models. In contrast to murine models, which require tumor seeding or DNA manipulation strategies, dogs develop OSA spontaneously in a manner similar to humans (Vail and Macewen, 2009; Withrow et al., 1991). In fact, canine OSA has approximately ten times the incidence rate (>10,000/year) and approximately twice the morbidity rate (>90%) when compared to humans (Morello et al., 2011). Additionally, dogs are common, genetically diverse as compared to rodent strains, and are often treated as in-home pets by humans. Cohabitation exposes both humans and canines to similar environmental stimuli, helping to eliminate distinguishing variables between species (Fenger et al., 2014; Morello et al., 2011). Given the similar bone structure and biomechanics of dogs and children, as well as the strong interest of pet owners to develop viable treatment options for canine OSA, use of the dog as a model for human OSA presents an excellent opportunity for research advancement. Thus, while the work performed will focus on a human OSA cell line, our findings may have implications for both humans and dogs affected by this debilitating and fatal disease.

High rates of metastases occur prior to diagnosis (Jaffe et al., 2010) making OSA treatments difficult. Metastasis of the OSA from the bone decreases the long-term survival rate of patients from 75% to 30% (Lee et al., 2008). While a robust number of studies have been performed examining the mechanisms of metastasis, elucidation of the

specific physiologic molecules, such as growth factors and cytokines, responsible for tumor cell invasion and metastasis is essential for understanding the mechanism and subsequent therapeutic treatment strategies. One such molecule that has proven to play an important role in these events through its mitogenic and chemotactic effects is PDGF-BB. Previous studies have shown that elevated levels of PDGF correlate with tumor growth, higher metastasis rates, reduced treatment efficacy, and decreased survival rates (Allam et al., 1992; Graves et al., 1984; Heldin et al., 1986; Seymour and Bezwoda, 1994; Seymour et al., 1993). Additionally, PDGF-BB has been shown to influence bone specific cells, such as osteoblasts and osteoclasts, for proliferation, activation, remodeling, invasion, and propagation of metastasis (Canalis et al., 1989; Caplan and Correa, 2011; Liu et al., 2011). These signaling cascades can directly influence tumor growth and cell survival. For these reasons, the role of PDGF-BB influence on OSA invasion is of primary interest for developing future clinical treatment strategies.

Platelet Derived Growth Factor-BB

Cellular invasion of the ECM is essential for many physiological and pathological processes, such as angiogenesis, tissue morphogenesis, wound healing, tissue repair, tumor growth, and metastasis (Alvarez et al., 2006; Bayless and Davis, 2003; Davis et al., 2000; Khanna et al., 2014; Maniscalco et al., 2012; Ostman and Heldin, 2001). It has been previously shown that PDGF-BB plays an important role during these events through both its mitogenic and chemotactic effects (Alvarez et al., 2006; Caplan and Correa, 2011; Hollinger et al., 2008b).

The PDGF family is a group of cationic homo- and hetero-dimeric growth factors composed of disulfide-bonded α- and β- polypeptide chains. The α- and β-chains of PDGFs are approximately 100 amino acid residues long and share approximately 60% amino acid sequence homology (Alvarez et al., 2006; Heldin and Westermark, 1999; Yarden et al., 1986). The three known forms of PDGF were recognized as PDGF-AA, -BB, and -AB until recent discovery of PDGF-CC and –DD. The ability for the A and B chains to dimerize creates a total of 5 known PDGF ligands (–AA, -AB, -BB, -CC, -DD) that bind PDGF receptors. Ligand binding occurs through tyrosine kinase receptors creating hetero- and homo-dimers that further influence the cell physiologic pathways to initiate proliferation, chemo kinesis, chemo taxis, and other important cellular events. PDGF receptors have three potential dimer combinations: PDGFR–αα, –αβ, –ββ. Phosphorylation at various residues of each receptor sub-type results in downstream signaling (Kim et al., 1999) through the MAK/Erk1/2, Akt/phosphidionsitol-3 kinase, and phospholipase Cγ (PLCγ) pathways; however, phosphorylation events do not appear to be specific to the individual PDGF ligand isoforms. PDGFR–α dimerization is initiated by PDGF-AA, -AB, -BB, and -CC but not PDGF-DD; while PDGF-BB initiates dimerization for all known receptor forms (Hollinger et al., 2008a). The ability of PDGF-BB to bind all known receptor combinations (PDGFR-αα, –αβ, –ββ) has led some scientists to term PDGF-BB as “the universal PDGF” (Hollinger et al., 2008a).

Various cell types, such as endothelial cells, megakaryocytes, fibroblasts, smooth muscle cells, macrophages, astrocytes, and glial cells, express various PDGF isoforms.

Within platelets, PDGF isoforms are not released into circulation but stored within the alpha granules (Bowen-Pope, 1986; Ross, 1989). Platelet-induced release of PDGF is triggered by platelet activation and degranulation secondary to activation stimuli such as thrombin. The ability to express, secrete, and respond to PDGF is critical in development and biological processes for cell growth, function, and maintenance of the pericellular environment. For example, PDGF is essential for embryonic development of kidneys, lungs, vascular networks, connective tissue, and central nervous system (Heldin and Westermark, 1988; Heldin and Westermark, 1999; Hoch, 2003; Levéen et al., 1994; Lindahl et al., 1997; Ostman and Heldin, 2001). In the context of angiogenesis, it is well known that angiogenic and vasculogenic endothelial networks express PDGF-BB, and that the appearance of PDGF-BB during angiogenesis recruits pericytes to stabilize newly formed vascular networks (Armulik, 2005; Gerhardt and Betsholtz, 2003). Lack of functional PDGF in these critical developmental stages has been shown to lead to loss of organ specific function or neonate death (Boström et al., 1996; Hoch, 2003; Levéen et al., 1994; Lindahl et al., 1997). In addition to developmental influence, PDGF has been shown to play a role in wound healing and fracture repair through PDGF-BB stimulated recruitment of pericytes (Caplan, 1988; Caplan and Correa, 2011). PDGF-BB stimulated recruitment of pericytes to wound or fracture sites, resulting in an increased level of expression and secretion of vascular endothelial growth factor (VEGF) from the recently recruited pericytes (Hellström et al., 2001; Reynolds et al., 2000). Interestingly, recent work has suggested that MSCs, or progenitor cells capable of reproducing skeletal tissues *in vitro*, are in effect pericytes (Caplan, 2008). The increased expression of

VEGF by pericytes and possibly MSCs subsequently triggers a downstream cascade, resulting in recruitment of endothelial cells for additional vascular network formation (Gehmert et al., 2011).

Due to the fact that PDGF-BB is critical during physiologic and pathologic processes, manipulation of the PDGF ligand-receptor signaling axis or critical downstream effector proteins may prove to be useful clinical targets. Although vascular networks assist in regulating PDGF-BB, PDGF-BB has also been linked to fibrosis, atherosclerosis, tumor growth, and metastasis. Currently, two possible scenarios exist for modulation of PDGF-BB: 1) stimulation and 2) inhibition of PDGF-BB; stimulation has shown to improve angiogenesis, wound healing, bone repair, and development (Caplan and Correa, 2011; Gehmert et al., 2011) while inhibition has been shown to limit malignant and non-malignant disease by blocking ligand-receptor binding or altering the signaling ability of the receptor tyrosine kinase (Hoch, 2003; McGary et al., 2002; Uehara et al., 2003). Thus, whether investigators choose to enhance or inhibit PDGF-BB expression, ligand-receptor binding, or down-stream signaling events; modulation of PDGF-BB may provide novel research and therapeutic strategies targeting downstream effector molecules responsible for cell invasion of 3D environments in response to PDGF. One important group of proteins involved in this process are the MMPs (Lu et al., 2012; Shi et al., 2011).

Matrix Metalloproteinases (MMPs)

MMPs, often termed matrixins, are proteolytic enzymes of the metzincin superfamily. MMPs have been shown to be highly involved in physiological processes

and disease progression and have been implicated in embryogenesis, nerve growth, ovulation, bone remodeling, wound healing, angiogenesis, apoptosis, atherosclerosis, cancer, arthritis, ulceration, and fibrosis (Bayless and Davis, 2003; Deryugina and Quigley, 2006; Egeblad and Werb, 2002; Lu et al., 2005; Nagase and Woessner, 1999; Sternlicht and Werb, 2001; Tang et al., 2013). The MMP family is subdivided into six groups: collagenases, gelatinases, stromelyins, matrilysins, membrane-type, and non-typical/other. Although classifications were organized to assist in identifying similar structure and function across the family of proteinases, this idea is likely inadequate as most MMPs are capable of degrading diverse matrix and non-matrix proteins (Nagase and Woessner, 1999). MMPs are endopeptidases, synthesized in an inactive or zymogen state. They are characterized by the presence of a highly conserved amino acid sequence shown to have a specificity for zinc at its catalytic site (Stocker et al., 1995). Beginning from the N-terminus, prototypical MMP contains a signal peptide, propeptide domain, catalytic domain, hinge region, and hemopexin domain. The signal peptide is present in all MMPs (except for MMP-17) and is present for targeting the translocon in the rough endoplasmic reticulum (rER) (Puente et al., 1996). Once the signal sequence is translated, it is cleaved, leaving the remaining domains to undergo post-translational modifications and eventual export from the cell.

The propeptide region contains a highly conserved cysteine residue, termed the cysteine switch, responsible for maintaining zymogen latency. For activation to occur, the propeptide domain must be cleaved or disrupted creating a conformational change, allowing the catalytic domain to bind preferential substrates for initiation of proteolysis.

Cleavage can be accomplished through substrate-mediated proteolysis by plasmin and other serine proteases, pH changes, free radicals, mechanical forces, and other activated MMPs (Vanwart and Birkedal-Hansen, 1990). Zymogen activation by these catalysts occurs after exportation from the cell, except when a furin-like recognition motif is present in the propeptide domain. This furin-like motif allows MMP-11, -14, -15, -16, and -17 to be activated within the cell due to a conserved region recognized by furin/pro-hormone convertase (Pei and Weiss, 1995). The convertase enzymes specialize in cleaving peptide sequences containing lysine and arginine to release the catalytic domain for activation. Once the catalytic domain is released, calcium ions stabilize the structure for enzymatic activity and proteolysis (Nagase and Woessner, 1999). In the case of MMP-2 and -9, the catalytic domain also contains a fibronectin repeat domain to assist in attachment and subsequent interaction with gelatin (Allan et al., 1995; Bányai et al., 1994). The catalytic domain is usually connected to the hemopexin domain through a flexible linker or "hinge" region. This hemopexin region is an ellipsoidal disk shape with a four blade β-propeller structure shown to be absolutely required for the collagenases but not essential for the other MMPs (Murphy and Knäuper, 1997). These structural differences in MMP regions aide in identifying group classification and functionality of specific proteolytic activity.

Currently, 25 MMPs are known to exist in vertebrates, with 22 being expressed in humans (Lohi et al., 2000; Sternlicht and Werb, 2001; Woessner, 1994; Woessner, 2002). In most cases, cells secrete MMPs into the cytosol or export the protein completely out of the cell; however, of the 22 human MMPs, six have been

characterized as MT-MMPs due to the presence of the transmembrane and cytoplasmic domains on the C-terminus of proteins.

Although much work has linked soluble MMPs such as MMP-1, -2, -3, -9, -10, and -13 to tumor invasion and metastasis (Himelstein et al., 1998; Proulx-Bonneau et al., 2011) other studies suggest that the MT-MMPs are the sub-family of MMPs required for the focused ECM proteolysis that occurs during angiogenic sprouting, tumor invasion, stem cell invasion, and tumor metastasis (Bayless and Davis, 2003; Bayless et al., 2009; Shiomi and Okada, 2003; Sternlicht and Werb, 2001). While MMPs have been linked to a myriad of tumor types such as chordomas, fibromas, fibrosarcoma, dermatofibrosarcoma, osteosarcomas, and tumors of the central nervous system, few studies exist linking MT-MMPs or other MMPs in to primary bone tumors such as OSA (Bjørnland et al., 2005; Bjørnland et al., 1999).

The multitude of contributing factors known to increase susceptibility of OSA make target treatment strategies difficult. Therefore, alternative options must be sought to reduce metastasis of OSA. The known role of PDGF-BB and its receptors in cell proliferation and invasion events, in addition to the strong support in the literature for the concept that MT-MMPs are required for focal ECM proteolysis during invasion, have led investigators to evaluate the role of PDGF-BB in direct correlation of increased expression and proteolytic activity of MMPs, more specifically MT-MMPs. These studies have been shown in our own preliminary data and previous publications in which MT-MMP activity is increased in response to PDGF-BB. Elucidation of expression and potential signaling cascades caused by PDGF-BB activation may prove useful in

treatment strategies for *in vivo* testing. In the present study, we evaluate the role of PDGF-BB in human OSA cell invasion into 3D collagen type I matrices via MMP proteolysis. We hypothesized that PDGF-BB would stimulate MG-63 cells to invade 3D collagen type I matrices in an MT-MMP dependent manner, while soluble MMPs would be less important to these events. Results detailed herein demonstrate invasion response of human osteosarcoma MG-63 cells to PDGF-BB by way of MT1-MMP proteolysis of collagen type I in a dose- and time-dependent manner. Our results provide insight into important cellular events and will prove useful for both investigators and clinicians considering translational treatment strategies of OSA.

MATERIALS AND METHODS

Cell Culture

MG-63 OSA cells were obtained from American Type Culture Collection (ATCC) and cultured with Dulbecco's Modified Eagle Medium (DMEM, Invitrogen, Carlsbad, CA), 10% heat-inactivated fetal bovine serum (FBS, Atlanta Biologicals, Inc., Flowery Branch, GA), 100μg/mL gentamicin (Invitrogen), and antimycotic (Invitrogen) containing 100U/mL of penicillin, 100μg/mL of streptomycin, and Fungizone and maintained at 37ºC with 5% CO_2. Cells were seeded at 500 cells/cm^2 on T75 tissue-culture plastic flask (Corning, Corning, NY) and media exchanged twice a week. Cells were allowed to reach 70-80% confluence before experimental use or incremental passage. After ten passages, cultured cells were discarded and a new cryopreserved vial thawed. Prior to each experiment, cells were washed with 10mLs of phosphate buffered

saline (PBS), trypsinized, neutralized with FBS, and centrifuged. Cells were washed in an additional 10mL volume of DMEM to remove residual serum and subsequently counted via hemocytometer in preparation for assays.

Chemotaxis/Migration Assay

Chemo taxis response was determined as previously described (Fisher et al., 2006) using a modified Boyden chamber (NeuroProbe, Inc., Gaitherburg, MD). Briefly, polycarbonate filters with 8µm pores (NeuroProbe) were pre-coated with 1mg/mL collagen type I in PBS for 24 hours prior to use. In configuring the Boyden chamber, 50µL of DMEM and 1:250 RSII (+) (transferrin, bovine serum albumin, oleic acid, insulin) (Fisher et al., 2006) media was supplemented with recombinant human PDGF-BB (R&D Systems, Minneapolis, MN) and pipetted into the lower chamber wells. Lower chamber wells were then covered with the collagen type I coated polycarbonate membrane. The remainder of the Boyden chamber was assembled and $3x10^4$ cells suspended in DMEM, 1:250 RSII, and 10µg/mL fibronectin added to the upper chamber wells. In some instances inhibitors were added to media for analysis. Cells were allowed to migrate for 4 hours at 37ºC with 5% CO_2 environment. After 4 hours, the Boyden chamber was disassembled and polycarbonate membrane fixed in 3% glutaraldehyde for 10 minutes. Upon fixation, membranes were stained with 0.1% amido black in 30% methanol and 10% acetic acid. Membrane adherent cells were quantified using a Bio-Rad Chemdoc™MP Imager and Quantity One software (Bio-Rad, version 5.2.1 build 11, Hercules, CA). Values were plotted against a previously established standard curve

to determine migrated cell number. Experimental groups were performed in quadruplicate to acquire mean ± standard deviation.

Collagen Invasion Assay

Collagen gels (n=3 gels/condition, 28µL volume) were prepared as previously described (Bayless et al., 2009). Briefly, 3D collagen gels were prepared at a final concentration of 3.75mg/mL in A/2 wells of 96 well plates (Corning). PDGF-BB was incorporated into gels at doses ranging from 0 to 1000ng/mL prior to polymerization and equilibrated at 37ºC and 5% CO_2. After polymerization, 100µL of FBS-free media containing 1:250 dilution of RSII and $2.5x10^5$ MG-63 cells were added to each well. In some instances, inhibitors were added to the culture media as follows: GM6001 (5µM), TAPI-0 (5µM), aprotinin (20KIU/mL), TIMP-1 (5µg/mL), TIMP-3 (5µg/mL), and AG1296 (5µM, 25µM, or 50µM). Cells were allowed to invade for 24-72 hours, at which point conditioned media were collected and gels fixed in 4% paraformaldehyde for 30 minutes. Fixed cultures were stained with 1µM DAPI for 30 minutes and invading cell nuclei counted with an ocular grid at 20x magnification. After invasion quantification, cultures were stained with 0.1% toluidine blue in 30% methanol for 30 minutes and subsequently destained with distilled water. Multiple focal plane microscopy images were acquired at 10x magnification. Afterwards, gels were extracted for sectioning analysis. Extracted gels were sagittally transected for imaging and invasion depth quantification (Cellsens, Olympus, Japan). Invading cell number and depth were recorded and mean ± standard deviation calculated.

MT-MMP Gene Expression

Isolation of RNA and subsequent gene expression evaluation was performed as previously described (Neupane et al., 2008). Total RNA was isolated from MG-63 cells using PureLink™ RNA Mini Kit (Life Technologies, Carlsbad, CA) and treated with DNase to remove contaminating DNA. Complementary DNA (cDNA) was synthesized from 2.5µg of total RNA using random hexamer primers and Superscript III reverse transcriptase (Invitrogen). Primers were commercially synthesized (Sigma-Aldrich) as follows: GAPDH (Kumar et al., 2010) Forward: ACCCACTCCTCCACCTTTG, Reverse: CTCTTGTGCTCTTGCTGGG; MT1-MMP (Primer 3) Forward: CAGAGAAGGCACACAAACGA, Reverse: CACTGGTGAGACAGGCTTGA; MT2-MMP (Primer 3) Forward: CGTGTCCTGCTTTACTGCAA, Reverse: GTCGGGGAAACAGAAACAAA; MT3-MMP (Primer 3) Forward: ATCTTGGCCTTATGCCTCCT, Reverse: CCTCTGGGTTTGAAAGGTCA; MT4-MMP (Primer 3) Forward: GGTGCGTGCACTCATGTACT, Reverse: TCATCGTCAAAGTGGGTGTC. PCR reactions (20µL) were prepared with 2µL of cDNA, 10nM of each primer, and 0.5 units of AmpliTaq Gold® 360 DNA Polymerase (Invitrogen). Cycling conditions were performed with an initial denaturation at 94°C for 5 minutes, followed by 35 cycles of: denature at 94°C for 0.5 minutes, anneal at 55°C for 0.5 minutes, extend at 72°C for 0.5 minutes, and a final extension at 72°C for 7 minutes. Upon completion, PCR products were separated on a 1.2% agarose gel by constant voltage electrophoresis for 60 minutes. PCR products were visualized using Gel

Green (Biotium, Hayward, CA) and images captured using BioRad Chemdoc™MP Imager and ImageLab software (version 5.2.1; Bio-Rad, Hercules, CA).

Transfection with siRNA

siGenome SMARTpool human MMP-1, MMP-2, MT1-MMP, MT2-MMP, and MT3-MMP siRNAs were obtained from General Electric Dharmacon (Lafayette, CO). Target Control #2 was used as a luciferase control. $3x10^5$ MG-63 cells were transfected with siRNA (50nM) in antibiotic-free media using siPORT Amine (Ambion, Naugatuck, CT) and the manufacturer's protocol. After 24 hours, cells were counted and seeded on polymerized collagen type I gels as described above. Protein expression was evaluated via Western blot and gelatin zymography.

Gelatin Zymography and Western Blotting

Conditioned media and cell lysates were collected from invasion assays and analyzed via gelatin zymography or Western blot analysis for protein expression and activation as previously described (Davis and Saunders, 2006; Fisher et al., 2006; Saunders et al., 2005). At the termination of the experiment, conditioned media was removed and gels extracted for lysate preparation. Gelatin zymography was performed with SDS-PAGE gels containing 8.5% acrylamide (Bio-Rad) and 1mg/mL porcine gelatin (Sigma-Aldrich, St. Louis, MO). Gel electrophoreses was performed at 150V for 55 minutes and subsequently incubated with three 20 minute periods in 2% Triton-X (Sigma-Aldrich) in milliQ water. Afterwards gels were washed and incubated overnight in developing buffer consisting of 25mM Tris HCL (Sigma-Aldrich) and 5mM $CaCl_2$ (Sigma-Aldrich). The following morning developing buffer was removed and gels were

stained with 0.1% Amido black in 30% methanol. After 20 minutes gels were destained in 30% methanol and 10% acetic acid in preparation for analysis and photography. Western blotting of cell lysates was performed with 7%, 10%, or 12% SDS-PAGE gels and probed against the following antibodies: MMP1 (Millipore; Billerica, MA), MT1-MMP (Epitomics; Burlingame, CA), MT2-MMP (Santa Cruz, Dallas, TX), MT3-MMP (Santa Cruz), PDGFR-β (Epitomics), PDGFR-α (Epitomics), and beta-actin (Millipore). In some instances, lysates were prepared in the presence of beta mercaptoethanol (BME, Sigma-Aldrich) for Western blot analysis.

Statistical Analysis

Descriptive statistics were generated and presented as mean ± standard deviation for all data. Analytical statistics included ANOVA with Tukey's post-hoc test. All statistics were performed with GraphPad Prism 6.0 (GraphPad Software, La Jolla, CA) Significance was established as $p \leq 0.05$.

RESULTS

PDGF-BB Stimulated Invasion

To determine if MG-63 cells were potentially responsive to PDGF-BB, Western blots were implemented to assess the presence of PDGF receptors α and β. In comparison to other cell types evaluated, MG-63 displayed robust expression of both receptor isoforms (Figure 2.1).

After demonstrating high levels of PDGF receptor expression in MG-63 cells as compared to other normal and neoplastic cells, evaluation of migration and invasion

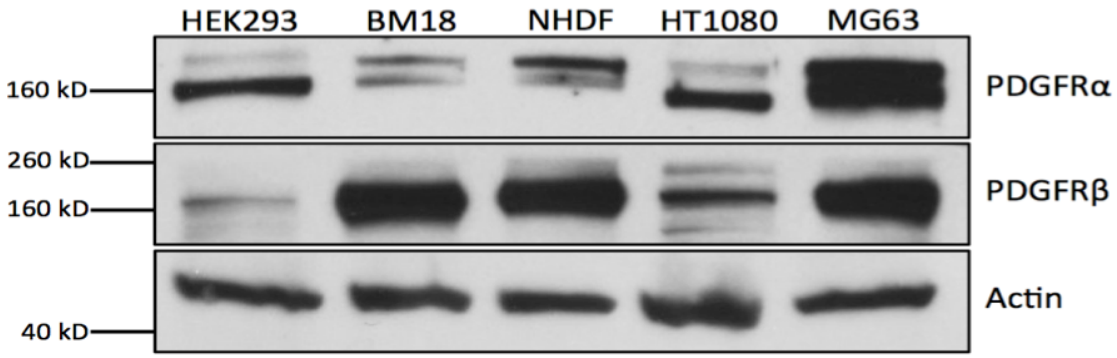

Figure 2.1. *PDGF receptor identification in normal and neoplastic cell types.* Western blot analysis of PDGFR-α and PDGFR-β levels in human embryonic kidney cells (HEK293), human bone marrow cells (BM18), normal human dermal fibroblast cells (NHDF), human fibrosarcoma cells (HT1080), and human osteosarcoma cells (MG-63), demonstrating robust levels of both α and β receptors for PDGF.

response to increasing concentrations of PDGF-BB using a Boyden camber (Figure 2.2) and 3D collagen type I matrices (Figure 2.3). As shown in Figure 2.2, using a modified Boyden chamber, MG-63 cells migrate through the membrane in the presence of PDGF-BB a dose dependent manner exhibiting migration in doses as low as 1 and 10ng/mL. For invasion assays, PDGF-BB was incorporated into collagen gels and assessed at 24- and 48-hours. As shown in representative images (overhead and sagittal) in Figure 2.3A, MG-63 cells invade in response to increasing dosages of PDGF. Inclusion of PDGF-BB resulted in a significant ($p<0.0001$) increase in invasion response in a dose dependent manner. While invading cell number is visually decreased at 24-hours in the 1000ng/mL, robust invasion is observed at the 48-hour time point. Invading cell number was quantified and mean ± SD calculated. Using two-way ANOVA, significant increases in invading cell number ($p<0.0001$) and invasion depth ($p<0.0001$) was observed in response to increasing concentrations of PDGF-BB and time as compared to controls (0 PDGF-BB, 24- vs. 48-hour); however, the 1000ng/mL condition at 24 hours confirm the visual representation of lower numbers of invading cells, Additionally, significant increases in cell invasion number and depth is present in high PDGF-BB dosage conditions when comparing similar PDGF-BB dosage of 24 vs. 48 hours ($p<0.0001$). Interestingly, when evaluating conditioned media and lysates for protein levels using Western blotting and gelatin zymography, increased expression of MMP-1 and activation of MMP-2 was observed, while MT-1 MMP appeared to remain unaffected by increasing doses of PDGF-BB (Figure 2.3C,D). While MMP-1 levels were substantially elevated, protein expression is visible for the latent conformation (52kDa) rather than the

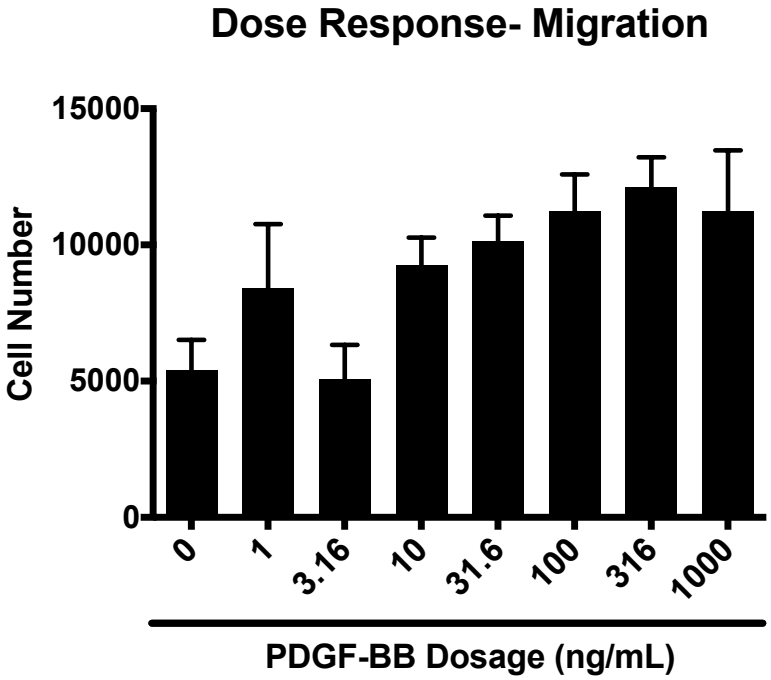

Figure 2.2. *MG-63 cells migrate in response to PDGF-BB.* PDGF-BB was incorporated in the lower wells of the modified Boyden chamber with a collagen coated, polycarbonate membrane overlaying lower wells. After assembly of the Boyden chamber, $3x10^4$ MG-63 cells were added to the upper wells and allowed to migrate for 4 hours. At the duration of 4 hours, the polycarbonate membrane was fixed, stained, and quantified for migrating cells using a predetermined standard curve. Graph represents mean ± standard deviation of migrating MG-63 cells in response to PDGF-BB dosages.

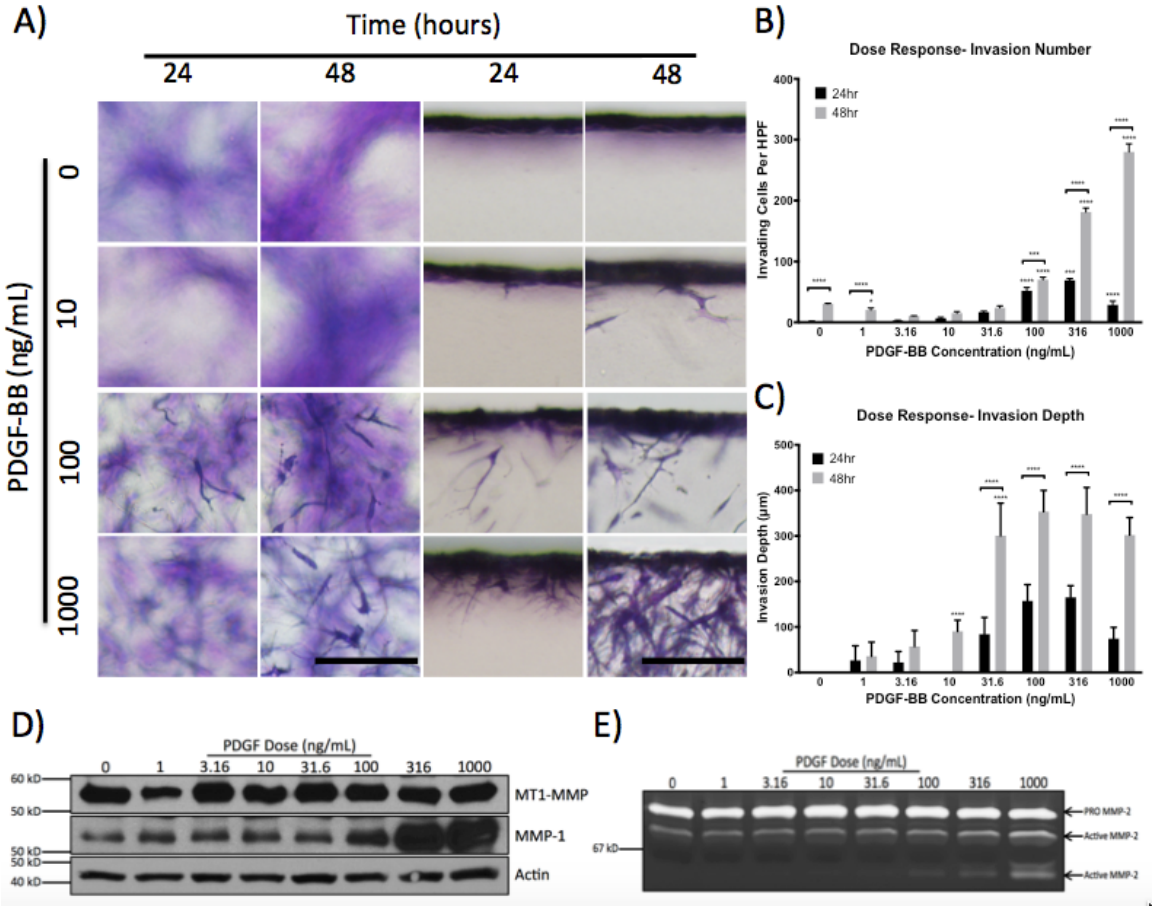

Figure 2.3. *PDGF-BB mediated MG-63 invasion in collagen type I matrices.* Collagen gels were polymerized as described with increasing concentrations of PDGF-BB. MG-63 cells were seeded on monolayer surfaces of gels and allowed to invade for 24 and 48 hours. **A)** Representative 10x overhead and sagittal microscopy images at 24 and 48 hours, demonstrating increased invasion (bar = 100µm) of MG-63 cells in response to PDGF-BB. **B)** Invading cells were manually counted using DAPI staining, fluorescence, and HPF and reported as mean ± SD. Invading cells significantly ($p<0.0001$) increased in a dose-dependent manner. **C)** Invasion depth was determined using data from panel A and reported as mean ± SD. **D)** Western blot analysis of MMP-1, MT1-MMP, and beta-actin, demonstrating corresponding increases in MMP-1 with increased concentration of PDGF-BB. **E)** Gelatin zymography analysis of conditioned media, demonstrating increased conversion of MMP-2 from the pro or latent form to active form with increasing concentrations of PDGF-BB.

active form (42kDa) (Figure 2.3D). On the contrary, gelatin zymography images in Figure 2.3E exhibit MMP-2 conversion from pro-MMP-2 (latent) (72kDa) to the active conformation (63kDA and 52kDa). These results indicate that PDGF-BB stimulates MG-63 cell migration and invasion in a dose-dependent manner Additionally, expression of MMP-1 and activation MMP-2 are increased during invasion.

Time Course Analysis of Invasion in Response to PDGF-BB

Time-dependent invasion in response to PDGF-BB was assessed at predetermined time points of 0-, 12-, 24-, 36-, 48-, and 72-hours. At each time point, conditioned media were collected, cell lysates prepared, and cultures fixed for quantification. Representative images (overhead and sagittal) of a 72-hour time-course of MG-63 cell invasion in response to PDGF-BB is shown in Figure 2.4A. As shown in the images and graphs, invading cell number and depth increased over time (Figure 2.4A,B,C). Using ANOVA and Tukey's correction, significant ($p<0.01$) increases were present in the number of MG-63 cells invading after 36 hours for both PDGF-BB incorporated and non-incorporated gels. While, depth of invasion was significantly increased over time ($p<0.0001$) in response to PDGF-BB, non-PDGF-BB containing wells did not display statistical differences. When comparing PDGF-BB treated and non-PDGF-BB treated conditions, significant increased invasion number ($p<0.0001$) and depth ($p<0.0001$) were present with increased time. Interestingly when evaluating conditioned media and lysates for MMP-1, MT1-MMP, and MMP-2 using Western blotting and gelatin zymography, increased expression was observed regardless of PDGF-BB treatment (Figure 2.4D,E). While MMP-1 remained in its latent conformation

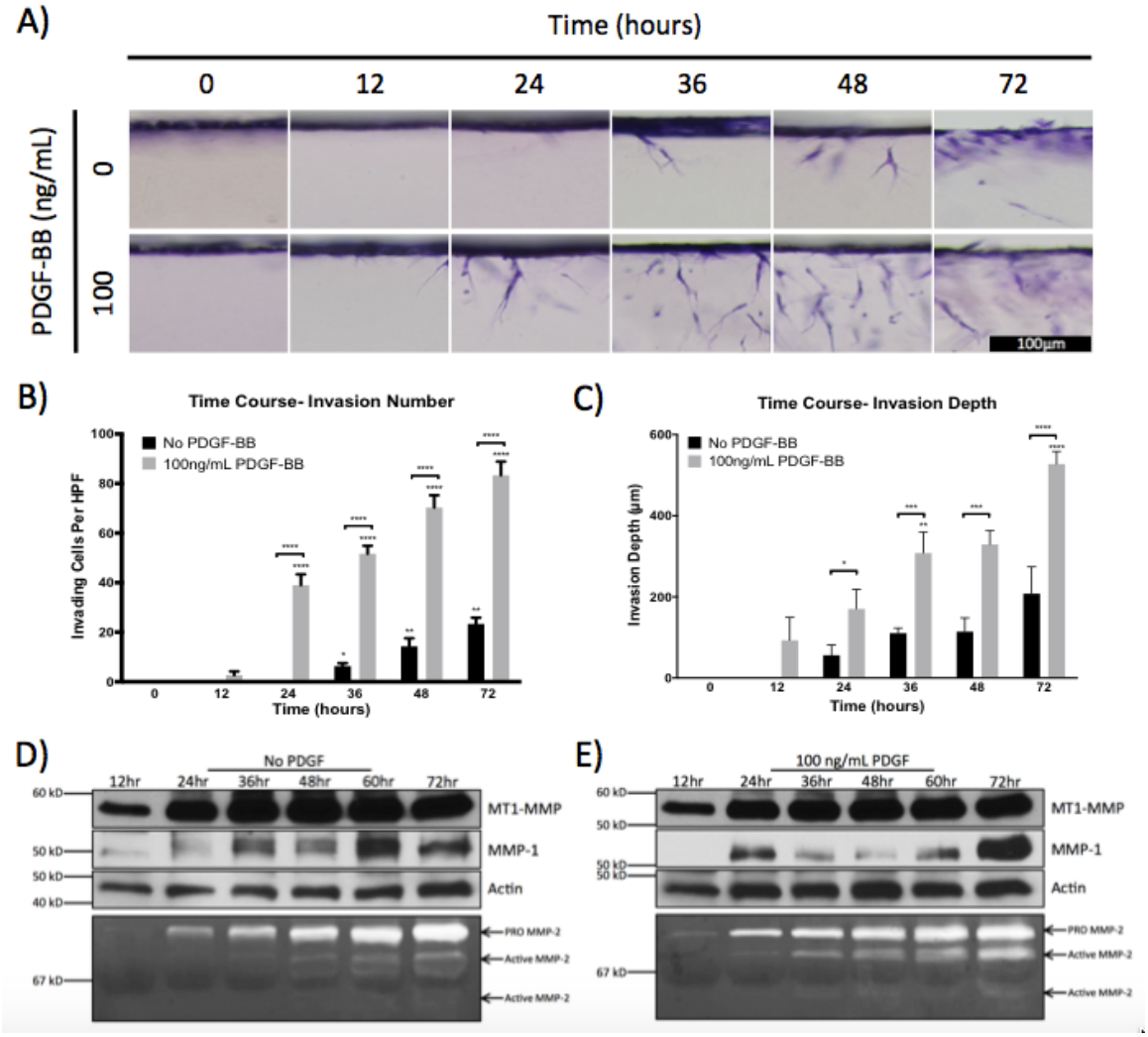

Figure 2.4. *Time course analysis of MG-63 invasion in response to PDGF-BB.* Collagen gels were polymerized as described with 100ng/mL PDGF-BB. MG-63 cells were seeded on monolayer surfaces of gels and allowed to invade for 0, 12, 24, 36, 48, or 72 hours. At each predetermined time point conditioned media were collected, gels fixed 4% paraformaldehyde, quantified, and photographed. **A)** Representative 10x microscopy images of invading MG-63 cells at each predetermined time point. **B)** Invading cells were manually counted using DAPI staining, fluorescence, and HPF and reported as mean ± SD. Invading cells significantly ($p<0.0001$) increased in a time-dependent manner. **C)** Invasion depth was determined using data from panel A and reported as mean ± SD. **D)** Western blot analysis, demonstrating MMP-1 and MT1-MMP levels. Gelatin zymography analysis of conditioned media, demonstrating increased.

(52ka), MMP-2 was detected in both its respective pro- (latent) and active states (63kDa and 52kDa). When comparing MMP-2 activation levels in the presence of PDGF-BB, conversion of pro-MMP-2 to its active state was visibly increased in the presence of PDGF-BB (Figure 2.4E). Although, MMP-1 and MMP-2 subjectively display robust increases in protein expression, MT-1 MMP expression was remained consistent (Figure 2.4E). These results indicate that PDGF-BB stimulates MG-63 cell invasion and that expression of MMP-1 (latent) and MT1-MMP increase over time regardless of PDGF-BB treatment. Additionally, pro-MMP-2 is converted from its pro- to active conformation with in the presence of PDGF-BB and increased time.

Effect of a Tyrosine Kinase Receptor Inhibitor on MG-63 Invasion

To evaluate the role of PDGF receptor signaling on the MG-63 invasion response, signaling was inhibited through the use of a known PDGF receptor tyrosine kinase inhibitor, AG1296. AG1296 has previously been shown to competitively inhibit autophosphorylation sites of PDGF receptor tyrosine kinase domains Try857 and Try751 (Kovalenko et al., 1997). In a dose-dependent manner (5μM, 25μM, 50μM), significant reduction ($p<0.0001$) of invasion at both 24- and 48-hours was observed when MG-63 cells were induced to invade in response to PDGF-BB in the presence of increasing concentrations of AG1296. As shown in Figure 2.5A, representative (overhead and sagittal) images demonstrate reduced invasion response in the presence of increasing concentrations of AG1296. Quantification of invading cell number (Figure 2.5B) in the presence of AG1296 demonstrated a significant decrease in the number of invading cells ($p<0.0001$) as compared to invasion control (PDGF-BB) and inhibitor carrier (DMSO)

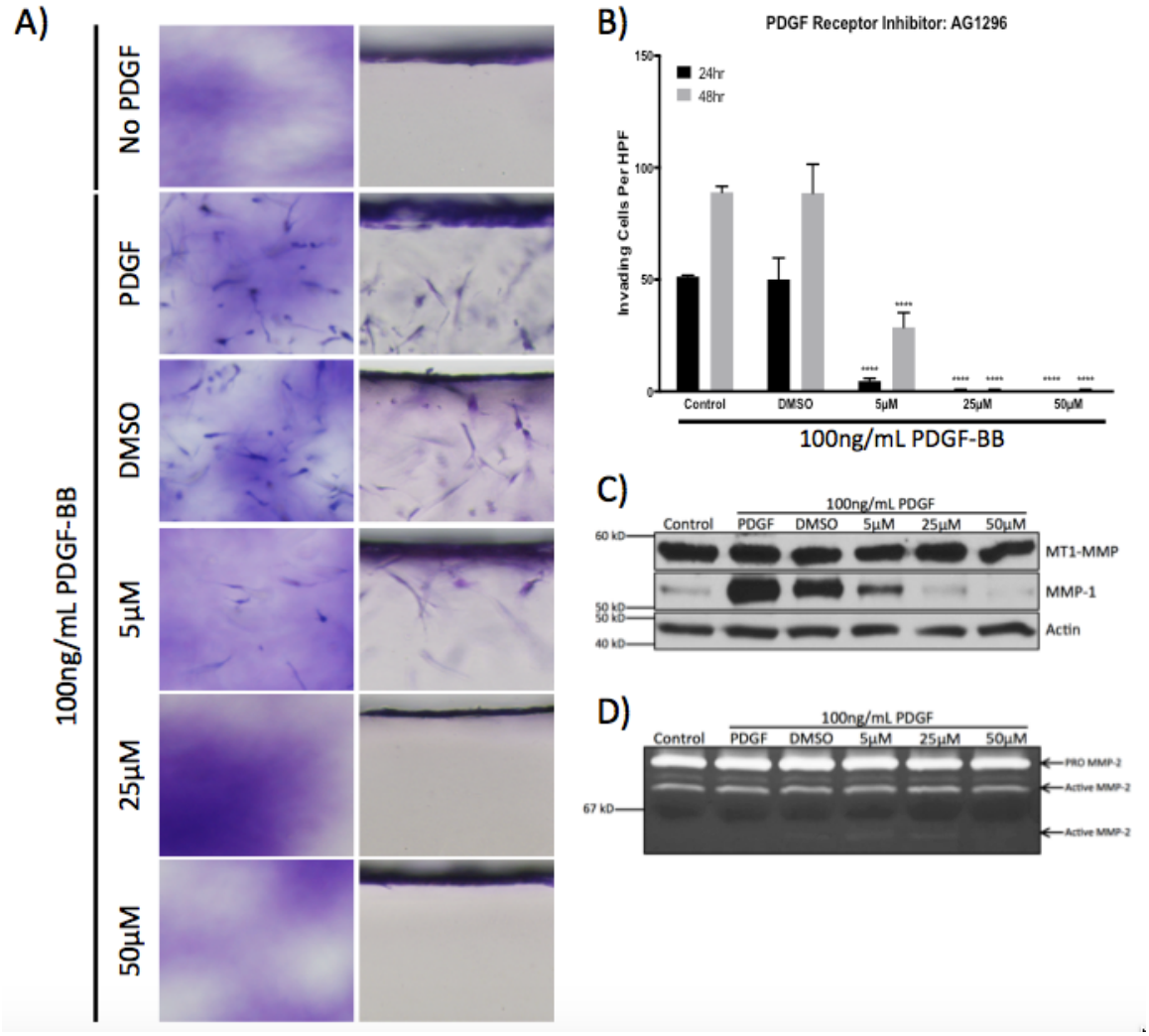

Figure 2.5. *Effect of PDGF receptor tyrosine kinase inhibitor on MG-63 cell invasion of collagen type I matrices.* Tyrosine kinase inhibitor, AG1296, was added to cultures to determine the correlation between PDGF-BB and MG-63 invasion. MG-63 cells were seeded on monolayer surfaces of gels containing 100ng/mL of PDGF-BB and allowed to invade for 24 or 48 hours prior to collection of culture media, fixation, quantification, and photography. **A)** Representative 10x overhead and sagittal microscopy images, demonstrating decreased invasion to relation to increasing concentrations of AG1296. **B)** Invading cell number was quantified and reported as mean ± SD. Invading cell number significantly ($p<0.0001$) decreased compared to PDGF-BB control and carrier (DMSO) conditions. **C)** Western blot analysis exhibiting decreased levels of MMP-1 as concentration of AG196 increases. **D)** Gelatin zymography analysis MMP-2 activation in conditioned media. Interestingly, no visual effect of MMP-2 activation is observed with increasing concentrations of AG1296.

wells. Interestingly, AG1296 inhibition decreased invading cell number to the level recorded for control wells lacking PDGF-BB (data not shown). As previously described, conditioned media and lysates from experiments in Figure 2.5A were evaluated with Western blot and gelatin zymography to analyze MMP-1, MMP-2, and MT1-MMP expression. AG1296 had limited to no effect on MT1-MMP levels (Figure 2.5C) or MMP-2 activation as both pro- and active forms are present (Figure 2.5D). These results notwithstanding, decreased MMP-1 protein levels were observed with increasing concentration of AG1296 (Figure 2.5C), suggesting that tyrosine kinase signaling is responsible increased MMP-1 expression that occurs upon exposure to PDGF-BB.

MT-MMPs are Required for Invasion of 3D Collagen Type I Matrices

Previous studies have shown the requirement of MMPs for cell-mediated invasion of 3D collagen matrices (Bayless and Davis, 2003; Fisher et al., 2006; Wolf et al., 2013). To evaluate the role of various classes of MMPs during MG-63 invasion of 3D collagen type I gels, MG-63 cells were induced to invade 3D collagen matrices containing PDGF-BB in the presence of several proteinase inhibitors. GM6001, TAPI-O, aprotinin, TIMP-1, and TIMP-3, were added to culture media in a step-wise process to determine the class/group of MMPs involved in MG-63 invasion. Representative images of cellular invasion (overhead and sagittal) are shown in Figure 2.6A. Invasion of MG-63 cells was completely inhibited in the presence of the broad-spectrum chemical MMP inhibitors GM6001 and TAPI-O ($p<0.0001$). Additionally, biologic MMP inhibitor TIMP-3, capable of inhibiting soluble and membrane-type MMPs, significantly inhibited invasion ($p<0.0001$). These results indicate that MMPs are required for MG-63 invasion

of collagen type I. To further elucidate the specific role of soluble versus membrane-type MMPs during MG-63 invasion, MG-63 cells were induced to invade in the presence of TIMP-1, a biologic inhibitor specific soluble MMPs. In contrast to GM6001 and TAPI-O, MG-63 cells were capable of invading in the presence of TIMP-1, although the invasion was slightly reduced as compared to PDGF-BB carrier control wells ($p<0.01$) (Figure 2.6B). However, when comparing invasion response in the presence of TIMP-3 and TIMP-1, there was a significant increase in invasion in the presence of TIMP-1 ($p<0.0001$). In addition, there was a significant decrease in invasion ($p<0.0001$) for MG-63 cells cultured in the presence of TIMP-3 when compared to PDGF-BB carrier control wells (Figure 2.6B). These results indicate that MT-MMPs are likely the required group of MMPs for MG-63 invasion of 3D collagen type I matrices.

Conditioned media and lysates were collected from experiments in Figure 2.6A and analyzed as described above. Using Western blot and gelatin zymography analyses, MMP-1, MMP-2, and MT1-MMP were expressed by MG-63s in culture (Figure 2.6C,D). As seen in previous figures (2.3-2.5), latent MMP-1 expression is increased in response to PDGF-BB (Figure 2.6C). Additionally, pro-MMP-2 is converted to an active conformation (Figure 2.6D). Interestingly, MMP-2 conversion to an activate state was visually decreased or absent in GM6001, TAPI-O, and TIMP-3 treatments, as noted by the absence of lower molecular weight bands (63kDa). However, MMP-2 activation was unaffected by the addition of TIMP-1. These results are of particular interest due to the known interaction between MMP-2 and MT1-MMP/TIMP-2 complex at the cell surface

Figure 2.6. *MT-MMPs are required for MG-63 invasion of 3D collagen type I matrices.* Collagen gels were polymerized with 100ng/mL PDGF-BB as previously described. MG-63 cells were seeded on monolayer surfaces of gels and allowed to invade for in the presence of the following proteinase inhibitors: no stimulus (Control), no inhibitor (PDGF-BB, positive control), DMSO (carrier control), 5μM GM6001, 5μM TAPI-O, 20KIU/mL aprotinin, 5μg/mL TIMP-1, or 5μg/mL TIMP-3. **A)** Representative 10x microscopy images after 48 hours, demonstration GM6001, TAPI-O, but not TIMP-1, suggesting that MT-MMPs are required for MG-63 invasion. **B)** Invading cells per HPF was quantified and reported as mean ± SD., demonstrating significant reduction ($p<0.0001$) of invading cell number when compared to DMSO (carrier control) wells. **C)** Western blot analysis displaying reduced MMP-1 expression in GM6001 and TAPI-O wells, while TIMP-1 and TIMP-3 had no effect on MMP-1 levels. **D)** Gelatin zymography assessment of MMP-2 expression and activation. Interestingly, MMP-2 activation was blocked by GM6001 and TAPI-O, reduced by TIMP-3, and remained unaffected by TIMP-1.

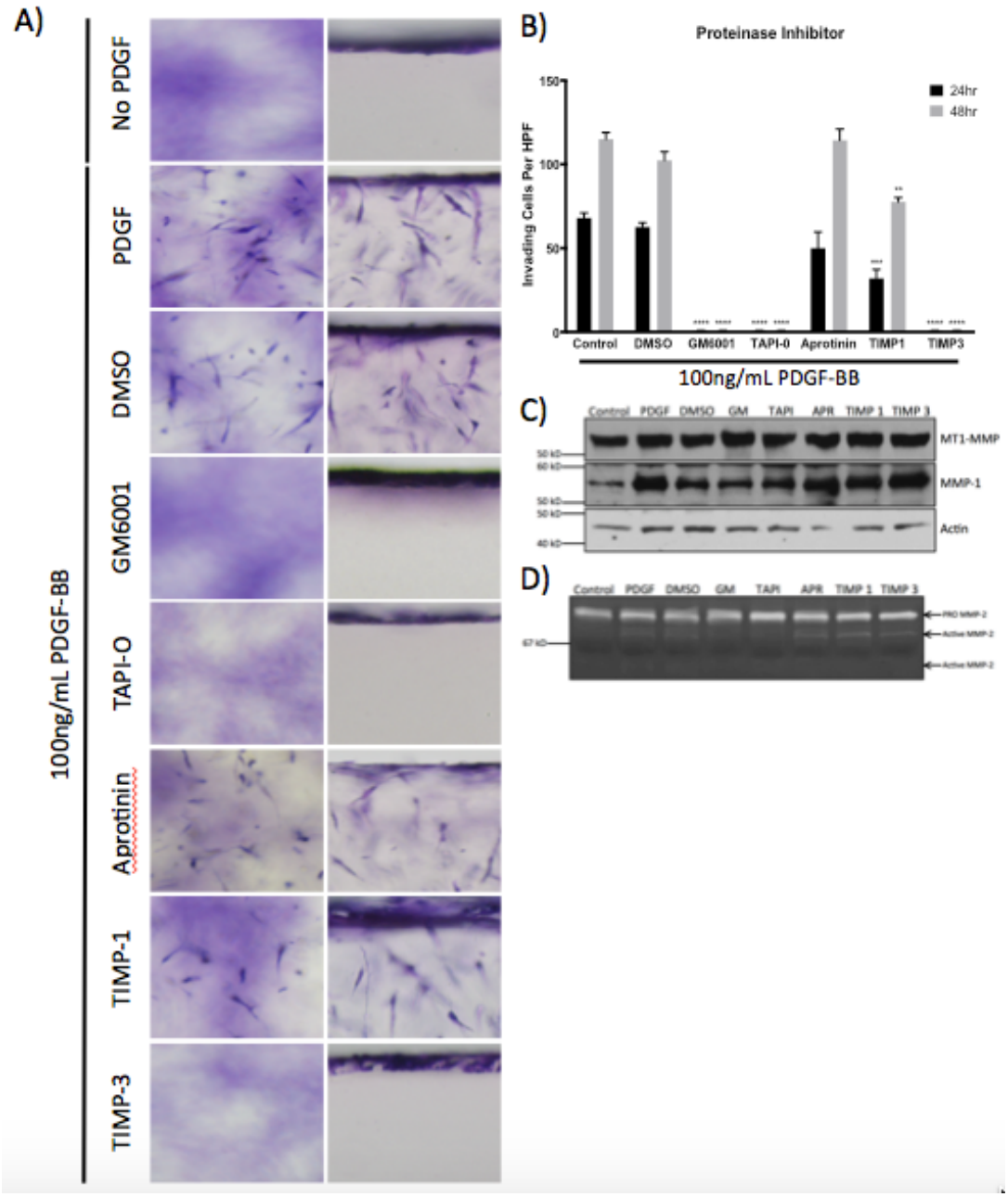
A)
No PDGF
PDGF
DMSO
GM6001
TAPI-O
Aprotinin
TIMP-1
TIMP-3
100ng/mL PDGF-BB
B)
Proteinase Inhibitor
24hr
48hr
Invading Cells Per HPF
150
100
50
0
Control
DMSO
GM6001
TAPI-0
Aprotinin
TIMP1
TIMP3
100ng/mL PDGF-BB
C)
Control
PDGF
DMSO
GM
TAPI
APR
TIMP 1
TIMP 3
MT1-MMP
MMP-1
Actin
D)
Control
PDGF
DMSO
GM
TAPI
APR
TIMP 1
TIMP 3

Figure 2.7. *MT-MMP gene expression in MG-63 cells.* MG-63 cells were qualitatively evaluated for MT-1, 2, 3, and 4-MMP using RT-PCR. MT-1, 2, and 3-MMP were positive when assessed using RT-PCR. Representative images of MT1 (172bp), MT2 (245bp), MT3 (250bp), and MT4 (216bp) gene expression demonstrating the absence of MT4-MMP.

(Sato et al., 1996). Through this triad, MMP-2 is activated by MT1-MMP, as such MMP-2 levels are often used as an indirect readout of MT1-MMP activity.

PDGF-BB Mediated Invasion of MG-63 Cells Requires MT1-MMP

Based on the results described in Figure 2.6, several MT-MMPs known to be involved in pericellular proteolysis and invasion were evaluated. MG-63 cells were evaluated for the presence of MT-1, -2, -3, and -4-MMP RNA using reverse transcription PCR. MG-63 cells were positive for MT-MMP 1, 2, and 3 transcripts, but negative for MT4-MMP (Figure 2.7). Based on these data, commercially available siRNAs for MT1, 2, and 3-MMP were acquired (Figure 2.8). Representative images (overhead and sagittal) of invading MG-63 cells transfected with the various siRNAs are shown in Figure 2.8A. There was a marked decrease in the number of invading cells in MG-63 cells treated with MT1-MMP siRNA, whereas invasion was unaffected by treatment with MT-2 or MT3-MMP. Moreover, quantification (mean ± SD) of Figure 2.8A confirms that significant differences in the number of invading cells ($p<0.0001$) were present when comparing MT1-MMP siRNA transfected cells to PDGF-BB control wells (Figure 2.8B). Protein expression confirmed knockdown of respective proteins (Figure 2.8C). These results indicate that MT1-MMP is required for PDGF-BB mediated invasion of 3D collagen matrices by MG-63 cells.

DISCUSSION

OSA is highly metastatic and pulmonary metastases are the most common cause of morbidity. The mechanism(s) by which OSA cells invade surrounding stroma and

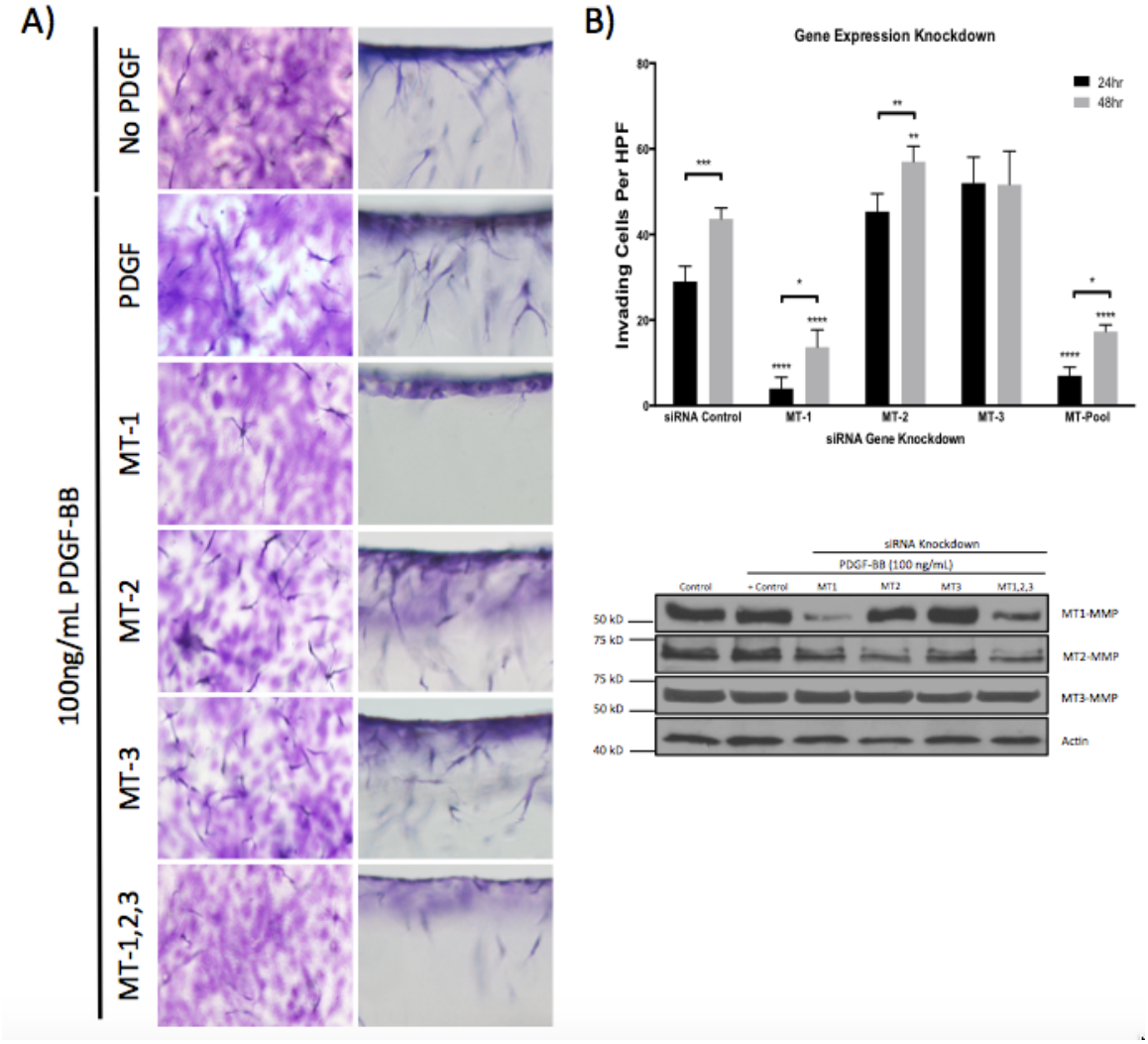

Figure 2.8. *PDGF-BB mediated MG-63 invasion of collagen type I requires MT1-MMP.* Knockdown of protein expression by siRNA was used to determine the specific MT-MMP responsible for MG-63 cells invasion in response to 100ng/mL PDGF-BB. MG-63 cells were siRNA transfected and subsequently seeded on monolayer surfaces of gels. Invasion response was evaluated at 24 or 48 hours. **A)** Representative 10x overhead and sagittal images display decreased invasion to no PDGF-BB (control) in MT1-MMP and MT-1, 2, 3 (MT-pool) wells, but not MT2- or MT3-MMP alone. **B)** Invading cells per HPF were quantified and reported as mean ± SD, demonstrating significant reduction ($p<0.0001$) in invading cell number in siMT1-MMP wells when compared to no-PDGF-BB control wells. **C)** Western blots expression confirms knockdown of MT-MMP protein levels.

eventually metastasize has yet to be fully elucidated. When prompted, cells must prove to be motile and proteolytic in traversing the extra cellular matrix, specifically collagen type I (Hotary et al., 2000; Murphy and Knäuper, 1997; Werb, 1997). It is thought that MMPs play a significant role in these functions. Although MMPs are often categorized based on either location or functionality (substrate specificity), a number of MMPs are thought to be involved in invasion. Previous literature has described soluble MMPs, such as MMP-1 (Colandrea et al., 2000), MMP-2 (Masson et al., 2005), and MMP-9 (Klein et al., 2004), invasion capabilities. However, other studies have focused on membrane-type MMPs' ability to promote invasion (Hotary et al., 2000; Sabeh et al., 2009). It has been previously shown that PDGF-BB plays an important role during many physiological and pathological processes, such as angiogenesis, wound healing, tumor growth, or metastasis, through both its mitogenic and chemotactic effects. The ability to express, secrete, and respond to PDGF is critical in development and biological processes for cell growth, function, and maintenance of the pericellular environment. In addition to developmental influence, PDGF has been shown to play a role in wound healing and fracture repair through PDGF-BB stimulated recruitment of pericytes (Caplan and Correa, 2011). PDGF-BB has also been linked to fibrosis, atherosclerosis, tumor growth, and metastasis. In addition, PDGF levels were elevated in a significant proportion of extensive metastatic breast cancers and osteosarcoma cell lines (Ariad et al., 1991; Takagi et al., 2014).

While previous studies have examined OSA cell lines MG-63, U2OS, SaOS, OHS, HOS, SaOS, and KPDX our accessibility and preliminary data (data not shown)

demonstrated a propensity of MG-63 to actively invade collagen type I matrices. In addition, previous studies have examined PDGF signal transduction and subsequent cellular response of MG-63 cells (Graves et al., 1984; Takagi et al., 2014; Thomas et al., 1997), but to the authors' knowledge 3D assays detailing proteolytic events of the extra cellular matrix in response to PDGF-BB have not been performed. Given the unique properties of PDGF-BB, the objective of this study was to examine invasion of human osteosarcoma MG-63 cells in 3D collagen type I matrices via MMP proteolysis in response to PDGF-BB. We hypothesized that PDGF-BB would stimulate MG-63 cells to invade 3D collagen matrices in an MT-MMP dependent manner, while soluble MMPs would be less important to these events.

The known role of PDGF-BB and its receptors in cell proliferation and invasion events, in addition to the strong support in the literature for the concept that MT-MMPs are required for focal ECM proteolysis during invasion, have led our laboratory to evaluate the role of PDGF-BB and MMPs, more specifically MT-MMPs, in invasion. Our results demonstrate both a significant time- and dose-dependent invasion of MG-63 human osteosarcoma cells in response to PDGF-BB. Furthermore, this process of invasion was dependent on PDGF receptor signaling and MT1-MMP. Therefore, based on the data presented herein we fail to reject our hypothesis that PDGF-BB would stimulate MG-63 cells to invade 3D collagen matrices in an MT-MMP dependent manner, while soluble MMPs would be less important to these events.

The MG-63 cell line in this study were passaged and expanded on traditional 2D tissue culture plastic for use in a serum-free 3D collagen type I invasion assay. Prior to

seeding, PDGF-BB was incorporated into collagen type I gels. Assessment of both dose- and time-dependent invasion exhibited significant increases in number and depth of invading cells. Interestingly, when assessing MMP levels of the dose response assay, MT1-MMP remains visually consistent with no increase or decrease in expression with increasing PDGF-BB concentrations. One explanation for the increased invasion may be the localization of MT1-MMP to the filapodia/lamelipodia processes in focal degradation of collagen type I matrices in response to PDGF. In contrast to MT1-MMP, MMP-1 expression levels increased in response to increasing concentrations of PDGF-BB. This increased protein expression may be the result of PDGF-BB activation of signaling cascades leading to transcription and expression of multiple genes with MMP-1 being one of the products. Previous studies have implicated phosphoinositide 3-kinase (PI3K) (Cheng et al., 2006), JAK-STAT (Andl, 2004), and C-terminal Src kinase (c-Src) (Leaner et al., 2010) pathways in tumorigenesis and increased MMP transcription. The PI3K pathway is activated by PDGF inducing arrangement of the Rho and Ras complexes (Auger et al., 1989; Coughlin et al., 1989; Kazlauskas et al., 1992) directing downstream cytoskeletal rearrangements (Kazlauskas et al., 1992). Furthermore, PI3K phosphorylates AKT initiating a cascade through IκB kinase (IKK) complex, a regulator for NF-κβ (Israel, 2010). Significantly, NF-κβ is known to be involved in gene transcription of MMPs (Bond et al., 1998; Vincenti and Brinckerhoff, 2002). Similar to PI3K, c-Src is implicated in AKT pathway activation for cell survival and gene transcription related to tumorigenesis and metastasis (Leaner et al., 2010). Lastly, Fossey et al, described activation of signal transducer and activator of transcription-3 (STAT3)

through the JAK-STAT pathway, leading to upregulation of gene transcription of MMPs (Fossey et al., 2009). These previous studies corroborate the data presented herein, in which MMP-1 expression is observed in the presence of PDGF-BB. While these signaling events directly link PDGF receptor-signaling to MMP gene transcription, further studies are needed to elucidate the specific pathway responsible for increased expression.

When evaluating potential signaling axis responsible for PDGF-BB and gene transcription/up-regulation we targeted the PDGF receptor tyrosine kinase using a synthetic inhibitor AG1296. In 1997, Kovalenko et al. suggested the role of AG1296 as a secondary inhibitor by allowing receptor tyrosine kinase to preferentially bind PDGF-BB and allow subsequent dimerization, but abolish the signaling cascade by competing with auto phosphorylation sites, Y857 and Y751 (Kovalenko et al., 1997). Thus, extinguishing the perpetuation of intra-cell signaling in response to ligand-receptor binding. Therefore, the addition of the PDGF receptor tyrosine kinase inhibitor AG1296 was of extreme interest. There was a significant reduction in MG-63 cell invasion when cultured in the presence of both PDGF-BB and increasing doses of AG1296. Moreover, when cultured in lower doses (5μM) of AG1296, limited invasion was still present while increasing concentrations (25μM and 50μM) of AG1296 eliminated invasion altogether. While AG1296 has a high specificity to PDGF receptor signaling inhibition, one limitation in is the ability of AG1296 to also inhibit fibroblast growth factor receptor (FGFR) at increased concentrations (12-18μM). Although other studies suggest alternate platelet-dependent signaling pathways, such as insulin-like growth factor-1 (IGF-1)

(Raile et al., 2003); data presented herein support that MG-63 invasion is driven at least in part by PDGF-BB.

Although previous studies described above discuss up regulation of MMP levels in response to PDGF, the specific MMPs implicated in invasion were not evaluated. To further our understanding, we explored the role of MMP-dependent proteolysis in invasion. In the presence of synthetic (GM6001 and TAPI-O) and biologic (TIMP-3) inhibitors of soluble and membrane-type MMPs, MG-63 cell invasion was completely absent (Figure 2.6A). These results indicate that MMPs are required for MG-63 cell invasion of 3D collagen type I gels. Moreover, inhibition of invasion by TIMP-3 (capable of inhibiting soluble and membrane-bound MMPs), but not TIMP-1 (inhibits soluble MMPs alone) suggests that MT-MMPs are required for MG-63 cell invasion. Interestingly, MMP-2 activation was blocked by GM6001 and TAPI-0, reduced by TIMP-3 and remained unaffected by TIMP-1. These findings are not surprising given that MMP-2 has shown to be activated by MT1-MMP/TIMP-2 complex on the cell surface (Sato et al., 1996).

Given the proteolytic response of MT1-MMP, increased expression of MMP-2 is not surprising. As described by Sato in 1996, through indirect activation, MT1-MMP conformationally activates MMP-2, using TIMP-2 as an intermediary binding structure (Sato et al., 1996). Briefly, MT1-MMP binds the N-terminus of TIMP-2 allowing MMP-2 to bind the C-terminal. Subsequently, an adjacent MT1-MMP activates MMP-2 to proMMP-2 while another MMP-2 enzyme removes the propeptide region creating a

fully activated/mature MMP-2 (Sato et al., 1996). The known relationship of this triad explains the increased activation levels of MMP-2 in our results.

While invasion was blocked in the presence of synthetic and biologic MT-MMP inhibitors, transcriptional blockade via siRNA was used to demonstrate the key influence of MT1-MMP in invasion. These findings were not surprising considering previous literature has shown invasion of other cell types is not dependent on MT2- and MT3-MMP (Hotary et al., 2000; Shimada et al., 1999). In addition, these findings were further corroborated when examining those of Bjornland et al., in which MT1-MMP was present in multiple osteosarcoma cells from both human and veterinary species (Bjørnland et al., 2005). Collectively, previous studies in combination findings presented above demonstrate the importance of MT1-MMP in MG-63 invasion of collagen type I matrices. While decreased invasion was present in MT1-MMP siRNA transfected wells was observed, invasion decrease was not equal to that of the robust inhibition seen in GM6001, TAPI-0, and TIMP-3 conditions (Figure 2.6). One explanation to limited invasion is that MT1-MMP is not genetically eliminated from the cellular transcript and thus residual protein would still be found in the cells even after siRNA blockade. Furthermore, whereas secreted MMPs are normally released as inactive zymogens, MT1-MMP is active before cell surface localization (Pei and Weiss, 1995; Sato et al., 1996; Yana and Weiss, 2000). Another alternative explanation to baseline MG-63 cell invasion may be the role of uninvestigated MT-MMPs or adamalysins-related membrane proteins (ADAMs) not addressed in this study. Additional studies are needed to identify and address the role of complementary molecules and their influence in MG-63 invasion.

Results presented herein demonstrate that PDGF-BB stimulates MT1-MMP-dependent MG-63 cell invasion, and thus, is critical in matrix proteolysis for tumor cell invasion. One question that remains to be answered is: how PDGF-BB stimulates intra-cellular pathways for gene transcription, in addition enabling MT1-MMP-dependent invasion. Further detailing of signaling mechanisms and key molecular proteins involved in localizing MT1-MMP to invasion sites will improve the understanding of how MG-63 and other neoplastic cell types invade their micro-stroma and eventually metastasize.

In conclusion, we elucidate an invasion response of human osteosarcoma MG-63 cells to PDGF-BB by way of MT1-MMP proteolysis of collagen type I. These results detail the importance of MT1-MMP in tumor cell proteolysis for motility and invasion. Interestingly, PDGF tyrosine kinase inhibitor, AG1296, neutralized MG-63 cell invasion in the presence of PDGF-BB. Moreover, given the significant reduction in invasion of MG-63 after reduction of MT1-MMP via siRNA, addition of TIMP-3, and addition of the PDGF-receptor tyrosine kinase inhibitors, each of these molecules/methods may be useful for investigators interested in reducing invasion of MG-63 cells, and possibly other osteosarcoma cells. Our results provide insight into important cellular events and will prove useful for both investigators and clinicians considering translational treatment strategies of osteosarcoma.

CHAPTER III

CHARACTERIZATION OF CANINE MULTIPOTENT STROMAL CELLS ISOLATED FROM SYNOVIUM, BONE MARROW, OR ADIPOSE TISSUE: A SUBJECT-MATCHED COMPARISON USING ASSAYS OPTIMIZED FOR THE DOG

SUMMARY

The dog represents an excellent large animal model for translational regenerative medicine studies; however, the ideal source of cMSCs for specific applications remains to be determined. The objective of this study was to comprehensively characterize cMSCs from bone marrow, adipose, and synovium using assays optimized for the dog. Tissues were isolated from five client owned dogs with cranial cruciate ligament rupture. All tissues produced plastic adherent, spindle shaped MSCs. Each cell preparation was assessed for MSC criteria using flow cytometry, colony forming unit (CFU) potential, tri-lineage differentiation, and immunomodulation assays. These cells were negative for CD 34, 45, STRO-1 and positive for CD 9, 44, 90. CD105 staining was variable across all cell preparations. There were significant differences between cMSCs as assessed by growth parameters, CFU potential, tri-lineage differentiation, and immunomodulatory response when comparing donor and tissue source. Synovial and marrow cMSCs exhibited superior short-term osteogenic activity, but when assessing long-term osteogenesis no significant differences were present. Additionally, synovial and adipose cMSCs proliferated more rapidly, displayed higher CFU potential, and formed larger chondrogenic pellets, although proteoglycan and collagen II staining was decreased when compared to marrow pellets. Lastly, all cMSCs reduced the concentration of

murine tumor necrosis factor alpha (TNF-α) in LPS-stimulated mouse macrophage co-culture assays, a novel finding for canine MSCs. As described in humans, we conclude that significant differences in cMSCs exist due to both tissue source and individual donor variability. Our findings and optimized methods will prove useful for future tissue engineering studies using the canine model.

INTRODUCTION

Translation of promising findings from rodent models to humans represents a significant hurdle for cell-based therapies. A number of large animal species have been used to bridge the gap from rodents to humans (Hatsushika et al., 2014; Horie et al., 2009; Horie et al., 2012b; Kon et al., 2000; Murphy et al., 2003). The dog is a compelling model species for these types of cell-based translational studies. When compared to rodents, dogs are large, long-lived, genetically diverse, and share many biochemical and physiological similarities with humans. Canine models have been used successfully for adult bone marrow transplantation, gene therapy, and development of protocols to overcome allograft rejection (Prentice et al., 1984; Socie and Blazar, 2009; Storb et al., 1970). Due to their response to learned behaviors such as treadmill exercise, dogs have been used to develop new therapies for cardiovascular and orthopedic diseases (Bockstahler et al., 2007; Kiviranta et al., 1988). From a biomechanical perspective, the canine skeleton undergoes loading in a manner that approximates that of the human skeleton (Bergmann et al., 1984; Liebschner, 2004). For these reasons, canine models of osteoarthritis, anterior cruciate ligament repair, meniscal injury, and non-

union fractures are well described (Arnoczky et al., 2010; Johnson et al., 1989; Liu et al., 2006; Nelson et al., 1988; Pond and Nuki, 1973; Shortkroff et al., 1996). Additionally, humans often consider dogs as in-home pets. Cohabitation exposes both humans and canines to similar environmental stimuli, helping to eliminate distinguishing variables between species (Fenger et al., 2014). For many of these reasons, the occurrence of adverse events in canine clinical trials appears to more reliably predict adverse events in humans. As such, performing clinical trials in dogs may allow investigators to more effectively identify and predict the benefits or unforeseen obstacles in humans.

MSCs hold much promise as therapeutic agents for many debilitating diseases. In addition to contributing to tissue and organ repair by homing, differentiation, and engraftment, MSCs are believed to improve tissue repair through production of growth factors, anti-inflammatory cytokines, direct modulation of the immune system, and anti-apoptosis effects (Augello et al., 2010). MSCs are most commonly isolated from bone marrow and adipose tissue (Neupane et al., 2008; Owen and Friedenstein, 1988; Peng et al., 2008; Sakaguchi et al., 2005; Takemitsu et al., 2012; Zuk et al., 2002). Recent literature has described the isolation of MSCs from synovium (De Bari et al., 2001), skeletal muscle (Kisiel et al., 2012), periosteum (De Bari et al., 2006) and dental pulp (Pierdomenico et al., 2005). While MSCs isolated from these diverse tissues meet established criteria for MSCs (Dominici et al., 2006), cell proliferation and differentiation vary widely when assessed by established in vitro assays. These differences may have important implications as investigators consider both the tissue source of MSCs as well as the model species for novel cell-based translational studies.

Although a robust foundation of literature exists describing synovium, bone marrow, and adipose-derived MSCs in humans, rodents, and other species (Arnhold et al., 2007; Niemeyer et al., 2010; Nishimura et al., 1999; Phinney, 2008; Stewart and Stewart, 2011; Vidal et al., 2007), a relatively modest number of reports exist describing he isolation and differentiation of cMSCs from these tissues (Kadiyala et al., 1997; Kisiel et al., 2012; Neupane et al., 2008; Volk et al., 2005; Volk et al., 2012). Drawing distinctions between the cMSCs isolated in these studies is difficult due to donor variation and differences in the isolation and culture techniques utilized by individual laboratories. Thus, a comprehensive report describing the characteristics of donor-matched cMSCs isolated from canine synovium, bone marrow, and adipose tissue is of utmost importance in order to facilitate the selection of cMSC for cell-based translational studies.

The objective of this study was to comprehensively characterize canine MSCs isolated from synovium, bone marrow, and adipose tissue using a donor-matched study and assays optimized for the canine species. Based on work in other species, we hypothesized that canine MSCs isolated from synovium, bone marrow, and adipose tissues would exhibit significant differences in isolation parameters, growth kinetics, CFU potential, flow cytometry profiles, tri-lineage differentiation, and immunomodulatory potential. As seen in other species, results detailed herein demonstrate variability in donor and tissue source when comparing the aforementioned characteristics. Our results provide insight into important similarities and differences

between cMSCs and will prove useful for investigators considering cMSCs for large animal translational studies.

MATERIALS AND METHODS

Tissue Collection and Cell Isolation

This study was performed under the supervision of the institutional animal care and use committee (IACUC) and an approved animal use protocol (AUP 2011-149). Canine synovium, bone marrow, and adipose tissues were obtained from four-castrated male and one spayed female dogs during knee arthroscopy for cranial cruciate ligament rupture. Median age was three years (range 2 to 6) with a median body weight of 39.4 kg (range 21.4 to 71.7 kg). Under general anesthesia, bone marrow aspirates were performed on the proximal humerus using 15 gauge Illinois biopsy needles. Adipose tissue was obtained from the infrapatellar fat pad prior to arthroscope insertion. Synovium/subsynovial tissues were isolated from the femoropatellar joint using arthroscopic biopsy forceps during knee arthroscopy. Sample weights and volumes are provided in Table 3.1.

Nucleated cells were isolated from bone marrow using gradient centrifugation (Ficoll-Paque Plus, GE Health Care Biosciences, Piscataway, NJ) as previously described (Pittenger, 2008). Following centrifugation at 1,800xG for 30 minutes, mononuclear cells were removed, washed twice with 15mL of Hank's Balanced Salt Solution (HBSS, Invitrogen, Carlsbad, CA), quantified, and assessed for viability using a hemocytometer and trypan blue exclusion. Adipose and synovial samples were washed

in HBSS and were manually minced into a paste consistency using sterile scalpel blades and scissors. Samples were subjected to enzymatic digestion using Liberase TM® (Roche Molecular Biochemical, Mannheim, Germany) with gentle agitation at 37°C for 3-6 hours (Sekiya et al., 2002). Digested samples were washed, centrifuged, and strained though a 40μm cell strainer. Residual non-digested tissues that were retained in the cell strainer were discarded. Strained cells were washed and centrifuged for quantification and assessment of viability.

Nucleated marrow cells were plated at $3x10^4$ cells/cm^2 in 150cm^2 tissue culture dishes in Complete Culture Medium (CCM) containing α-MEM, 100U/mL penicillin, 100μg/mL streptomycin (Invitrogen), and 10% premium select fetal bovine serum (Atlanta Biological, Inc., Flowery Branch, GA), while nucleated cells from adipose and synovium were plated at 200 cells/cm^2. Cells were incubated at 37°C and 5% humidified CO_2 for 24 hours. For the following three days, plates were washed with PBS to remove non-adherent cells followed by media exchange. Culture dishes were subsequently monitored for expansion of the primary cell population (passage 0) with media exchange performed every other day. At 70% confluence (5-12 days) cells were lifted with 0.5% trypsin/EDTA solution (Invitrogen) and re-seeded at 100 cells/cm^2 for expansion of passage 1 cells. Media was exchanged every other day until cells were 70% confluent. Passage 1 cells were cryopreserved in α-MEM with 5% DMSO (Sigma-Aldrich, St. Louis, MO) and 30% FBS in preparation for subsequent experiments. With exception of the CFU assays, passage 1 cells were thawed, plated at 100 cells/cm^2, and expanded to 70% confluent passage 2 cells for use in experiments.

Colony Forming Unit (CFU) Assay

CFU ability of the primary cell population was determined on the day of tissue harvest by plating isolated cells in triplicate on 55cm^2 dishes at 4.5x10^5 total cells/dish for bone marrow and 1x10^3 total cells/dish for synovium and adipose tissue as previously described (Digirolamo et al., 1999; Pochampally, 2008; Prockop et al., 2001). Cells were incubated at 37°C in 5% humidified CO_2 for 24 hours in CCM. Plates were washed with PBS twice followed by media exchange with CCM at 24 and 48 hours. After the 48-hour wash, plates were incubated 21 additional days without media exchange. At 21 days, plates were stained with 0.3% crystal violet solution (Sigma-Aldrich) for 30 minutes. Plates were washed, photographed, and colony number and size were quantified using Image J FIJI Colony Counter (Schneider et al., 2012).

Expression of Plasticity Associated Genes

Isolation of RNA and subsequent gene expression evaluation was performed as previously described (Neupane et al., 2008). Total RNA was isolated from passage 2 cells using PureLink™ RNA Mini Kit (Life Technologies, Carlsbad, CA) and treated with DNase to remove contaminating DNA. Complementary DNA (cDNA) was synthesized from 2.5µg of total RNA using random hexamer primers and Superscript III reverse transcriptase (Invitrogen). Primers were commercially synthesized (Sigma-Aldrich) as follows: GAPDH (Okui et al., 2008) Forward: GGAGAAAGCTGCCAAATATG, Reverse: ACCAGGAAATGAGCTTGACA; NANOG (Neupane et al., 2008) Forward: GAATAACCCGAATTGGAGCAG, Reverse: AGCGATTCCTCTTCACAGTTG; OCT4 (Neupane et al., 2008) Forward:

GAGTGAGAGGCAACCTGGAG, Reverse: GTFAAGTGAGGGCTCCCATA; SOX2 (Neupane et al., 2008) Forward: AGTCTCCAAGCGACGAAAAA, Reverse: GCAAGAAGCCTCTCCTTGAA. PCR reactions (20µL) were prepared with 2µL of cDNA, 10nM of each primer, and 0.5 units of AmpliTaq Gold® 360 DNA Polymerase (Invitrogen). Cycling conditions were performed with an initial denaturation at 94°C for 5 minutes, followed by 35 cycles of: denature at 94°C for 0.5 minutes, anneal at 55°C for 0.5 minutes, extend at 72°C for 0.5 minutes, and a final extension at 72°C for 7 minutes. Upon completion, PCR products were separated on a 1.2% agarose gel by constant voltage electrophoresis for 60 minutes. PCR products were visualized using Gel Green (Biotium, Hayward, CA) and images captured using BioRad Chemdoc™MP Imager and ImageLab software (version 5.2.1; Bio-Rad, Hercules, CA).

Flow Cytometry

Passage 2 cMSCs were trypsinized, washed in PBS, counted, resuspended to $6x10^5$ cells/mL, and divided into individual aliquots containing $3x10^5$ cells in 50µL of PBS and 2% FBS. Commercially available antibodies were acquired for cell analysis from AbD Serotec (CD-9, -34, -44, -45, -90; Raleigh, North Carolina), Santa Cruz (CD-105; Santa Cruz, CA), and R&D (STRO-1; Minneapolis, MN). Cells were incubated in primary antibody (CD34-, 44-, 45-, 90- 100µg/mL, CD9- 10µg/mL, CD105- 40µg/mL, STRO1- 150µg/mL) for 30 minutes, washed twice, and resuspended in 300µL of PBS and 2% FBS. For CD44, CD90, and STRO-1 cells were resuspended in 50µL of PBS and 2% FBS for incubation in secondary antibody at 6.25µg/mL for 30 minutes, then washed twice, and resuspended in 300µL of PBS and 2% FBS for analysis (Stewart and

Stewart, 2001; Stewart et al., 1999). Cell fluorescence was determined by flow cytometry using a FACSCalibur flow cytometer (BD Biosciences, San Jose, CA), CellQuest (BD Biosciences) acquisition software, and FlowJo analysis software version 9.8.3 (TreeStar, Inc, Ashland, Oregon). Prior to analysis, propidium iodide was added at 100μg/mL to identify and remove non-viable cells. The filters used were 610/20 for propidium iodide and 530/30 for FITC. Flow cytometry results are presented as percentage positive staining relative to unstained control cells, in which percentage positive is defined as the number of viable cells that stained positive for each marker divided by the total number of viable cells evaluated for that marker.

Proliferation Assay- Short-term Proliferation

To compare the short term proliferation of synovium, marrow, and adipose cMSCs, cells were plated at 100 cells/cm^2 in triplicate wells on 12-well tissue culture plates in CCM as described above. Cells were washed with PBS, fixed in 500μL of DNA quantification buffer at 24-hour intervals for 10 days, and quantified by fluorescence DNA incorporation assay as previously described (Krause et al., 2011). After application of DNA quantification buffer, cells were frozen and stored at -20°C until assay completion. After thawing to room temperature, cell monolayers were disassociated and DNA released from them by adding 1mg/mL collagenase (Sigma), 1U/mL *HindIII* (Invitrogen), and 1U/mL *Eco*RI (Invitrogen) for incubation at 37°C for 16 hours. The following day, cell suspensions were transferred to 1.5mL tubes and Sytox Orange (Life Technologies) was added in a 1000-fold dilution. Cell suspensions were centrifuged at 15,000xG for 20 minutes and supernatant added to opaque 96-well plates

in triplicate to determine fluorescence (Krause et al., 2011). Individual cell numbers were determined by referencing a linear standard curve consisting of pre-determined numbers of cMSCs.

Proliferation Assay- Long-term Proliferation

To compare the long-term proliferation of cMSCs over multiple passages, cells were plated in triplicate at 100 cells/cm^2 on 55cm^2 dishes and cultured in CCM with media exchange every other day. After five days, cells were trypsinized, manually counted, and re-plated at 100 cells/cm^2. This process was repeated for a total of five cell passages (25 cumulative days in culture). At each passage, cell yield per plate was determined using a hemocytometer and trypan blue exclusion (n=3 plates/cell line) and data reported as the mean population doubling number for each cell preparation. Population doubling was determined as previously described by Greenwood et al. as follows: population doubling (PD) is equal to the log of the ratio of the final cell count (N) to the starting cell count (X_0), divided by the log of 2; that is PD= [log(N ÷ X_0)] ÷ log2 (Greenwood et al., 2004).

Adipogenesis

Canine MSCs were plated in CCM at 2x10^4 cells/cm^2 in 12-well plates (n=4 wells/condition). The following day, cells were treated with CCM or modified adipogenic medium developed by making slight modifications to existing cMSC literature (Al-Nbaheen et al., 2012; Csaki et al., 2007; Kisiel et al., 2012; Neupane et al., 2008; Reger et al., 2008; Schwarz et al., 2012; Sekiya et al., 2002). Adipogenic medium consisted of α-MEM containing 1nM dexamethasone (Sigma), 5mM rosiglitazone

(Sigma), 50mM pantothenate (Enzo Life Sciences, Farmingdale, NY), 10mM insulin (Sigma), 30mM biotin (Enzo), 50mM isobutylmethylxanthine (Sigma), and 10% serum [5% FBS, 5% rabbit serum (Atlanta Biological)]. Media were exchanged twice weekly. After 21 days, cells were washed with PBS and fixed in 10% neutral buffered formalin prior to staining in 0.5% Oil Red O (Sigma) to document lipid vacuole formation. Cells were photographed prior to extraction of Oil Red O stain for quantification as previously described (Sekiya et al., 2002).

Short-term Assay of Osteogenesis - Alkaline Phosphatase (ALP) Activity

Canine MSCs were plated in CCM at $5x10^3$ cells/cm^2 in 12-well plates (n=3 wells/ condition). The following day (Day 1), cells were treated with control medium (CCM), or osteogenic basal medium optimized for the dog. Osteogenic basal medium (OBM) consisted of α-MEM, 5% FBS, 10μg/mL beta-glycerophosphate (βGP, Sigma), 50mg/mL ascorbate-2-phosphate (Sigma), or OBM supplemented with 50 or 100-ng/mL of recombinant human bone morphogenic protein-2 (rhBMP-2; R&D Systems) as previously described (Krause et al., 2011; Volk et al., 2005). Media were exchanged on day four. At day seven, cells were washed twice with PBS and incubated with 500μL of 4°C ALP activity buffer containing 1mM magnesium chloride (Sigma), 0.1% Triton-X (Sigma), and 100mM sodium chloride (Sigma) in PBS. 500μL of 4°C ALP substrate p-nitrophenylphosphate (P-NPP, Thermo Fisher Scientific; West Palm Beach, FL) was added to each well to initiate the assay. Absorbance was determined for each well at 405nm in one minute intervals for 20 minutes at 37°C using an automated plate reader (HT Synergy, BioTek, Winooski, VT) and Gen3Bio software. Kinetic ALP activity

curves were generated for each well and the ALP activity per well was calculated by determining the slope of each activity curve using a linear curve fit technique. ALP activity of each well was normalized to the number of cells in each well using the DNA quantification technique described above.

Long-term Assay of Osteogenesis - Alizarin Red Stain (ARS) Mineralization

Detachment of high-density monolayers from the tissue culture surface of long-term mineralization assays is a phenomenon that is not uncommon in cMSC mineralization assays (unpublished observations). This problem has been described in prior cMSC literature (Kadiyala et al., 1997; Volk et al., 2005; Volk et al., 2012). In order to prevent monolayer detachment, cMSCs were plated in CCM at $2x10^4$ cells/cm^2 in 12-well plates (n=4 wells/condition). Prior to plating, the periphery of wells was mechanically scored using a sterile stone Dremel bit and associated hand chuck in order to create a circular etching around the margin of each well. Wells were coated with human fibroblast derived fibronectin (Sigma) at 5mg/mL in PBS for 30 minutes at 37°C. Excess fibronectin was removed and cells were seeded in each well. The following day, cells were treated with CCM, OBM, or OBM supplemented with 200ng/mL rhBMP-2. Media were exchanged twice weekly. After seven days, 1nM dexamethasone was added to OBM and OBM + BMP-2 wells, creating osteogenic differentiation media (ODM) to induce mineralization (Krause et al., 2008; Reger et al., 2008; Volk et al., 2005). At 21 days, cells were washed with PBS and fixed in 500µL of 10% neutral buffered formalin prior to staining in 40nM alizarin red stain (ARS; Sigma) to visualize calcium deposition within osteogenic monolayers. Wells were photographed prior to extraction of ARS for

semi-quantification via spectrophotometry using an acetic acid extraction technique as previously described (Krause et al., 2011).

Chondrogenesis

Micromass cultures of cMSCs were generated using slight modifications to the previously described technique (Sekiya et al., 2002). Briefly, passage 2 cMSCs were washed in PBS, trypsinized, counted, and resuspended to $1x10^6$ cells/mL in chondrogenic medium. Chondrogenic medium consisted of α-MEM supplemented with a 1:250 dilution of ITS+ culture supplement, 50µg/mL ascorbate-2-phosphate, 40µg/mL L-proline (Sigma), 100µg/mL sodium pyruvate (Sigma), 10^{-7}M dexamethasone, 10ng/mL recombinant human transforming growth factor-β3 (rhTGF-β3, R&D Systems), and 500ng/mL of rhBMP-2. Cells were pelleted in 15mL conical tubes ($5x10^5$ cells/tube) by centrifugation at 500xG for 5 minutes (n=3 pellets/cell line). Chondrogenic medium was exchanged twice weekly. After 21 days, chondrogenic pellets were fixed in 10% neutral buffered formalin. Pellets were photographed and area (mm^2) was determined using digital morphometry. Pellets were subsequently embedded in paraffin and sectioned for histologic evaluation using 1% toluidine blue/sodium borate (Sigma) stain.

Immunohistochemistry

Paraffin-embedded sections were deparaffinized in CitraSolv (Thermo Fisher Scientific) and rehydrated using a graded alcohol series. Antigen retrieval was performed with boiling citrate buffer and endogenous peroxidase activity was quenched by incubating sections in methanol containing 1% hydrogen peroxide for 15 minutes at

room temperature. Sections were then incubated with rabbit anti-collagen type II IgG (Abcam, Cambridge, MA; 10μg/ml in PBS containing 1% BSA) or rabbit IgG (Rockland, Limerick, PA) as a negative control for 16 hours at 4°C. Immunoreactive protein was visualized using the Vectastain ABC Kit (Vector Laboratories Inc., Burlingame, CA) according to kit instructions with 3,3′-diaminobenzidine tetrahydrochloride (Sigma) as the color substrate. Sections were lightly counterstained with Gill's hematoxylin, dehydrated, and coverslipped for photography (Gao et al., 2008; Spencer et al., 1999).

Immunomodulation

To assess macrophage-mediated immunomodulation, mouse macrophage cells (RAW 264.7 cell line, ATCC TIB-71) were seeded at $1x10^4$ cells/cm^2 in 12-well plates in CCM and allowed to attach overnight. After 24 hours (approximately 60% confluence), cMSCs were titrated in triplicate ($1x10^3$, $1x10^4$, $2.5x10^4$, and $5x10^4$ cells/well) to initiate a 24 hour co-culture (n=3 replicates/cMSC dosage). Lipopolysaccharide (E. coli 055:B5 strain, Sigma) was introduced to each well at 0.5μg/mL to induce macrophage activation. Co-cultures were allowed to respond for 18 hours, at which point conditioned media were collected and stored at -20°C. Upon evaluation of all 15 cMSC preparations, media were thawed on ice and analyzed for murine TNF-α and interleukin-6 (IL-6) protein concentrations via enzyme-linked immunosorbent assay (ELISA) according to manufacturer's protocol (R&D).

Statistical Analysis

Descriptive statistics were generated using GraphPad Prism 6.0 (GraphPad Software, La Jolla, CA) and were reported as mean ± standard deviation. Data were imported into a commercial statistical software program (SAS, version 9.4; SAS Institute Inc., Cary, NC, USA) for analysis. Repeated measures ANOVA was used to determine if each parameter differed significantly by tissue type and treatment group, as appropriate, with donor dog regarded as a random effect. The Tukey method was used to adjust for multiple pairwise comparisons. For all analyses, p-values < 0.05 were considered significant.

RESULTS

Results presented herein summarize data from five individual donors. Detailed descriptions for individual donors can be found in the APPENDIX.

Cell Isolation and Colony Forming Unit (CFU) Potential

Nucleated cells were successfully isolated from each donor and tissue sample. Synovium ($46.6 \times 10^3 \pm 62.8 \times 10^3$ cells/gram of tissue) provided greater numbers of nucleated cells when compared to bone marrow ($18.7 \times 10^3 \pm 28.1 \times 10^3$) and adipose tissue ($12.9 \times 10^3 \pm 12.0 \times 10^3$), although these differences were not significantly different ($p=0.2$). In addition, there was no difference in the number of total nucleated cells isolated from bone marrow or adipose tissue ($p=0.8$) (Figure 3.1A. Table 3.1). After 7-14 days of culture, cMSCs were identified in primary expansion plates as

Table 1. Isolation data of cell samples from five individual donors				
Source	Sample weight (grams)	Nucleated cell no. (x10^3 cells)/volume of weight	Colony no./ nucleated cells	Mean colony Area
Synovium	0.24 ± 0.10	46.60 ± 62.8	6.48 ± 3.49	0.28 ± 0.03
Marrow	4.20 ± 0.80	18.70 ± 28.10	0.01 ± 0.01	0.26 ± 0.12
Adipose	0.31 ± 0.10	12.90 ± 12.00	2.63 ± 2.17	0.26 ± 0.13

Table 3.1. *Nucleated cell isolation and CFU potential of synovium, marrow, and adipose cMSCs.* Synovium, marrow, and adipose tissues were obtained from five canine donors presenting for rupture of the cranial cruciate ligament. Cells were isolated using Ficoll™ centrifugation (marrow) or enzymatic digestion (synovium, adipose) and plated at clonal density. Tissue sample weights from all donor specimen collections are shown (mean ± SD) and nucleated cell number adjusted per gram of tissue of all cell preparations acquired (mean ± SD). Post isolation, CFU potential of primary cell populations for all 15 donors was performed. $1x10^3$ total cells (synovium and adipose) or $4.5x10^5$ total cells (marrow) were seeded on 55 cm^2 plates and incubated for 21 days. Plates were stained with 0.3% Crystal Violet and colony number (mean ± SD) and surface area (mean ± SD) was quantified for each plate.

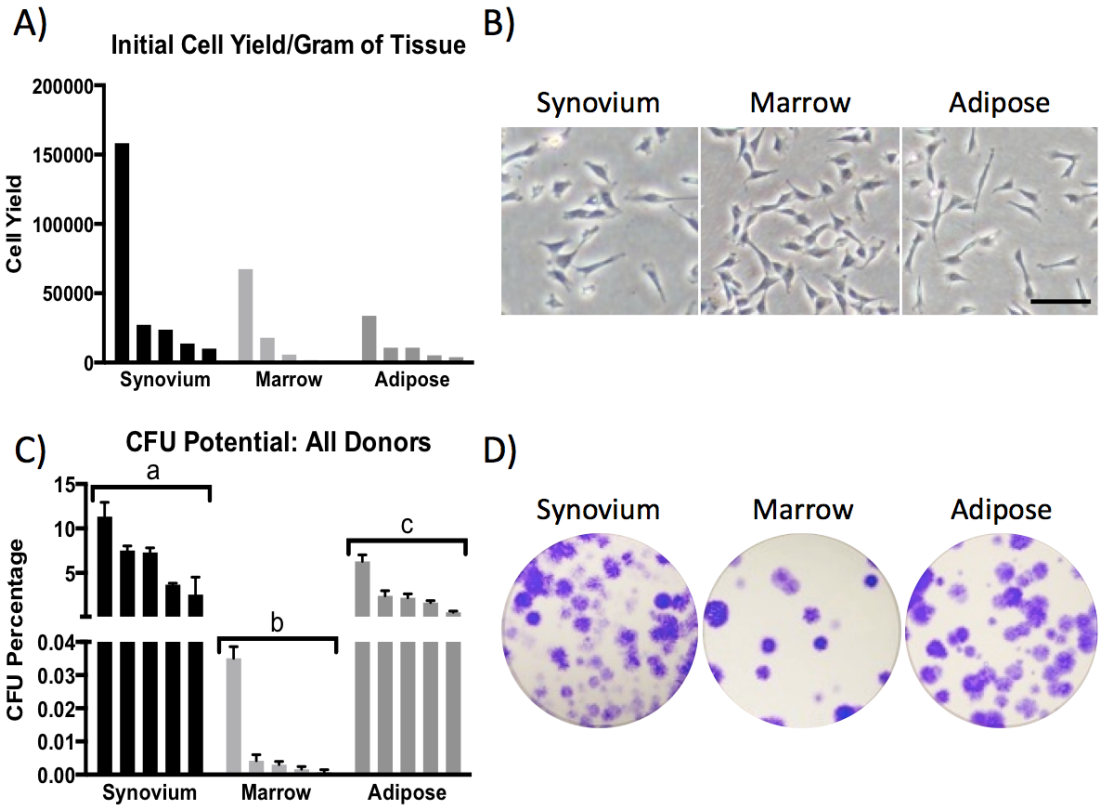

Figure 3.1. *Nucleated cell isolation and CFU potential of synovium, marrow, and adipose cMSCs.* Synovium, marrow, and adipose tissues were obtained from five canine donors presenting for rupture of the cranial cruciate ligament. Cells were isolated using Ficoll™ centrifugation (marrow) or enzymatic digestion (synovium, adipose) and plated at clonal density. **A)** Initial nucleated cell yield for all 15 donors, normalized to tissue weight. **B)** Representative 10X objective phase contrast microscopy images seven days post isolation (Bar=100µm). **C)** CFU potential of primary cell populations for all 15 donors. $1x10^3$ total cells (synovium and adipose) or $4.5x10^5$ total cells (marrow) were seeded on 55 cm^2 plates and incubated for 21 days. Plates were stained with 0.3% Crystal Violet and colony counts were performed on each plate. CFU potential is defined as the number of colonies present divided by total number of seeded cells, expressed as a percentage of the total seeded cells. Data are reported as mean ± SD (n=3 plates/tissue). Letters a, b, and c denote significant differences between tissue sources of cMSCs ($p<0.0001$). **D)** Photographs of CFU plates from a single representative donor. For panels A and C, data are reported in descending order for each tissue.

plastic-adherent, spindle shaped cells (Figure 3.1B). All primary nucleated cell populations obtained from the 15-tissue samples exhibited some degree of CFU potential. Using repeated measures ANOVA, significant differences were observed in the CFU potential between the three tissues ($p<0.0001$), with synovium (6.48 ± 3.49%) and adipose tissue (2.63 ± 2.17%) exhibiting markedly higher CFU potential when compared to bone marrow (0.009 ± 0.01%). These CFU values are consistent with findings in human MSCs (Sakaguchi et al., 2005). Specifically, the CFU potential of synovium cMSCs was significantly greater than both adipose ($p<0.001$) and bone marrow ($p<0.0001$) derived cells; while CFU potential of adipose cMSCs was significantly greater than bone marrow derived cells ($p<0.01$) (Table 3.1, Figure 3.1C,D).

Cell Surface Expression

Flow cytometry was used to characterize each preparation of cMSCs for cell surface markers (Figure 3.2, Table 3.2). All cMSC were negative for the leukocyte markers CD34 and CD45. Cells were consistently positive for CD9, CD44, and CD90. Interestingly, there was variable staining for CD105 (Endoglin), with synovium (46.16 ± 21.78%) and adipose (59.84 ± 15.57%) cMSCs exhibiting higher percentage positive staining cells when compared to marrow cMSCs (17.12 ± 8.85%). Additionally, cMSCs were negative for STRO-1, despite confirming cross reactivity of the commercially available STRO-1 antibody on canine peripheral blood (data not shown). Histograms from a representative donor's marrow-derived cMSCs are shown in Figure 3.2.

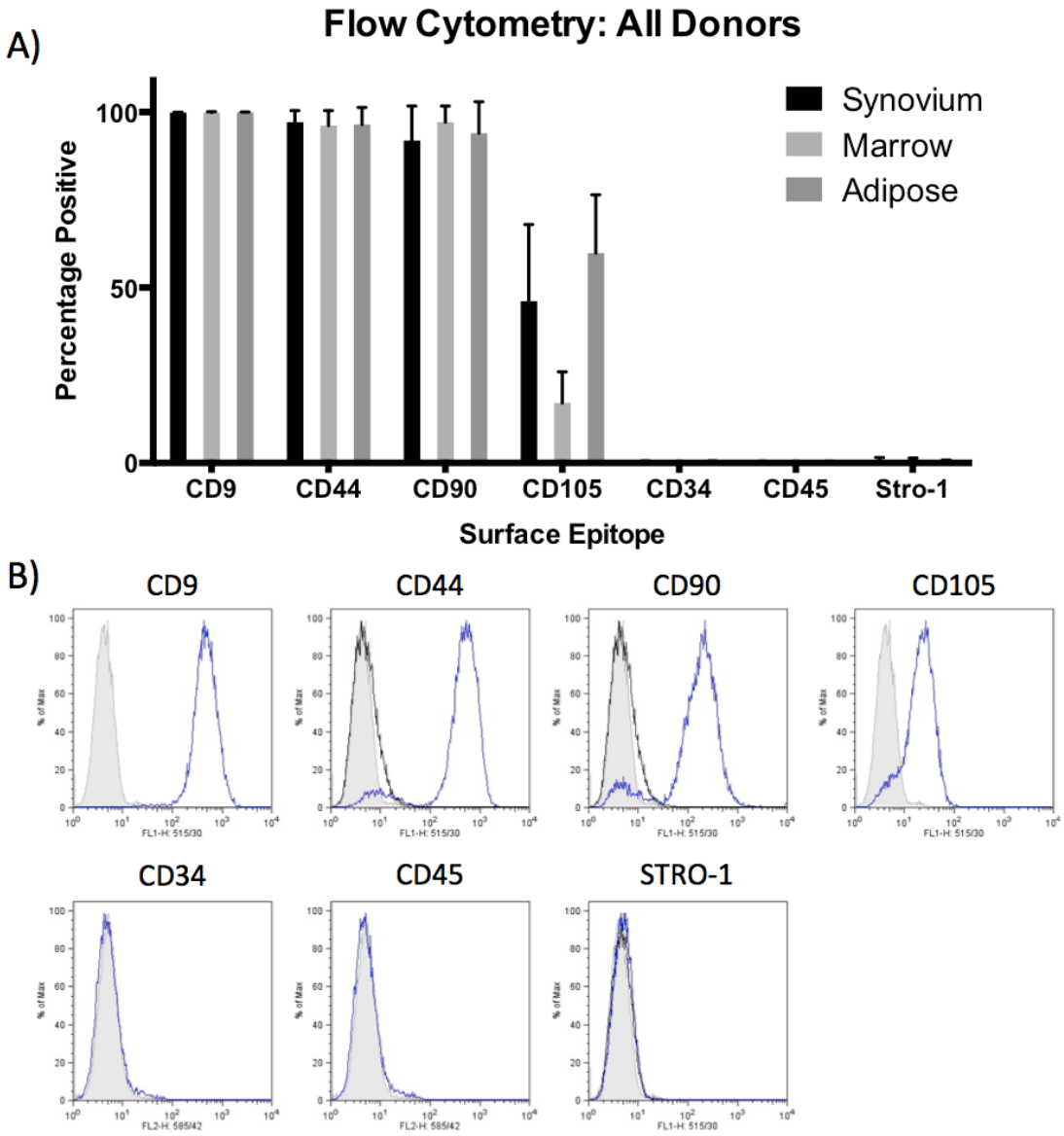

Figure 3.2. *Flow cytometry analysis of synovium, marrow, and adipose cMSCs.* **A)** Percentage positive cells reported as mean ± SD for synovium, marrow, and adipose cMSCs isolated from five canine donors. **B)** Representative histograms demonstrating staining of marrow cMSCs from a single donor in which grey shading denotes unstained control cells, black outline denotes secondary control staining, and blue outline denotes staining of interest.

Table 2. Flow cytometry percentage positive cell surface markers							
Source	CD9	CD44	CD90	CD105	CD34	CD45	STRO-1
Synovium	99.88 ± 0.11	97.16 ± 3.32	91.94 ± 9.81	46.16 ± 21.78	0.34 ± 0.27	0.29 ± 0.22	0.01 ± 1.55
Marrow	99.86 ± 0.26	96.21 ± 4.25	97.17 ± 4.55	17.12 ± 8.86	0.30 ± 0.13	0.23 ± 0.12	0.26 ± 1.14
Adipose	99.98 ± 0.05	96.49 ± 4.88	93.99 ± 8.99	59.84 ± 16.57	0.33 ± 0.26	0.27 ± 0.26	0.00 ± 1.1

Table 3.2. *Flow cytometry analysis of synovium, marrow, and adipose cMSCs.* Percentage positive cells reported as mean ± SD for synovium, marrow, and adipose cMSCs isolated from five canine donors.

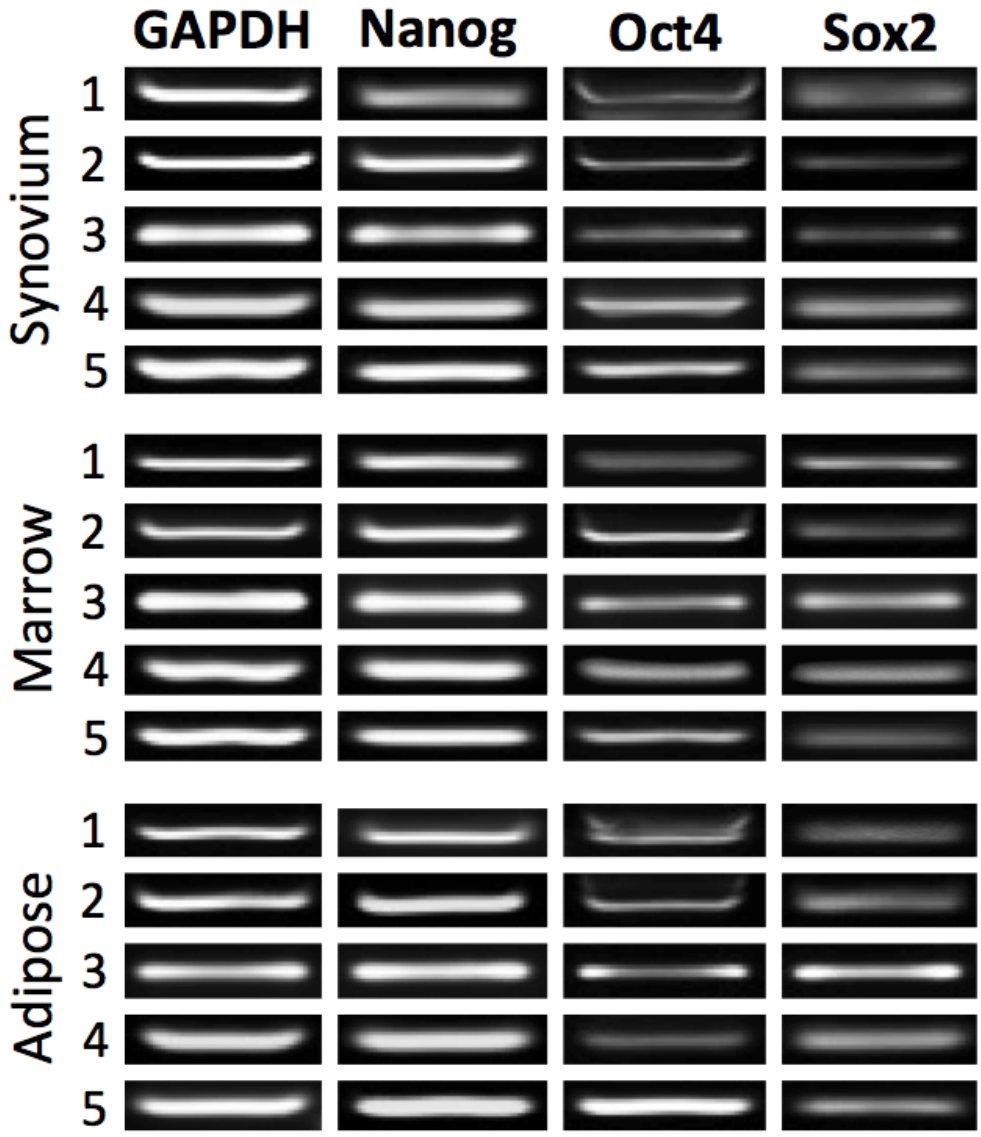

Figure 3.3. *Expression of plasticity-associated genes in synovium, marrow, and adipose cMSCs.* Passage 2 cMSCs were qualitatively evaluated for the plasticity-associated genes NANOG, OCT4, and SOX.2 using RT-PCR. All 15 cMSC cell preparations were positive when assessed using RT-PCR. Representative images of NANOG (274bp), OCT4 (141bp), and SOX2 (142bp) gene expression from synovium, marrow, and adipose derived cMSCs of a single donor are shown. Canine GAPDH was used as a housekeeping gene.

Gene Expression

Reverse-transcription PCR was used to evaluate all cell preparations for pluripotent associated transcription factors, NANOG, OCT4, and SOX2, as previously described (Neupane et al., 2008). All cMSCs displayed positive indication for plasticity associated gene expression and GAPDH control (Figure 3.3).

Proliferation Assays

Both short- and long-term proliferation assays were used to assess the proliferation characteristics of donor-matched cMSCs derived from synovium, marrow, and adipose tissues. In short-term proliferation assays, there were significant differences in proliferation between synovium, marrow, and adipose cMSCs ($p<0.01$). Consistent with findings in previously described literature (Sakaguchi et al., 2005), adipose and synovium cMSCs proliferated more rapidly than marrow cMSCs. A proliferation curve from a representative donor is shown in Figure 3.4A. Scatter plots reporting the number of recovered cells at day 5 and day 10 for all 15 cMSC isolates are shown in Figure 3.4B. Using repeated measures ANOVA, adipose cMSC proliferation was significantly greater than marrow ($p<0.01$) and synovium ($p<0.05$). While synovium cMSCs tended to proliferate more rapidly than marrow cMSCs, values were not significantly different in the short-term proliferation assay ($p=0.1$). These results indicate that despite donor variation, tissue source of cMSCs affects short-term proliferation of cMSCs, with adipose cMSCs proliferating more rapidly than synovium or marrow cMSCs. These findings are consistent with publications in other species (Sekiya et al., 2002).

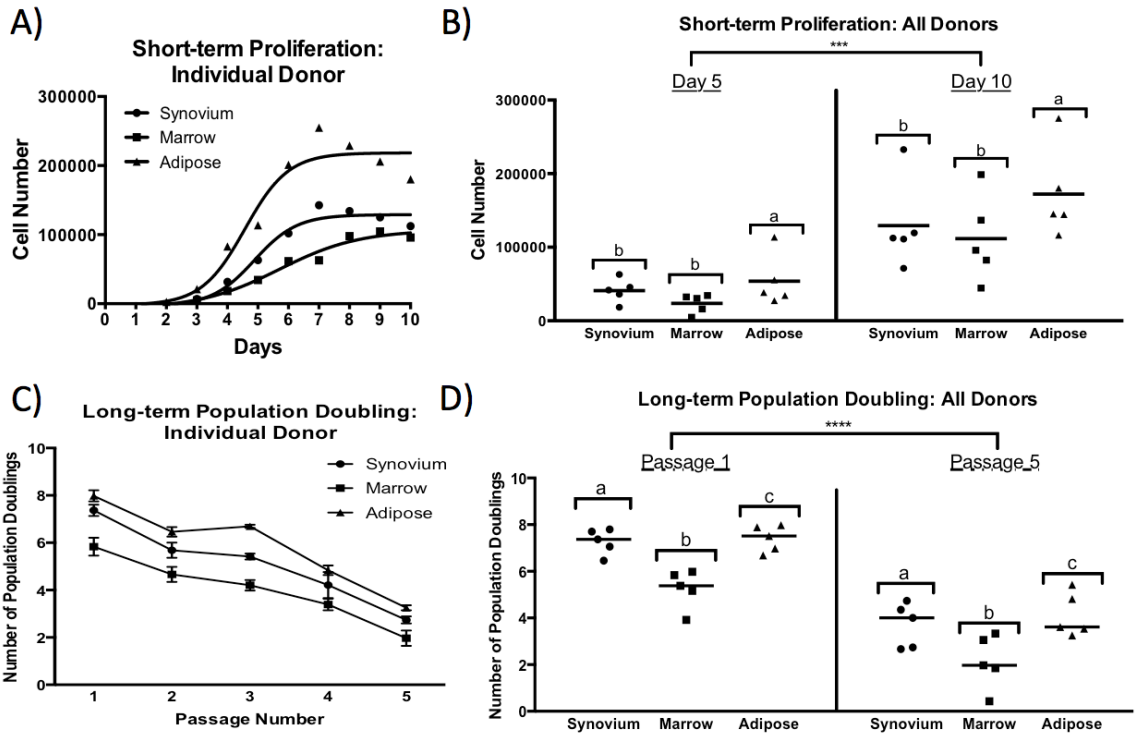

Figure 3.4. *Short- and long-term proliferation of synovium, marrow, and adipose cMSCs.* Passage 2 cMSCs were seeded at 100 cells/cm^2 in CCM on 12-well plates (n=3 wells/cell preparation) with media exchange every other day. Mean cell number was determined daily for 10 consecutive days using DNA quantification. **A)** Mean short-term proliferation of a representative donor, demonstrating higher proliferation rates of adipose and synovium cMSCs. **B)** Scatter-plot demonstrating the number of cMSCs for all 15 cell preparations at days 5 and 10. Each data point represents the cell number for an individual cMSC preparation (bar=mean cell yield across the five donors). Long-term proliferation was determined over a 5 passage, 25-day time course. Passage 2 cMSCs were seeded at 100 cells/cm^2 in CCM on 55 cm^2 plates (n=3 plates/cell preparation/passage) with media exchange every other day. At 5 day intervals, cells were washed, trypsinized, recovered, cell number determined using a hemocytometer, and re-plated at 100 cells/cm^2. Long-term proliferation rates were determined using the population doubling equation. **C)** Population doubling (mean ± SD) of a representative donor, demonstrating increased doubling rate of adipose and synovium cMSCs, particularly at passages 1-3. **D)** Population doubling scatter-plot for all 15 cMSC preparations at Passage 1 and 5. Each data point denote population-doubling rate for an individual cMSC preparation (bar=mean population doubling rate across the 5 donors). Note: for panels B and D, asterisks represent significant differences in the cell number: (***) $p<0.001$; (****) $p<0.0001$. Letters a, b, c denote significant differences between tissue sources ($p<0.05$).

In long-term assays, tissue source of cMSCs had a significant effect on the number of recovered cells over the five passage, 25-day time course ($p<0.0001$) (Figure 3.4C,D). As previously reported in other species, population doubling decreased significantly with sequential passaging ($p<0.0001$). Results for a representative donor are shown in Figure 3.4C. The mean population doubling at Passage 1 and Passage 5 for all cMSC preparations are shown in Figure 3.4D. Using repeated measures ANOVA, population doubling of both adipose ($p<0.0001$) and synovium ($p<0.0001$) cMSCs was significantly greater than marrow cMSCs across all passages. Additionally, the population doubling of adipose and synovium cMSCs was significantly different ($p=0.02$). These results demonstrate the superior proliferation abilities of adipose and synovium cMSCs as well as the finite proliferation of cMSCs derived from all three tissues.

Tri-lineage Differentiation- Adipogenesis

Adipogenic potential was evaluated at 21 days by both visual assessment of lipid vacuole accumulation and quantification of Oil Red O staining. All cMSCs underwent varying degrees of adipogenesis, with increased vacuole formation and Oil Red O staining when compared to control (CCM) (Figure 3.5). Adipogenic differentiation of a representative donor is shown in Figure 3.5A,B. Morphologically, synovium and adipose cMSCs produced medium to large, grape-like vacuoles, whereas marrow cMSCs produced small, diffuse vacuoles. Oil Red O extraction for this individual donor confirms significant increases in lipid accumulation for all three tissues when compared to control (CCM) ($p<0.005$), with adipose cMSCs exhibiting significantly greater Oil

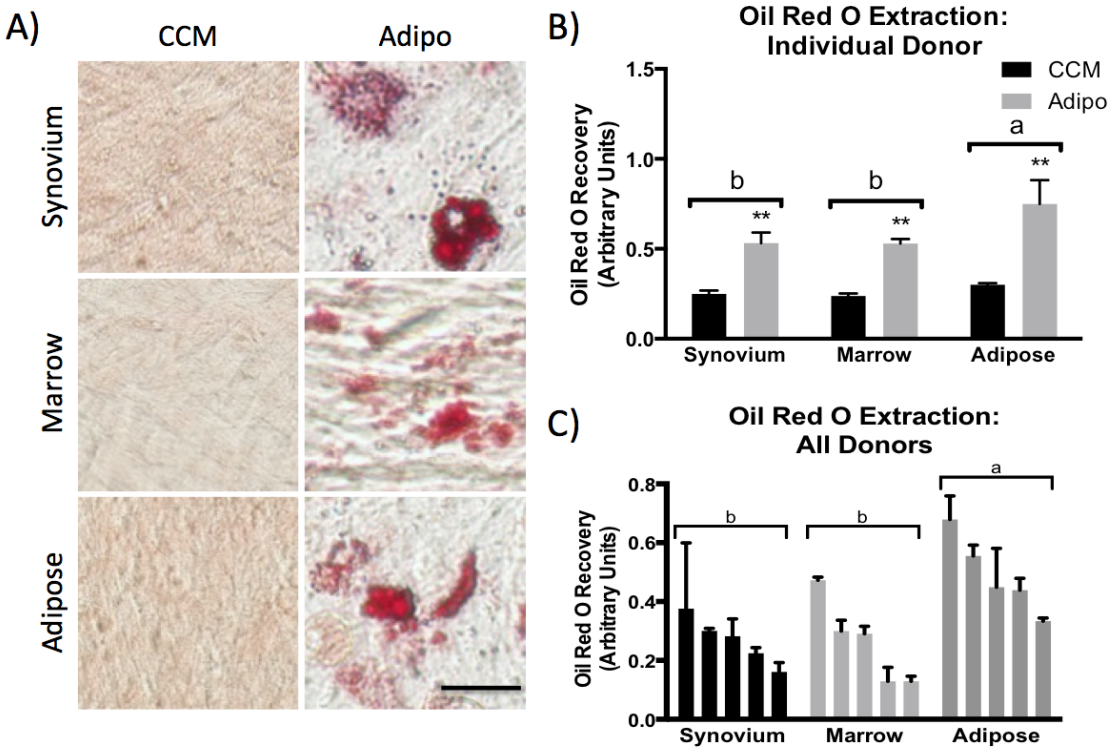

Figure 3.5. *Adipogenesis of synovium, marrow, and adipose cMSCs.* **A)** Passage 2 cMSCs were cultured in quadruplicate wells in CCM or modified adipogenic media with media exchange twice weekly. At 21 days, cells were formalin fixed and evaluated for lipid accumulation with Oil Red O (bar=25µm). **B)** Oil Red O quantification (mean ± SD) for a representative donor. Asterisks (**) denote significantly different Oil Red O quantification between treatment conditions ($p<0.01$). **C)** Mean ± SD Oil Red O quantification for all 15 cMSC isolates. CCM values have been subtracted from adipogenic values to facilitate presentation of results. Data are reported in descending order for each tissue. For panels B and C, letters a and b denote significant differences between tissue sources of cMSCs ($p<0.001$).

Red O extraction as compared to synovium ($p<0.05$) or marrow derived ($p<0.05$) cMSCs.

Oil Red O extraction values for all 15 cMSC cell preparations are reported in Figure 3.5C. Using repeated measures ANOVA, there was a significant increase in Oil Red O extraction in cMSCs treated with adipogenic media as compared to control ($p<0.0001$, data not shown). In addition, there were significant differences in Oil Red O extraction based on tissue source of the cMSCs ($p<0.001$). Using the Tukey post-hoc test, adipose cMSCs had significantly greater Oil Red O extraction values across all donors when compared to bone marrow ($p<0.01$) and synovium ($p<0.001$) cMSCs; however, there was no difference in Oil Red O extraction between synovium and marrow cMSCs ($p=0.1$). These results indicate that while synovium, marrow, and adipose cMSCs are capable of undergoing adipogenesis, adipose cMSCs are superior in their adipogenic ability.

Tri-lineage Differentiation- Osteogenesis

Two assays were utilized to evaluate the osteogenic potential of donor-matched cMSCs. The ALP activity assay was used to assess early commitment to osteogenic differentiation after seven days while the Alizarin Red Stain (ARS) mineralization assay was used to assess mineralizing osteogenesis at 21 days.

ALP Activity Assay

In contrast to MSCs derived from other species, it has previously been reported that cMSCs require osteogenic medium supplemented with exogenous BMP-2 in order to exhibit robust ALP activity (Volk et al., 2005; Volk et al., 2012). To confirm this

finding, we performed ALP activity assays on all 15 cMSC isolates after initiation of osteogenesis with OBM or OBM containing 50 or 100ng/mL rhBMP-2. In support of prior publications, there were marked differences in ALP activity in response to rhBMP-2. An ALP assay from a representative donor (marrow cMSCs) is shown in Figure 3.6A. Over the 20-minute kinetic assay, we were unable to detect ALP activity in cMSCs treated with CCM or OBM; however, OBM containing rhBMP-2 induced a dose-dependent increase in ALP activity. The slope of each ALP activity assay was determined and normalized to a per cell basis using DNA quantification. The ALP activity per cell for synovium, marrow, and adipose cMSCs from a representative donor is provided in Figure 3.6B. There was no significant difference in ALP activity when synovium, marrow, and adipose cMSCs were treated with OBM ($p=0.999$), a medium known to induce robust ALP activity in human MSCs. In the presence of OBM containing rhBMP-2, there was a dose-dependent increase in ALP activity for synovium, marrow, and adipose cMSCs (OBM+50ng/mL rhBMP-2, $p<0.001$; OBM+100ng/mL rhBMP02, $p<0.0001$). Furthermore, there were marked differences in the response to rhBMP-2 based on the tissue source of cMSCs. Synovium ($p<0.001$) and marrow ($p<0.001$) cMSCs exhibited significantly greater ALP activity in response to OBM + rhBMP-2 as compared to adipose cMSCs.

ALP activity values for all 15 cMSC lines are shown in Figure 3.6C. Using repeated measures analysis of variance (ANOVA), there were significant differences in ALP activity based on osteogenic media condition ($p<0.0001$) as well as the cMSC tissue source ($p<0.01$). There was no difference in ALP activity between cMSCs

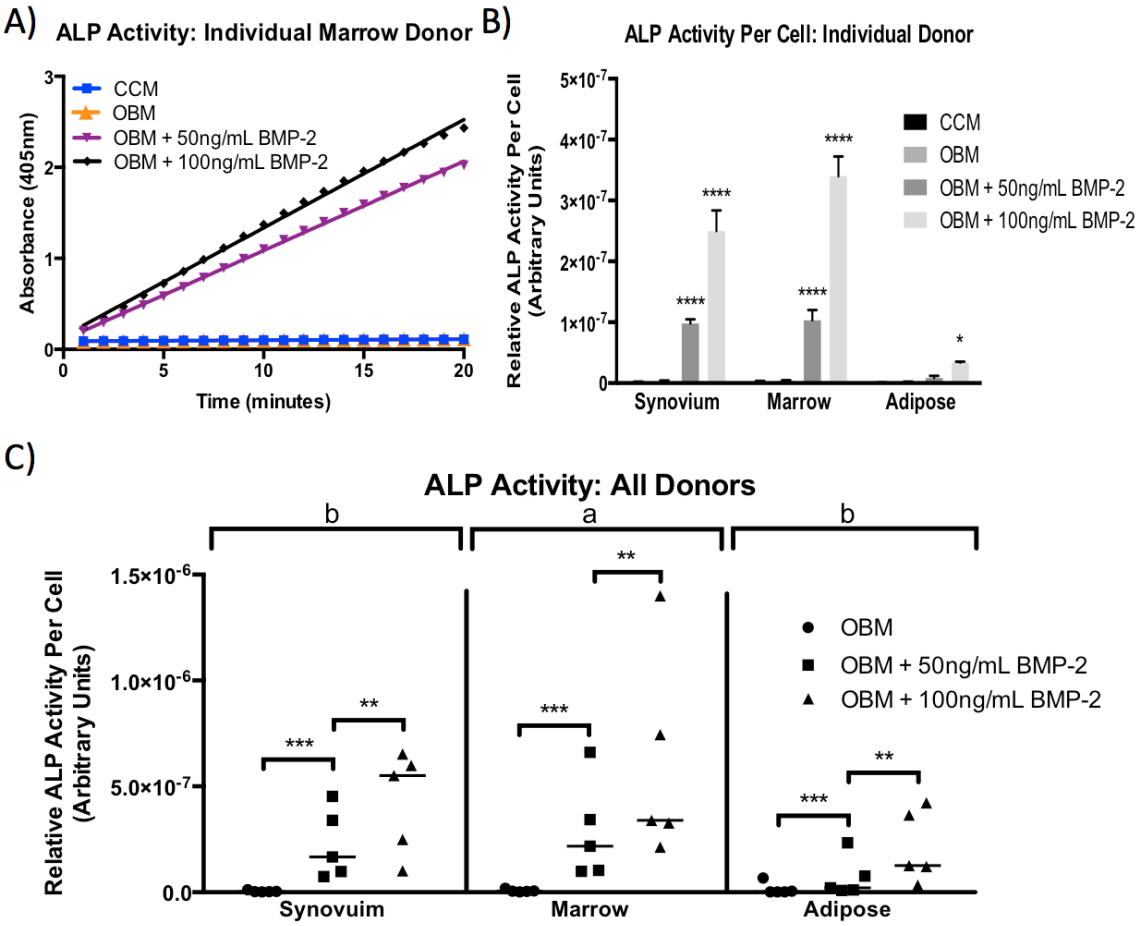

Figure 3.6. *Short-term osteogenesis of synovium, marrow, and adipose cMSCs.* Short-term osteogenesis was determined using the ALP assay. Passage 2 cMSCs were cultured in CCM, OBM, or OBM + rhBMP-2 for 7 days and evaluated for the ability to convert the colorless substrate PNPP to colorimetric PNP over time. **A)** ALP activity was determined by spectrophotometer (absorbance 405nM) over a 20-minute time course. Kinetic ALP activity results for a single cMSC preparation from a representative donor are shown. **B)** ALP activity normalized to cell number by DNA quantification for synovium, marrow, and adipose cMSCs from a representative donor are shown, demonstrating the minimal response of adipose cMSCs to OBM. **C)** Scatter plots demonstrating ALP activity for all 15 cMSC preparations organized by tissue and media condition. Each data point represents the ALP activity per cell for an individual cMSC preparation and a given media condition (bar=mean across the 5 donors). For panels B and C, asterisks denote significant differences between treatment groups; (*) denotes $p<0.05$, (**) denotes $p<0.01$, (***) denotes $p<0.001$, (****) denotes $p<0.0001$. The letters a and b denote significant differences between tissue sources of cMSCs ($p<0.01$).

cultured in CCM or OBM (data not shown, $p=0.999$). ALP activity was significantly higher for cMSCs treated with OBM+50ng/mL rhBMP-2 ($p<0.001$) and OBM+100ng/mL rhBMP-2 ($p<0.0001$) when compared to CCM or OBM. Additionally, cMSCs treated with OBM+100ng/mL BMP-2 exhibited significantly higher ALP activity as compared to cMSCs treated with OBM+50ng/mL rhBMP-2 ($p<0.001$). When considering the cMSC tissue source, marrow-derived cMSCs exhibited significantly greater ALP activity when compared to adipose cMSCs ($p<0.001$) and synovium cMSCs ($p<0.05$), while no significant difference in ALP activity was observed between synovium and adipose cMSCs ($p=0.1$). Collectively, these data clearly demonstrate that cMSCs require exogenous BMP-2 to exhibit detectible ALP activity, and that rhBMP-2 supplementation drives ALP activity in a dose-dependent manner. Moreover, while synovium and marrow cMSCs from individual donors respond robustly to OBM + BMP-2, adipose derived cMSCs from the same donors exhibit significantly reduced short-term osteogenic differentiation as assessed by the ALP activity assay.

Alizarin Red Stain (ARS) Mineralization Assay

Long-term, biomineralizing osteogenesis was evaluated at 21 days by both visual assessment of calcium accumulation within monolayers and quantification of ARS extraction. All cMSCs underwent varying degrees of osteogenesis as assessed by ARS binding (Figure 3.7). The ARS results for a representative donor are shown in Figure 3.7A,B. While ARS did not stain control wells (CCM), or in wells treated with ODM lacking BMP-2 (not shown), ARS accumulation was robust in synovium, marrow, and adipose cMSCs treated with ODM + 200ng/mL rhBMP-2. Quantification of ARS

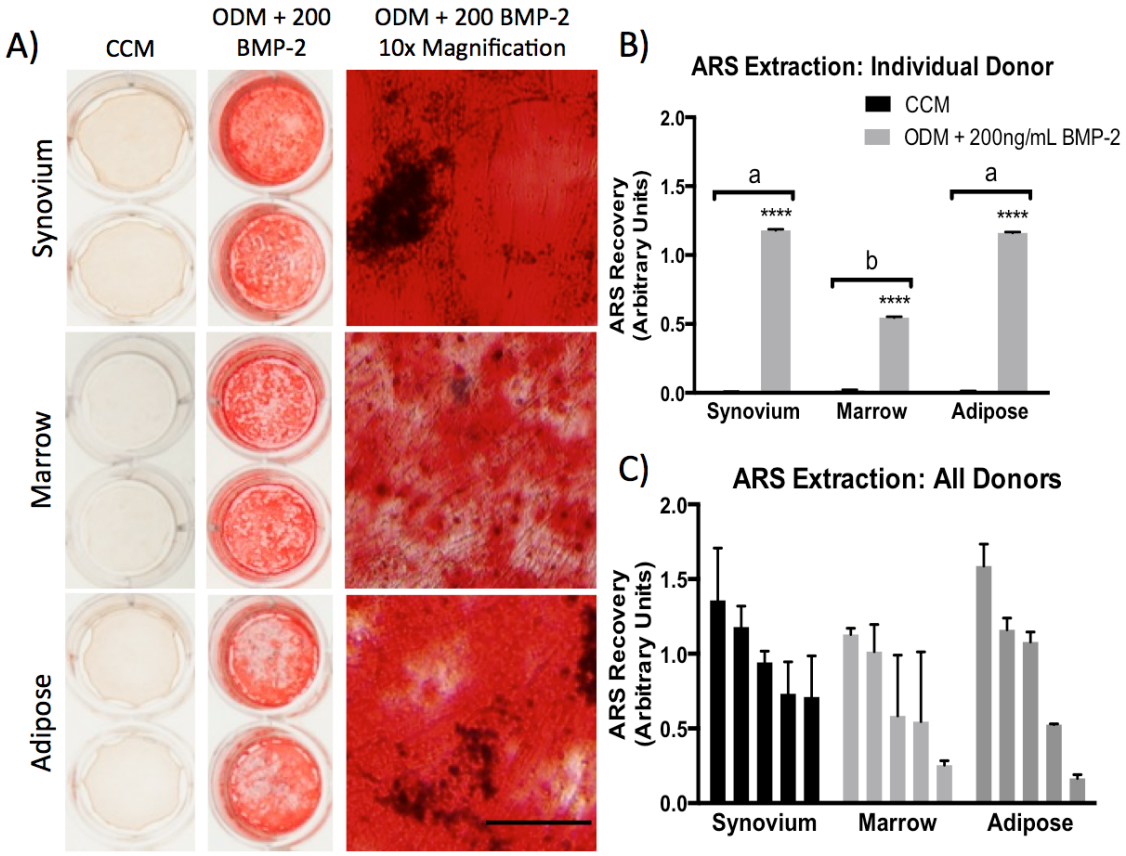

Figure 3.7. *Long-term osteogenesis of synovium, marrow, and adipose cMSCs.* Passage 2 cMSCs were cultured in triplicate wells in CCM or ODM with media exchange twice weekly. **A)** After 21 days of culture in CCM (left column) or ODM + 200ng/mL of rhBMP-2 (middle and right columns) monolayers were fixed in 10% formalin and stained with ARS. Plates were photographed (left and middle columns) and imaged with 10X objective light microscopy (right column) to document ARS accumulation (bar=125µm). **B)** ARS extraction (mean ± SD) for a representative donor. Asterisks (****) denote significant differences between treatment groups ($p<0.0001$). **C)** Mean ± SD ARS extraction values for all 15 cMSC preparations. CCM values have been subtracted from osteogenic values to facilitate presentation of results. Data are reported in descending order for each tissue. For panels B and C, letters a and b denote significant differences between tissue sources of cMSCs, if present ($p<0.0001$).

extraction for the donor in panel A demonstrates a marked increase in ARS for all three tissues when compared to control (CCM) ($p<0.0001$), with synovium ($p<0.0001$) and adipose ($p<0.0001$) cMSCs exhibiting significantly greater ARS extraction as compared to marrow cMSCs. ARS extraction values for all 15 cMSC cell lines are reported in Figure 3.7C. Using repeated measures ANOVA, there was a significant increase in ARS extraction in cMSCs treated with ODM + 200ng/mL rhBMP-2 as compared to control (data not shown, $p<0.0001$). However, in contrast to the ALP activity assay there was no significant difference in ARS extraction based on tissue source of the cMSCs ($p=0.5$). These results suggest that while adipose cMSCs may exhibit reduced osteogenic differentiation in the short term ALP activity assay, all tissue sources of cMSCs underwent osteogenesis when assessed using a long-term mineralization assay.

Tri-lineage Differentiation- Chondrogenesis

The classic micromass culture system was used to evaluate the chondrogenic potential of donor-matched cMSCs derived from synovium, marrow, and adipose tissues (Sekiya et al., 2002). All cMSCs underwent chondrogenic differentiation and increased in size over 21 days. Chondrogenesis was assessed using digital morphometry to quantify pellet size and histology to assess proteoglycan (toluidine blue) and collagen type II (immunohistochemistry) accumulation. Results from a representative donor are shown in Figure 3.8A,B. Synovium ($p<0.0001$) and adipose ($p<0.001$) cMSCs produced larger chondrogenic pellets as compared to marrow cMSCs. For this donor, adipose pellets were significantly larger than synovium pellets ($p<0.05$). While marrow cMSCs were smaller in size, they consistently displayed a deeper and more uniform staining for

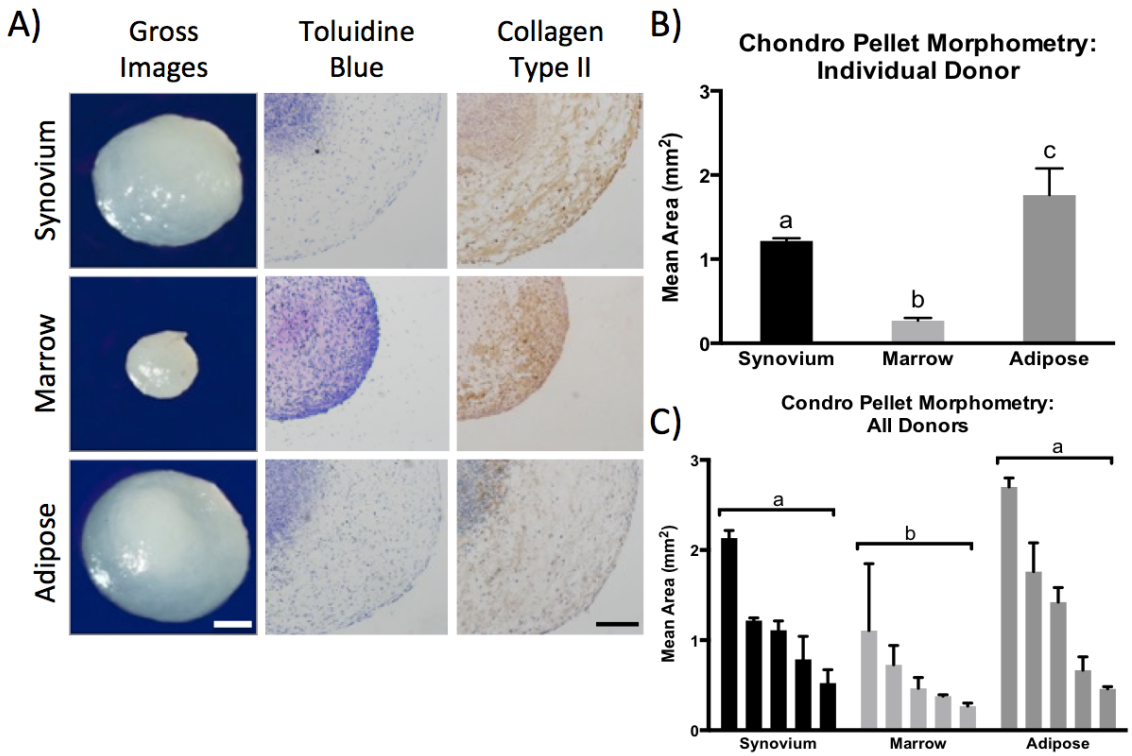

Figure 3.8. *Chondrogenesis of synovium, marrow, and adipose cMSCs.* Passage 2 cMSCs were evaluated for chondrogenesis using the micromass pellet technique. $5x10^7$ cells from each cMSC preparation were pelleted in triplicate and incubated for 21 days in chondrogenic medium with media exchange twice weekly. **A)** Pellets were photographed (gross images, bar=300µm), formalin fixed, and sectioned for histology. Pellets were positive for proteoglycan (toluidine blue) and collagen type II (10X objective, bar=150µm), although the intensity of staining varied across donor and tissue source of cMSC. **B)** Pellet morphometry for a representative donor (mean ± SD). **C)** Mean ± SD pellet area (mm^2) of chondrogenic pellets for all 15 cMSC preparations. Data are reported in descending order for each tissue. For panels B and C, letters a, b, and c denote significant differences between tissue source of cMSCs ($p<0.01$).

toluidine blue and collagen Type II (Figure 3.8A, middle row). Although adipose cMSCs tended to produce the largest chondrogenic pellets, toluidine blue and collagen type II immunohistochemistry was less uniform, with much of the periphery of the structures devoid of toluidine blue stain or collagen type II signal.

Digital morphometric results for all 15 cMSC isolates are provided in Figure 3.8C. Using repeated measures ANOVA, there was a significant difference in chondrogenic pellet size based on the cMSC tissue of origin ($p<0.01$). Both adipose ($p<0.001$) and synovium ($p<0.01$) cMSC chondrogenic pellets were significantly larger than marrow cMSC pellets. There was no significant difference in pellet size when comparing synovium or adipose chondrogenic cMSCs ($p=0.1$). Collectively, the results suggest that synovium and marrow cMSCs may generate superior chondrogenic pellets when employing the micromass system. Subjectively assessing toluidine blue and collagen type II stain accumulation, marrow cMSC chondrogenic pellets exhibited an increased staining compared to synovium and adipose derived cMSC chondrogenic pellets. These findings suggest higher levels of proteoglycan and collagen type II for marrow cMSCs, although these pellets were significantly smaller than those generated from synovium or adipose cMSCs. However, when assessed based on pellet size, adipose and synovium cMSCs generated the largest chondrogenic structures.

Immunomodulation

While the dog has been used to study graft-vs-host disease (Prentice et al., 1984; Socie and Blazar, 2009; Storb et al., 1970), to the authors' knowledge, the ability of cMSCs to modulate inflammation in vitro has yet to be examined. For this reason, we

established macrophage and cMSC co-culture experiments in which a murine macrophage cell line (RAW 264.7 cell line) was cultured alone or in combination with cMSCs (1 x 10^3 to 50 x 10^3 cells/well). Cultures were stimulated with LPS to stimulate toll-like receptors on the macrophages and thereby initiate an inflammatory response. Levels of secreted murine TNF-α and IL-6 were then assayed in conditioned media to measure inflammatory responses by the RAW cells and also assess whether cMSCs could affect the production of these two cytokines. The concentration of TNF-α detected in a representative co-culture experiment is shown in Figure 3.9A,B. As has been described in other species (Chen et al., 2012; Choi et al., 2011; Oh et al., 2012), cMSC co-culture resulted in a dose-dependent decrease in the concentration of murine TNF-α detected in conditioned media, suggesting that cMSCs have the ability to modulate the expression of murine TNF-α. In order to make direct comparisons across all 15 cMSC preparations, the measured concentrations of TNF-α were normalized to the positive control (murine cells alone stimulated with LPS) for each assay and reported as the percentage TNF-α relative to control (Figure 3.9B).

The relative concentrations of TNF-α for all 15 cMSC co-culture experiments are shown in Figure 3.9C. Using repeated measures ANOVA, there were significant differences in TNF-α based on the number of cMSCs present within the co-cultures ($p<0.0001$), whereas the tissue source of cMSCs had no effect on TNF-α ($p<0.5$). Using the Tukey method, TNF-α concentrations were significantly decreased in co-cultures containing 50 x 10^3 cells ($p<0.0001$) and 25 x 10^3 cells ($p<0.01$) when compared to co-cultures containing 1 x 10^3 cells/well. These results suggest that cMSCs are capable of

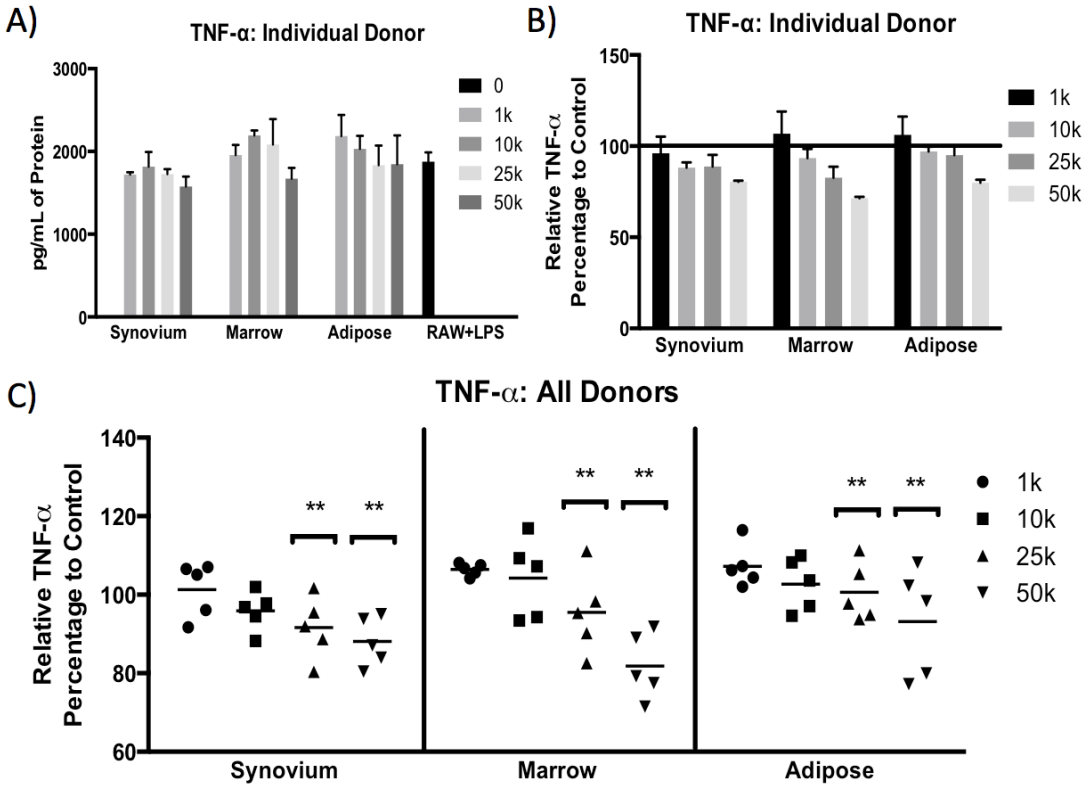

Figure 3.9. *Immunomodulation of murine TNF-α by synovium, marrow, and adipose cMSCs.* Passage 2 cMSCs ($1x10^3$–$50x10^3$) were co-cultured with $1x10^4$ murine macrophage cells in 12 well plates in CCM (n=3 wells/condition). After 24hrs, LPS (0.5μg/mL) was added to co-cultures to activate macrophages and to assess cMSCs immunomodulation. After 18hrs, media were collected and ELISA performed to determine the concentration of secreted murine TNF-α. **A)** Representative murine TNF-α concentrations (mean ± SD) for an individual donor. RAW + LPS denotes TNF-α concentration from murine macrophages (RAW cells) in the absence of cMSCs (positive control). **B)** Data from panel A were transformed to reflect the percentage change in TNF-α relative to the RAW + LPS positive control in preparation for comparative analysis across all 15 cMSC preparations and are reported as mean ± SD. **C)** Scatter plots demonstrating the percentage change of TNF-α concentration relative to positive control for all 15 cMSC preparations, organized by tissue and number of cMSCs present within co-cultures. Each data point represents the relative murine TNF-α for an individual cell preparation and "dose" of cMSC (bar=mean across the 5 donors). For all three tissues, TNF-α concentrations decreased in response to increasing numbers of co-cultured cMSCs. Marrow-derived cMSCs had the largest effect on TNF-α concentration, suggesting that marrow-derived cMSCs had the largest immunomodulatory effect on TNF-α in this in vitro co-culture system; however, differences between tissue source of cMSCs was not significant (p=0.5). Asterisks denote significant differences between numbers of co-cultured cMSCs: (*) $p<0.05$, (***) $p<0.001$, (****) $p<0.0001$.

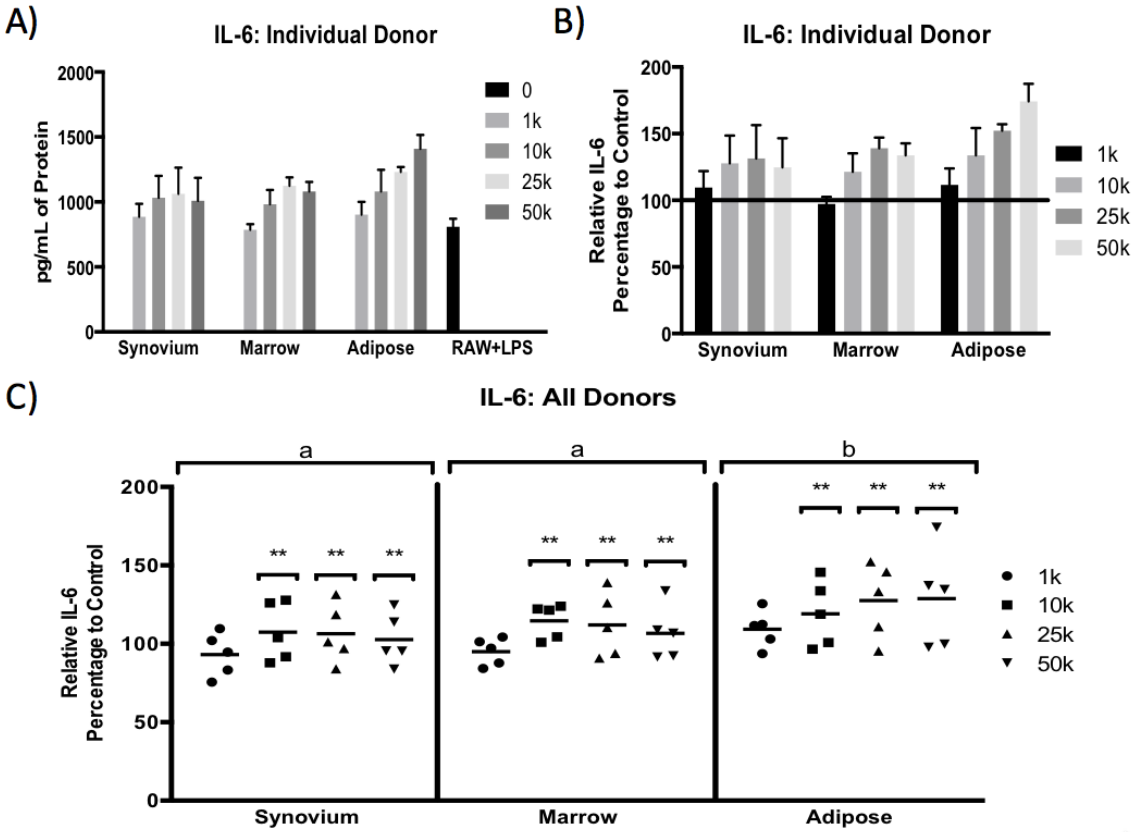

Figure 3.10. *Immunomodulation of murine IL-6 by synovium, marrow, and adipose cMSCs.* Passage 2 cMSCs ($1x10^3$–$50x10^3$) were co-cultured with $1x10^4$ murine macrophage cells in in CCM (n=3 wells/condition). After 24hrs, LPS (0.5µg/mL) was added to co-cultures to activate macrophages and to assess cMSCs immunomodulation. After 18hrs in LPS stimulated co-culture, media were collected and ELISA performed to determine the concentration of secreted murine IL-6. **A)** Representative murine IL-6 concentrations (mean ± SD) for an individual donor. RAW + LPS denotes IL-6 concentration from murine macrophages (RAW cells) in the absence of cMSCs (positive control). **B)** Data from panel A were transformed to reflect the percentage change in IL-6 relative to the RAW + LPS positive control in preparation for comparative analysis across all 15 cMSC preparations and are reported as mean ± SD. **C)** Scatter plots demonstrating the percentage change in IL-6 concentration relative to positive control for all 15 cMSC preparations, organized by tissue an number of cMSCs present within co-cultures. Each data point represents the relative murine IL-6 for an individual cell preparation and "dose" of cMSCs (bar=mean across the 5 donors). For all three tissues, IL-6 concentrations significantly increased in response to increasing number of co-cultured cMSCs. While cMSCs resulted in a dose-dependent increase in measured murine IL-6, adipose cMSCs had the largest effect. Asterisks denote significant differences between numbers of co-cultured cMSCs: (**) $p<0.01$, (***) $p<0.001$. Letters a and b denote significant differences in IL-6 concentrations ($p<0.05$).

modulating macrophage-mediated inflammation in the described in vitro co-culture system. Furthermore, it appears the cMSCs obtained from synovium, marrow, and adipose tissues are able to modulate murine TNF-α levels. Interestingly, we also assayed co-culture conditioned media for murine IL-6 (Figure 3.10). In contrast to TNF-α results, co-culture of cMSCs with murine macrophages activated with LPS resulted in an increase in the detected concentration of murine IL-6, a finding that has yet to be reported in other species. As shown in Figure 3.10C, co-cultures containing adipose derived cMSCs contained significantly higher levels of IL-6 when compared to the other tissue types ($p<0.001$). Collectively, these results indicate that cMSCs are indeed capable of modulating an LPS-mediated inflammatory response in the in vitro setting, and that when co-cultured with cMSC, murine macrophages may differentially modulate specific inflammatory cytokines.

DISCUSSION

While a modest number of studies have described the isolation and multi-lineage differentiation of canine MSCs derived from various mesenchymal tissues, selecting the ideal MSC tissue source for specific translational studies remains a challenge due to donor variation, small sampling size, tissue comparison discrepancies, differences in cell isolation and culture techniques, and diverse tri-lineage differentiation protocols. Existing canine studies often utilize differentiation protocols developed for human MSCs, despite evidence that human MSC protocols may not be completely effective for differentiation of canine MSCs (Kisiel et al., 2012; Volk et al., 2005). Canine MSCs

appear to require rhBMP-2 supplementation for consistent osteogenic differentiation (Volk et al., 2005; Volk et al., 2012); in addition, optimization of lineage specific media including pantothenate, biotin, rosiglitazone, and insulin are needed for consistent adipogenic differentiation (Al-Nbaheen et al., 2012; Csaki et al., 2007; Kisiel et al., 2012; Neupane et al., 2008; Park et al., 2012; Schwarz et al., 2012; Volk et al., 2012). Additionally, the immunomodulatory effects of MSCs have received much recent attention in human, murine, and equine MSCs (Carrade et al., 2012; English, 2012; Le Blanc, 2003). To the authors' knowledge, immunomodulatory experiments have not been included in prior donor-matched canine MSC characterization studies.

Given the unique properties of cMSCs, the objective of this study was to comprehensively characterize canine MSCs isolated from synovium, bone marrow, and adipose tissue using a donor-matched study design and assays optimized for the canine species. We hypothesized that given the differences among donor and tissue source, significant differences would exist in the properties of these cells. Canine MSCs were successfully isolated from all donor tissues. While the resulting 15 cMSC preparations met established criteria for MSCs, there were significant differences in isolation numbers, CFU potential, proliferation rates, and tri-lineage differentiation. Therefore, we were unable to reject our hypothesis.

MSCs were first isolated from bone marrow and adipose tissue (Friedenstein et al., 1970; Zuk et al., 2002). It was subsequently discovered that MSCs are present in many adult mesenchymal tissues such as: synovium, periosteum, muscle, and dental pulp (Kisiel et al., 2012; Pierdomenico et al., 2005). We selected synovium, bone

marrow, and adipose tissue for extensive characterization because of the strong clinical interest, the likely use of these tissues in translational canine studies, the ability to acquire these tissues using minimally invasive techniques such as bone marrow aspiration or arthroscopy, and the ability of these tissues to produce robust numbers of MSCs.

The canine MSCs isolated from five adult dogs in this study were spindle-shaped, adherent to tissue culture plastic, exhibited positive plasticity-associated markers, and demonstrated CFU capability. Digests of synovium and subsynovial tissues produced the highest number nucleated cells per gram of tissue. Furthermore, nucleated cells isolated from synovial digests exhibited a significantly higher CFU efficiency (~6.5%) as compared to adipose tissue digests (~2.6%). These results indicate that synovium is a potentially suitable alternative to marrow or adipose tissue and, consistent with reports in humans, synovial tissue contains high numbers of MSCs (Fan et al., 2009; Mochizuki et al., 2006; Sakaguchi et al., 2005). Although bone marrow aspirates produced a large number of nucleated cells, the CFU efficiency (~0.01%) of bone marrow was approximately 100-fold less than synovium or adipose tissue, a finding that is well described for human bone marrow MSCs.

Canine MSCs were characterized for surface epitopes using flow cytometry. As has been described in other species, canine MSCs were consistently $CD34^-$, $CD45^-$, $CD9^+$, $CD44^+$, and $CD90^+$. Whereas all cell preparations were strongly positive for CD9, CD44, and CD90, the frequency of CD105 (Endoglin) staining varied dramatically. CD105 values for our five canine donors ranged from 16-75% for synovium, 3-25% for

bone marrow, and 48-89% for adipose tissues. The diverse CD105 results obtained on our passage 2 cMSCs indicates that subsequent to isolation and expansion, the tissue of origin affects the epitope profile of canine MSCs (Figure 3.2, Table 3.2). It is also possible that the reduced CD105 staining of our canine MSCs may represent incomplete antibody binding to the canine CD105 epitope, as commercially available antibodies designed for other species were used to evaluate our canine cells. Lastly, the cMSCs examined in this study were negative for STRO-1, regardless of cell source. While STRO-1 has been linked to colony-forming osteogenic progenitor cells from humans (Gronthos et al., 1994; Gronthos et al., 1999), STRO-1 may be rapidly lost in culture (Stewart et al., 1999). Additional studies report variable STRO-1 staining of human marrow and adipose MSCs (Colter et al., 2001; Gronthos et al., 2001; Hung et al., 2002; Zuk et al., 2002), and negative STRO-1 staining of human synovial MSCs (Sakaguchi et al., 2005). The STRO-1 antibody used in the present study did not label any of the 15 cMSC preparations, despite staining canine peripheral blood mononuclear cells (data not shown). Our ability to perform more extensive epitope characterization via flow cytometry was limited by access to commercially available antibodies capable of cross-reacting with canine isoforms of additional cell surface epitopes. The flow cytometry reagents and methods described in the present report should prove useful to investigators attempting to characterize cMSCs via flow cytometry.

The ability of MSCs to self-renew and rapidly expand in culture is of considerable importance when selecting a potential tissue source for MSC translational studies. The present study assessed short and long-term proliferation using a donor-

matched study design. For all five canine donors, adipose and synovium proliferated more rapidly when compared to marrow derived MSCs. In our short-term assay, we utilized DNA quantification to assess proliferation of cMSCs plated at clonal density of 100 cells/cm^2 (350 cells/3.5 cm^2 well) over a 10-day time course. Using this method, adipose cMSCs proliferated more rapidly than synovium, and synovium more rapidly than marrow MSCs, although the latter finding was not statistically significant. Importantly, regardless of their source, substantial cMSCs proliferation is observed from day five to day ten, consistent with the lag and logarithmic phases of proliferation reported in human MSCs (Sakaguchi et al., 2005). In our long-term passaging assay, cMSCs were plated at 100 cells/cm^2 (15,000 cells/150 cm^2 plate) and assessed by manual counting over five sequential passages to simulate large scale expansion. Population doubling of synovium, marrow, and adipose cMSCs were significantly different. Population doubling of all cell preparations decreased with subsequent passages. Adipose and synovium cMSCs exhibited significantly higher population doubling rates as compared to marrow cMSCs. Additionally, the long-term passaging assay confirmed the finite capacity of cMSCs to self-renew, a known property of MSCs in other species. The discrepancy in proliferation between the short term proliferation assay (day 0-10) and our long-term passaging assay (day 0-5) can be contributed to the difference in methods utilized for quantifying MSCs and the total number of cells seeded in each assay (350 total cells assayed by fluorometric DNA quantification versus 5,500 total cells assayed over time via manual counting). Collectively, our results indicate that

if rapid proliferation of cMSCs is needed for a specific translational application in the dog, adipose and synovium should be considered as the source of MSCs.

An important criterion of MSCs is the ability to differentiate from a progenitor state to a cell with a specific mesenchymal lineage. Our goal was to describe optimized differentiation assays relying heavily on existing canine MSC differentiation literature (Neupane et al., 2008; Volk et al., 2005; Volk et al., 2012) and to evaluate tri-lineage differentiation of cMSCs using our donor matched study design and multiple canine donors. This optimization involved development of specific plating densities, FBS ratios, application of matrix substrates, mechanical scoring of well, and development of ideal differentiation media "recipes" to improve the differentiation of cMSCs. We believe the methods and results reported herein will be useful for investigators unfamiliar with MSCs, as well as for investigators relying heavily on in vitro differentiation results to select a source of cMSCs for translational studies.

We examined the adipo-, osteo-, and chondro-genic differentiation capabilities of 15 preparations of canine MSCs. Adipogenic differentiation was confirmed in all cell preparations using the optimized adipogenic protocol. Importantly, the morphology and size of lipid vacuoles produced after adipogenic differentiation varied based on the tissue source of cMSCs. Adipose and synovium cMSCs produced classic, large, grape-like lipid clusters compared to the small, diffuse vacuoles produced by bone marrow derived cMSCs. These morphologic findings were confirmed by quantification of Oil Red O staining. The superior adipogenic differentiation of adipose-derived MSCs is not surprising due to the pericellular cues that are likely provided to adipose cMSCs in their

native environment. Interestingly, synovium performed as an intermediate in adipogenic assays, forming large grape-like lipid vacuoles, but forming them with less frequency when compared to adipose tissue. Additional mechanistic studies evaluating the PPARγ signaling axis would be necessary to further assess our findings.

Our lab is specifically interested in use of cMSCs in translational bone healing studies. In order to determine if an ideal tissue source exists for these studies, we compared the osteogenic differentiation of cMSCs isolated from synovium, marrow, and adipose tissues using a short-term kinetic ALP activity assay and the long-term monolayer ARS mineralization assay. While quantifiable PCR and microarrays are considered by some to be more modern methods of assessing osteogenic differentiation of MSCs, generating and validating canine PCR primers can be a challenge due to the fact that the sequence of many canine mRNA transcripts associated osteogenic differentiation are predicted sequences based on whole-genome sequencing. We selected the ALP activity assay because it is a kinetic assay requiring living cells to catabolize an ALP substrate. This assay has been shown to detect early osteogenic differentiation due to the fact that ALP is required to hydrolyze phosphate for eventual bone mineralization in the form of calcium phosphate deposition (Alves et al., 2011; Ashton et al., 1985; Brey et al., 2010) and it has been previously evaluated in the canine MSC literature (Volk et al., 2005; Volk et al., 2012). In 2005, Volk assessed the osteogenic differentiation of canine marrow MSCs and demonstrated that a combination of ascorbate-2-phosphate and rhBMP-2 were necessary to detect ALP activity in early osteogenic marrow-derived cMSC cultures (Volk et al., 2005). The results of the present

study evaluating 15 cell lines from three canine mesenchymal tissues confirm that rhBMP-2 supplementation is necessary to detect ALP activity in early canine osteogenic cultures. One potential explanation for our findings and those of Volk is: species-specific differences in bone biology or the loss of BMP-2 expression after cMSC isolation and culture result in an absence of endogenous (cMSC derived) BMP-2 in canine osteogenic differentiation cultures.

Early osteogenic differentiation as assessed by ALP activity was widely variable across the three tissue sources of cMSC. While none of the cMSC cell preparations displayed ALP activity in control (CCM) or OBM at seven days of culture, synovium and bone marrow cMSCs exhibited a strong response to rhBMP-2 when compared to adipose derived MSCs, with bone marrow consistently exhibiting the highest ALP activity within each donor. These findings are not surprising given that adipose MSCs were isolated from fat, and that signaling pathways such as PPARγ compete with osteogenic signaling pathways such as canonical Wnt during differentiation (Bennett et al., 2002; Farmer, 2005; Krause et al., 2010; Moldes et al., 2003; Takada et al., 2009a; Takada et al., 2009b). Interestingly, all three tissue sources of cMSCs produced calcium-binding mineral in long-term monolayer cultures, although mineralization did not occur in cultures in which rhBMP-2 was not supplied (not shown). Using quantification of ARS, adipose and synovium cMSCs demonstrated higher ARS values in some donors, although these differences were not significant when evaluated collectively across all donors. Our long-term osteogenic results suggest that while adipose cMSCs appear to be refractory to early osteogenic differentiation (even in the presence of rhBMP-2), adipose

derived cMSCs are capable of transitioning to osteogenic cultures over time. Alternatively, adipose derived cMSCs may utilize alternative mineralization pathways in vitro, such as the pathways associated with dystrophic mineralization of vascular calcification (Doherty et al., 2003; Vattikuti and Towler, 2004). Thus, investigators considering adipose tissue as a source for cMSC osteogenic cells should closely consider both osteogenic induction media and number of days in culture to optimize osteogenic differentiation. The performance of synovium cMSCs in our osteogenic assays was not surprising given the prior synovium MSC literature (Innes et al., 2013; Sakaguchi et al., 2005; Yokoyama et al., 2005). Synovium MSCs have been shown to exhibit robust ARS stain in long-term cultures (Sakaguchi et al., 2005), although to our knowledge early osteogenic differentiation of synovium MSCs has not been previously examined using the ALP activity assay.

In contrast to the adipogenic and osteogenic differentiation assays, the well-described serum-free micromass chondrogenesis technique did not require major adjustments for use with cMSCs. Using this technique, all fifteen cMSC preparations formed chondrogenic pellets. When assessing pellet size using morphometry, synovium and adipose cMSC produced larger pellets as compared to bone marrow, but demonstrated reduced staining for proteoglycan (toluidine blue) and collagen type II when assessed histologically. Despite their small size, bone marrow derived chondrogenic pellets were the only cell preparations to consistently have intense staining for proteoglycan (toluidine blue) and collagen type II (immunohistochemistry); however, one obvious limitation regarding the chondrogenic capacity of marrow cMSCs is the

reduced pellet size when compared to synovium and adipose cMSCs. Synovium provided intermediate chondrogenic results, with pellets considerably larger than those produced by marrow cMSCs containing toluidine blue and collagen type II staining slightly reduced as compared to marrow cMSCs. Additional work is necessary to optimize cMSC chondrogenesis to produce larger micromass pellets with high intensity staining for proteoglycans and collagen type II for canine translational cartilage repair studies.

Many investigators now include immunomodulatory capacity as an inherent characteristic of MSCs, but this has not been substantially documented for cMSCs. Therefore, our goal was to determine whether cMSCs from various sources had the universal capacity to inhibit some key features of the innate immune response and to determine if the source of cMSCs affected this process using a simplified macrophage-based assay.

In the present report, we evaluated the ability of cMSCs to modulate secretion of two key inflammatory cytokines in an LPS-induced murine macrophage (RAW cell) co-culture system. When LPS was added to RAW cells, there was a robust secretion of TNF-α that could be measured by ELISA. Inclusion of cMSCs resulted in a significant and dose-dependent decrease in the measured concentration of secreted murine TNF-α. Furthermore, this response was observed for all 15 cMSC cell preparations and the tissue source of cMSCs did not appear to affect the reduction of measured TNF-α.

It has recently been suggested that MSCs are not constitutively immunosuppressive and require activation or licensing to initiate immunomodulatory

effects (English, 2012; English et al., 2007; Liotta et al., 2008). Our immunomodulation results portray that activation of specific toll-like receptors (TLRs) may license MSCs differently, with TLR3 activation driving anti-inflammatory properties, and TLR4 activation leading to a pro-inflammatory response through IL-6, IL-8, or TGF-β production (English, 2012; Németh et al., 2008). TLRs have been implicated in this process, and LPS is a known ligand of TLR4. Although LPS has been shown to activate through ligand-receptor binding, recent studies depict non-canonical pathway signaling in which immune response is elicited without LPS-TLR4 binding (Kayagaki et al., 2013; Waterman et al., 2010). This differential licensing through canonical and non-canonical mechanisms may explain our IL-6 results, namely that inclusion of cMSCs in LPS-stimulated co-cultures resulted in an increase in the measured concentration of murine IL-6. The rationale for increased production of IL-6 in response to MSCs exposed to inflammatory stimuli has been to initiate a pro-inflammatory pathogen clearance mechanism (Bouffi et al., 2010). This may occur through the NF-κβ pathway and PGE production (Choi et al., 2011; Németh et al., 2008) but further studies are needed to fully appreciate the primary signaling pathways.

In conclusion, in this study we successfully isolated MSCs from canine synovium, bone marrow, and adipose tissues. While all cMSC preparations exhibited characteristics of MSCs using *in vitro* assays optimized for the canine species, both tissue of origin and donor affected cMSC performance. Synovium cMSCs exhibit robust short- and long-term osteogenic differentiation. Combining their ease of isolation, CFU potential, rapid proliferation, and presence within the intra-articular niche, synovium

MSCs appear to be an excellent choice for orthopedic translational cell-based studies. While marrow cMSCs have a lower CFU potential and proliferate more slowly, our findings indicate that marrow cMSCs are capable of marked short-term and long-term osteogenic differentiation and produce chondrogenic pellets that stain intensely for proteoglycan and collagen type II, making bone marrow an excellent source of cMSCs for orthopedic applications. Given the inability of adipose cMSCs to demonstrate detectible ALP activity even in the presence of substantial BMP-2 supplementation, adipose tissue may not be an ideal source for osteogenic cells if short-term cultures are required; however, adipose tissue produces large numbers of cMSCs with high CFU and proliferation potential. Moreover, adipose cMSCs produce calcium rich long-term monolayer osteogenic cultures, and thus may be suitable for long term culture of tissue engineering constructs. Interestingly, cMSCs isolated from synovium, marrow, and adipose tissue appear to modulate TNF-α levels in LPS-stimulated macrophage co-culture assays, suggesting that all tissue sources may be useful in immunomodulatory translational studies. Our results provide insight into important similarities and differences between cMSCs and will prove useful for investigators considering these canine tissues for large animal translational studies.

CHAPTER IV

COMPARISON OF CONVENTIONAL AND NOVEL FABRICATION METHODS FOR POLYETHYLENE GLYCOL DIACRYLATE (PEG-DA) HYDROGELS AS THREE-DIMENSIONAL (3D) SCAFFOLDS FOR CANINE ARTICULAR CARTILAGE TISSUE ENGINEERING

SUMMARY

Tissue engineering approaches using 3D scaffolds and progenitor cells, such as multipotent stromal cells (MSCs), represent a promising treatment for restoring the osteochondral interface in focal cartilage lesions. Synthetic hydrogel scaffolds constructed of poly(ethylene)glycol-diacrylate (PEG-DA) have been extensively investigated for numerous applications, including cartilage tissue engineering. In an effort to extend their properties, our collaborative group, led by Dr. Melissa Grunlan recently developed a method of fabricating PEG-DA hydrogels using solvent induced phase separation (SIPS) with a solvent-casted particulate-leaching system (SCPL), thereby creating a series of tunable interconnecting pores throughout the scaffold to improve opportunities for cell proliferation, migration, and tissue in-growth. The presence of pores within PEG-DA hydrogel scaffolds has the potential to confront several limitations of conventional fabrication methods. Addressing the inability of cells to migrate within the construct in addition allowing for host tissue to migrate into the scaffold. While this SIPS/SCPL-PEG-DA system holds much promise, the ability of SIPS/SCPL-PEG-DA hydrogels to serve as viable scaffolds for cells has yet to be examined. The objective of this study was to compare PEG-DA hydrogels fabricated with “conventional” photoinitiators, Igracure 651 or Igracure 2959, and the novel

SIPS/SCPL hydrogels as putative scaffolds for cell adhesion, survival, and proliferation in preparation for articular cartilage tissue engineering work. The secondary objective of this study was to evaluate the biocompatibility of PEG-DA hydrogel scaffolds in vivo. Due to our lab's expertise and long-term goals, we utilized bone marrow cMSCs for in vitro studies. Using a 21-day time course, cell-scaffold co-cultures were assessed with live-dead staining, lactate dehydrogenase (LDH) cytotoxicity assay, proliferation, storage modulus, and SEM. Canine MSCs seeded on SIPS/SCPL-PEG-DA hydrogels exhibited significantly greater proliferation when compared to those photoencapsulated within conventional hydrogels. Cell attachment, spreading, and proliferation on SIPS/SCPL-PEG-DA were confirmed using SEM. Canine MSCs cultured on SIPS/SCPL-PEG-DA hydrogels exhibited minimal cytotoxicity when assessed by live-dead staining, whereas those cultured within conventional hydrogels demonstrated substantial cytotoxicity. These findings were confirmed using the LDH assay. Lastly, using the rat subcutaneous and intra-articular implant models, SIPS/SCPL-PEG-DA hydrogels were biocompatible, as determined by an appropriate vascular, cellular, and fibrous tissue response 21 days post-implantation. In summary, this study demonstrates that the fabrication method of PEG-DA hydrogel scaffolds has important effects on cMSC survival and proliferation. PEG-DA hydrogels fabricated via SIPS/SCPL may be preferential to conventional PEG-DA hydrogels for articular cartilage tissue-engineering scaffold studies utilizing cMSCs.

INTRODUCTION

Articular cartilage has poor intrinsic healing potential. Consequently, developmental and degenerative joint diseases in humans and veterinary species, such as OC and traumatic joint injuries, are chronic and progressive diseases. They are characterized by articular cartilage degradation, thinning, inflammation, and fibrosis. Regardless of the inciting cause (trauma, OC, genetics, cyclical fatigue over time, etc.), focal articular cartilage lesions predictably progress to widespread, generalized OA of the joint. The global economic impact of OA in humans has been estimated to be 60 billion dollars per year (Buckwalter et al., 2004). In the United States alone, approximately 52.5 million adults are affected by OA and an estimated growth to 67 million by 2030 is predicted (Barbour et al., 2013). In the domestic veterinary species, approximately 70% of canines over two years of age are also afflicted by OA. OA affects quality of life, economic productivity, and life expectancy in humans and domestic animals (Woolf and Pfleger, 2003; Ytrehus et al., 2007). Additionally, high OA prevalence in dogs places considerable strain on the medical system and financial burden on clients/owners without many viable treatment options.

Traditional treatment of small, focal cartilage lesions are divided into two broad categories: medical management and surgical intervention. Medical management through use of NSAIDs or corticosteroids focuses on alleviation of pain and reduction of joint inflammation. Although effective, medical management typically requires life-long treatment (Moran et al., 2003). Long-term administration of medications such as NSAIDS and corticosteroids carries some risk of major complications due to significant

side effects. Additional medical management options can be explored for patients who fail to respond completely to oral medications; including direct injection of joint lubricants or anti-inflammatory agents, physical therapy, weight management, and non-traditional treatments such as acupuncture (Adams et al., 1995; Brandt et al., 2000; Christensen et al., 2005; Katz et al., 2013; Takeda and Wessel, 1994).

Due to the fact that medical management is not a curative treatment, surgical intervention often becomes necessary. The first line of defense for early, focal cartilage lesions and OA focus on minimally invasive surgical treatments such as arthroscopic surgical debridement, microfracture to induce fibrocartilage formation, OAT, and ACI. While these treatments are minimally invasive and provide short-term alleviation of pain, they may not provide the desired long-term resolution of symptoms and clinical signs. Thus, major surgical intervention becomes necessary. These treatments include partial or total joint replacement. Although joint replacement can be highly effective, it is costly and not without its own complications such as incomplete restoration of function, implant loosening, infection, luxation, or fracture (Clohisy et al., 2004; Ranawat, 1986).

Translation of promising treatment strategies for articular cartilage injuries from rodent models to humans represents a significant hurdle for cell-based therapies. While a number of large animal species have been used to bridge the gap from rodents to humans (Hatsushika et al., 2014; Horie et al., 2009; Horie et al., 2012b; Kon et al., 2000; Murphy et al., 2003), the dog represents the most compelling model species for cell-based tissue engineering studies. A recent review highlights the advantages of using dogs and other

companion animals for translational cell-based clinical trials (Hoffman and Dow, 2016). From a biomechanical perspective, the canine skeleton undergoes loading in a manner that approximates that of the human skeleton (Bergmann et al., 1984; Liebschner, 2004). In addition, due to their response to learned behaviors such as treadmill exercise, dogs have been used to develop new therapies for cardiovascular and orthopedic diseases (Bockstahler et al., 2007; Kiviranta et al., 1988). For these reasons, canine models of osteoarthritis, anterior cruciate ligament repair, meniscal injury, and non-union fractures are well described (Arnoczky and Warren, 1983; Johnson et al., 1989; Liu et al., 2006; Nelson et al., 1988; Pond and Nuki, 1973; Shortkroff et al., 1996). For many of these reasons, the occurrence of adverse events in canine clinical trials appears to more reliably predict adverse events in humans. As such, performing clinical trials in dogs may allow investigators to more effectively identify and predict adverse events in humans.

Due to the limitations of current treatment options and the increasing economic impact of OA in human and veterinary populations, development of new treatment strategies, focusing on tissue repair or replacement are necessary. One increasingly popular strategy to repair or replace injured tissues is the use of regenerative medicine, specifically tissue engineering. Tissue engineering utilizes a combination of cells, scaffolds, and biologically active factors in order to repair, restore, or replace injured tissues. While not a true tissue engineering treatment, one method currently in use in human and veterinary medicine involves the direct injection of autologous or allogeneic MSCs into the injured joint (Black et al., 2008; Black et al., 2007; Ferris et al., 2014;

Guercio et al., 2012; Wong et al., 2013). Although injected cells appear to provide relief of symptoms and clinical signs, these affects are likely transient due to the rapid clearance of MSCs from the site of injection. MSCs can be obtained from a variety of tissue types (Sakaguchi et al., 2005) and are capable of in vitro (and in some cases in vivo) differentiation into specialized cells in response to environmental cues. While these characteristics make MSCs an exemplary candidate for tissue engineering, the ideal delivery method to localize cells at the site of injury has yet to be determined. Recent studies have shown over 90% of MSCs injected at a site of injury are not present 24 hours post application (Krause et al., 2010). Another experimental animal study showed that injected MSCs could not be detected at 7 days post injection in a meniscal injury model (Horie et al., 2012b) . Moreover, recent work has shown that joint fluid from dogs with OA induces substantial cytotoxicity to cMSCs (Kiefer et al., 2015). This study by Kiefer et al. certainly brings into question the efficacy of MSC injections and raises questions on the ethics of autologous MSC injections in the presence of limited evidence-based medicine (Jeffery and Granger, 2012; Prockop and Olson, 2007).

Given the current limitations of direct injection of MSCs detailed above, a tissue engineering approach involving specific scaffolds for cell retention and tissue regeneration is a promising alternative for restoring the native osteocondral interface. The current clinical focus of cartilage tissue engineering is to develop methods with consistent regenerative potential, capable of forming hyaline cartilage that can be implemented using surgically feasible techniques and ultimately, minimally invasive methods of delivery.

Current articular cartilage tissue engineering methods employ 3D scaffolds as a means of delivering cells and biologic agents. While polymers such as collagen, alginate, and polyurethane have been used in articular cartilage tissue engineering studies, the most common component of such constructs is PEG. PEG is considered the "gold standard" of synthetic biopolymers and has been extensively investigated as a scaffold material for the regeneration of numerous types of tissues (Pasut, 2014). PEG based hydrogels have been shown to be hydrophilic, tissue compatible, and tunable to necessary specifications (Bailey et al., 2012; Bailey et al., 2013; Gacasan et al., 2016; Rafat et al., 2008; Wallace et al., 2001). In particular, PEG based hydrogels are especially popular because of their immunologically inert properties, preventing non-specific protein adhesion that would induce immune and inflammatory responses (Bailey et al., 2012; Pasut, 2014). The ability of PEG based scaffolds to act as "biologic blank slates" enables targeted control of cellular response through the addition of specific cytokines and growth factors (Burdick et al., 2002; Lu and Anseth, 2000; Mason et al., 2001; West and Hubbell, 1995). This ability to incorporate the chemical and physical cues necessary for tailored cell adhesion and differentiation may allow for the creation of tissue engineering therapies customized for an individual or injury. While these properties are advantageous, PEG based scaffolds are not without limitations such as poor media exchange, oxygen inhibition at the cell-macromer interface, free radical propagation, cross-linking networks resulting in shrinkage and incomplete double bond conversion, and others (Park et al., 2007). The potential consequences of the aforementioned fabrication limitations include the inability of cells to migrate with

hydrogel constructs, increased apoptosis, and reduction of host tissue integration. Thus, current PEG fabrication methods present obstacles for cell-based scaffold advancement in tissue-engineering strategies. Further confirming these obstacles, to date, articular cartilage tissue engineering studies employing PEG scaffolds have not proven effective for restoring the osteochondral interface. This is likely due to the inability to reproduce the structure, function, and biomechanical properties of natural tissue within the scaffold, and the inability of the scaffold to interface, or bond, with healthy host tissue (de Girolamo et al., 2015).

In order to overcome the limitations of PEG-DA scaffolds fabricated through conventional methods, our collaborative group, led by Dr. Melissa Grunlan, developed a series of novel PEG hydrogel fabrication technique termed SIPS/SCPL (Bailey et al., 2012; Gacasan et al., 2016). This method creates a series of interconnecting pores within the scaffold with the goal of enhancing cell attachment, proliferation, migration, and tissue ingrowth (Gacasan et al., 2016). In the present study we compared PEG-DA hydrogels fabricated with conventional methods to SIPS/SCPL-PEG-DA hydrogels as putative scaffolds for cMSCs tissue engineering constructs. Our null hypothesis is that fabrication method would have no effect on cell attachment, cytotoxicity, proliferation, or mechanical properties of cell-hydrogel constructs. Results detailed herein identify a synthetic hydrogel scaffold fabrication system that is compatible with cMSCs and is shown to integrate with surrounding tissue when implanted into a rat model. Our results provide insight into hydrogel fabrication techniques in combination with cMSCs, this work will prove useful for further articular cartilage tissue engineering strategies.

MATERIALS AND METHODS

Tissue Collection and Cell Isolation

Passage 1, bone marrow-derived cMSCs were thawed and expanded as previously described in Chapter III. The clinical portion of this study was performed under the supervision of the Texas A&M University IACUC and an AUP (2015-0072). Briefly, canine bone marrow was obtained via bone marrow aspirate of the proximal humerus using a 15 gauge Illinois biopsy needle while under general anesthesia. Nucleated cells were isolated from bone marrow using gradient centrifugation (Ficoll-Paque Plus, GE Health Care Biosciences, Piscataway, NJ) using previously described techniques (Pittenger, 2008). Following centrifugation at 1800 x g for 30 minutes, mononuclear cells were removed, washed twice with 15mL of Hank's Balanced Salt Solution (HBSS, Invitrogen, Carlsbad, CA), quantified, and assessed for viability using a hemocytometer and trypan blue exclusion. Nucleated marrow cells were plated at 30,000 cells/cm^2 in 150 mm diameter tissue culture dishes in CCM containing α-MEM, 100 units/ml penicillin, 100 μg/ml streptomycin (Invitrogen), and 10% premium select fetal bovine serum (PS-FBS; Atlanta Biological, Inc., Flowery Branch, GA). Cells were incubated at 37°C and 5% humidified CO_2 for 24 hours. Plates were washed with PBS to remove non-adherent cells followed by media exchange. This process was repeated daily for two additional days. Culture dishes were subsequently monitored for expansion of the primary cell population (Passage 0) with media exchange performed every other day. Upon reaching 70% confluence (5-12 days) cells were lifted with 0.5% trypsin/EDTA solution (Invitrogen) and re-seeded at 100 cells/cm^2 for expansion of Passage 1 cells.

Media exchanged was performed every other day until 70% confluence was reached. Passage 1 cells were cryopreserved in α-MEM with 5% DMSO (Sigma-Aldrich, St. Louis, MO) and 30% FBS in preparation for subsequent experiments. For these assays, passage 1 cells were thawed, plated, and subsequently expanded as passage 2 cultures. Cells were confirmed as MSCs using the classification as described by Dominic et al. in 2006 (Dominici et al., 2006). This included morphological assessment, colony forming capacity, flow cytometry, and tri-lineage differentiation. Prior to each experiment, passage 2 cMSCs were washed with PBS, trypsinized (Invitrogen), neutralized with FBS, and centrifuged. Cells were washed in an additional 10 mL volume of α-MEM to remove residual serum and subsequently counted via hemocytometer in preparation for hydrogel studies.

Polyethylene Glycol Diaacrylate (PEG-DA) Synthesis

PEG-DA (3.4kDa) was synthesized as previously reported (Bailey et al., 2012). Briefly, PEG-3400 (23.5 g, 7.0 mmol), Et_3N (1.95 ml, 14.0 mmol) and acryloyl chloride (2.27 ml, 28.0 mmol) were reacted overnight under N2 atmosphere to obtain PEG-DA. The product was washed with K_2CO_3, precipitated in ether and dried under reduced pressure (14.7 psi) (13.8 g, 59% yield). 1H-NMR end-group analysis determined the M_n of resultant PEG-DA to be 3393 g/mM (~3400 g/mM).

"Conventional" Hydrogel Fabrication with Encapsulation of cMSCs

Hydrogels containing cMSCs were fabricated in planar slab formation as previously described(Munoz-Pinto et al., 2012). Briefly, hydrogels were prepared by the

photopolymerization of: PEG-DA (3.4 kDa), ACRL-PEG-DA-RGD (3.9 mg/mL), PBS, and one of two photoinitiators (10µL/mL). Photoinitiators consisted of either 1) Igracure 651: consisting of 2,2-dimethyl-2-phenyl-acetophenone (DMAP, Sigma-Aldrich, St. Louis, MO) in 1-vinyl-2-pyrrolidinone (NVP, Sigma) or 2) Igracure 2959: consisting of 100mg 2-hydroxy-4'-(2-hydroxyethoxy)-2-methylpropiophenone in 70% ethanol. PEG-DA Solutions were prepared using 10% weight by 90% volume ratio of PEG-DA to PBS, and photoinitiator sequentially added at 10µL/mL. Final solution was vortexed and .22µm polyethersulfone (PES) membrane filtered. Sterile precursor solution was used to resuspend cells at a concentration $1x10^6$ cMSCs/mL. After cell resuspension, solution was immediately added to 1.5mm prefabricated glass molds and exposed to longwave ultra-violet (UV) light (UV-Transilluminator, 6mW/cm2, 365nm). Using Igracure 651, UV exposure was limited to 2 minutes, while the use of photocatalyst Igracure 2959 required UV exposure for 6 minutes. After removal from the mold, 1.5mm thick planar gels were washed in PBS and 8mm diameter disks created using a sterile skin biopsy punch (Acuderm; Fort Lauderdale, FL). 1.5mm x 8mm disks were transferred to sterile 48-well non tissue-culture polystyrene wells for long-term culture and experimental analysis.

SIPS/SCPL Hydrogel Fabrication and cMSC Seeding

Cylindrical porous hydrogel constructs were fabricated as recently described (Gacasan et al., 2016) by first placing 3g of a 5% weight NaCl to water mixture into a 3mL glass vial (OD = 15 mm) with the appropriate salt size. The mixture was then centrifuged (4000 RPM, 10 minutes) and dried overnight at room temperature creating a

salt template. Precursor solutions were prepared at total macromer concentrations of 30% weight 3.4 kDa PEG-DA to total mass of solution in dichloromethane (DCM) with 10μL of photoinitiator (30% weight DMAP in NVP) per milliliter of solution. Solutions were added to the salt template (~1 mL), sealed, and centrifuged at 2000 rpm for 5 minutes to distribute the macromer solution. The vials were subsequently cured for 6 minutes via exposure to ultra-violet light (UV-transilluminator, 6 mW cm-2, 365nm). After air-drying overnight to remove solvent, hydrogel cylinders were removed from the vial, sectioned to 1.2mm using a vibratome (LEICA VT1000S), and subsequently soaked in deionized (DI) water for 48 hours at 100rpm to allow for swelling and leaching of salt, remaining DCM, and any impurities to create hydrated disks (15mm diameter x 1.5mm height). After final elution, hydrogels were sterilized with room temperature incubation of 70% ethanol washes at 2-, 4-, and 18-hours with PBS washes occurring between. Following the 18-hour ethanol wash, two PBS washes were performed with additional overnight PBS wash. At the end of final PBS wash, 1.5mm high x 8mm wide disks were created using a sterile skin biopsy punch as described above. Individual disks were transferred to 48-well plates, $1x10^4$ bone marrow MSCs in 50μL of CCM were applied to the monolayers of each disk. Cell seeded hydrogels were allowed 30 minutes of incubation before adding 500μL of CCM to each well.

Cell Adhesion and Visual Assessment of Viability

Cell seeded hydrogels were prepared as described above and cultured in CCM containing 10% FBS. After 1-, 3-, 10-, and 21-days (n=3 gels per time point) medium was removed and two PBS washes performed. After final PBS wash, medium was

removed and 500 μL of fresh PBS containing 0.2 μM calcein (Sigma) and 100μg/mL propidium iodide (Botinium, Hayward, CA) were added to each hydrogel. Hydrogels were incubated at 37°C for 30 minutes and evaluated for live/dead staining using an Olympus microscope and fluorescent microscopy. Images were merged and overlays produced using SPOT software (version 5.1; Sterling Heights, MI).

Cytotoxicity

Hydrogels containing cMSCs were cultured for 24- and 72-hours without media exchange to assess cytotoxicity. At day 1 and 3, conditioned culture media (n=3) were collected in 200μL aliquots and stored at -20°C. Media was allowed to thaw on ice and assessed for LDH levels following manufacturer's instructions for an LDH Cytotoxicity assay kit (Roche, Indianapolis, IN). As a cellular and comparative control, conditioned media were also collected from passage 2 cMSCs cultured on traditional two-dimensional (2D) tissue-culture plastic.

Cell Proliferation

To assess proliferation of cMSCs on conventional vs. SIPS/SCPL PEG-DA hydrogel scaffolds, cMSCs were encapsulated or seeded as described above in triplicate. At pre-determined time points (1, 3, 10, and 21 days) hydrogels were washed with PBS, transferred to 1.7mL Eppendorf tubes, and placed in DNA quantification buffer consisting of: 500μL PBS containing (100mM) Trizma HCL (Sigma) and (1mM) Magnesium Chloride (Sigma) as previously described (Krause et al., 2011). After application of DNA quantification buffer, hydrogels were manually homogenized with RNAse free (pestles) and stored at -20°C. On the day of analysis, samples were allowed

to thaw to room temperature. Collagenase (1mg/mL; Sigma), *Hind*III (1U/mL, Invitrogen, Carlsbad, CA), and *Eco*RI (1U/mL; Invitrogen) were added to the sample tubes and allowed to incubate at 37°C overnight. The following morning tubes were centrifuged at 15,000 X g for 20 minutes and supernatant suspensions transferred to an opaque 96-well plate. Sytox Orange (Life Technologies) was added to samples at a 1:1000 dilution and absorbance determined via automated plate reader (HT Synergy, BioTek, Winooski, VT) and Gen3Bio software. Individual cell numbers were determined by referencing a pre-determined linear standard curve containing a known number of cMSCs.

Scanning Electron Microscopy

At pre-determined time points (1, 3, 10, and 21 days), hydrogel disks containing cMSCs were washed twice with PBS and fixed with 4% paraformaldehyde (Electron Microscopy Sciences; Hatfield, PA) for one hour at room temperature. Afterwards, disks were dehydrated in a graded ethanol series. Following the final dehydration step, hydrogels were flash frozen in liquid nitrogen for one minute and lyophilized overnight at -50°C and 0.02mBar of vacuum (Labconco Centri Vap Gel Dryer System, Kansas City, MO). The following day, hydrogels were gold sputter coated and imaged with a field emission scanning electron microscope (FEI Quanta 600 FE-SEM) at an accelerated electron energy of 10keV as previously described (Bailey et al., 2012).

Dynamic Mechanical Analysis

At pre-determined time points (1, 3, 10, and 21 days), three groups of hydrogel disks (n=5 disk/group) were analyzed for biomechanical properties over time. Groups

consisted of: 1) hydrogel disks without cells, cultured in CCM; and 2) hydrogel disks containing cMSCs, cultured in CCM. Prior to analysis, culture media were removed and hydrogel disks manually blotted for preparation of compression analysis. Compression analysis was performed as previously described (Bailey et al., 2013). Storage modulus (*G'*) was measured in compression with a dynamic mechanical analyzer (TA Instruments Q800) equipped with parallel-plate compression clamp with a diameter of 40mm (bottom) and 15mm (top). Disks samples were clamped between plates, and tested in a multi-frequency strain mode (1 to 30Hz). Frequency output was quantified and mean ± standard deviation calculated.

Biocompatibility- Subcutaneous Studies

In vivo biocompatibility studies were approved by the Texas A&M University IACUC committee under protocol #2015-0072 and an approved AUP. Based on results of in vitro studies reported below, and the intended use of SIPS/SCPL-PEG-DA scaffolds in the intra-articular (IA) space, subcutaneous biocompatibility studies were limited to the SIPS/SCPL-PEG-DA hydrogel scaffolds. Based on previous studies proving the biocompatibility of PEG (Burdick et al., 2002; Wallace et al., 2001) and our efforts to reduce the number of live animals utilized in our study, we elected to limit evaluation of hydrogel scaffolds in the subcutaneous space to the SIPS/SCPL-PEG-DA condition, as this construct appeared to be most promising based on our in vitro and comparative intra-articular in vivo studies. Hydrogels were prepared as previously described and 3mm high x 6mm wide plugs were created using a sterile skin biopsy punch. Sterile plugs were implanted subcutaneously in the caudolateral area of 12-week-

old Sprague-Dawley rats (n=10 rats/treatment group). Sample size for number of rats needed was determined based on previous literature and the ISO-10993-6 standard. Anesthesia was induced via isoflurane, and a surgical plane of general anesthesia was maintained using mask inhalation of isoflurane (2%-3.5% adjusted to effect). After induction, rats received 0.05mg/kg of buprenorphine via intraperitoneal injection and 5mg/kg of enrofloxacin via intramuscular injection. In addition, rats received 5ml/kg of warm 0.9% Lactated Ringer's solution subcutaneously. The hair was clipped and removed from dorsal midline. A sterile surgical preparation was performed using alternating scrubs of chlorohexidine and sterile saline. Using sterile technique, a 3cm skin incision was made on the caudal aspect of the dorsal midline. One small subcutaneous pocket was generated on the left side of the midline using a combination of blunt and sharp dissection. A single hydrogel plug fabricated with the small pore SIPS/SCPL-PEG-DA fabrication method was applied on the left side of midline. Care was taken to place implants caudal to the last rib and cranial to the ilial wing, in a location preventing secondary trauma to the implants by hind-leg scratching. After irrigation, subcutaneous and dermal tissues were closed using 4-0 Monocryl™ suture in a simple interrupted pattern and intradermal pattern, respectively. Rats were recovered from anesthesia and observed everyday for 21 days. At 21 days, a period expected to coincide with resolution of acute inflammation, rats were humanely euthanized using CO_2 asphyxiation and fixed with 10% neutral buffer formalin in preparation for histological examination.

Biocompatibility- Intra-Articular Studies

This study was approved by the Texas A&M University IACUC committee under protocol #2015-0072 and an approved AUP. Based on results of in vitro studies reported below, and the intended use of PEG-DA scaffolds in the intra-articular (IA) space, intra-articular biocompatibility studies were performed using conventional PEG-DA hydrogels fabricated using Igracure 651 as well as hydrogels fabricated using the SIPS/SCPL-PEG-DA technique. Hydrogels were fabricated using sterile technique as described above and 3mm high x 2mm wide plugs created using a sterile skin biopsy punch. Sterile plugs were implanted into the trochlear groove of the femoropatellar joint of 12-week-old Sprague-Dawley rats. Briefly, after induction of anesthesia and pre-medication as described above, hair was clipped and removed from the left stifle followed by a sterile surgical preparation using alternating scrubs of chlorohexidine and sterile saline. Using sterile technique, a 3cm skin and subcutaneous incision was created on the craniolateral aspect of the stifle. A lateral parapatellar arthrotomy was created using a #15 blade and the patella was luxated medially. The midline of the femoral trochlea was located. A 1.94mm wide x 3mm deep defect was created within each trochlea using a high-speed drill and constant saline irrigation. A single hydrogel plug fabricated with either Igracure 651-PEG-DA or small pore SIPS/SCPL-PEG-DA was manually inserted into the defect. Care was taken to ensure the exposed surface of each gel was flush with the tangential surface of adjacent cartilage. After irrigation, joint capsule and fascia lata were closed using 4-0 Monocryl™ suture in a simple interrupted pattern. Skin and subcutaneous tissue was closed using 4-0 Monocryl in an intradermal

pattern. At 21 days, rats were humanely euthanized as described above. Operated limbs were removed and skin, subcutaneous tissues, and musculature dissected. Limbs containing the femur, tibia, patella, patellar tendon, and intact joint capsule were fixed with 10% neutral buffer formalin in preparation for histological examination.

Histologic Assessment

Following formalin fixation, femur and skin specimens containing hydrogel implants were routinely processed and slides prepared for histological evaluation. Briefly for subcutaneous samples, skin with subcutis containing the hydrogel implant were sectioned perpendicular to the skin surface through the implant, photographed to document gross appearance and hydrogel location, and routinely processed for paraffin embedding. Once embedded, serial sections (5µm thick) were created using a rotary microtome (Mirom HM 355 S, ThermoFisher Scientific, Waltham, MA). Sections were slide mounted, stained (hematoxylin: Electron Microscopy Services, Hatfield, PA and esosin: Ricca Chemical Company, Arlington, TX; or trichrome: Ricca Chemical Company), and coverslipped. Briefly, for intra-articular samples, hindlimb skin and superficial musculature was removed after formalin fixation. A micro x-ray unit (X-tek Systems, Ltd., Herts, United Kingdom) was used to take orthogonal views (lateromedial and craniocaudal) of each formalin-fixed specimen for identification of the hydrogel site. After micro x-rays, stifles with associated portions of femur and tibia were submerged in formalin decalcification solution (Formacal-4, Statlab Medical Products, McKinney, TX) and placed on an oscillating mixer for 44-52 hours. Specimens were removed from decalcification solution, thoroughly rinsed with deionized water, and placed in isotonic

phosphate-buffered saline until sectioning. Orthogonal micro x-ray images were used to approximate sagittal sectioning to create stifle hemisections. Each hemisection was routinely processed, embedded in paraffin, and serially sectioned (5μm thick) using a rotary microtome. Sections were mounted, stained, and coverslipped as described above. A board-certified veterinary pathologist and veterinary pathology resident, blinded to treatment group, evaluated each hydrogel implant using a semi-quantitative, ordinal scoring system for inflammation, angiogenesis, and fibrosis using modifications to previous described methods (Karahan et al., 2001). Within each category, the ordinal scoring systems ranged from 0-5 (0=none observed, 1=minimal, 2=mild, 3=moderate, 4=marked, 5=severe) in which zero represents complete lack of a response and 5 represents a maximum response

Statistics

Descriptive and analytic statistics for *in vitro* studies were generated and were reported as mean ± standard deviation. Results of *in vitro* assays were assessed using ANOVA and Tukey's post-hoc. For *in vivo* biocompatibility studies, ordinal data sets were compared using the Fisher's exact test. Significance was established at $p<0.05$. Descriptive and analytical statistics were performed with GraphPad Prism 6.0 (GraphPad Software, La Jolla, CA) and JMP Pro 11 (JMP® Pro 11.0.0, Cary NC).

RESULTS

Canine MSC Characterization

Marrow derived cMSCs were characterized using criteria established by Dominici (Dominici et al., 2006). Cells were adherent to tissue culture plastic and exhibited a spindle-shaped morphology (Figure 4.1A). When seeded at clonal density and incubated 21 days without media exchange, cMSCs demonstrated CFU capacity (Figure 4.1B). Additionally, cMSCs exhibited adipo-, osteo-, and chondrogenic ability (Figure 4.1,C-E) when assessed using differentiation methods optimized for canine MSCs (Chapter 3). Additionally, cells were positive for CD 9, 44, 90, and 105 and were negative for CD 34 and 45 when assessed by flow cytometry (data not shown). Collectively, these results confirmed that the cells used in subsequent studies met established criteria for MSCs

PEG-DA Hydrogel Fabrication

Figure 4.2 demonstrates the gross appearance of PEG-DA hydrogel scaffolds fabricated using conventional and SIPS/SCPL fabrication methods. Conventional PEG-DA hydrogels fabricated using Igracure 651 and Igracure 2959 were visually translucent polymer mesh structures with well-defined peripheral edges (Figure 4.2A). In contrast, SIPS/SCPL fabricated hydrogels contained an interconnecting series of 268 ± 35μm pores (voids within the hydrogel), resulting in a slightly opaque hydrogel with indistinct margins. Regardless of fabrication method, hydrogels were 1.5mm high x 8mm wide disks. The porous nature of the SIPS/SCPL-PEG-DA hydrogel is clearly visible in

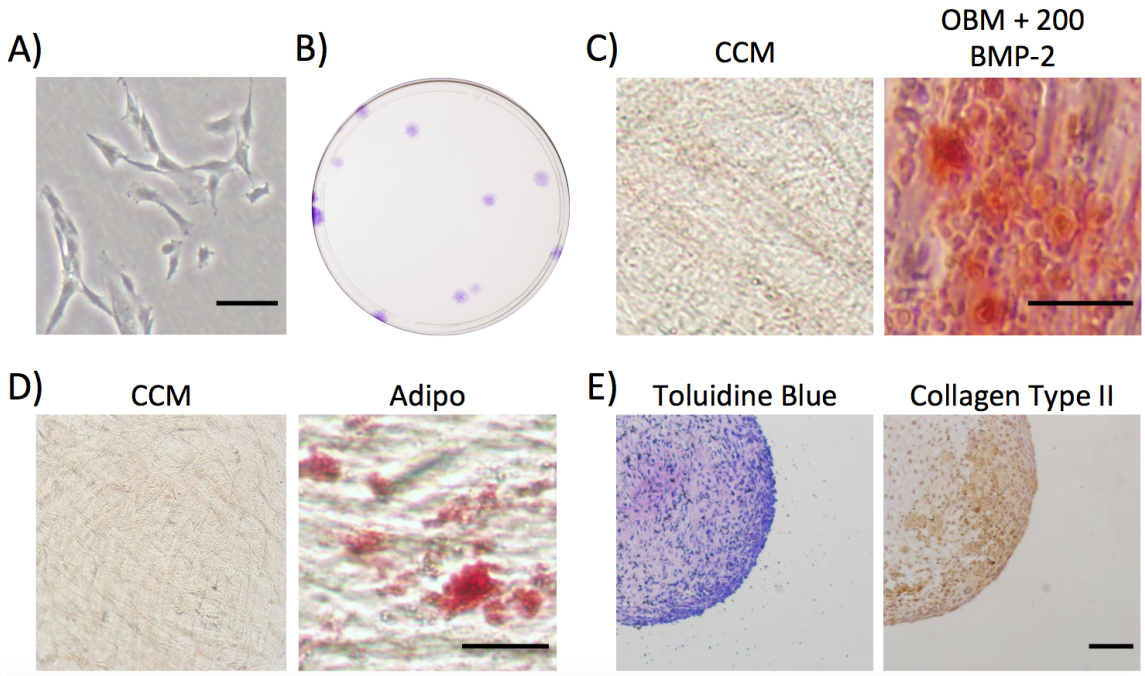

Figure 4.1. *Characterization of canine bone marrow MSCs.* **A)** Representative 10x objective phase contrast microscopy image of bone marrow cMSCs demonstrating the classic plastic-adherent, spindle shaped morphology typical of MSCs (bar=100µm). **B)** Representative photograph of a CFU plate from freshly isolated bone marrow cells. **C)** Microscopic images of osteogenic cultures fixed and stained with Alizarin Red after 21 days of culture in OBM containing 200ng/mL rhBMP-2 (bar=125µm). **D)** Microscopic images of adipogenic cultures fixed and stained with Oil Red O after 21 days of culture in adipogenic media (Bar= 25µm). **E)** Microscopic images of chondrogenic micromass cultures fixed and assessed for proteoglycan (toluidine blue) and collagen type II content (immunohistochemistry) after 21 days of culture in chondrogenic media (bar=150µm).

Figure 4.2A. Importantly, the SIPS/SCPL process is tunable, allowing modulation of pore size for specific applications. To demonstrate this property, the SIPS/SCPL method (Figure 4.2B, top row) was tuned/modulated using varying salt sizes to created pores termed "small" (181 ± 29μm), "medium" (268 ± 35μm), or "large" (459 ± 69μm). In order to more clearly demonstrate the effect of salt size on pore size, SEM was performed on small, medium, and large SIPS/SCPL-PEG-DA hydrogels (Figure 4.2B, bottom row). These images demonstrate the interconnectivity of the pores in addition to the variation in pore dimensions.

cMSC Morphology and Viability

To assess morphology and viability of cMSCs seeded on PEG hydrogel scaffolds, preliminary studies were performed to confirm cellular attachment would occur when cMSCs were seeded upon the surface of hydrogel constructs (data not shown). Upon successful completion of 2D monolayer attachment, 3D assessment of cMSC attachment was assessed in three-dimensions. Canine MSCs were encapsulated in conventional PEG-DA or seeded on SIPS/SCPL-fabricated hydrogels and cultured for 1, 3, 10, and 21 days. Viability was assessed with live/dead staining (Figure 4.3). Representative 10x objective overlay images of live and dead fluorescence demonstrated a marked increase in number of propidium iodide (red=PI positive) stained cMSCs in both Igracure-651 and Igracure-2559 as compared to SIPS/SCPL fabricated hydrogels. Additionally, while cMSCs stained positive for calcein in both conventional hydrogel scaffolds, the number of calcein positive cells subjectively decreased over the 21-day time course. Moreover, cMSCs appeared as rounded, isolated cells in both conventional

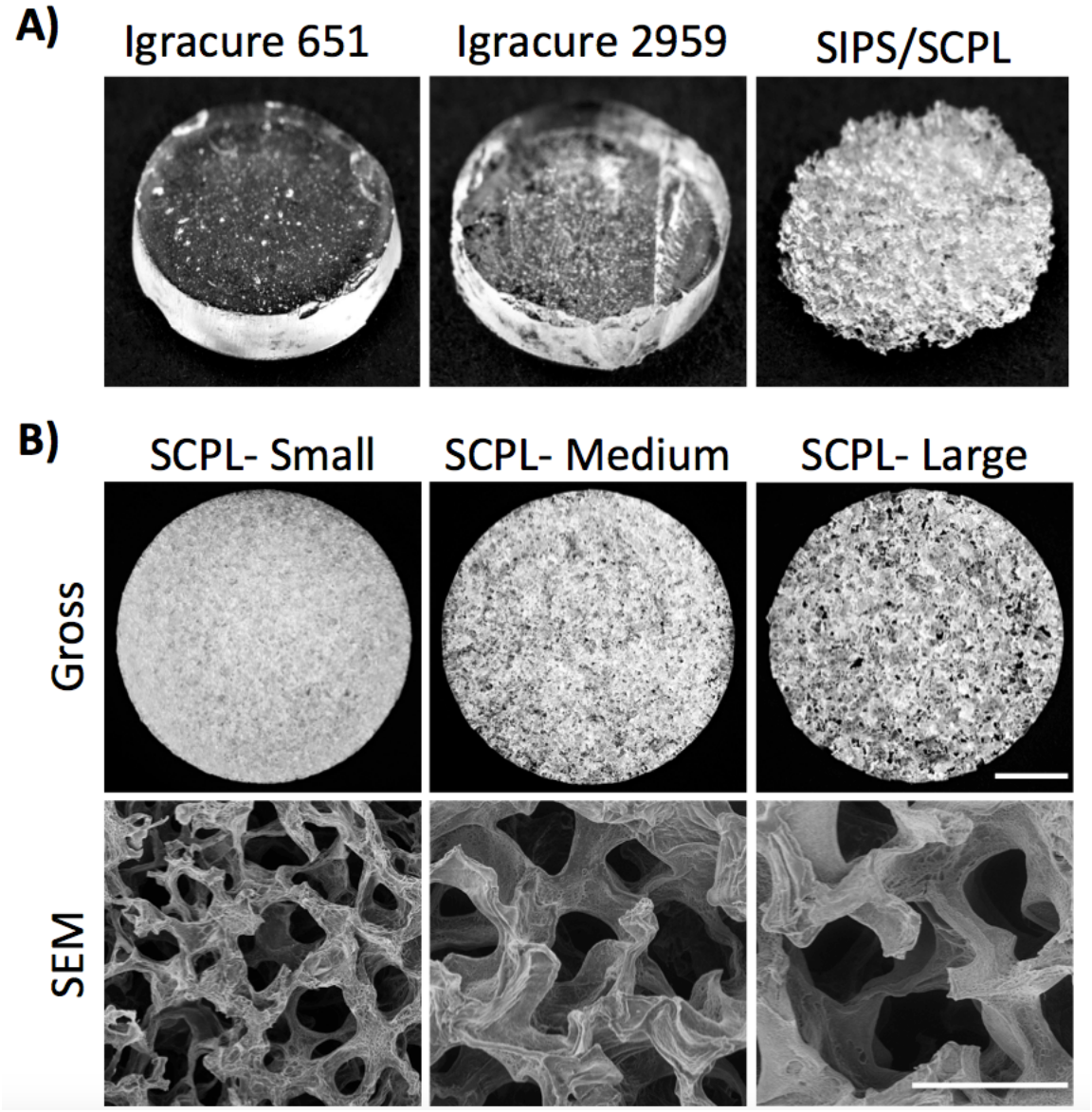

Figure 4.2. *Varying PEG-DA hydrogel fabrication methods.* PEG-DA hydrogel constructs were prepared using conventional photoinitiators Igracure 651 and Igracure 2959 of SIPS/SCPL for evaluation with canine bone marrow MSCs. **A)** Representative gross images of Igracure 651 (left), Igracure 2959 (center), and SIPS/SCPL (right) fabricated hydrogels demonstrating 3D properties (1.5mm high x 8mm diameter). **B)** SIPS/SCPL hydrogels were fabricated with varying salt sizes: "small" (181 ± 29µm), "medium" (268 ± 35µm), and "large" (459 ± 69µm). Representative gross images (top row) demonstrating a low magnification effect of salt size on SIPS/SCPL scaffold properties (bar=2mm). Representative SEM (bottom row) images demonstrating the effect of salt size on scaffold pore interconnectivity (bar=500µm).

hydrogel systems and the number of cells present within these scaffolds remained constant over the 21-day time course. In contrast, there was robust calcein staining of cMSCs cultured on the SIPS/SCPL-fabricated PEG-DA scaffolds containing "medium" pore sizes (268μm ± 35μm). Although occasional PI positive cells were noted, the vast majority of cMSCs were calcein positive. In addition, at all time points cell morphology was spindle-shaped. Lastly, the number of cells present within the SIPS/SCPL-fabricated hydrogels displayed subjective dramatic increase over the 21-day time course based on live/dead staining, whereas the number of cells in conventional PEG-DA hydrogels was subjectively reduced. These results suggest that encapsulation of cMSCs in conventional PEG-DA hydrogels results in substantial loss of viability and the confinement of cells to a rounded or spherical morphology. In contrast, culture of cMSCs on SIPS/SCPL-fabricated hydrogels resulted in robust cell viability, development of a spindle-shaped morphology, and an increase in cells number over time.

Effect of Pore Size on Cell Morphology and Viability as Assessed by Live/Dead Staining

To further determine the effect of pore size on cell morphology and viability, SIPS/SCPL hydrogels were fabricated with a series of small, medium, or large interconnecting pores. Cells were seeded onto SIPS/SCPL hydrogels and were assessed at 1, 3, 10, and 21 days for viability and cell morphology using live/dead staining. Representative 10x objective overlay images (Figure 4.4) demonstrate an increase in calcein positive cells over time with scarce PI positive cells, regardless of hydrogel pore size or time point. As with medium pore SIPS/SCPL hydrogels, cells cultured on small and large pore SIPS/SCPL hydrogels demonstrated spindle-shaped/mesenchymal

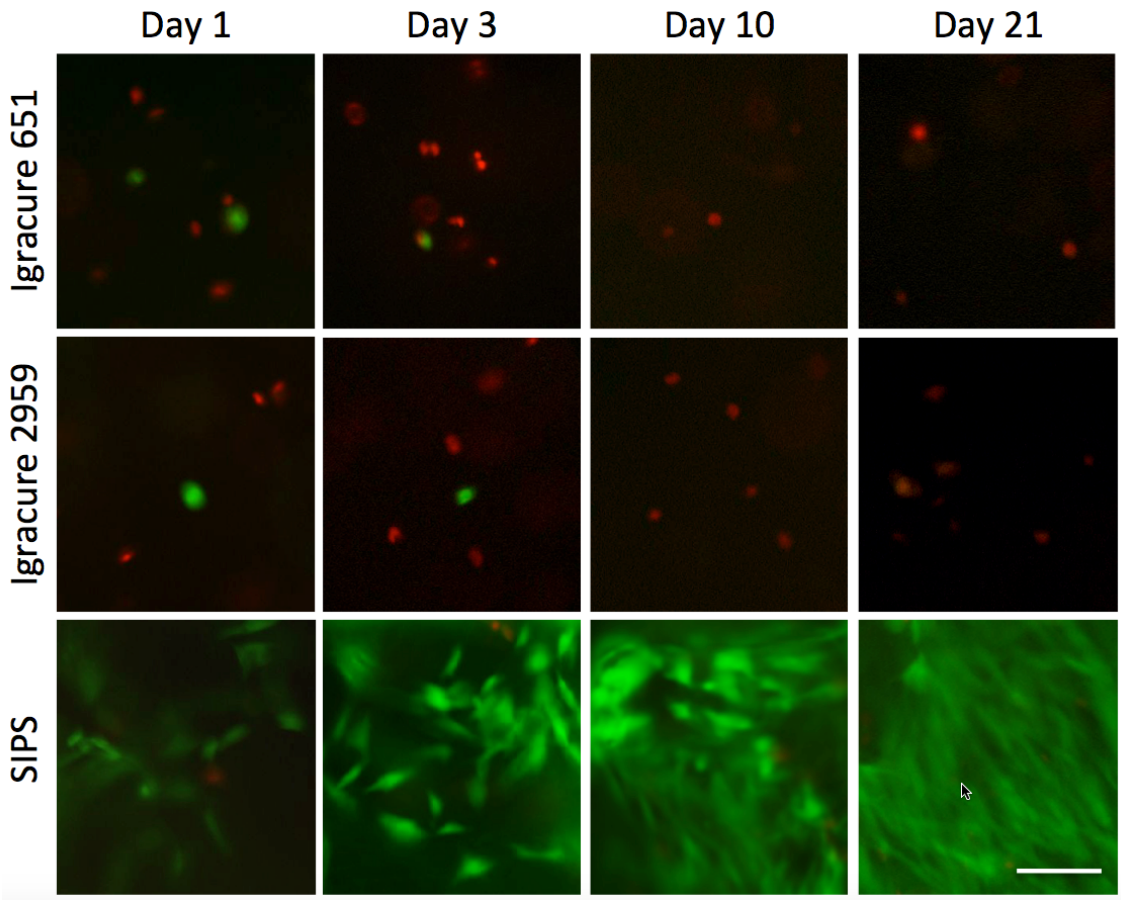

Figure 4.3. *cMSC morphology and viability when seeded in varying fabrication methods of PEG-DA hydrogels*. Bone marrow cMSCs encapsulated in conventional PEG-DA or seeded on SIPS/SCPL-fabricated hydrogels were culture for 1, 3, 10, and 21 days. At each pre-determined time point hydrogels containing cMSCs were assessed for live (green=calcein positive) and dead (red=propidium iodide positive) fluorescence. Representative 10x fluorescent overlay images of cell-encapsulated, photoinitiator Igracure 651- (top row) and Igracure 2959- (center row) fabricated hydrogels demonstrating an isolated, rounded morphology and increased propidium iodide staining. In contrast, representative 10x fluorescent overlay images of cell-seeded, medium SIPS/SCPL-fabricated hydrogels (bottom row) exhibit robust calcein staining with spindle-shaped cell morphology (bar=125µm).

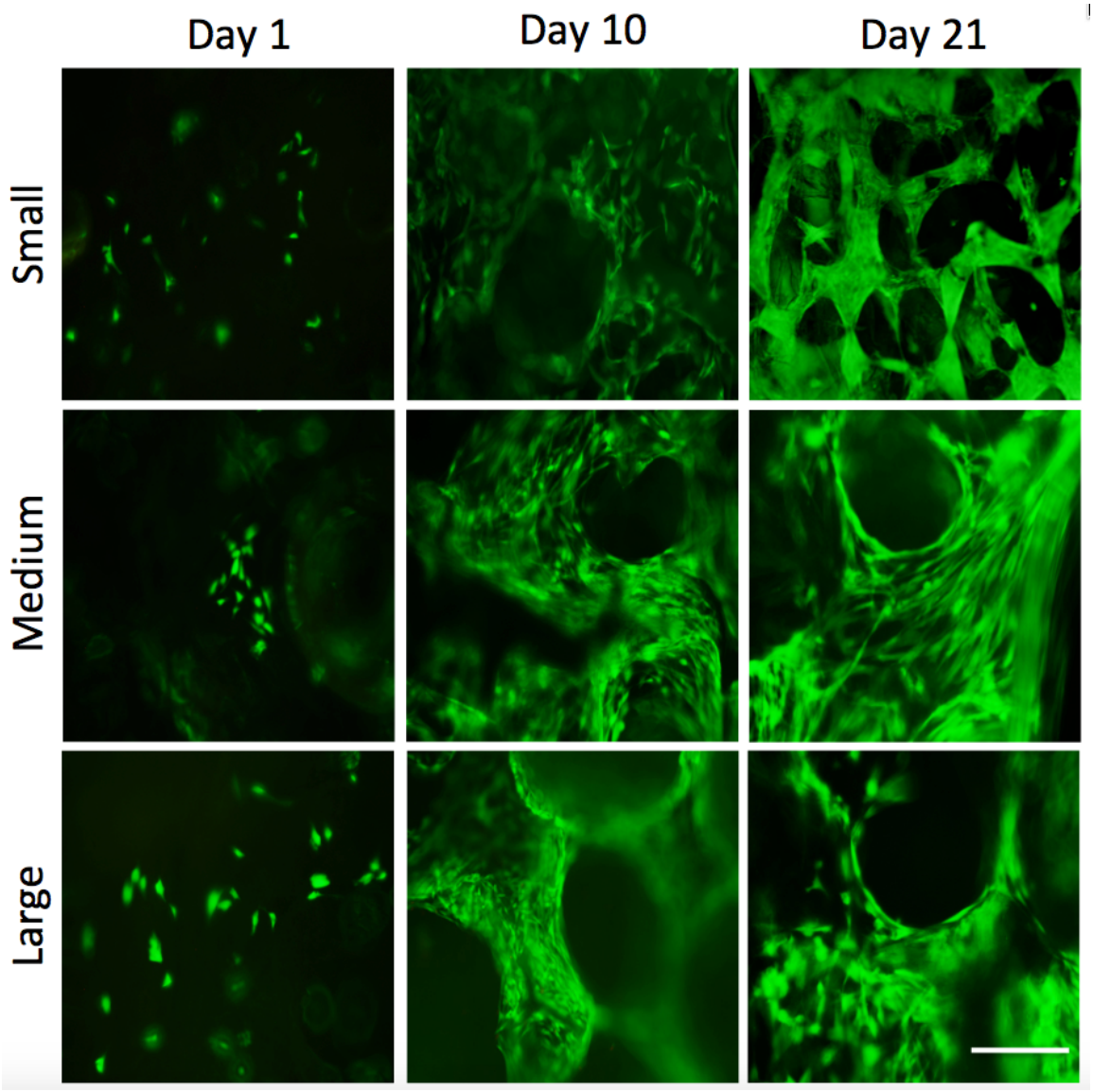

Figure 4.4. *Effect of SIPS/SCPL pore size on cMSC cell morphology and viability.* SIPS/SCPL hydrogels were fabricated with a series of small (181 ± 29μm), medium (268 ± 35μm), and large (459 ± 69μm) interconnecting pores. Bone marrow cMSCs were seeded onto the various pore size SIPS/SCPL-fabricated hydrogels and cultured for 1, 3, 10, and 21 days. At each pre-determined time point, hydrogels containing cMSCs were assessed for live (green=calcein positive) and dead (red=propidium iodide positive) fluorescence. Representative 10x fluorescent overlay images, demonstrating robust calcein staining and spindle-shape cell morphology for cMSC-seeded small (top row), medium (center row), and large (bottom row) SIPS/SCPL-fabricated hydrogels (bar=125μm).

morphology and subjectively increased in number to cover more surface area of the hydrogels over time. These results suggest that SIPS/SCPL-fabricated hydrogels containing pores of varying sizes appear to be effective hydrogel scaffolds for cMSCs.

Cell Stress/Cytotoxicity as Assessed by Lactate Dehydrogenase (LDH)

Cytotoxicity of cMSCs cultured in PEG-DA hydrogel scaffolds was assessed by assaying LDH levels in conditioned media at day 1 and 3 (Figure 4.5A). Canine MSCs cultured in conventional hydrogels fabricated with Igracure 651 exhibited significantly increased LDH levels at day 1 as compared to cMSCs cultured on 2D tissue culture polystyrene plastic ($p<0.0001$), but levels were significantly reduced when evaluated at day 3 ($p<0.05$). Canine MSCs cultured in conventional hydrogels fabricated with Igracure 2959 exhibited significantly decreased LDH levels at both day 1 and day 3 when compared to 2D cultures ($p<0.0001$). Canine MSCs cultured on SIPS/SCPL hydrogels exhibited significantly reduced LDH levels at both day 1 and day 3 when compared to 2D cultures ($p<0.0001$). Importantly, LDH levels were significantly ($p<0.0001$) reduced in the SIPS/SCPL-fabricated hydrogels as compared to conventional hydrogels fabricated with Igracure 651 or 2959 at day 1. Additionally, at day 3, SIPS/SCPL-fabricated hydrogels exhibited significantly reduced LDH levels compared to 2D, Igracure 651 ($p<0.0001$), and Igracure 2959 ($p<0.05$).

Proliferation

Proliferation assays were used to assess growth characteristics of canine bone marrow MSCs cultured on PEG-DA hydrogel scaffolds and to confirm results from Figures 4.3 and 4.4 (Figure 4.5B,C). There was no significant difference in the number

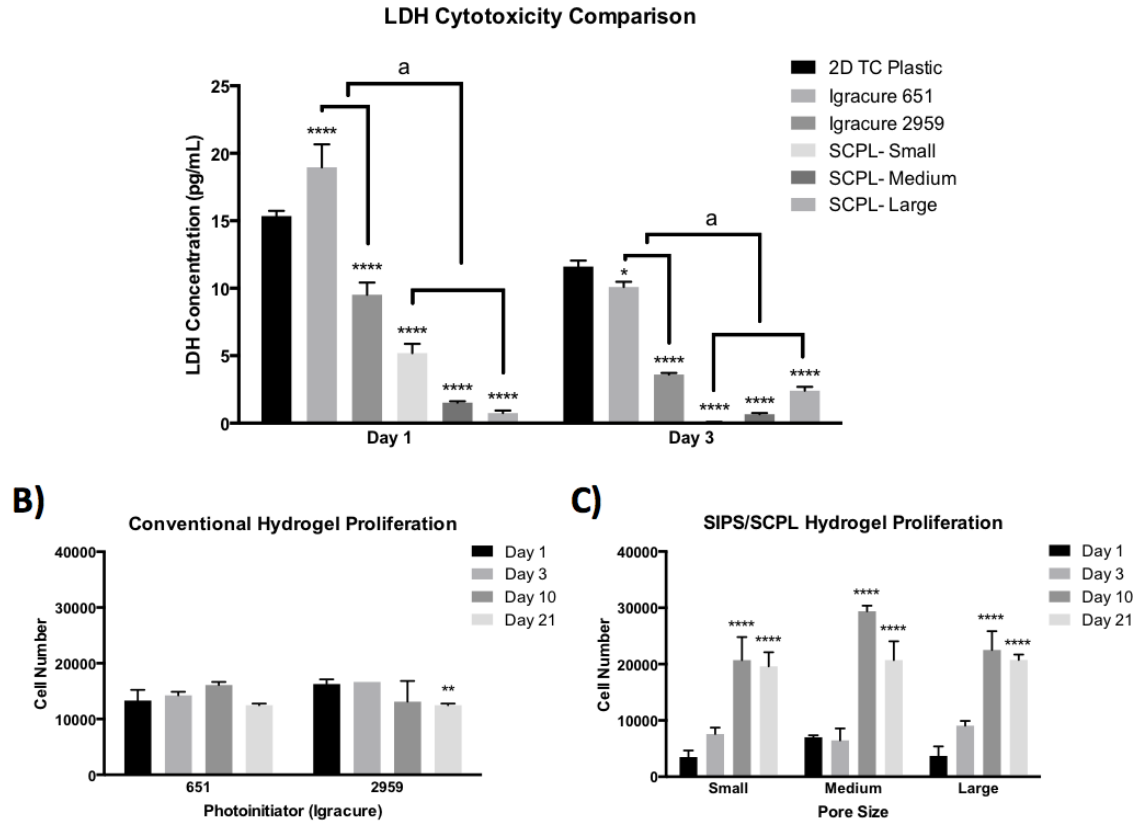

Figure 4.5. *Assessment of cMSC cytotoxicity and proliferation in varying fabrication methods of PEG-DA hydrogels.* Bone marrow cMSCs on traditional 2D tissue-culture (TC) plastic, encapsulated in conventional PEG-DA, or seeded on SIPS/SCPL-fabricated hydrogels were cultured for 1 and 3 days. At each time point, conditioned media were collected for evaluation of cell stress/cytotoxicity as assessed by LDH levels. **A)** Representative LDH concentrations (mean ± SD) for all conditions. Asterisks denote significance as statistically compared to 2D TC plastic cultured cells: (*) $p<0.05$, (****) $p<0.0001$. Letters denote significance differences between conventional and SIPS/SCPL-fabricated hydrogels ($p<0.05$). Proliferation for cell encapsulated conventional PEG-DA or cell-seeded, SIPS/SCPL-fabricated hydrogels was determined at 1, 3, 10, and 21 days (n=3 hydrogels/fabrication method). Mean cell number was determined using DNA quantification. **B)** Mean ± SD proliferation of cMSC-encapsulated, conventional hydrogels, demonstrating baseline or decreased proliferation rates. **C)** Mean ± SD proliferation of cMSC-seeded, SIPS/SCPL fabricated hydrogels, demonstrating increased proliferation rates at 10 and 21 days. Note: for panels B and C, asterisks denote significant differences in cell number: (**) $p<0.01$; (****) $p<0.0001$.

of canine MSCs recovered from conventional hydrogels fabricated with Igracure 651 at any of the pre-determined time points ($p=0.19$). There was a significant decrease ($p<0.01$) in cell number after 21 days for cMSCs recovered from conventional hydrogels fabricated with Igracure 2959 (Figure 4.5B). In contrast, significant increases in cMSC cell number was present in the SIPS/SCPL hydrogels at days 10 ($p<0.0001$), and 21 ($p<0.0001$) (Figure 4.5C). Furthermore, all three pore sizes (small, medium, and large) exhibited significant ($p<0.0001$) increases in cell number over 21 days. When comparing conventional and SIPS/SCPL-fabricated hydrogels, there were significant increases in the number of recovered cells in the SIPS/SCPL-fabricated hydrogels ($p<0.0001$). These results demonstrate that PEG-DA hydrogel fabrication technique has a direct impact on the proliferation of cMSCs. Specifically, the number of cMSCs cultured in SIPS/SCPL-fabricated hydrogels increased over time, whereas the number of cMSCs for conventional hydrogels remained unchanged and in some cases decreased over time. These results confirm the subjective visual assessment of increased cell number in SIPS/SCPL-fabricated hydrogels over time (Figure 4.3).

Scanning Electron Microscopy (SEM)

To further assess cell morphology and spreading of the varying pore size SIPS/SCPL-fabricate hydrogel scaffolds, SEM was performed to obtain high magnification images. Canine MSCs were seeded onto to SIPS/SCPL gels and assessed at 1, 3, 10, and 21 days for cell monolayer appearance (day 1 and 3 data not shown). Representative 200X images at day 10 and 21 (Figure 4.6A) subjectively confirm live/dead-imaging results that SIPS/SCPL-fabricated hydrogels containing pores of

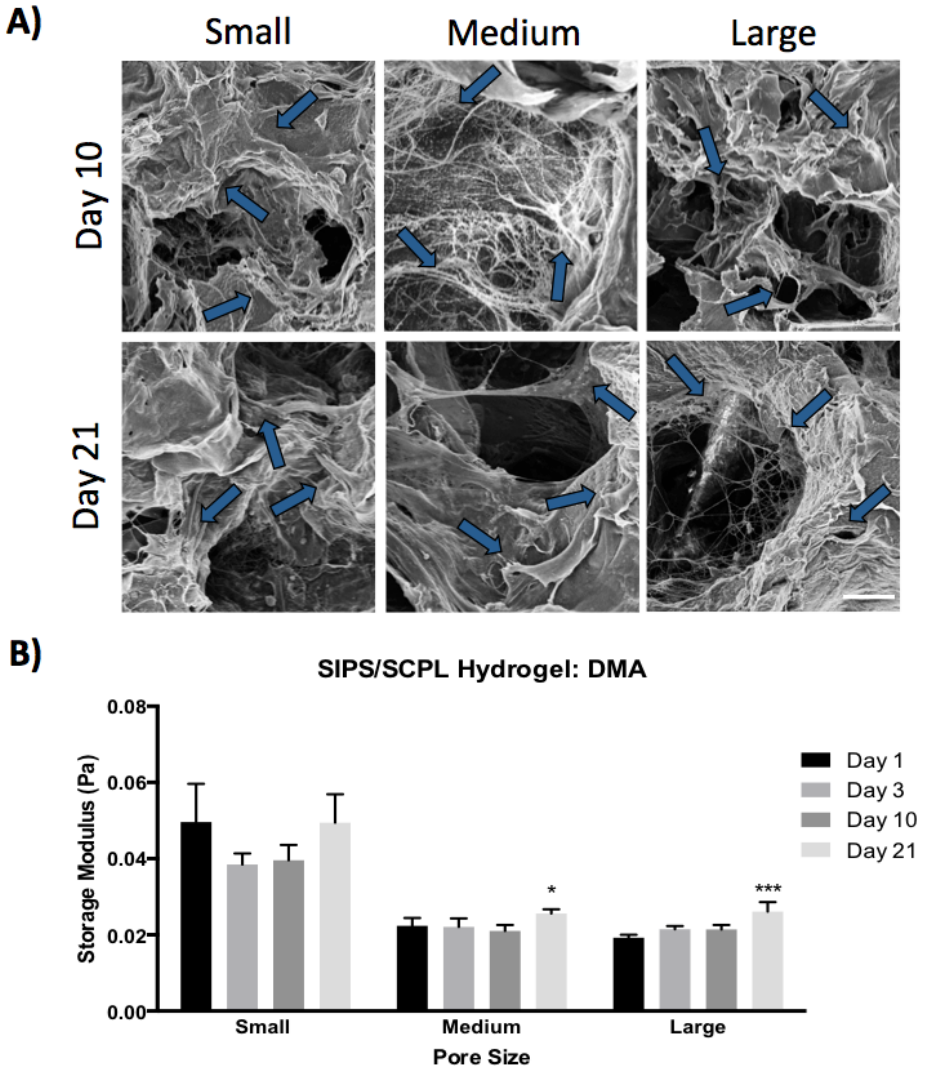

Figure 4.6. *SEM and DMA of cMSC seeded SIPS/SCPL fabricated hydrogels.* SIPS/SCPL hydrogels were fabricated with a series of small, medium, and large interconnecting pores. Bone marrow cMSCs were seeded onto various pore size SIPS/SCPL-fabricated hydrogels and cultured for 1, 3, 10, and 21 days. At each pre-determined time point, hydrogels containing cMSCs were assessed for cell morphology, spreading, and biomechanical properties. **A)** Representative 200x magnification SEM images, demonstrating cMSCs-hydrogel attachment and cell spreading on small (left column), medium (center column), and large (right column) pore SIPS/SCPL hydrogels at 10 (top row) and 21 (bottom row) days (bar=125μm). Arrows denote hydrogel-adherent cells. Storage modulus (G') was assessed using DMA and 10Hz data recorded and plotted as mean ± SD. **B)** Representative storage modulus (G') quantification (mean ± SD) of cMSC-seeded, SIPS/SCPL-fabricated hydrogels (n=5 hydrogel fabrication method/day). Asterisks denote significance when compared to day 1. (*) $p<0.05$; (***) $p<0.001$.

varying sizes appear to be effective hydrogel scaffolds for cMSCs. Interestingly, cells seeded on medium and large pore size SIPS/SCPL-fabricated hydrogels appear to cover more scaffold surface area and displayed increased cell processes. These increased cell processes are evident in the cells' ability to span the pore vacancies.

Dynamic Mechanical Analysis (DMA)

To assess the biomechanical properties of conventional or SIPS/SCPL-fabricated hydrogels cultured with cMSCs over time, storage modulus (*G'*) was measured by DMA to assess gel stiffness at each time point. Canine MSCs cultured with small pore size SIPS/SCPL-fabricated hydrogel scaffolds exhibited significantly increased storage modulus as compared to medium or large pores at all time points ($p<0.0001$) (Figure 4.6B). There were significant increases in storage modulus at day 21 as compared to day 1 in medium ($p<0.05$) and large ($p<0.001$) pore hydrogels. These data demonstrate that small pore size SIPS/SCPL hydrogel scaffolds display increased stiffness as compared to medium or large pore hydrogels, but that the stiffness of medium and large pore SIPS/SCPL-fabricated hydrogels increases over time.

Biocompatibility

Hydrogel implants and surrounding tissue were histologically evaluated to determine biocompatibility.

Subcutaneous SIPS/SCPL hydrogel implants were surrounded by a thin (10-200μm) capsule composed of mature, well-organized fibrous connective tissue (Figure 4.7A). Within the capsule, tissue reaction was similar in all sections, with uniform, consistent invasion of hydrogel pores (Figure 4.7B,C). Hydrogel margins were line by a

layer of cells comprising abundant epithelioid macrophages with frequent multinucleated giant cells (Figure 4.7D) accompanied by minimal to moderate fibroplasia, mild to moderate fibrosis, neovascularization, and small to moderate numbers of lymphocytes, and plasma cells. Occasional sections had scant to moderate numbers of eosinophils. Changes to connective tissues and skeletal muscle in immediate contact with the hydrogel were minimal. Trichrome staining confirmed the presence of a well-organized, mature collagen capsule surrounding the hydrogels and minimal to mild fibrosis within hydrogel interstices.

Conventional and SIPS/SCPL-fabricated hydrogels implanted intra-femorally were histologically evaluated to determine biocompatibility. SIPS/SCPL-fabricated hydrogels exhibited consistent tissue invasion of hydrogel pores (Figure 4.8A) resulting in a trabecular network of fibrous connective tissue with neovascularization and occasional woven bone formation (Figure 4.8B). Woven bone often extended from adjacent epiphyseal trabeculae along connective tissue struts (osteoconductive) and also formed novel islands within central portions of intra-porous connective tissue ingrowth (osteoinductive). Small, often discontiguous bands of fibroplasia and fibrosis surround the outer hydrogel margins, but did not form a discrete capsule as seen with subcutaneous hydrogel implants (Figure 4.8A). Inflammation is mild to moderate and characterized by a layer of epithelioid macrophages and multinucleated giant cells along the hydrogel interface, with fewer numbers of lymphocytes, plasma cells, and rare eosinophils. Epithelioid macrophages and multinucleated giant cells occasionally have a finely granular appearance to the cytoplasm, suggesting hydrogel phagocytosis. The

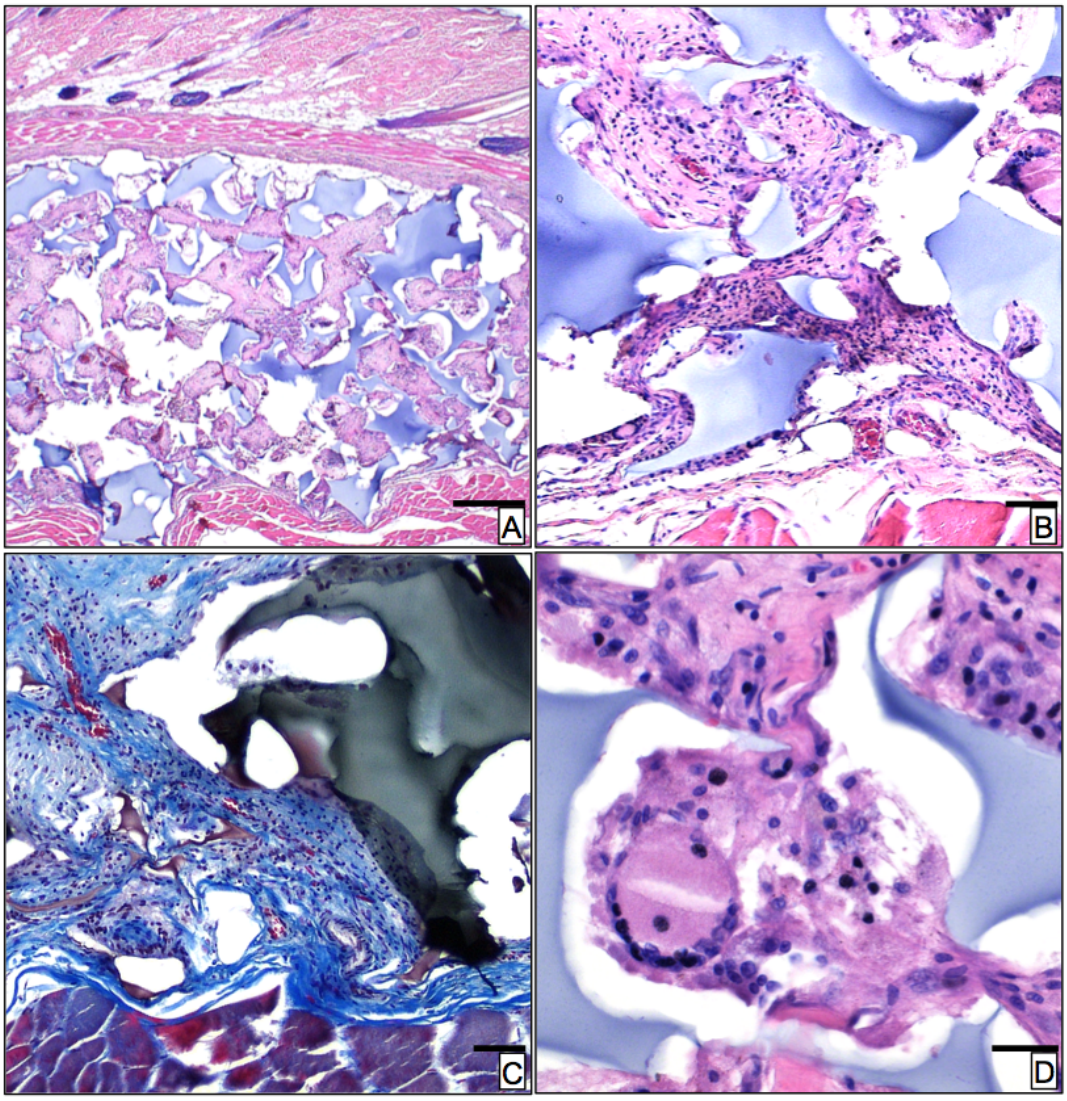

Figure 4.7. *Subcutaneous SIPS/SCPL hydrogel implant biocompatibility.* **A)** Representative H&E stained, 4x magnification (bar=40µm) image of a SIPS/SCPL hydrogel within the subcutaneous tissue 21 days post-surgical implantation. Widespread ingrowth of fibrous connective tissue and neovascularization is observed within the hydrogel pores while the hydrogel periphery contains only a small fibrous connective tissue capsule. **B)** Representative H&E stained, 10x magnification (bar=60µm) image detailing fibrous connective tissue and neovascularization of hydrogel pores. Mild hypercellularity is present within the fibrous trabeculae. **C)** Representative Trichrome stained, 10x magnification (bar=60µm) image indicating the presence of collagen (blue) within connective tissue trabeculae. **D)** H&E stained, 40x magnification (bar=25µm) image exhibiting H&E staining of epithelioid macrophages and foreign-body giant cells lining the hydrogel interface. Small numbers of lymphocytes and plasma cells are also present throughout the fibrous connective tissue intercalated within the hydrogel pores.

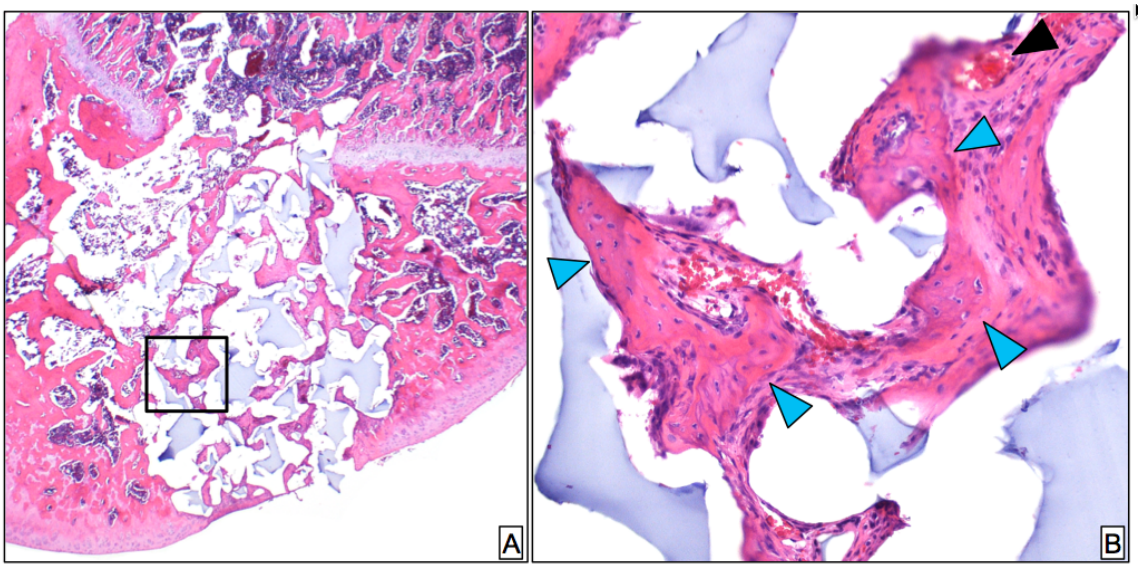

Figure 4.8. *SIPS/SCPL hydrogel intra-femoral biocompatibility.* **A)** Representative H&E stained, 2x magnification (bar=50µm) image of a SIPS/SCPL hydrogel exhibiting increased fibrous connective tissue porous ingrowth, with woven bone formation within connective tissue trabeculae. **B)** 20x magnification (bar=20µm) of the boxed region in Panel A denoting numerous islands of woven bone within connective tissue trabeculae (blue arrowheads). Additionally the presence of numerous small caliber vessels was noted (black arrow head), indicative of good neovascularization of connective tissue trabeculae.

subarticular bony plate overlying the hydrogel implant at the surgical site is often incomplete and lacks fibrocartilage (Figure 4.8A). Of note, four (4/20, 20%) femora with SIPS/SCPL hydrogels had small fragments of hydrogels that were displaced into the intra-articular space. Hydrogel fragments typically adhered to the synovium (Figure 4.9A) and invoked localized granulomatous inflammation with increased collagen and mild synovial hyperplasia (Figure 4.9B).

In contrast to SIPS/SCPL-fabricated hydrogels, conventionally fabricated hydrogels were devoid of tissue ingrowth (Figure 4.10A). Inflammation was minimal to mild and limited to the peripheral hydrogel interface, comprising a single discontinuous layer of epithelioid macrophages and multinucleated giant cells (Figure 4.10B), with very rare lymphocytes, plasma cells, and eosinophils. Occasionally, inflammatory cells were absent, resulting in direct contact of the hydrogel with the adjacent epiphyseal trabecular bone along the longitudinal cranial and caudal axes. Despite direct hydrogel contact, bony reaction is not observed at these sites (Figure 4.10C). Fibroplasia/fibrosis peripheral to the hydrogel was absent to very minimal. Notably, conventional hydrogel implants consistently demonstrated the reconstitution of a broad plate of subchondral bone covered by a layer of articular fibrocartilage (Figure 4.10A) at the surgical site overlying the implant.

Statistical evaluation indicated no significant differences between conventional and SIPS/SCPL-fabricated hydrogels in regards to eosinophilic, neutrophilic, and granulomatous inflammation, periarticular changes, bone marrow progenitor cell proliferation/maturation, and femoral articular cartilage alteration. However, significant

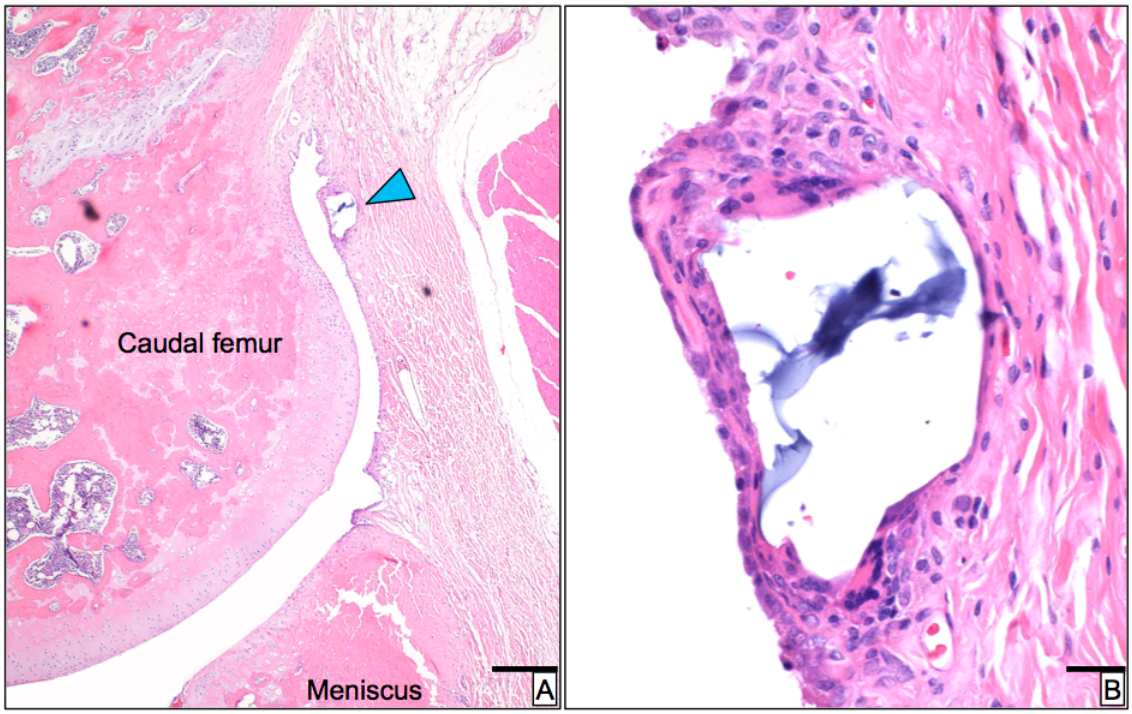

Figure 4.9. *Intra-articular hydrogel displacement.* **A)** 4x magnification (bar=125µm), H&E stained images displaying a small fragment of SIPS/SCPL hydrogel retained within the synovial recesses of the caudal femur. **B)** 40x magnification (bar=25µm) image of area noted by blue arrowhead in Panel A. Displaced hydrogel fragment adhered to the synovium and surrounded by granulomatous inflammation, increased collagen, and mild synovial hyperplasia.

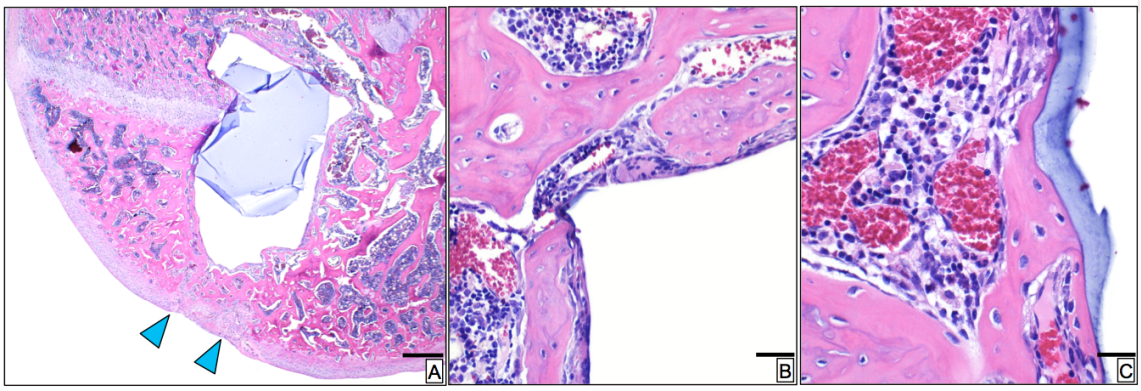

Figure 4.10. *Conventional hydrogel intra-femoral biocompatibility.* **A)** Representative H&E stained, 2x magnification (bar=50µm) image exhibiting the absence of tissue ingrowth into the gel matrix. Additionally, minimal peripheral inflammatory infiltration is present. Of note, woven bone spans the surgical site (bony bridging) and is covered by a layer of fibrocartilage (blue arrowheads). Wrinkling and retraction of the hydrogel is artifactual. **B)** H&E stained, 20x magnification (bar=35µm) image of the hydrogel-intrafemoral interface. Peripheral inflammation at the hydrogel interface comprises multinucleated giant cells and epithelioid macrophages, with rare lymphocytes and plasma cells. **C)** H&E stained, 40x magnification (bar=25µm) image detailing the hydrogel interface devoid of inflammatory cells, allowing for direct bony contact. The hydrogel-bone interface is quiescent and does not appear to elicit any reaction from adjacent bony trabeculae.

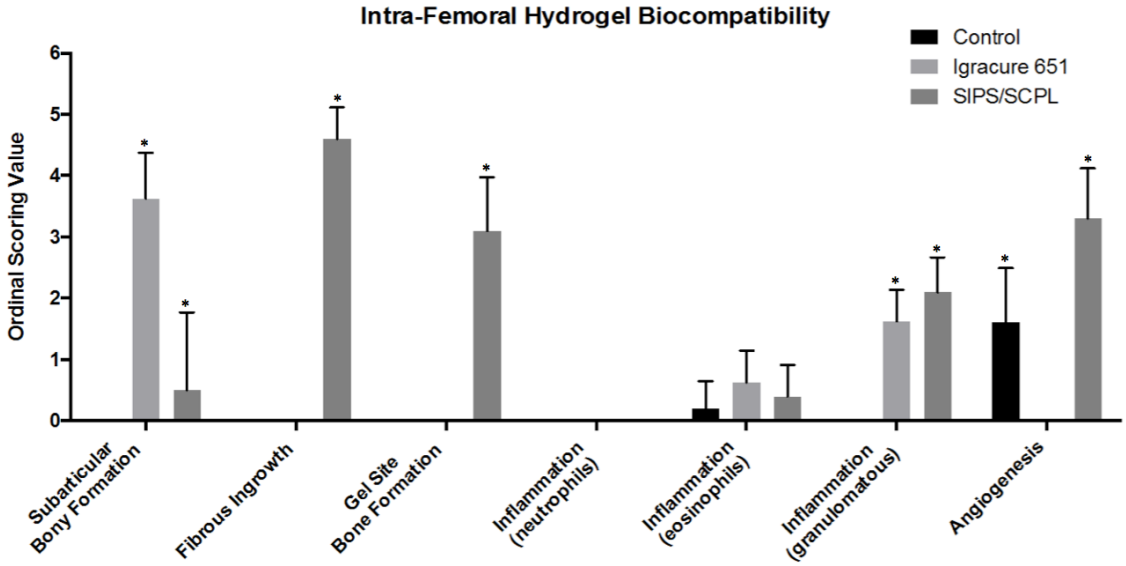

Figure 4.11. *Intra-articular SIPS/SCPL hydrogel implant biocompatibility*. Ordinal scoring of key biocompatibility features evaluated using decalcified, paraffin-embedded, H&E stained sections containing conventional (Igracure 651) or SIPS/SCPL fabricated PEG-DA hydrogels, or sham surgical site (control, no hydrogel). Intra-femoral implant (or control) has a significant effect on the presence of subarticular bony formation, ingrowth of fibrous connective tissue, woven bone formation within implant site, and degree of angiogenesis, (*) $p<0.0001$.

differences between SIPS/SCPL-fabricated and conventional hydrogels included the development of subarticular bony bridging ($p<0.0001$), ingrowth of fibrous connective tissue into the hydrogel matrix ($p<0.0001$), development of woven bone within the hydrogel matrix ($p<0.0001$), neovascularization within the matrix ($p<0.0001$), and presence of lymphocytes and plasma cells ($p<0.0184$) (Figure 4.11).

Artifactual hydrogel changes induced as a result of routine paraffin processing were observed for both conventional and SIPS/SCPL-fabricated hydrogels and included wrinkling, mild to moderate attenuation, and/or fragmentation.

DISCUSSION

The objective of this study was to compare PEG-DA hydrogels fabricated with conventional (photoencapsulated) and SIPS/SCPL methods as potential scaffolds for cMSC articular cartilage tissue engineering. We selected PEG-DA because of the increasing evidence in the literature describing the tunable, biocompatible, and immunologically inert nature of PEG-DA hydrogel scaffolds (Bailey et al., 2012; Bailey et al., 2013; Pasut, 2014; Rafat et al., 2008; Wallace et al., 2001). Based on our results, we reject our hypothesis that fabrication method would have no effect on cellular or mechanical properties of cMSCs-hydrogel constructs. Visual and quantitative assessment of appearance, proliferation, cytotoxicity, and histology demonstrated that SIPS/SCPL hydrogels were superior as compared to conventional fabrication techniques.

Recent studies have suggested that MSCs in combination with conventional PEG-DA based scaffolds as a viable option for translation to clinical therapies (Buxton

et al., 2007; Munoz-Pinto et al., 2012; Shin et al., 2005) due to the proven success of MSC incorporation, subsequent cellular response to scaffold-tethered growth factors, and mechanical construct changes. While these findings are encouraging for conventional PEG based tissue-engineering scaffolds, successful translation to the in vivo setting using a number of animal models has yet to be fully accomplished. This may be due to scaffold limitations such as poor media exchange, oxygen inhibition at the cell-macromer interface, free radical propagation, increase cross-linkage resulting in shrinkage, and smaller mesh/pore size (Bryant and Anseth, 2002). For these reasons, our group aimed to enhance porosity and interconnectivity by introducing a series of interconnecting pores within the PEG-DA hydrogel scaffolds using a novel SCPL fabrication technique. Increased porosity and interconnectivity likely provides a more conducive environment for media exchange and cell movement; thus facilitating increased in-growth of surrounding tissue. This was confirmed when analyzing SIPS/SCPL-cMSC constructs, as they displayed traditional spindle-shaped morphology, increased fluorescent staining, proliferation, and tissue in-growth as compared to conventionally prepared hydrogels. Moreover, cell stress/cytotoxicity as assessed by LDH concentrations was reduced in SIPS/SCPL hydrogels. Histologic analysis revealed extensive intraporous connective tissue permeation in subcutaneous and intrafemoral SIPS/SCPL hydrogel implants. Additionally, intrafemoral hydrogel implants demonstrated the formation of woven bone formation within nascent connective tissue ingrowth, indicating a microenvironment suitable for osseous regeneration.

To further evaluate the SIPS/SCPL system pore size was altered to include small and large pore comparisons. As with initial studies using the medium pore size hydrogels, no increased cell stress/cytotoxicity was present in any of the pore sizes when assessed by LDH levels. Additionally, live/dead fluorescent staining was increased over the 21 day time period. Furthermore, surface area coverage was visually evident between the varying pore sizes. Small pore hydrogels appeared to be confluent with cell monolayers while maintaining pore interconnectivity and integrity. As pore size increased the scaffold surface remained inundated with cells but did not have the intensity of fluorescent staining the small pore hydrogels exhibited. One rationale for this may be smaller area to which cells had access when adhering to the reduced pore size structures. Another potential rationale relates to the cells' ability to be more spread out due to the larger surface area. Rationale for the second hypothesis can be supported when evaluating proliferation (Figure 4.5C) and SEM (Figure 4.6A). Qualitative SEM data demonstrated that cells on medium and large pore size hydrogels appeared to cover more hydrogel surface area, spanning the pores with lamellipodia/filopodia like cell processes. In agreement with this concept, cell number was relatively similar across all pore sizes at 21 days of culture.

Articular cartilage contains unique properties due to its ability to respond to frictional, compressive, shear, and tensile mechanical loads assessed by the joint, such as the knee and hip. Tissue-engineering constructs have aimed at reproducing native mechanical properties in an effort to restore function. Storage modulus or stiffness (*G'*) of industrial materials such as steel (200GPa) and wood (10GPa) exhibit significantly

higher mechanical stiffness when compared to mechanical properties of healthy cartilage, in which *G'* ranges from 0.45MPa to 0.80MPa (Mansour, 2003). These values are significantly lowered as degeneration and disease of focal lesions and osteoarthritis progress (Buschmann et al., 1999). One pitfall in translating synthetic PEG-DA-based biomaterials into clinical treatment strategies has been the inability to mimic native biomechanical properties of cartilage. Previous studies evaluating PEG-DA-based SIPS scaffolds for cartilage tissue engineering found constructs to range from 60kPa to 75kPa. This was a promising finding due to the higher mechanical stiffness when compared to previously describe conventionally prepared hydrogels, Igracure 651 and Igracure 2959 (Bailey et al., 2012; Bryant and Anseth, 2002; Gacasan et al., 2016; Zhang et al., 2011). Based on these previous studies, the present study evaluated PEG-DA-based SIPS/SCPL-fabricated hydrogels' storage modulus (*G'*) using dynamic mechanical analysis (DMA). SIPS/SCPL hydrogels displayed decreased (in an order of magnitude) *G'* (~20mPa to 40mPa) as compared to previously described SIPS hydrogels (Bailey et al., 2012). When assessing pore size differences, small pore size SIPS/SCPL hydrogels exhibited substantially higher *G'* (~50mPa) as compared to medium or large pore sizes (~20mPa). Collectively, conventional hydrogels are stiffer as compared to SIPS/SCPL-fabricated hydrogels. Furthermore, increased pore size decreases *G'*. Contributing factors believed to be responsible for these observations are 1) the increasing macroporous morphology, reducing hydrogel surface area as compared to conventional hydrogels; 2) increased pore sizes, leading to less hydrogel structure. As seen in gross and SEM images, increased pore size correlates decreased amount of scaffold material

needed to support mechanistic changes. Although, SIPS/SCPL-fabricated hydrogels do not approach mechanical properties of native cartilage or conventional hydrogels, one promising finding was observed in the increased *G'* with increased time across all pore sizes. This increasing stiffness may be due cMSCs synthesis and secretion of extracellular matrix. Further studies are needed to determine if these data can be confirmed and subsequently enhanced to provide a more similar biomechanical structure to that of native cartilage.

While the results presented herein provide a promising avenue for future translational studies, our study is not without pitfalls. One such is example is the decreased mechanical strength as compared to conventional hydrogels or native cartilage. Albeit concerning, this obstacle is navigable by modulating hydrogel properties using previously described chemical compounds such as polydimethylsiloxane$_{star}$ (PDMS$_{star}$) (Bailey et al., 2012; Munoz-Pinto et al., 2012). These recent studies detail the ability of PDMSstar to direct MSC differentiation to osteogenic lineage while increasing the storage modulus of the scaffold. Additionally, the percentage of PEG-DA and the molecular weight of PEG may also be adjusted to improve hydrogel stiffness. Another route of study to enhance cMSC-hydrogel constructs, particularly the SIPS/SCPL system, involves cellular influence. Results presented above evaluate cells for viability, morphology, and growth characteristic but not for differentiation capacity. Future studies should include the study of tissue specific differentiation media, incorporation of growth factors in the hydrogel, and the addition of biocompatible polymers, such as PDMS, to evaluate the cellular modulation capacity

in an effort to create the optimal cell-based scaffold. Optimizing mechanical properties and hydrogel architecture of the SIPS/SCPLS system are important areas of future focus in order to minimize the potential for scaffold fragmentation and displacement within the joint space. It is possible that targeted changes to scaffold architecture and biomechanical properties will result in a more robust subchondral bone plate, as was observed with the conventionally fabricated intra-articular PEG-DA hydrogel implants.

Confirmed through our statistical analysis, subarticular bone (the subchondral plate) and articular fibrocartilage restoration was largely absent in SIPS/SCPL-fabricated hydrogels (Figure 4.8A) whereas a layer of subchondral bone and established fibrocartilage were consistently present overlying conventional hydrogels (Figure 4.9A). Additionally, occasional small hydrogel fragments were noted remotely within the synovial lining of the joint. When present, these small fragments were associated with focal and mild granulomatous response (4.10). Combining the limited subchondral bone and fibrocartilage healing in the SIPS/SCPL hydrogels with the observance of remote hydrogel fragments suggest that either hydrogel architecture, biomechanical properties, of both, resulted in insufficient biomechanical support for restoration of the subchondral plate.

The restoration of subchondral bone in the knees that received conventional PEG-DA hydrogels likely occurred due to an increased stiffness of hydrogel when compared to those fabricated via SIPS/SCPL. However, the comparatively dense composition of the conventional PEG-DA hydrogels significantly inhibited tissue ingrowth, including fibroplasia/fibrous connective tissue formation and

neovascularization (Figure 4.9A,B). Although lymphocyte and plasma cell infiltration was more significant in SIPS/SCPL hydrogels ($p<0.0184$), cellular infiltration was minimal to mild and this scoring difference likely reflects a relative increase in overall cellularity given extensive intraporous tissue invasion. To summarize, the results of our intra-articular PEG-DA hydrogel scaffold *in vivo* study suggest that while the conventional PEG-DA hydrogel scaffolds allowed a more robust healing of the subchondral plate and an associated layer of fibrocartilage that bridged the articular surface in most cases, there was zero incorporation or "bonding" of conventional PEG-DA hydrogels with the subchondral bone, as evidence by a complete lack of fibrous tissue, bone, or vascular ingrowth. In contrast, PEG hydrogels fabricated via SIPS/SCPL allowed marked tissue ingrowth, including fibrous tissue, neovascularization, and consistent islands of bone both in the periphery of the hydrogel constructs, but also interspersed more deeply within the hydrogels. While these findings confirm tissue ingrowth and improved bonding of the SIPS/SCPL system, we believe the biomechanical properties of the SIPS/SCPL system explain why the subchondral bone and fibrous tissue incompletely covered the articular cartilage lesions in these knees. We propose that the next generation of hydrogel scaffolds contain a series of interconnecting pores for improved cell survival via attachment, proliferation, and migration events (encouraging tissue ingrowth and bonding), but that the biomechanical properties of the SIPS/SCPL be improved using the methods described above, or through "hybridization" of these two systems, namely a hydrogel scaffold in which 90% or more of the scaffold contains pores fabricated through SIPS/SCPL, but that the superficial

portion of the scaffold in contact with the joint space be composed of a stiffer zone of conventionally fabricated PEG-DA hydrogel.

In conclusion, the ability to modulate scaffold properties of pore size and interconnectivity is of the utmost importance in regards to developing an optimal cell infused construct for focal lesions of articular cartilage. In this study we have identified a synthetic hydrogel scaffold fabrication method that is compatible with bone marrow cMSCs and is shown to integrate with surrounding tissue when implanted in vivo in experimentally induced osteochondral defects. This work is foundational for further development of the SIPS/SCPL-PEG-DA hydrogel scaffolds for focal osteochondral lesions, experimental and translational animal studies, and in the future, veterinary and human clinical trials.

CHAPTER V

CONCLUSIONS AND FUTURE DIRECTIONS

This dissertation outlines the importance of OC and focal cartilage injury, both of which lead to progressive joint OA. The purpose of the research presented herein is to explore the use of tissue engineering strategies utilizing cMSCs and novel 3D hydrogel scaffolds as a mechanism for treating focal cartilage lesions in the clinical setting. While the focus of the present work is orthopedic injuries, the results are more broadly applicable to cell-matrix interactions, the selection and use of tissue-specific MSCs for tissue engineering strategies, and the development of custom tissue engineering scaffolds, or "devices", to restore structure and function to injured tissues.

First, in Chapter II, a well-described, 3D, serum-free collagen system was used as a model system to demonstrate the importance of growth factors and cell-matrix interactions in 3D environments. The role of molecular cell signaling, protein expression, and proteinase activation were examined; specifically, the role of PDGF-BB and MMP influence on human osteosarcoma invasion in 3D collagen type I matrices. In Chapter III, canine MSCs were isolated from synovium, bone marrow, and adipose tissue and comprehensively characterize using a donor-matched study and assays optimized for the canine species. Characterization was assessed on CFU potential, differentiation markers, mRNA expression, proliferation rates, immunomodulatory capabilities, and tri-lineage differentiation. Lastly, in Chapter IV, using previously characterized cMSCs (Chapter III), two PEG based hydrogel fabrication methods were compared *in vitro*. Additionally, these scaffolds were evaluated for biocompatibility *in*

vivo in both the cutaneous and intra-articular spaces. Collectively, these studies have the potential to impact the field of regenerative medicine, specifically tissue engineering, in the context of articular cartilage injury and repair.

In Chapter II, the ability of PDGF-BB to stimulate human OSA cell (MG-63) invasion and MMP expression was explored. In particular, study results elucidated the specific MT-MMPs involved in 3D collagen type I proteolysis and invasion. Using a well-described, quantifiable, serum-free, 3D collagen invasion system, human MG-63 osteosarcoma cells were seeded on 3.75mg/mL collagen type I matrices containing varying dosages of PDGF-BB. Using this system, cells were evaluated in a biologic, serum-free environment in which the experimental conditions and supplemental media were known. MG-63 invasion was assessed in response to PDGF-BB, and the requirement for both PDGF-BB and MMPs was demonstrated using MMP inhibitors, tyrosine kinase receptor inhibitors, and knockdown of MMP gene expression. Collectively, these studies demonstrated that MG-63 cells undergo significant invasion in response to PDGF-BB in a dose- and time-dependent manner. Furthermore, MT1-MMP was shown to be the central MMP involved in MG-63 cellular invasion into collagen type I matrices, while soluble MMPs such as MMP-1 and MMP-2 were shown to be less critical. Despite these pre-clinical observations, one limitation to translational use would be that only one cell line of osteosarcoma was evaluated. To further advance the field, multiple osteosarcoma cell lines should be assessed for similar responses to PDGF-BB prior to considering translational treatment targets. Using data found herein, investigators may wish to quantify the MMP profile of other osteosarcoma cell lines, and

to confirm their specific roles in invasion responses. In addition, specific molecular signaling proteins that are initiated in response to PDGF-BB and subsequent involvement in increased transcription and translation for downstream protein expression need to be further elucidated. These collective studies would provide important target therapies for potential translational treatments.

In Chapter III, a comprehensive isolation and characterization study of cMSCs was performed using a donor-matched study design. Canine MSCs were successfully isolated from synovium, bone marrow, and adipose tissues of five individual canine donors during surgical treatment for CCL rupture. Nucleated cells were isolated and expanded for subsequent studies. Cells were shown to be spindle-shaped, adherent to tissue culture plastic, and exhibited a flow cytometry profile typical of MSCs in other species. In addition, all cell preparations displayed positive expression for genes associated with plasticity or multi-potency. Using assays optimized for the canine cells, it was determined that significant differences in cMSCs existed based on tissue source and individual donor variability. While all cMSCs exhibited positive expression of plasticity-associated markers, NANOG, OCT4, and SOX2, and likewise demonstrated CFU capacity, synovial and adipose MSCs proliferated more rapidly and displayed higher CFU potential. In osteogenic assays, synovial and marrow cMSCs exhibited markedly superior ALP activity as compared to adipose MSCs, although adipose cMSC osteogenic differentiation improved with ARS staining of long-term assays. Adipose cMSCs exhibited superior adipogenic differentiation. In evaluating chondrogenic studies, synovial and adipose cMSCs formed larger chondrogenic pellets although

proteoglycan and collagen type II staining varied across cell lines and appeared to be more intense in bone marrow pellets. Lastly, it has been recently accepted that immunomodulation is a fundamental component of MSCs. To determine if cMSCs possess immunomodulatory potential, we established a macrophage/cMSC co-culture assay, the first of its kind in the field of cMSCs. Murine macrophages were cultured alone or in combination with increasing numbers of cMSCs. Cultures were supplied with LPS to initiate activation of macrophages and a subsequent immune response. Conditioned culture media were collected and assessed for murine TNF-α and IL-6 concentrations. These cytokines were used as general indicators of the murine macrophage's inflammatory response to LPS. Significant decreases were observed in TNF-α concentration levels with increasing number of cMSCs, regardless of the tissue or donor source. In contrast to TNF-α results, IL-6 concentrations were significantly increased with increasing cell numbers of cMSCs. Moreover, adipose cMSCs induced a significant increase in IL-6 when compared to other tissue sources of cMSCs. Based on our comprehensive characterization study, it was determined that all cell preparations met established criteria for MSCs. This work will prove useful as a foundation for investigators interested in using cMSCs for translational tissue-engineering studies. However, future studies are necessary to determine if the tissue source is relevant in the context of injection of cMSCs in solution to palliate joint pain, or in the context of using cMSCs in combination with 3D scaffolds as tissue engineering devices. The question can be stated succinctly as: "Are cMSCs more efficacious in treating focal joint injury and OA through tissue engineering strategies/devices or as a therapeutic injection?" To

fully answer this question, further work must be performed to analyze the properties of cMSCs in both the *in vitro* and *in vivo* environments. One key focus for the strategy of using cMSCs as a symptomatic agent is the role of cMSCs-toll-like receptor binding and subsequent immunomodulatory signaling. Determining the presence and role of specific receptors, molecular signaling, and pathways of cMSCs is utmost importance. Additional optimization must also be performed to thoroughly understand the mechanistic route in which cMSC affect pro- and anti-inflammatory responses. Clearly defining the response of cMSCs to local cues, in both the *in vitro* and *in vivo*, will enable hypothesis-driven studies, evaluation of dosing and dose frequency studies, and ultimately lead to properly designed clinical trials (appropriately powered and controlled) to determine whether injection of cMSCs in solution into injured joint spaces is efficacious.

In regards to the use of cMSCs as a component of tissue engineering "devices", the ability to drive cMSC differentiation through biologic or synthetic cues is an appealing treatment option. One of the main goals of the lab is to develop novel tissue engineering strategies for use in osteochondral and osteoarthritic clinical treatments. To this end, studies were performed in Chapter IV to evaluate bone marrow cMSCs in combination with PEG-DA hydrogels fabricated with conventional or novel methods. PEG hydrogels were selected for evaluation due to the fact that they have been shown to be tunable and immunologically inert (biocompatible). These studies proved that conventionally fabricated PEG hydrogels with photoinitiators Igracure 651 and Igracure 2959 were not optimal for improved cell health or proliferation of canine bone marrow

MSCs. To navigate these obstacles, we evaluated a newly described SIPS/SCPL fabrication system. This novel fabrication method created a series of interconnecting pores allowing for more accessible media exchange, cell motility, and cell proliferation. Bone marrow cMSCs cultured on SIPS/SCPL prepared hydrogels proved to be a highly promising cell-scaffold combination, as determined by significant cell proliferation, adherence, and spreading as compared to conventionally prepared hydrogels. The promising results of these initial studies led to further evaluation of cMSCs on the SIPS/SCPL PEG-DA hydrogel system. SIPS/SCPL prepared hydrogels were adjusted to modulate pore size from ~181μm to ~459μm and further evaluated in combination with bone marrow cMSCs. These studies further confirmed the increased adherence, proliferation, and spreading of cMSCs, regardless of the size of the interconnecting hydrogel pores. Moreover, mechanical testing exhibited an increased storage modulus (i.e. the hydrogels became stiffer) at day 21 as compared to Day 1. These data in combination with proliferation and cell morphology results suggest that increased cMSCs are coating the SIPS/SCPL hydrogel scaffolds. It is likely that the cMSCs are also depositing provisional matrix proteins.

Due to the impressive performance of the SIPS/SCPL system in vitro, comparative studies were performed assessing both the "conventional" Igracure 651 hydrogel and SIPS/SCPL hydrogels in vivo in the intra-articular space. "Conventional" and SIPS/SCPL prepared hydrogels were implanted into 12-week old Sprague-Dawley rats and evaluated at 21 days. Results of these studies demonstrated that while the conventional PEG-DA hydrogel scaffolds allowed a more robust healing of the

subchondral plate and an associated layer of fibrocartilage that bridged the articular surface in most cases, incorporation or "bonding" did not occur with the subchondral bone. In contrast, PEG hydrogels fabricated via SIPS/SCPL encouraged tissue ingrowth (consistent with our in vitro experiments) and led to islands of bone in the peripheral and deep zones of the scaffolds. As detailed in Chapter IV, we propose that the next generation of hydrogel scaffold contain a series of interconnecting pores for cell attachment, tissue ingrowth and bonding with adjacent host tissues, but that the superficial zone of the SIPS/SCPL hydrogel scaffold be modulated to markedly increase stiffness or that the scaffold be "hybridized" with a thin, yet stiff layer of conventionally fabricated PEG-DA hydrogel at the joint surface.

While these studies provide a foundation for use of the SIPS/SCPL hydrogel system for translational articular cartilage tissue engineering studies, further in vitro and laboratory animal studies are likely necessary prior to moving to a large animal or human setting. Important questions remain surrounding the influence of scaffold properties and culture media. Does lineage specific culture media as described in Chapter III influence differentiation within 3D scaffolds? Experiments to address this question would involve comparing control culture conditions with osteogenic or chondrogenic differentiation media using differentiation assays, histology, and real-time PCR analyses. Does the modulation of tensegrity (mechanical properties of the scaffold) or addition of chemical substrates induce differentiation of MSCs to a specific phenotype? One such additional chemical compound that should be studied is $PDMS_{star}$. $PDMS_{star}$ is a polymer previously shown to be incorporated into PEG-based scaffolds,

altering structural properties and exhibiting inherent osteoinductive properties (Bailey et al., 2012; Munoz-Pinto et al., 2012). Initial studies performed in our lab evaluating cMSCs cultured in the presence of $PDMS_{star}$ indicated that there was no significant detriment of $PDMS_{star}$ on cMSC cell health, adhesion, or proliferation. Unfortunately, this study currently remains as preliminary data, as it was determined that $PDMS_{star}$ did not remain fully incorporated within the PEG-DA scaffold. However, some degree of $PDMS_{star}$ was present within the scaffold. Thus the results of our preliminary $PDMS_{star}$ experiments leads to the question of the effect of PDMSstar on cMSC viability, proliferation, and differentiation. Further analysis and modifications to methods for fully incorporating $PDMS_{star}$ are necessary prior to initiation of $PDMS_{star}$ studies.

In conclusion, when comparing the conventionally-fabricated hydrogels to the SIPS/SCPL system, bone marrow cMSCs exhibited increased cell-scaffold adhesion, viability, and proliferation on PEG-DA hydrogels fabricated using the SIPS/SCPL system. Moreover, tuning SIPS/SCPL scaffold pore size did not cause any significant differences to the aforementioned assessments.

Further exploration of cMSCs in combination with both biologic and synthetic scaffolds should be considered to develop a tissue-engineering device for the treatment of osteochondral lesions such as OC, small traumatic joint injuries, or focal OA. Collectively, this dissertation outlines the importance of OC, traumatic cartilage injury, OA, and the use of 3D scaffolds as a potential tissue engineering treatment in the clinical setting. Work presented herein clearly demonstrates the modulation of both biologic and

synthetic 3D systems for translation into *in vivo* studies. These data may lead to novel treatments of OC and OA in clinical patients, both human and veterinary.

REFERENCES

Adams, M., Atkinson, M., Lussier, A., Schulz, J., Siminovitch, K., Wade, J. and Zummer, M. (1995). The role of viscosupplementation with hylan G-F 20 (Synvisc) in the treatment of osteoarthritis of the knee: a Canadian multicenter trial comparing hylan G-F 20 alone, hylan G-F 20 with non-steroidal anti-inflammatory drugs (NSAIDs) and NSAIDs alone. *Osteoarthr. Cartil.* **3**, 213–225.

Al-Nbaheen, M., Vishnubalaji, R., Ali, D., Bouslimi, A., Al-Jassir, F., Megges, M., Prigione, A., Adjaye, J., Kassem, M. and Aldahmash, A. (2012). Human stromal (mesenchymal) stem cells from bone marrow, adipose tissue and skin exhibit differences in molecular phenotype and differentiation potential. *Stem Cell Rev and Rep* **9**, 32–43.

Al-Shaikh, R., Chou, L., Mann, J., Dreeben, S. and Prieskorn, D. (2002). Autologous osteochondral grafting for talar cartilage defects. *Foot Ankle Int* **23**, 381–389.

Allam, M., Martinet, N. and Martinet, Y. (1992). Differential migratory response of U-2 OS osteosarcoma cell to the various forms of platelet-derived growth factor. *Biochimie* **74**, 183–186.

Allan, J., Docherty, A., Barker, P., Huskission, N., Reynolds, J. and Murphy, G. (1995). Binding of gelatinases A and B to type-I collagen and other matrix components. *Biochem. J.* **309**, 299–306.

Alvarez, R., Kantarjian, H. and Cortes, J. (2006). Biology of platelet-derived growth factor and its involvement in disease. *Mayo Clinic Proceedings* **81**, 1241–1257.

Alves, H., Dechering, K., Van Blitterswijk, C. and De Boer, J. (2011). High-throughput assay for the identification of compounds regulating osteogenic differentiation of human mesenchymal stromal cells. *PLoS ONE* **6**, e26678.

Andl, C. (2004). EGFR-induced cell migration is mediated predominantly by the JAK-STAT pathway in primary esophageal keratinocytes. *AJP: Gastrointestinal and Liver Physiology* **287**, G1227–G1237.

Ariad, S., Seymour, L. and Bezwoda, W. (1991). Platelet-derived growth factor (PDGF) in plasma of breast cancer patients: correlation with stage and rate of progression. *Breast Cancer Res. Treat.* **20**, 11–17.

Armulik, A. (2005). Endothelial/Pericyte Interactions. *Circulation Research* **97**, 512–523.

Arnhold, S., Goletz, I., Klein, H., Stumpf, G., Beluche, L., Rohde, C., Addicks, K. and Litzke, L. (2007). Isolation and characterization of bone marrow-derived equine mesenchymal stem cells. *American Journal of Veterinary Research* **68**, 1095–1105.

Arnoczky, S. and Warren, R. (1983). The microvasculature of the meniscus and its response to injury. *The American Journal of Sports Medicine* **11**, 131–141.

Arnoczky, S., Cook, J., Carter, T. and Turner, A. (2010). Translational models for studying meniscal repair and replacement: What they can and cannot tell us. *Tissue Eng Part B Rev* **16**, 31–39.

Ashton, B., Abdullah, F., Cave, J. and Williamson, M. (1985). Characterization of cells with high alkaline phosphatase activity derived from human bone and marrow: Preliminary assessment of their osteogenicity. *Bone* **6**, 313–319.

Augello, A., Kurth, T. and De Bari, C. (2010). Mesenchymal stem cells: A perspective from in vitro cultures to in vivo migration and niches. *Eur Cell Mater* **20**, 121–133.

Auger, K., Serunian, L., Soltoff, S., Libby, P. and Cantley, L. (1989). PDGF-dependent tyrosine phosphorylation stimulates production of novel polyphosphoinositides in intact cells. *Cell* **57**, 167–175.

Bailey, B., Fei, R., Munoz-Pinto, D., Hahn, M. and Grunlan, M. (2012). PDMSstar-PEG hydrogels prepared via solvent-induced phase separation (SIPS) and their potential utility as tissue engineering scaffolds. *Acta Biomaterialia* **8**, 4324–4333.

Bailey, B., Nail, L. and Grunlan, M. (2013). Continuous gradient scaffolds for rapid screening of cell-material interactions and interfacial tissue regeneration. *Acta Biomaterialia* **9**, 8254–8261.

Barbour, K., Helmick, C., Theis, K., Murphy, L., Hootman, J., Brady, T. and Cheng, Y. (2013). Prevalence of doctor-diagnosed arthritis and arthritis-attributable activity limitation - United States, 2010-2012. *MMWR Morb. Mortal. Wkly. Rep.* **62**, 869–873.

Bayless, K. and Davis, G. (2003). Sphingosine-1-phosphate markedly induces matrix metalloproteinase and integrin-dependent human endothelial cell invasion and lumen formation in three-dimensional collagen and fibrin matrices. *Biochemical and Biophysical Research Communications* **312**, 903–913.

Bayless, K., Kwak, H. and Su, S. (2009). Investigating endothelial invasion and sproutingbehavior in three-dimensional collagen matrices. *Nature Protocols* **4**, 1888–1898.

Bányai, L., Tordai, H. and Patthy, L. (1994). The gelatin-binding site of human 72 kDa type IV collagenase (gelatinase A). *Biochem. J.* **298 (Pt 2)**, 403–407.

Bennett, C., Ross, S., Longo, K., Bajnok, L., Hemati, N., Johnson, K., Harrison, S. and MacDougald, O. (2002). Regulation of Wnt signaling during adipogenesis. *Journal*

of Biological Chemistry **277**, 30998–31004.

Bergmann, G., Siraky, J., Rohlmann, A. and Koelbel, R. (1984). A comparison of hip-joint forces in sheep, dog and man. *Journal of Biomechanics* **17**, 907–921.

Bjørnland, K., Flatmark, K., Pettersen, S., Aaasen, A., Fodstad, Ø. and Mælandsmo, G. (2005). Matrix metalloproteinases participate in osteosarcoma invasion. *Journal of Surgical Research* **127**, 151–156.

Bjørnland, K., Winberg, J., Ødegaard, O., Hovig, E., Loennechen, T., Aaasen, A., Fodstad, Ø. and Mælandsmo, G. (1999). S100A4 involvement in metastasis deregulation of matrix metalloproteinases and tissue inhibitors of matrix metalloproteinases in osteosarcoma cells transfected with an anti-*S100A4* ribozyme. *Cancer Research* **59**, 4702–4708.

Black, L., Gaynor, J., Adams, C., Dhupa, S., Sams, A., Taylor, R., Harman, S., Gingerich, D. A. and Harman, R. (2008). Effect of intraarticular injection of autologous adipose-derived mesenchymal stem and regenerative cells on clinical signs of chronic osteoarthritis of the elbow joint in dogs. *Vet. Ther.* **9**, 192–200.

Black, L., Gaynor, J., Gahring, D., Adams, C., Aron, D., Harman, S., Gingerich, D. and Harman, R. (2007). Effect of adipose-derived mesenchymal stem and regenerative cells on lameness in dogs with chronic osteoarthritis of the coxofemoral joints: a randomized, double-blinded, multicenter, controlled trial. *Vet. Ther.* **8**, 272–284.

Bockstahler, B., Skalicky, M., Peham, C., Müller, M. and Lorinson, D. (2007). Reliability of ground reaction forces measured on a treadmill system in healthy dogs. *The Veterinary Journal* **173**, 373–378.

Bond, M., Fabunmi, R., Baker, A. and Newby, A. (1998). Synergistic upregulation of metalloproteinase-9 by growth factors and inflammatory cytokines: an absolute requirement for transcription factor NF-κB. *FEBS Letters* **435**, 29–34.

Boström, H., Willetts, K., Pekny, M., Levéen, P., Lindahl, P., Hedstrand, H., Pekna, M., Hellström, M., GebreMedhin, S., Schalling, M., et al. (1996). PDGF-A signaling is a critical event in lung alveolar myofibroblast development and alveogenesis. *Cell* **85**, 863–873.

Bouffi, C., Bony, C., Courties, G., Jorgensen, C. and Noël, D. (2010). IL-6-dependent PGE2 secretion by mesenchymal stem cells inhibits local inflammation in experimental arthritis. *PLoS ONE* **5**, e14247.

Bowen-Pope, D. (1986). The growth factor-platelet-transformation connection. *Dev Biol* **3**, 111–128.

Brandl, F., Sommer, F. and Goepferich, A. (2007). Rational design of hydrogels for tissue engineering: Impact of physical factors on cell behavior. *Biomaterials* **28**, 134–146.

Brandt, K., Smith, G. and Simon, L. (2000). Intraarticular injection of hyaluronan as treatment for knee osteoarthritis: What is the evidence? *Arthritis Rheum* **43**, 1192–1203.

Breur, G. and Lambrechts, N. (2011). Osteochondrosis. In *Veterinary Surgery: Small Animal*, pp. 1178–1189.

Brey, D., Motlekar, N., Diamond, S., Mauck, R., Garino, J. and Burdick, J. (2010). High-throughput screening of a small molecule library for promoters and inhibitors of mesenchymal stem cell osteogenic differentiation. *Biotechnol. Bioeng.* **108**, 163–174.

Bruder, S., Fink, D. and Caplan, A. (1994). Mesenchymal stem cells in bone development, bone repair, and skeletal regeneration therapy. *J. Cell. Biochem.* **56**, 283–294.

Bryant, S. and Anseth, K. (2002). Hydrogel properties influence ECM production by chondrocytes photoencapsulated in poly(ethylene glycol) hydrogels. *J. Biomed. Mater. Res.* **59**, 63–72.

Buckwalter, J., Saltzman, C. and Brown, T. (2004). The impact of osteoarthritis. *Clin Orthop Relat Res* **427**, S6–S15.

Burdick, J., Mason, M., Hinman, A., Thorne, K. and Anseth, K. (2002). Delivery of osteoinductive growth factors from degradable PEG hydrogels influences osteoblast differentiation and mineralization. *J Control Release* **83**, 53–63.

Buschmann, M., Kim, Y., Wong, M., Frank, E., Hunziker, E. and Grodzinsky, A. (1999). Stimulation of aggrecan synthesis in cartilage explants by cyclic loading is localized to regionsof high interstitial fluid flow. *Archives of Biochemistry and Biophysics* **366**, 1–7.

Buxton, A., Zhu, J., Marchant, R., West, J., Yoo, J. and Johnstone, B. (2007). Design and characterization of poly(ethylene glycol) photopolymerizable semi-interpenetrating networks for chondrogenesis of human mesenchymal stem cells. *Tissue Engineering* **13**, 2549–2560.

Canalis, E., McCarthy, T. and Centrella, M. (1989). Effects of platelet-derived growth factor on bone formation in vitro. *J. Cell. Physiol.* **140**, 530–537.

Caplan, A. (1988). Bone development. *Cell and molecular biology of vertebrate hard tissues* **136**, 3–16.

Caplan, A. (1991). Mesenchymal stem cells. *J. Orthop. Res.* **9**, 641–650.

Caplan, A. (2008). All MSCs Are Pericytes? *Cell Stem Cell* **3**, 229–230.

Caplan, A. and Correa, D. (2011). PDGF in bone formation and regeneration: New insights into a novel mechanism involving MSCs. *J. Orthop. Res.* **29**, 1795–1803.

Carrade, D., Lame, M., Kent, M., Clark, K., Walker, N. and Borjesson, D. (2012). Comparative analysis of the immunomodulatory properties of equine adult-derived mesenchymal stem cells. *cell med* **4**, 1–11.

Chen, C., Tsai, P. and Huang, C. (2012). Anti-inflammation effect of human placental multipotent mesenchymal stromal cells is mediated by prostaglandin E2 via a myeloid differentiation primary response gene 88-dependent pathway. *Anesthesiology* **117**, 568–579.

Cheng, J., Chou, C., Kuo, M. and Hsieh, C. (2006). Radiation-enhanced hepatocellular carcinoma cell invasion with MMP-9 expression through PI3K/Akt/NF-κB signal transduction pathway. *Oncogene* **25**, 7009–7018.

Choi, H., Lee, R., Bazhanov, N., Oh, J. and Prockop, D. (2011). Anti-inflammatory protein TSG-6 secreted by activated MSCs attenuates zymosan-induced mouse peritonitis by decreasing TLR2/NF- B signaling in resident macrophages. *Blood* **118**, 330–338.

Christensen, R., Astrup, A. and Bliddal, H. (2005). Weight loss: The treatment of choice for knee osteoarthritis? A randomized trial. *Osteoarthritis and Cartilage* **13**, 20–27.

Clair, B., Johnson, A. and Howard, T. (2009). Cartilage repair: Current and emerging options in treatment. *Foot & Ankle Specialist* **2**, 179–188.

Clohisy, J., Calvert, G., Tull, F., McDonald, D. and Maloney, W. (2004). Reasons for revision hip surgery. *Clin Orthop Relat Res* **429**, 188–192.

Colandrea, T., D'Armiento, J., Kesari, K. and Chada, K. (2000). Collagenase induction promotes mouse tumorigenesis by two independent pathways. *Mol. Carcinog.* **29**, 8–16.

Colter, D., Sekiya, I. and Prockop, D. (2001). Identification of a subpopulation of rapidly self-renewing and multipotential adult stem cells in colonies of human marrow stromal cells. *Proceedings of the National Academy of Sciences* **98**, 7841–7845.

Constantinou, L., Cobb, T. and Walden, A. (2014). Long-term follow-up of osteochondral autologous transplantation in the metacarpophalangeal joints. *Hand* **9**,

335–339.

Coughlin, S., Escobedo, J. and Williams, L. (1989). Role of phosphatidylinositol kinase in PDGF receptor signal transduction. *Science* **243**, 1191–1193.

Csaki, C., Matis, U., Mobasheri, A., Ye, H. and Shakibaei, M. (2007). Chondrogenesis, osteogenesis and adipogenesis of canine mesenchymal stem cells: A biochemical, morphological and ultrastructural study. *Histochem Cell Biol* **128**, 507–520.

Daar, A. and Greenwood, H. (2007). A proposed definition of regenerative medicine. *J Tissue Eng Regen Med* **1**, 179–184.

Danišovič, Ľ., Polák, Š. and Vojtaššák, J. (2013). Adult stem cells derived from skeletal muscle — biology and potential. *cent.eur.j.biol.* **8**, 215–225.

Davis, G. and Saunders, W. (2006). Molecular balance of capillary tube formation versus regression in wound repair: Role of matrix metalloproteinases and their inhibitors. *J Investig Dermatol Symp Proc* **11**, 44–56.

Davis, G., Bayless, K., Davis, M. and Meininger, G. (2000). Regulation of tissue injury responses by the exposure of matricryptic sites within extracellular matrix molecules. *AJPA* **156**, 1489–1498.

De Bari, C., Dell'Accio, F., Tylzanowski, P. and Luyten, F. (2001). Multipotent mesenchymal stem cells from adult human synovial membrane. *Arthritis Rheum* **44**, 1928–1942.

De Bari, C., Dell'Accio, F., Vanlauwe, J., Eyckmans, J., Khan, I., Archer, C., Jones, E., McGonagle, D., Mitsiadis, T. A., Pitzalis, C., et al. (2006). Mesenchymal multipotency of adult human periosteal cells demonstrated by single-cell lineage analysis. *Arthritis Rheum* **54**, 1209–1221.

de Girolamo, L., Niada, S., Arrigoni, E., Di Giancamillo, A., Domeneghini, C., Dadsetan, M., Yaszemski, M., Gastaldi, D., Vena, P., Taffetani, M., et al. (2015). Repair of osteochondral defects in the minipig model by OPF hydrogel loaded with adipose-derived mesenchymal stem cells. *Regenerative Medicine* **10**, 135–151.

Deryugina, E. and Quigley, J. (2006). Matrix metalloproteinases and tumor metastasis. *Cancer Metastasis Rev.* **25**, 9–34.

Digirolamo, C., Stokes, D., Colter, D., Phinney, D., Class, R. and Prockop, D. (1999). Propagation and senescence of human marrow stromal cells in culture. *British Journal of Haematology,* **107**, 275–281.

Doherty, T., Asotra, K., Fitzpatrick, L., Qiao, J., Wilkin, D., Detrano, R., Dunstan, C., Shah, P. and Rajavashisth, T. (2003). Calcification in atherosclerosis: Bone biology and chronic inflammation at the arterial crossroads. *Proceedings of the National Academy of Sciences* **100**, 11201–11206.

Dominici, M., Slaper-Cortenbach, I., Marini, F., Krause, D., Deans, R., Keating, A., Prockop, D. and Horwitz, E. (2006). Minimal criteria for defining multipotent mesenchymal stromal cells. The International Society for Cellular Therapy position statement. *Cytotherapy* **8**, 315–317.

Duan, P., Pan, Z., Cao, L., He, Y., Wang, H., Qu, Z., Dong, J. and Ding, J. (2013). The effects of pore size in bilayered poly(lactide-co-glycolide) scaffolds on restoring osteochondral defects in rabbits. *J. Biomed. Mater. Res.* **102**, 180–192.

Egeblad, M. and Werb, Z. (2002). New functions for the matrix metalloproteinases in cancer progression. *Nat. Rev. Cancer* **2**, 161–174.

Engler, A., Sen, S., Sweeney, H. and Discher, D. (2006). Matrix elasticity directs stem cell lineage specification. *Cell* **126**, 677–689.

English, K. (2012). Mechanisms of mesenchymal stromal cell immunomodulation. *Immunology and Cell Biology* **91**, 19–26.

English, K., Barry, F., Field-Corbett, C. and Mahon, B. (2007). IFN-γ and TNF-α differentially regulate immunomodulation by murine mesenchymal stem cells. *Immunology Letters* **110**, 91–100.

Erices, A., Conget, P. and Minguell, J. (2000). Mesenchymal progenitor cells in human umbilical cord blood. *British Journal of Haematology,* **109**, 235–242.

Fan, J., Varshney, R., Ren, L., Cai, D. and Wang, D. (2009). Synovium-derived mesenchymal stem cells: A new cell source for musculoskeletal regeneration. *Tissue Eng Part B Rev* **15**, 75–86.

Farmer, S. (2005). Regulation of PPARγ activity during adipogenesis. *Int J Obes Relat Metab Disord* **29**, S13–S16.

Fenger, J., London, C. and Kisseberth, W. (2014). Canine osteosarcoma: A naturally occurring disease to inform pediatric oncology. *ILAR Journal* **55**, 69–85.

Ferris, D., Frisbie, D., Kisiday, J., McIlwraith, C., Hague, B., Major, M., Schneider, R., Zubrod, C., Kawcak, C. and Goodrich, L. (2014). Clinical outcome after intra-articular administration of bone marrow derived mesenchymal stem cells in 33 horses with stifle injury. *Veterinary Surgery* **43**, 255–265.

Fisher, K., Pop, A., Koh, W., Anthis, N., Saunders, W. and Davis, G. (2006). Tumor cell invasion of collagen matrices requires coordinate lipid agonist-induced G-protein and membrane-type matrix metalloproteinase-1-dependent signaling. *Mol Cancer* **5**, 69–69.

Fossey, S., Liao, A., McCleese, J., Bear, M., Lin, J., Li, P., Kisseberth, W. and London, C. (2009). Characterization of STAT3 activation and expression in canine and human osteosarcoma. *BMC Cancer* **9**, 81–81.

Fraser, J., Zhu, M., Wulur, I. and Alfonso, Z. (2008). Adipose-derived stem cells. In *Methods in Molecular Biology* (eds. Prockop, D., Phinney, D., and Bunnell, B., pp. 59–67. Humana Press.

Friedenstein, A., Chailakhjan, R. and Lalykina, K. (1970). The development of fibroblast colonies in monolayer cultures of guinea‐pig bone marrow and spleen cells. *Cell Proliferation* **3**, 393–403.

Friedenstein, A., Chailakhyan, R. and Gerasimov, U. (1987). Bone marrow osteogenic stem cells: In vitro cultivation and transplantation in diffusion chambers. *Cell Tissue Kinet* **20**, 263–272.

Gacasan, E., Sehnert, R., Ehrhardt, D. and Grunaln, M. (2016). Macroporous PEG-DA hydrogels for osteochondral tissue regeneration. *Journal of Materials Chemistry B* **under review**.

Gao, H., Wu, G., Spencer, T., Johnson, G. and Bazer, F. (2008). Select nutrients in the ovine uterine lumen. II. Glucose transporters in the uterus and peri-implantation conceptuses. *Biology of Reproduction* **80**, 94–104.

Gao, J., Dennis, J., Solchaga, L., Awadallah, A., Goldberg, V. and Caplan, A. (2001). Tissue-engineered fabrication of an osteochondral composite graft using rat bone marrow-derived mesenchymal stem cells. *Tissue Eng* **7**, 363–371.

Garrison, K., Donell, S., Ryder, J., Shemilt, I., Mugford, M., Harvey, I. and Song, F. (2007). Clinical effectiveness and cost-effectiveness of bone morphogenetic proteins in the non-healing of fractures and spinal fusion: A systematic review. *Health Technol Assess* **11**, 1–4.

Gehmert, S., Gehmert, S., Hidayat, M., Sultan, M., Berner, A., Klein, S., Zellner, J., Müller, M. and Prantl, L. (2011). Angiogenesis: The role of PDGF-BB on adipose-tissue derived stem cells (ASCs). *Clin Hemorheol Microcirc* **48**, 5–13.

Gerhardt, H. and Betsholtz, C. (2003). Endothelial-pericyte interactions in angiogenesis. *Cell Tissue Res* **314**, 15–23.

Gobbi, A., Francisco, R., Lubowitz, J., Allegra, F. and Canata, G. (2006). Osteochondral lesions of the talus: Randomized controlled trial comparing chondroplasty, microfracture, and osteochondral autograft transplantation. *Arthroscopy: The Journal of Arthroscopic and Related Surgery* **22**, 1085–1092.

Gorlick, R. (2009). Current concepts on the molecular biology of osteosarcoma. In *Cancer Treatment and Research*, pp. 467–478. Boston, MA: Springer US.

Granero-Moltó, F., Weis, J., Miga, M., Landis, B., Myers, T., O'Rear, L., Longobardi, L., Jansen, E., Mortlock, D. and Spagnoli, A. (2009). Regenerative effects of transplanted mesenchymal stem cells in fracture healing. *Stem Cells* **27**, 1887–1898.

Graves, D., Antoniades, H., Williams, S. and Owen, A. (1984). Evidence for functional platelet-derived growth factor receptors on MG-63 human osteosarcoma cells. *Cancer Research* **44**, 2966–2970.

Greenwood, H., Singer, P., Downey, G., Martin, D., Thorsteinsdóttir, H. and Daar, A. (2006). Regenerative medicine and the developing world. *PLoS Med.* **3**, e381–e381.

Greenwood, S., Hill, R., Sun, J., Armstrong, M., Johnson, T., Gara, J. and Galloway, S. (2004). Population doubling: A simple and more accurate estimation of cell growth suppression in the in vitro assay for chromosomal aberrations that reduces irrelevant positive results. *Environ. Mol. Mutagen.* **43**, 36–44.

Grinnell, F. and Petroll, W. (2010). Cell motility and mechanics in three-dimensional collagen matrices. *Annu. Rev. Cell Dev. Biol.* **26**, 335–361.

Gronthos, S., Franklin, D., Leddy, H., Robey, P., Storms, R. and Gimble, J. (2001). Surface protein characterization of human adipose tissue-derived stromal cells. *J. Cell. Physiol.* **189**, 54–63.

Gronthos, S., Graves, S., Ohta, S. and Simmons, P. (1994). The STRO-1+ fraction of adult human bone marrow contains the osteogenic precursors. *Blood* **84**, 4164–4173.

Gronthos, S., Zannettino, A. and Graves, S. (1999). Differential cell surface expression of the STRO-1 and alkaline phosphatase antigens on discrete developmental stages in primary cultures of human bone. *Journal of Bone and Mineral Research* **14**, 47–56.

Guercio, A., Di Marco, P., Casella, S., Cannella, V., Russotto, L., Purpari, G., Di Bella, S. and Piccione, G. (2012). Production of canine mesenchymal stem cells from adipose tissue and their application in dogs with chronic osteoarthritis of the humeroradial joints. *Cell. Biol. Int.* **36**, 189–194.

Gunatillake, P. and Adhikari, R. (2003). Biodegradable synthetic polymers for tissue engineering. *Eur Cell Mater* **5**, 1–16.

Guo, B. and Ma, P. (2014). Synthetic biodegradable functional polymers for tissue engineering: A brief review. *Sci. China Chem.* **57**, 490–500.

Harris, J., Siston, R., Brophy, R., Lattermann, C., Carey, J. and Flanigan, D. (2011). Failures, re-operations, and complications after autologous chondrocyte implantation. *Osteoarthritis and Cartilage* **19**, 779–791.

Hatsushika, D., Muneta, T., Nakamura, T., Horie, M., Koga, H., Nakagawa, Y., Tsuji, K., Hishikawa, S., Kobayashi, E. and Sekiya, I. (2014). Repetitive allogeneic intra-articular injections of synovial mesenchymal stem cells promote meniscus regeneration in a porcine massive meniscus defect model. *Osteoarthritis and Cartilage* 1–10.

Heldin, C. and Westermark, B. (1988). Role of platelet-derived growth factor in vivo. In *The Molecular and cellular Biology of Wound Repair* (ed. Clark, R., pp. 249–273. Springer Science & Business Media.

Heldin, C. and Westermark, B. (1999). Mechanism of action and in vivo role of platelet-derived growth factor. *Physiol. Rev.* **79**, 1283–1316.

Heldin, C., Johnsson, A., Wennergren, S., Wernstedt, C., Betsholtz, C. and Westermark, B. (1986). A human osteosarcoma cell line secretes a growth factor structurally related to a homodimer of PDGF A-chains. *Nature* **319**, 511–514.

Hellström, M., Gerhardt, H., Kalén, M., Li, X., Eriksson, U., Wolburg, H. and Betsholtz, C. (2001). Lack of pericytes leads to endothelial hyperplasia and abnormal vascular morphogenesis. *The Journal of Cell Biology* **153**, 543–553.

Himelstein, B., Asada, N., Carlton, M. and Collins, M. (1998). Matrix metalloproteinase-9 (MMP-9) expression in childhood osseous osteosarcoma. *Med Pediatr Oncol* **31**, 471–474.

Hoch, R. (2003). Roles of PDGF in animal development. *Development* **130**, 4769–4784.

Hoffman, A. and Dow, S. (2016). Concise review: Stem cell trials using companion animal disease models. *Stem Cells Translational and Clinical Research* 1–21.

Hollinger, J., Hart, C., Hirsch, S., Lynch, S. and Friedlaender, G. (2008a). Recombinant human platelet-derived growth factor: Biology and clinical applications. *J Bone Joint Surg Am* **90**, 48.

Hollinger, J., Onikepe, A., MacKrell, J., Einhorn, T., Bradica, G., Lynch, S. and

Hart, C. (2008b). Accelerated fracture healing in the geriatric, osteoporotic rat with recombinant human platelet-derived growth factor-BB and an injectable beta-tricalcium phosphate/collagen matrix. *J. Orthop. Res.* **26**, 83–90.

Horie, M., Choi, H., Lee, R., Reger, R., Ylostalo, J., Muneta, T., Sekiya, I. and Prockop, D. (2012a). Intra-articular injection of human mesenchymal stem cells (MSCs) promote rat meniscal regeneration by being activated to express Indian hedgehog that enhances expression of type II collagen. *Osteoarthritis and Cartilage* **20**, 1197–1207.

Horie, M., Driscoll, M., Sampson, H., Sekiya, I., Caroom, C., Prockop, D. and Thomas, D. (2012b). Implantation of allogenic synovial stem cells promotes meniscal regeneration in a rabbit meniscal defect model. *J Bone Joint Surg Am* **94**, 701–712.

Horie, M., Sekiya, I., Muneta, T., Ichinose, S., Matsumoto, K., Saito, H., Murakami, T. and Kobayashi, E. (2009). Intra-articular injected synovial stem cells differentiate into meniscal cells directly and promote meniscal regeneration without mobilization to distant organs in rat massive meniscal defect. *Stem Cells* **27**, 878–887.

Horwitz, E., Prockop, D., Fitzpatrick, L., Koo, W., Gordon, P., Neel, M., Sussman, M., Orchard, P., Marx, J., Pyeritz, R., et al. (1999). Transplantability and therapeutic effects of bone marrow-derived mesenchymal cells in children with osteogenesis imperfecta. *Nature Medicine* **5**, 309–313.

Hotary, K., Allen, E., Punturieri, A., Yana, I. and Weiss, S. (2000). Regulation of cell invasion and morphogenesis in a three-dimensional type I collagen matrix by membrane-type matrix metalloproteinases 1, 2, and 3. *The Journal of Cell Biology* **149**, 1309–1323.

Hou, Y., Schoener, C., Regan, K., Munoz-Pinto, D., Hahn, M. and Grunlan, M. (2010). Photo-cross-linked PDMS star-PEG hydrogels: Synthesis, characterization, and potential application for tissue engineering scaffolds. *Biomacromolecules* **11**, 648–656.

Hu, X., Yu, A., Qi, B., Fu, T., Wu, G., Zhou, M., Luo, J. and Xu, J. (2010). The expression and significance of IDH1 and p53 in osteosarcoma. *J Exp Clin Cancer Res* **29**, 43–53.

Huck, J., Biery, D., Lawler, D., Gregor, T., Runge, J., Evans, R., Kealy, R. and Smith, G. (2009). A longitudinal study of the influence of lifetime food restriction on development of osteoarthritis in the canine elbow. *Veterinary Surgery* **38**, 192–198.

Hung, S., Chen, N., Hsieh, S., Li, H., Ma, H. and Lo, W. (2002). Isolation and characterization of size‐sieved stem cells from human bone marrow. *Stem Cells* **20**, 249–258.

Innes, J., Gordon, C., Vaughan-Thomas, A., Rhodes, N. and Clegg, P. (2013). Evaluation of cartilage, synovium and adipose tissue as cellular sources for

osteochondral repair. *The Veterinary Journal* **197**, 619–624.

Israel, A. (2010). The IKK complex, a central regulator of NF-kB activation. *Cold Spring Harbor Perspectives in Biology* **2**, 1–13.

Jaffe, N., Bruland, O. and Bielack, S. (2010). *Pediatric and Adolescent Osteosarcoma*. (eds. Jaffe, N., Bruland, O., and Bielack, S. Springer Science & Business Media.

Jeffery, N. and Granger, N. (2012). Is "stem cell therapy" becoming 21st century snake oil? *Veterinary Surgery* **41**, 189–190.

Jin, Y., Tipoe, G., Liong, E., Lau, T., Fung, P. and Leung, K. (2001). Overexpression of BMP-2/4, -5 and BMPR-IA associated with malignancy of oral epithelium. *Oral Oncol.* **37**, 225–233.

Johnson, E., Urist, M., Schmalzried, T., Chotivichit, A., Huang, H. and Finerman, G. (1989). Autogeneic cancellous bone grafts in extensive segmental ulnar defects in dogs. *Clin Orthop Relat Res* **243**, 254–265.

Johnston, S. (1997). Osteoarthritis. Joint anatomy, physiology, and pathobiology. *The Veterinary clinics of North America. Small animal practice* **27**, 699–723.

Kadiyala, S., Young, R., Thiede, M. and Bruder, S. (1997). Culture expanded canine mesenchymal stem cells possess osteochondrogenic potential in vivo and in vitro. *Cell transplantation* **6**, 125–134.

Karahan, S., Kincaid, S., Kammermann, J. and Wright, J. (2001). Evaluation of the rat stifle joint after transection of the cranial cruciate ligament and partial medial meniscectomy. *Comp. Med.* **51**, 504–512.

Katz, J., Brophy, R., de Chaves, L., Cole, B., Dahm, D., Donnell-Fink, L., Guermazi, A., Haas, A., Jones, M., Levy, B., et al. (2013). Surgery versus physical therapy for a meniscal tear and osteoarthritis. *N Engl J Med* **368**, 1675–1684.

Kayagaki, N., Wong, M., Stowe, I. and Ramani, S. (2013). Noncanonical inflammasome activation by intracellular LPS independent of TLR4. *Science* **341**, 1246–1249.

Kazlauskas, A., Kashishian, A. and Cooper, J. (1992). GTPase-activating protein and phosphatidylinositol 3-kinase bind to distinct regions of the platelet-derived growth factor receptor beta subunit. *Molecular and Cellular Biology* **12**, 2534–2544.

Khanna, C., Fan, T., Gorlick, R., Helman, L., Kleinerman, E., Adamson, P., Houghton, P., Tap, W., Welch, D., Steeg, P., et al. (2014). Toward a drug development path that targets metastatic progression in osteosarcoma. *Clin. Cancer Res.*

20, 4200–4209.

Kiefer, K., O'Brien, T., Pluhar, E. and Conzemius, M. (2015). Canine adipose-derived stromal cell viability following exposure to synovial fluid from osteoarthritic joints. *Vet Rec Open* **2**, e000063.

Kim, W., Mohan, R. and Wilson, S. (1999). Effect of PDGF, IL-1alpha, and BMP2/4 on corneal fibroblast chemotaxis: Expression of the platelet-derived growth factor system in the cornea. *Investigative ophthalmology & visual science* **40**, 1364–1372.

Kirschner, C. and Anseth, K. (2013). Hydrogels in healthcare: From static to dynamic material microenvironments. *Acta Materialia* **61**, 931–944.

Kisiel, A., McDuffee, L., Masaoud, E., Bailey, T., Esparza Gonzalez, B. and Nino-Fong, R. (2012). Isolation, characterization, and in vitro proliferation of canine mesenchymal stem cells derived from bone marrow, adipose tissue, muscle, and periosteum. *American Journal of Veterinary Research* **73**, 1305–1317.

Kiviranta, I., Tammi, M., Jurvelin, J., Säämänen, A. and Helminen, H. (1988). Moderate running exercise augments glycosaminoglycans and thickness of articular cartilage in the knee joint of young beagle dogs. *J. Orthop. Res.* **6**, 188–195.

Klein, G., Vellenga, E., Fraaije, M., Kamps, W. and de Bont, E. (2004). The possible role of matrix metalloproteinase (MMP)-2 and MMP-9 in cancer, e.g. acute leukemia. *Critical Reviews in Oncology/Hematology* **50**, 87–100.

Kon, E., Muraglia, A., Corsi, A., Bianco, P., Marcacci, M., Martin, I., Boyde, A., Ruspantini, I., Chistolini, P., Rocca, M., et al. (2000). Autologous bone marrow stromal cells loaded onto porous hydroxyapatite ceramic accelerate bone repair in critical-size defects of sheep long bones. *J. Biomed. Mater. Res.* **49**, 328–337.

Kovalenko, M., Ronnstrand, L., Heldin, C., Loubtchenkov, M., Gazit, A., Levitzki, A. and Böhmer, F. (1997). Phosphorylation site-specific inhibition of platelet-derived growth factor beta-receptor autophosphorylation by the receptor blocking tyrphostin AG1296. *Biochemistry* **36**, 6260–6269.

Krause, U., Harris, S., Green, A., Ylostalo, J., Zeitouni, S., Lee, N. and Gregory, C. A. (2010). Pharmaceutical modulation of canonical Wnt signaling in multipotent stromal cells for improved osteoinductive therapy. *Proceedings of the National Academy of Sciences* **107**, 4147–4152.

Krause, U., Seckinger, A. and Gregory, C. (2008). Assays of osteogenic differentiation by cultured human mesenchymal stem cells. In *Methods in Molecular Biology* (eds. Prockop, D., Phinney, D., and Bunnell, B., pp. 215–230. Humana Press.

Krause, U., Seckinger, A. and Gregory, C. A. (2011). Assays of osteogenic differentiation by cultured human mesenchymal stem cells. In *Methods in Molecular Biology*, pp. 215–230. Totowa, NJ: Humana Press.

Kumar, A., Salimath, B., Stark, G. and Finkenzeller, G. (2010). Platelet-derived growth factor receptor signaling is not involved in osteogenic differentiation of human mesenchymal stem cells. *Tissue Engineering Part A* **16**, 983–993.

Le Blanc, K. (2003). Immunomodulatory effects of fetal and adult mesenchymal stem cells. *Cytotherapy* **5**, 485–489.

Leaner, V., Chick, J., Donninger, H., Linniola, I., Mendoza, A., Khanna, C. and Birrer, M. (2010). Inhibition of AP-1 transcriptional activity blocks the migration, invasion, and experimental metastasis of murine osteosarcoma. *AJPA* **174**, 265–275.

Lee, J., Kim, M., Kim, D., Lim, J., Park, K., Cho, W., Song, W., Lee, S. and Jeon, D. (2008). Postoperative infection and survival in osteosarcoma patients. *Ann Surg Oncol* **16**, 147–151.

Lee, S. and Shin, H. (2007). Matrices and scaffolds for delivery of bioactive molecules in bone and cartilage tissue engineering. *Advanced Drug Delivery Reviews* **59**, 339–359.

Levéen, P., Pekny, M., Gebre-Medhin, S., Swolin, B., Larsson, E. and Betsholtz, C. (1994). Mice deficient for PDGF B show renal, cardiovascular, and hematological abnormalities. *Genes & Development* **8**, 1875–1887.

Liebschner, M. (2004). Biomechanical considerations of animal models used in tissue engineering of bone. *Biomaterials* **25**, 1697–1714.

Lindahl, P., Johansson, B., Levéen, P. and Betsholtz, C. (1997). Pericyte loss and microaneurysm formation in PDGF-B-deficient mice. *Science* **277**, 242–245.

Liotta, F., Angeli, R., Cosmi, L., Filì, L., Manuelli, C., Frosali, F., Mazzinghi, B., Maggi, L., Pasini, A., Lisi, V., et al. (2008). Toll-Like receptors 3 and 4 Are expressed by human bone marrow-derived mesenchymal stem cells and can inhibit their T-cell modulatory activity by impairing notch signaling. *Stem Cells* **26**, 279–289.

Liu, Q., Jernigan, D., Zhang, Y. and Fatatis, A. (2011). Implication of platelet-derived growth factor receptor alpha in prostate cancer skeletal metastasis. *Chin J Cancer* **30**, 612–619.

Liu, W., Burton-Wurster, N., Glant, T., Tashman, S., Sumner, D., Kamath, R., Lust, G., Kimura, J. and Cs-Szabo, G. (2006). Spontaneous and experimental osteoarthritis in dog: Similarities and differences in proteoglycan levels. *J. Orthop. Res.* **21**, 730–737.

Lohi, J., Lehti, K., Valtanen, H., Parks, W. and Keski-Oja, J. (2000). Structural analysis and promoter characterization of the human membrane-type matrix metalloproteinase-1 (MT1-MMP) gene. *Gene* **242**, 75–86.

Lu, C., Miclau, T., Hu, D., Hansen, E., Tsui, K., Puttlitz, C. and Marcucio, R. (2005). Cellular basis for age-related changes in fracture repair. *J. Orthop. Res.* **23**, 1300–1307.

Lu, P., Weaver, V. and Werb, Z. (2012). The extracellular matrix: A dynamic niche in cancer progression. *The Journal of Cell Biology* **196**, 395–406.

Lu, S. and Anseth, K. (2000). Release behavior of high molecular weight solutes from poly(ethylene glycol)-based degradable networks. *Macromolecules* **33**, 2509–2515.

Madry, H., Grün, U. and Knutsen, G. (2011). Cartilage repair and joint preservation: Medical and surgical treatment options. *Dtsch Arztebl Int* **108**, 669–677.

Maniscalco, L., Iussich, S., Morello, E., Martano, M., Biolatti, B., Riondato, F., Salda, Della, L., Romanucci, M., Malatesta, D., Bongiovanni, L., et al. (2012). PDGFs and PDGFRs in canine osteosarcoma: New targets for innovative therapeutic strategies in comparative oncology. *The Veterinary Journal* **195**, 41–47.

Mansour, J. (2003). Biomechanics of cartilage. *Biomechanical Princip* 67–79.

Martin, I., Miot, S., Barbero, A., Jakob, M. and Wendt, D. (2007). Osteochondral tissue engineering. *Journal of Biomechanics* **40**, 750–765.

Martin, J. and Buckwalter, J. (2000). The role of chondrocyte-matrix interactions in maintaining and repairing articular cartilage. *Biorheology* **37**, 129–140.

Mason, M., Metters, A., Bowman, C. and Anseth, K. (2001). Predicting controlled-release behavior of degradable PLA-b-PEG-b-PLA hydrogels. *Macromolecules* **34**, 4630–4635.

Masson, V., la Ballina, de, L., Munaut, C., Wielockx, B., Jost, M., Maillard, C., Blacher, S., Bajou, K., Itoh, T., Itohara, S., et al. (2005). Contribution of host MMP-2 and MMP-9 to promote tumor vascularization and invasion of malignant keratinocytes. *The FASEB Journal* **19**, 234–236.

McGary, E., Weber, K., Mills, L., Doucet, M., Lewis, V., Lev, D., Fidler, I. and Bar-Eli, M. (2002). Inhibition of platelet-derived growth factor-mediated proliferation of osteosarcoma cells by the novel tyrosine kinase inhibitor STI571. *Clin. Cancer Res.* **8**, 3584–3591.

Miller, C., Aslo, A., Won, A., Tan, M. and Lampkin, B. (1996). Alterations of the

p53, Rb and MDM2 genes in osteosarcoms. *J Cancer* **122**, 559–565.

Miller, S., Lloyd, R., Bruenger, F., Krahenbuhl, M., Polig, E. and Romanov, S. (2003). Comparisons of the skeletal locations of putative plutonium-induced osteosarcomas in humans with those in beagle dogs and with naturally occurring tumors in both species. *Radiat. Res.* **160**, 517–523.

Miyamoto, S., Teramoto, H., Coso, O. A., Gutkind, J., Burbelo, P., Akiyama, S. and Yamada, K. (1995). Integrin function: Molecular hierarchies of cytoskeletal and signaling molecules. *The Journal of Cell Biology* **131**, 791–805.

Mochizuki, T., Muneta, T., Sakaguchi, Y., Nimura, A., Yokoyama, A., Koga, H. and Sekiya, I. (2006). Higher chondrogenic potential of fibrous synovium– and adipose synovium–derived cells compared with subcutaneous fat–derived cells. *Arthritis Rheum* **54**, 843–853.

Moldes, M., Zuo, Y., Morrison, R., Silva, D., Park, B., Liu, J. and Farmer, S. (2003). Peroxisome-proliferator-activated receptor gamma suppresses Wnt/beta-catenin signalling during adipogenesis. *Biochem. J.* **376**, 607–613.

Moran, M., Khan, A., Sochart, D. and Andrew, G. (2003). Evaluation of patient concerns before total knee and hip arthroplasty. *The Journal of Arthroplasty* **18**, 442–445.

Morello, E., Martano, M. and Buracco, P. (2011). Biology, diagnosis and treatment of canine appendicular osteosarcoma: Similarities and differences with human osteosarcoma. *The Veterinary Journal* **189**, 268–277.

Munoz-Pinto, D., Jimenez-Vergara, A., Hou, Y., Hayenga, H., Rivas, A., Grunlan, M. and Hahn, M. (2012). Osteogenic potential of poly(ethylene glycol)–poly(dimethylsiloxane) hybrid hydrogels. *Tissue Engineering Part A* **18**, 1710–1719.

Murphy, G. and Knäuper, V. (1997). Relating matrix metalloproteinase structure to function: Why the "hemopexin" domain? *Matrix Biology* **15**, 511–518.

Murphy, J., Fink, D., Hunziker, E. and Barry, F. (2003). Stem cell therapy in a caprine model of osteoarthritis. *Arthritis Rheum* **48**, 3464–3474.

Nagase, H. and Woessner, J. (1999). Matrix Metalloproteinases. *Journal of Biological Chemistry* **274**, 21491–21494.

Nauta, A. and Fibbe, W. (2007). Immunomodulatory properties of mesenchymal stromal cells. *Blood* **110**, 3499–3506.

Nelson, B., Anderson, D., Brand, R. and Brown, T. (1988). Effect of osteochondral

defects on articular cartilage. *Acta Orthop Scand* **59**, 574–579.

Neupane, M., Chang, C., Kiupel, M. and Yuzbasiyan-Gurkan, V. (2008). Isolation and characterization of canine adipose–derived mesenchymal stem cells. *Tissue Engineering Part A* **14**, 1007–1015.

Németh, K., Leelahavanichkul, A., Yuen, P., Mayer, B., Parmelee, A., Doi, K., Robey, P., Leelahavanichkul, K., Koller, B., Brown, J., et al. (2008). Bone marrow stromal cells attenuate sepsis via prostaglandin E2–dependent reprogramming of host macrophages to increase their interleukin-10 production. *Nature Medicine* **15**, 42–49.

Niederauer, G., Slivka, M., Leatherbury, N., Korvick, D., Harroff, H., Ehler, W., Dunn, C. and Kieswetter, K. (2000). Evaluation of multiphase implants for repair of focal osteochondral defects in goats. *Biomaterials* **21**, 2561–2574.

Niemeyer, P., Fechner, K., Milz, S., Richter, W., Suedkamp, N., Mehlhorn, A., Pearce, S. and Kasten, P. (2010). Comparison of mesenchymal stem cells from bone marrow and adipose tissue for bone regeneration in a critical size defect of the sheep tibia and the influence of platelet-rich plasma. *Biomaterials* **31**, 3572–3579.

Nishida, T., Kubota, S., Kojima, S., Kuboki, T., Nakao, K., Kushibiki, T., Tabata, Y. and Takigawa, M. (2004). Regeneration of defects in articular cartilage in rat knee joints by CCN2 (connective tissue growth factor). *Journal of Bone and Mineral Research* **19**, 1308–1319.

Nishimura, K., Solchaga, L., Caplan, A., Yoo, J., Goldberg, V. and Johnstone, B. (1999). Chondroprogenitor cells of synovial tissue. *Arthritis Rheum* **42**, 2631–2637.

Nooeaid, P., Salih, V., Beier, J. and Boccaccini, A. (2012). Osteochondral tissue engineering: Scaffolds, stem cells and applications. *J. Cell. Mol. Med.* **16**, 2247–2270.

Ochi, M., Uchio, Y., Tobita, M. and Kuriwaka, M. (2001). Current concepts in tissue engineering technique for repair of cartilage defect. *Artif Organs* **25**, 172–179.

Oh, J., Choi, H., Lee, R., Roddy, G., Ylöstalo, J., Wawrousek, E. and Prockop, D. (2012). Identification of the HSPB4/TLR2/NF-κB axis in macrophage as a therapeutic target for sterile inflammation of the cornea. *EMBO Mol Med* **4**, 435–448.

Okui, Y., Kano, R., Maruyama, H. and Hasegawa, A. (2008). Cloning of canine Toll-Like receptor 7 gene and its expression in dog tissues. *Veterinary Immunology and Immunopathology* **121**, 156–160.

Ostman, A. and Heldin, C. (2001). Involvement of platelet-derived growth factor in disease: Development of specific antagonists. *Adv. Cancer Res.* **80**, 1–38.

Owen, M. and Friedenstein, A. (1988). Stromal stem-sells: Marrow-derived osteogenic precursors. *Ciba Found. Symp.* **136**, 42–60.

Pacifici, M., Golden, E., Adams, S. and Shapiro, I. (1991). Cell hypertrophy and type X collagen synthesis in cultured articular chondrocytes. *Experimental Cell Research* **192**, 266–270.

Park, H., Temenoff, J. and Mikos, A. (2007). Biodegradable orthopedic implants. In *Topics in Bone Biology* (eds. Bronner, F., Farach-Carson, M., and Mikos, A., pp. 55–68. Springer Science and Business Media.

Park, J., Ye, M. and Park, K. (2005). Biodegradable polymers for microencapsulation of drugs. *Molecules* **10**, 146–161.

Park, S., Seo, M., Kim, H. and Kang, K. (2012). Isolation and characterization of canine amniotic membrane-derived multipotent stem cells. *PLoS ONE* **7**, e44693.

Park, Y., Kim, H., Oh, J. and Lee, S. (2001). The co-expression of p53 protein and P-glycoprotein is correlated to a poor prognosis in osteosarcoma. *International Orthopaedics (SICOT)* **24**, 307–310.

Pasut, G. (2014). Polymers for protein conjugation. *Polymers* **6**, 160–178.

Pei, D. and Weiss, S. (1995). Furin-dependent intracellular activation of the human stromelysin-3 zymogen. *Nature* **375**, 244–247.

Peng, L., Jia, Z., Yin, X., Zhang, X., Liu, Y., Chen, P., Ma, K. and Zhou, C. (2008). Comparative analysis of mesenchymal stem cells from bone marrow, cartilage, and adipose tissue. *Stem Cells and Development* **17**, 761–774.

Peterson, L., Minas, T., Brittberg, M., Nilsson, A., Sjögren-Jansson, E. and Lindahl, A. (2000). Two- to 9-year outcome after autologous chondrocyte transplantation of the knee. *Clin Orthop Relat Res* **374**, 212–234.

Phinney, D. (2008). Isolation of mesenchymal stem cells from murine bone marrow by immunodepletion. In *Methods in Molecular Biology* (eds. Prockop, D., Phinney, D., and Bunnell, B., pp. 171–186. Humana Press.

Pierdomenico, L., Bonsi, L., Calvitti, M., Rondelli, D., Arpinati, M., Chirumbolo, G., Becchetti, E., Marchionni, C., Alviano, F., Fossati, V., et al. (2005). Multipotent mesenchymal stem cells with immunosuppressive activity can be easily isolated from dental pulp. *Transplantation* **80**, 836–842.

Pittenger, M. (2008). Mesenchymal stem cells from adult bone marrow. In *Methods in Molecular Biology* (eds. Prockop, D., Phinney, D., and Bunnell, B., pp. 27–44. Humana

Press.

Pochampally, R. (2008). Colony forming unit assays for MSCs. *Methods Mol. Biol.* **449**, 83–91.

Pond, M. and Nuki, G. (1973). Experimentally-induced osteoarthritis in the dog. *Annals of the Rheumatic Diseases* **32**, 387–388.

Prentice, H., Janossy, G. and Price-Jones, L. (1984). Depletion of T lymphocytes in donor marrow prevents significant graft-versus-host disease in matched allogeneic leukaemic marrow transplant recipients. *The Lancet* **323**, 472–476.

Prockop, D. (1997). Marrow stromal cells as stem cells for nonhematopoietic tissues. *Science* **276**, 71–74.

Prockop, D. and Olson, S. (2007). Clinical trials with adult stem/progenitor cells for tissue repair: Let's not overlook some essential precautions. *Blood* **109**, 3147–3151.

Prockop, D., Sekiya, I. and Colter, D. (2001). Isolation and characterization of rapidly self- renewing stem cells from cultures of human marrow stromal cells. *Cytotherapy* **3**, 393–396.

Proulx-Bonneau, S., Guezguez, A. and Annabi, B. (2011). A concerted HIF-1α/MT1-MMP signalling axis regulates the expression of the 3BP2 adaptor protein in hypoxic mesenchymal stromal cells. *PLoS ONE* **6**, e21511.

Puente, X., Pendás, A., Llano, E., Velasco, G. and López-Otín, C. (1996). Molecular cloning of a novel membrane-type matrix metalloproteinase from a human breast carcinoma. *Cancer Research* **56**, 944–949.

Rafat, M., Li, F., Fagerholm, P., Lagali, N. and Watsky, M. (2008). PEG-stabilized carbodiimide crosslinked collagen–chitosan hydrogels for corneal tissue engineering. *Biomaterials* **29**, 3960–3972.

Raile, K., Hille, R., Laue, S., Schulz, A., Pfeifer, G., Horn, F. and Kiess, W. (2003). Insulin-like growth factor I (IGF-I) stimulates proliferation but also increases caspase-3 activity, Annexin-V binding, and DNA-fragmentation in human MG63 osteosarcoma cells: Co-activation of pro- and anti-apoptotic pathways by IGF-I. *Horm. Metab. Res.* **35**, 786–793.

Ranawat, C. (1986). The patellofemoral joint in total condylar knee arthroplasty. *Clin Orthop Relat Res* **205**, 93–99.

Rasmusson, I. (2006). Immune modulation by mesenchymal stem cells. *Experimental Cell Research* **312**, 2169–2179.

Reger, R., Tucker, A. and Wolfe, M. (2008). Differentiation and characterization of human MSCs. In *Methods in Molecular Biology* (eds. Prockop, D., Phinney, D., and Bunnell, B., pp. 93–107. Humana Press.

Reynolds, L., Grazul-Bilska, A. and Redmer, D. A. (2000). Angiogenesis in the corpus luteum. *Endocrine* **12**, 1–9.

Robertson, W., Kelly, B. and Green, D. (2003). Osteochondritis dissecans of the knee in children. *Curr. Opin. Pediatr.* **15**, 38–44.

Ross, R. (1989). Platelet-derived growth factor. *The Lancet* **333**, 1179–1182.

Runge, J., Biery, D., Lawler, D., Gregor, T., Evans, R., Kealy, R., Szabo, S. and Smith, G. (2008). The effects of lifetime food festriction on the development of osteoarthritis in the canine shoulder. *Veterinary Surgery* **37**, 102–107.

Sabeh, F., Li, X., Saunders, T., Rowe, R. and Weiss, S. (2009). Secreted versus membrane-anchored collagenases: Relative roles in fibroblast-dependent collagenolysis and invasion. *Journal of Biological Chemistry* **284**, 23001–23011.

Sakaguchi, Y., Sekiya, I., Yagishita, K. and Muneta, T. (2005). Comparison of human stem cells derived from various mesenchymal tissues: Superiority of synovium as a cell source. *Arthritis Rheum* **52**, 2521–2529.

Sandberg, A. and Bridge, J. (2003). Updates on the cytogenetics and molecular genetics of bone and soft tissue tumors: osteosarcoma and related tumors. *Cancer Genet. Cytogenet.* **145**, 1–30.

Sato, H., Kinoshita, T., Takino, T., Nakayama, K. and Seiki, M. (1996). Activation of a recombinant membrane type 1-matrix metalloproteinase (MT1-MMP) by furin and its interaction with tissue inhibitor of metalloproteinases (TIMP)-2. *FEBS Letters* **393**, 101–104.

Saunders, W., Bayless, K. and Davis, G. (2005). MMP-1 activation by serine proteases and MMP-10 induces human capillary tubular network collapse and regression in 3D collagen matrices. *Journal of Cell Science* **118**, 2325–2340.

Schneider, C., Rasband, W. and Eliceiri, K. (2012). NIH image to ImageJ: 25 years of image analysis. *Nature Methods* **9**, 671–675.

Schwarz, C., Leicht, U., Rothe, C., Drosse, I., Luibl, V., Röcken, M. and Schieker, M. (2012). Effects of different media on proliferation and differentiation capacity of canine, equine and porcine adipose derived stem cells. *Research in Veterinary Science* **93**, 457–462.

Sekiya, I., Larson, B., Smith, J., Pochampally, R., Cui, J. and Prockop, D. (2002). Expansion of human adult stem cells from bone marrow stroma: Conditions that maximize the yields of early progenitors and evaluate their quality. *Stem Cells* **20**, 530–541.

Seymour, L. and Bezwoda, W. (1994). Positive immunostaining for platelet-derived growth-factor (PDGF) is an adverse prognostic factor in patients with advanced breast-cancer. *Breast Cancer Res. Treat.* **32**, 229–233.

Seymour, L., Dajee, D. and Bezwoda, W. (1993). Tissue platelet derived-growth factor (PDGF) predicts for shortened survival and treatment failure in advanced breast cancer. *Breast Cancer Res. Treat.* **26**, 247–252.

Sherwood, J., Riley, S., Palazzolo, R., Brown, S., Monkhouse, D., Coates, M., Griffith, L., Landeen, L. and Ratcliffe, A. (2002). A three-dimensional osteochondral composite scaffold for articular cartilage repair. *Biomaterials* **23**, 4739–4751.

Shi, C., Ma, Y., Liu, H., Zhang, Y., Wang, Z. and Jia, H. (2011). The non-receptor tyrosine kinase c-Src mediates the PDGF-induced association between furin and pro-MT1-MMP in HPAC pancreatic cells. *Mol Cell Biochem* **362**, 65–70.

Shields, L., Raque, G., Glassman, S., Campbell, M., Vitaz, T., Harpring, J. and Shields, C. (2006). Adverse effects associated with high-dose recombinant human bone morphogenetic protein-2 use in anterior cervical spine fusion. *Spine* **31**, 542–547.

Shimada, T., Nakamura, H., Ohuchi, E., Fujii, Y., Murakami, Y., Sato, H., Seiki, M. and Okada, Y. (1999). Characterization of a truncated recombinant form of human membrane type 3 matrix metalloproteinase. *Eur. J. Biochem.* **262**, 907–914.

Shin, H., Temenoff, J., Bowden, G., Zygourakis, K., Farach-Carson, M., Yaszemski, M. and Mikos, A. (2005). Osteogenic differentiation of rat bone marrow stromal cells cultured on Arg–Gly–Asp modified hydrogels without dexamethasone and β-glycerol phosphate. *Biomaterials* **26**, 3645–3654.

Shiomi, T. and Okada, Y. (2003). MT1-MMP and MMP-7 in invasion and metastasis of human cancers. *Cancer Metastasis Rev.* **22**, 145–152.

Shortkroff, S., Barone, L., Hsu, H., Wrenn, C., Gagne, T., Chi, T., Breinan, H., Minas, T., Sledge, C., Tubo, R., et al. (1996). Healing of chondral and osteochondral defects in a canine model: The role of cultured chondrocytes in regeneration of articular cartilage. *Biomaterials* **17**, 147–154.

Smith, G., Paster, E., Powers, M., Lawler, D., Biery, D., Shofer, F., McKelvie, P. and Kealy, R. (2006). Lifelong diet restriction and radiographic evidence of osteoarthritis of the hip joint in dogs. *J Am Vet Med Assoc* **229**, 690–693.

Socie, G. and Blazar, B. (2009). Acute graft-versus-host disease: From the bench to the bedside. *Blood* **114**, 4327–4336.

Spencer, T., Bartol, F., Bazer, F., Johnson, G. and Joyce, M. (1999). Identification and characterization of glycosylation-dependent cell adhesion molecule 1-like protein expression in the ovine uterus. *Biology of Reproduction* **60**, 241–250.

Sternlicht, M. and Werb, Z. (2001). How matrix metalloproteinases regulate cell behavior. *Annu. Rev. Cell Dev. Biol.* **17**, 463–516.

Stewart, C. and Stewart, J. (2001). Cell preparation for the identification of leukocytes. *Methods in Cell Biology* **63**, 217–251.

Stewart, K., Walsh, S., Screen, J., Jefferiss, C., Chainey, J., Jordan, G. and Beresford, J. (1999). Further characterization of cells expressing STRO-1 in cultures of adult human bone marrow stromal cells. *Journal of Bone and Mineral Research* **14**, 1345–1356.

Stewart, M. and Stewart, A. (2011). Mesenchymal stem cells: Characteristics, sources, and mechanisms of action. *Veterinary Clinics of NA: Equine Practice* **27**, 243–261.

Stocker, W., Grams, F., Baumann, U., Reinemer, P., Gomisruth, F., McKay, D. and Bode, W. (1995). The metzincins- Topological and sequential relations between the astacins, adamalysins, serralysins, and matrixins (collagenases) define a superfamily of zinc-peptidases. *Protein Sci* **4**, 823–840.

Storb, R., Epstein, R., Graham, T. and Thomas, E. (1970). Methotrexate regimens for control of graft-versus-host disease in dogs with allogeneic marrow grafts. *Transplantation* **9**, 240–246.

Takada, I., Kouzmenko, A. and Kato, S. (2009a). Molecular switching of osteoblastogenesis versus adipogenesis: Implications for targeted therapies. *Expert Opin. Ther. Targets* **13**, 593–603.

Takada, I., Kouzmenko, A. and Kato, S. (2009b). Wnt and PPARγ signaling in osteoblastogenesis and adipogenesis. *Nature Publishing Group* **5**, 442–447.

Takagi, S., Takemoto, A., Takami, M., Oh-hara, T. and Fujita, N. (2014). Platelets promote osteosarcoma cell growth through activation of the platelet-derived growth factor receptor-Akt signaling axis. *Cancer Science* **105**, 983–988.

Takeda, W. and Wessel, J. (1994). Acupuncture for the treatment of pain of osteoarthritic knees. *Arthritis Care Res* **7**, 118–122.

Takemitsu, H., Zhao, D., Yamamoto, I., Harada, Y., Michishita, M. and Arai, T.

(2012). Comparison of bone marrow and adipose tissue-derived canine mesenchymal stem cells. *BMC Veterinary Research* **8**, 1–9.

Tang, Y., Rowe, R., Botvinick, E., Kurup, A., Putnam, A., Seiki, M., Weaver, V., Keller, E., Goldstein, S., Dai, J., et al. (2013). MT1-MMP-dependent control of skeletal stem cell commitment via a b1-integrin/YAP/TAZ signaling axis. *Developmental Cell* **25**, 402–416.

Thomas, J., Venugopalan, M., Galvin, R., Wang, Y., Bokoch, G. and Vlahos, C. (1997). Inhibition of MG-63 cell proliferation and PDGF-stimulated cellular processes by inhibitors of phosphatidylinositol 3-kinase. *J. Cell. Biochem.* **64**, 182–195.

Thomas, R., Wang, H., Tsai, P., Langford, C., Fosmire, S., Jubala, C., Getzy, D., Cutter, G., Modiano, J. and Breen, M. (2009). Influence of genetic background on tumor karyotypes: Evidence for breed-associated cytogenetic aberrations in canine appendicular osteosarcoma. *Chromosome Res* **17**, 365–377.

Tibbitt, M. and Anseth, K. (2009). Hydrogels as extracellular matrix mimics for 3D cell culture. *Biotechnol. Bioeng.* **103**, 655–663.

Toma, J., Akhavan, M. and Fernandes, K. (2001). Isolation of multipotent adult stem cells from the dermis of mammalian skin. *Nat Cell Biol* **3**, 778–784.

Tsubota, K., Satake, Y. and Kaido, M. (1999). Treatment of severe ocular-surface disorders with corneal epithelial stem-cell transplantation. *The New England Journal of Medicine* **340**, 1697–1703.

Uccelli, A., Moretta, L. and Pistoia, V. (2006). Immunoregulatory function of mesenchymal stem cells. *Eur. J. Immunol.* **36**, 2566–2573.

Uehara, H., Kim, S., Karashima, T., Shepherd, D., Fan, D., Tsan, R., Killion, J., Logothetis, C., Mathew, P. and Fidler, I. (2003). Effects of blocking platelet-derived growth factor-receptor signaling in a mouse model of experimental prostate cancer bone metastases. *J Natl Cancer Inst* **95**, 458–470.

Ulbricht, J., Jordan, R. and Luxenhofer, R. (2014). On the biodegradability of polyethylene glycol, polypeptoids and poly(2-oxazoline)s. *Biomaterials* **35**, 4848–4861.

Vail, D. and Macewen, E. (2009). Spontaneously occurring tumors of companion animals as models for human cancer. *Cancer Investigation* **18**, 781–792.

van der Flier, A. and Sonnenberg, A. (2001). Function and interactions of integrins. *Cell Tissue Res* **305**, 285–298.

Vanwart, H. and Birkedal-Hansen, H. (1990). The cysteine switch- A principle of

regulation of metalloproteinase activity with potential applicability to the entire matrix metalloproteinase gene family. *Proceedings of the National Academy of Sciences* **87**, 5578–5582.

Vattikuti, R. and Towler, D. (2004). Osteogenic regulation of vascular calcification: An early perspective. *AJP: Endocrinology and Metabolism* **286**, e686–e696.

Vidal, M., Kilroy, G., Lopez, M., Johnson, J., Moore, R. and Gimble, J. (2007). Characterization of equine adipose tissue-derived stromal cells: Adipogenic and osteogenic capacity and comparison with bone marrow-derived mesenchymal stromal cells. *Veterinary Surgery* **36**, 613–622.

Vincenti, M. and Brinckerhoff, C. (2002). Transcriptional regulation of collagenase (MMP-1, MMP-13) genes in arthritis: Integration of complex signaling pathways for the recruitment of gene-specific transcription factors. *Arthritis Res.* **4**, 157–164.

Volk, S., Diefenderfer, D., Christopher, S., Haskins, M. and Leboy, P. (2005). Effects of osteogenic inducers on cultures of canine mesenchymal stem cells. *American Journal of Veterinary Research* **66**, 1729–1737.

Volk, S., Wang, Y. and Hankenson, K. (2012). Effects of donor characteristics and ex vivo expansion on canine mesenchymal stem cell properties: Implications for MSC-based therapies. *Cell transplantation* **21**, 2189–2200.

Walkley, C., Qudsi, R., Sankaran, V., Perry, J., Gostissa, M., Roth, S., Rodda, S., Snay, E., Dunning, P., Fahey, F., et al. (2008). Conditional mouse osteosarcoma, dependent on p53 loss and potentiated by loss of Rb, mimics the human disease. *Genes & Development* **22**, 1662–1676.

Wallace, D., Cruise, G., Rhee, W., Schroeder, J., Prior, J., Ju, J., Maroney, M., Duronio, J., Ngo, M., Estridge, T., et al. (2001). A tissue sealant based on reactive multifunctional polyethylene glycol. *J. Biomed. Mater. Res.* **58**, 545–555.

Waterman, R., Tomchuck, S., Henkle, S. and Betancourt, A. (2010). A new mesenchymal stem cell (MSC) paradigm: Polarization into a pro-inflammatory MSC1 or an immunosuppressive MSC2 phenotype. *PLoS ONE* **5**, e10088.

Werb, Z. (1997). ECM and cell surface proteolysis: Regulating cellular ecology. *Cell* **91**, 439–442.

West, J. and Hubbell, J. (1995). Photopolymerized hydrogel materials for drug delivery applications. *Reactive Polymers* **25**, 139–147.

Wilke, V., Robinson, D., Evans, R., Rothschild, M. and Conzemius, M. (2005). Estimate of the annual economic impact of treatment of cranial cruciate ligament injury

in dogs in the United States. *J Am Vet Med Assoc* **227**, 1604–1607.

Wilson, W., van Donkelaar, C., van Rietbergen, R. and Huiskes, R. (2005). The role of computational models in the search for the mechanical behavior and damage mechanisms of articular cartilage. *Medical Engineering & Physics* **27**, 810–826.

Withrow, S., Powers, B., Straw, R. and Wilkins, R. (1991). Comparative aspects of osteosarcoma. Dog versus man. *Clin Orthop Relat Res* **270**, 159–168.

Woessner, J. (1994). The family of matrix metalloproteinases. *Annals of the New York Academy of Sciences* **732**, 11–21.

Woessner, J. (2002). MMPs and TIMPs-- A historical perspective. *Mol Biotechnol* **22**, 33–49.

Wolf, K., teLindert, M., Krause, M., Alexander, S., teRiet, J., Willis, A., Hoffman, R., Figdor, C., Weiss, S. and Friedl, P. (2013). Physical limits of cell migration: Control by ECM space and nuclear deformation and tuning by proteolysis and traction force. *The Journal of Cell Biology* **201**, 1069–1084.

Wong, K., Lee, K., Tai, B., Law, P., Lee, E. and Hui, J. (2013). Injectable cultured bone marrow derived mesenchymal stem cells in varus knees with cartilage defects undergoing high tibial osteotomy: A prospective, randomized controlled clinical trial with 2 years' follow-up. *Arthroscopy: The Journal of Arthroscopic and Related Surgery* **29**, 2020–2028.

Woolf, A. and Pfleger, B. (2003). Burden of major musculoskeletal conditions. *Bull. World Health Organ.* **81**, 646–656.

Yana, I. and Weiss, S. (2000). Regulation of membrane type-1 matrix metalloproteinase activation by proprotein convertases. *Mol. Biol. Cell* **11**, 2387–2401.

Yarden, Y., Escobedo, J., Kuang, W., Yang-Feng, T., Daniel, T., Tremble, P., Chen, E., Ando, M., Harkins, R. and Francke, U. (1986). Structure of the receptor for platelet-derived growth factor helps define a family of closely related growth factor receptors. *Nature* **323**, 226–232.

Yokoyama, A., Sekiya, I., Miyazaki, K., Ichinose, S., Hata, Y. and Muneta, T. (2005). In vitro cartilage formation of composites of synovium-derived mesenchymal stem cells with collagen gel. *Cell Tissue Res* **322**, 289–298.

Ytrehus, B., Carlson, C. and Ekman, S. (2007). Etiology and pathogenesis of osteochondrosis. *Veterinary Pathology* **44**, 429–448.

Zhang, H., Wang, L., Song, L., Niu, G., Cao, H., Wang, G., Yang, H. and Zhu, S.

(2011). Controllable properties and microstructure of hydrogels based on crosslinked poly(ethylene glycol) diacrylates with different molecular weights. *J. Appl. Polym. Sci.* **121**, 531–540.

Zuk, P., Zhu, M., Ashjian, P., De Ugarte, D., Huang, J., Mizuno, H., Alfonso, Z., Fraser, J., Benhaim, P. and Hedrick, M. (2002). Human adipose tissue is a source of multipotent stem cells. *Mol. Biol. Cell* **13**, 4279–4295.

APPENDIX

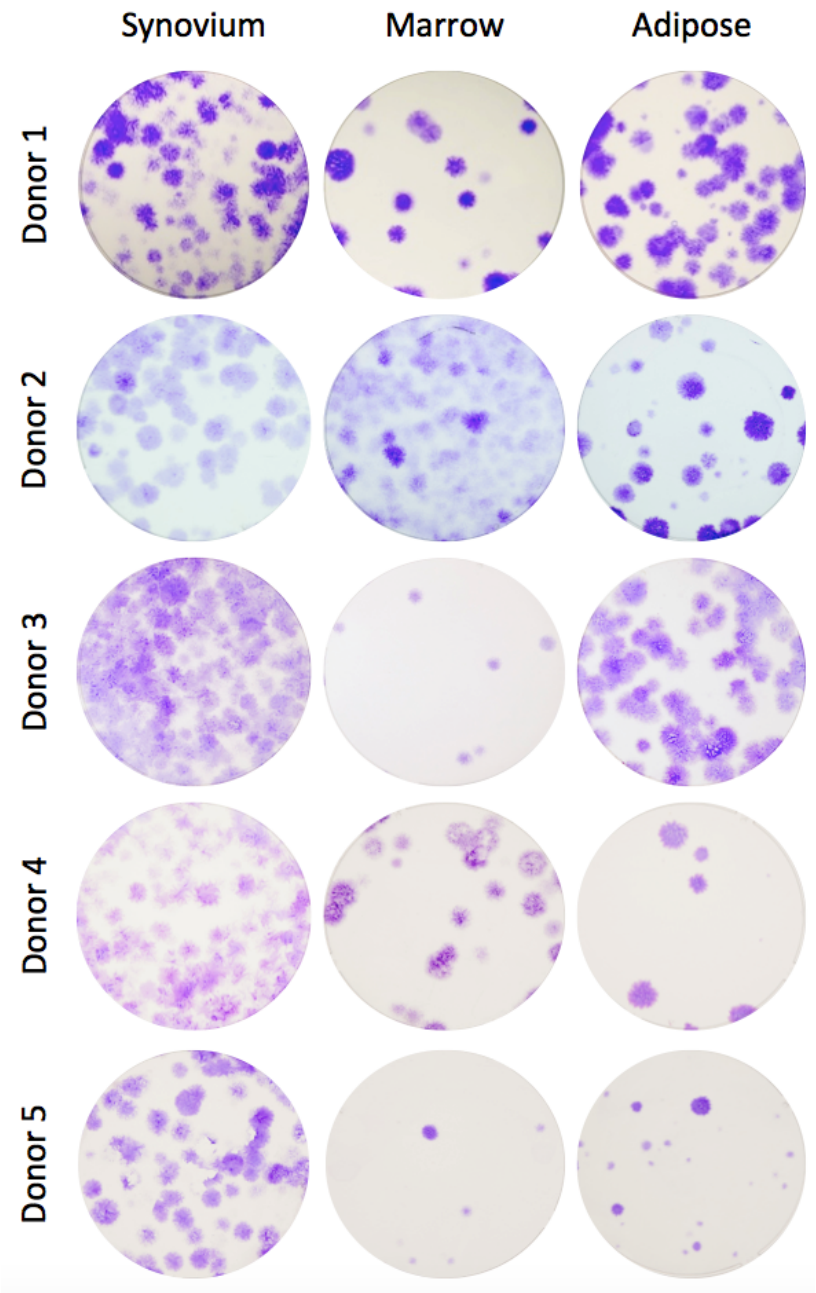

Appendix 1.1 *Colony forming unit (CFU) assay for all 15 cell preparations*. Colony forming unit (CFU) potential of primary cell populations for all 15 donors was assessed. $1x10^3$ total cells (synovium and adipose) or $4.5x10^5$ total cells (marrow) were seeded on 55 cm^2 plates (n=3) and incubated for 21 days without media exchange. Plates were stained with 0.01% Crystal Violet and colony counts were performed on each plate. Representative photographs of CFU plates for each tissue from each individual donor.

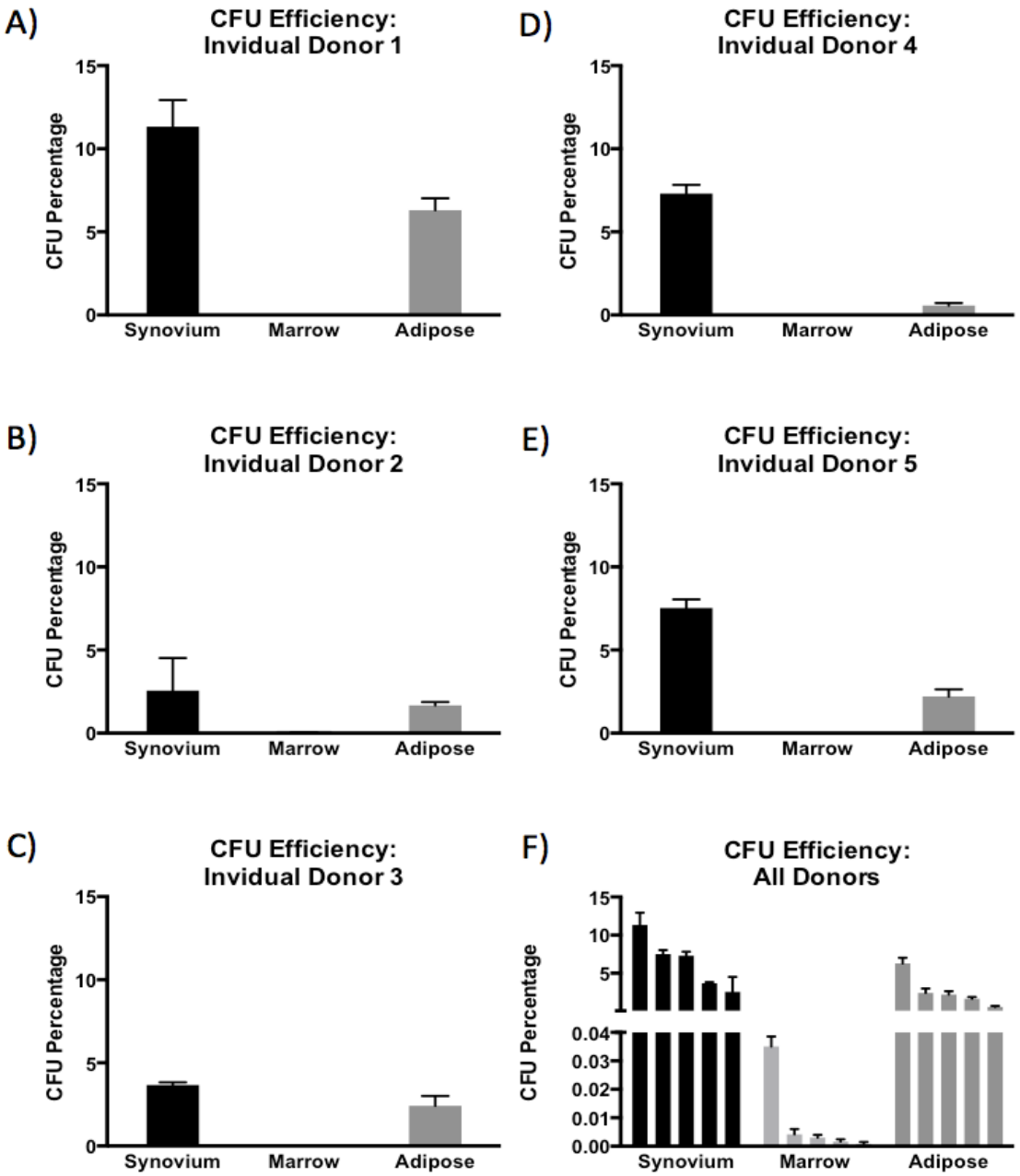

Appendix 1.2. *Colony forming unit efficiency.* Colony forming unit (CFU) potential of primary cell populations for all 15 tissue samples. $1x10^3$ total cells (synovium and adipose) or $4.5x10^5$ total cells (marrow) were seeded on 55 cm^2 plates (n=3) and incubated for 21 days without media exchange. Plates were stained with 0.01% Crystal Violet and colony counts were performed on each plate. CFU efficiency is defined as the number of colonies present divided by total number of seeded cells. Data are reported as mean ± SD (n=3 plates/tissue). **A-E)** Individual donor CFU efficiency. **F)** All donor CFU efficiency organized in descending order.

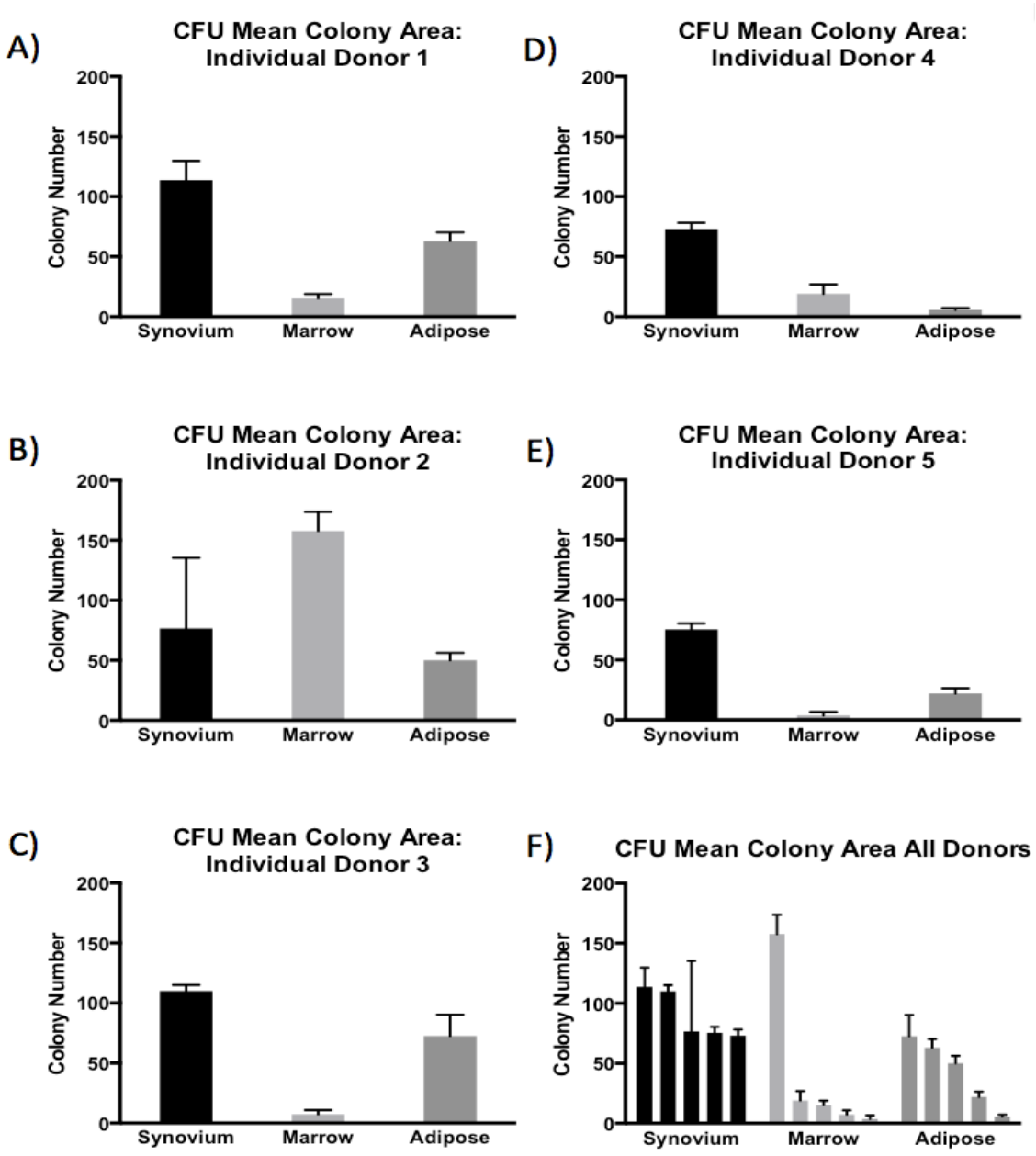

Appendix 1.3. *Colony forming unit (CFU) mean colony area.* Colony forming unit (CFU) mean colony area of primary cell populations for all 15 tissue samples. $1x10^3$ total cells (synovium and adipose) or $4.5x10^5$ total cells (marrow) were seeded on 55 cm^2 plates and incubated for 21 days without media exchange. Plates were stained with 0.01% Crystal Violet and individual colony area measured (n=3 plates/tissue) using ImageJ software. CFU mean colony area is defined as colony surface area (cm^2) divided by the number of colonies. Data are reported as mean ± SD. **A-E)** Individual donor CFU mean colony area. **F)** All donor CFU mean colony area organized in descending order.

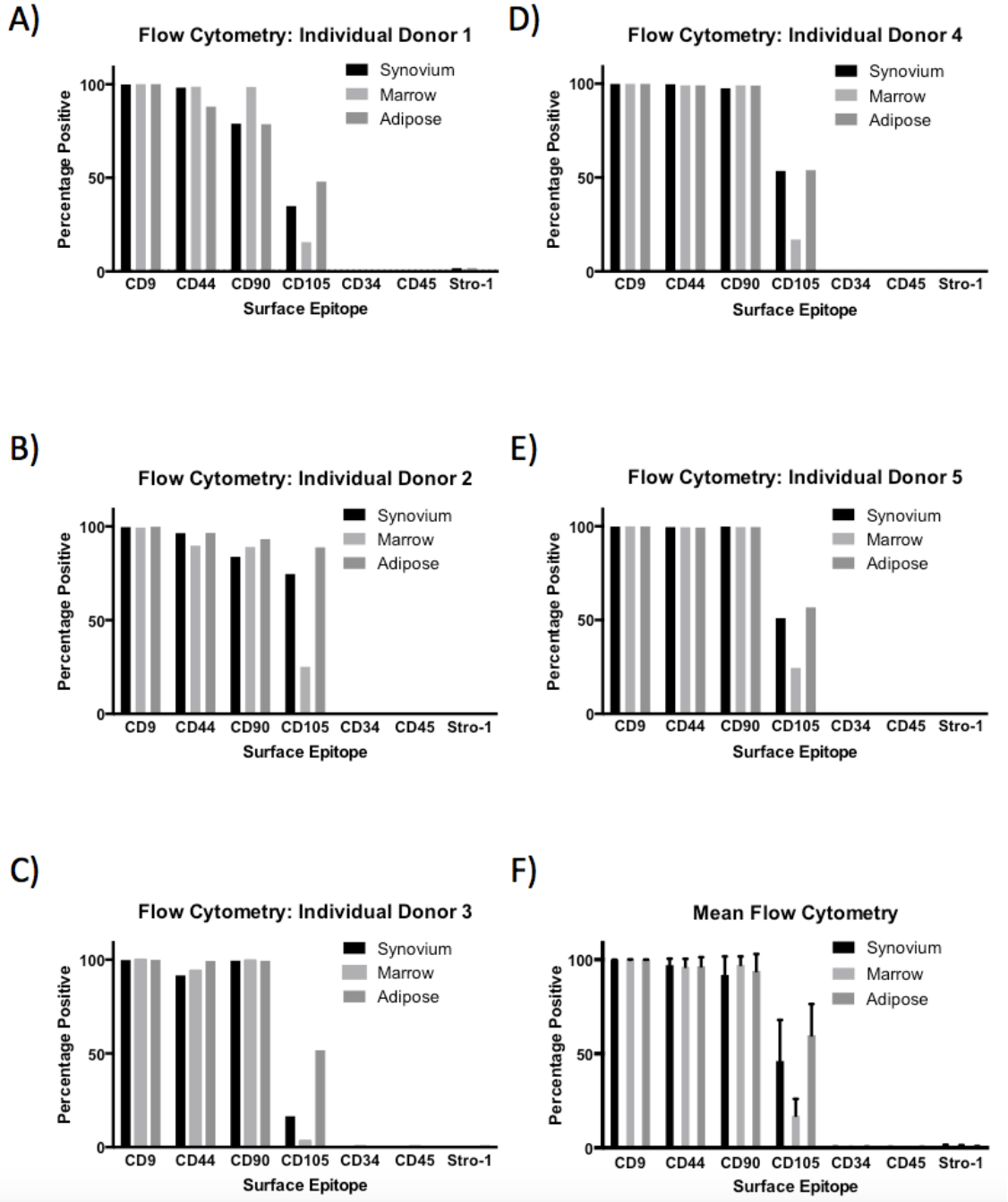

Appendix 1.4. *Flow cytometry for all 15 cell preparations*. **A-E)** Percentage positive cells from synovium, marrow, and adipose cMSCs isolated from five individual canine donors. **F)** Mean ± SD percentage positive cells synovium, marrow, and adipose cMSCs isolated from all five canine donors.

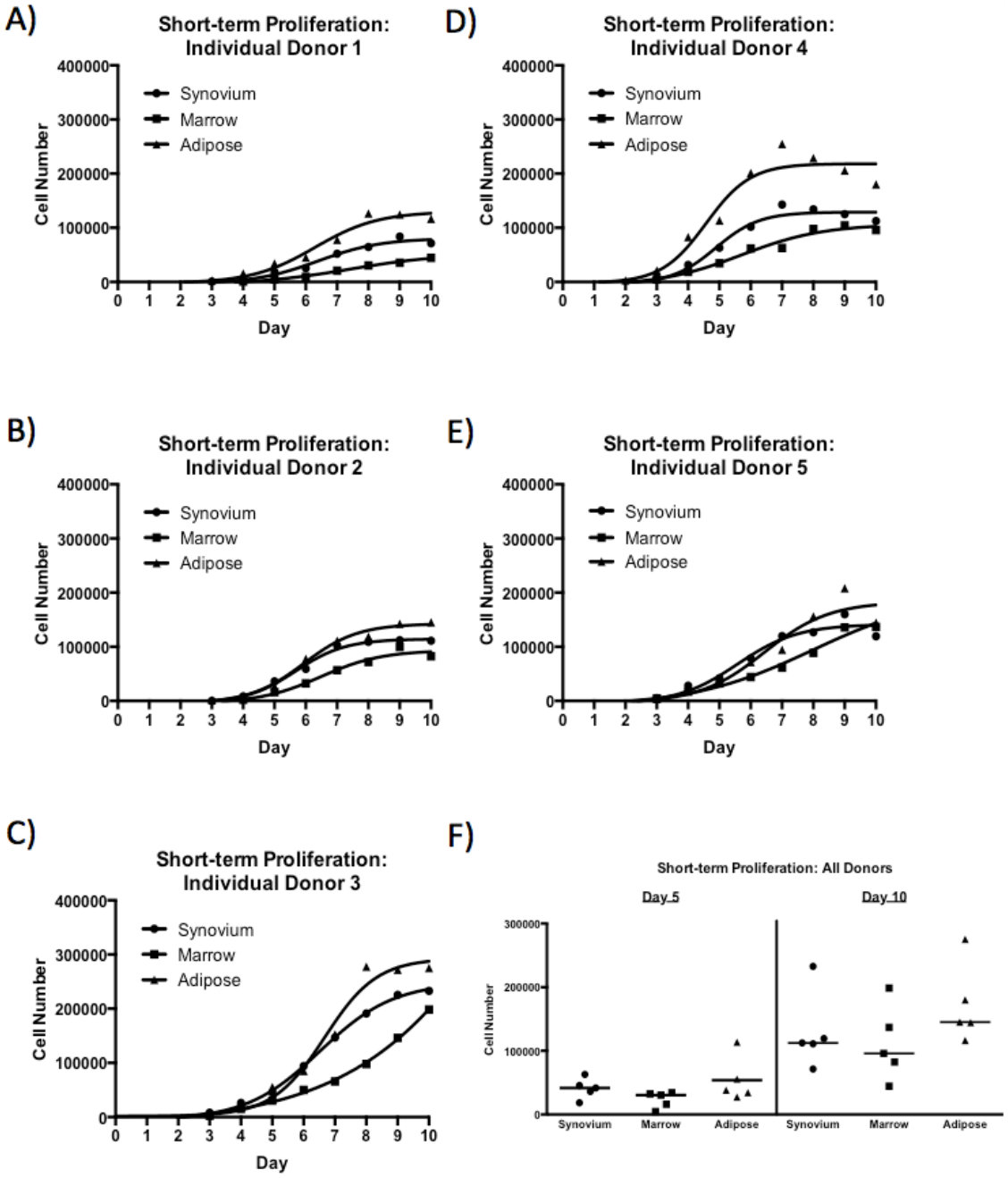

Appendix 1.5. *Short-term proliferation rates of cMSCs from synovium, bone marrow, and adipose tissues.* Short-term proliferation was determined over a 10 day time course. Passage 2 cells were seeded at 100 cells/cm^2 in CCM on 12-well plates (n=3 wells/cell line) with media exchange every other day. **A-E)** Mean cell number from each individual donor was determined daily using DNA quantification. **F)** Scatter-plot demonstrating proliferation of all cell lines at days 5 and 10. Each data point represents the cell number for an individual cell line (bar=mean).

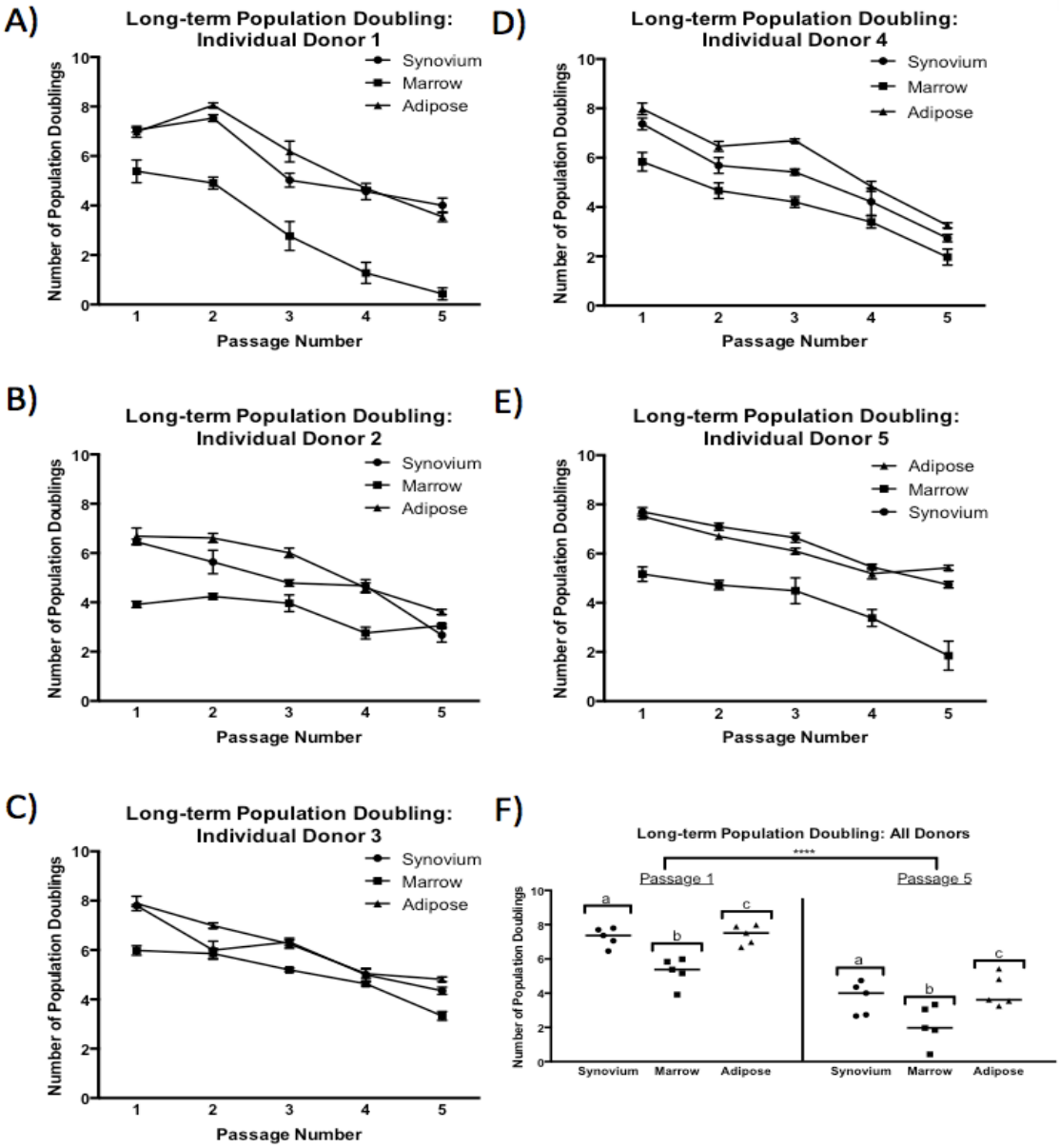

Appendix 1.6. *Long-term proliferation rates of cMSCs from synovium, bone marrow, and adipose tissues.* Long-term proliferation was determined over a 5 passage, 25 day time course. Passage 2 cMSCs were seeded at 100 cells/cm^2 in CCM on 55 cm^2 plates (n=3 plates/cell preparation/passage) with media exchange every other day. At 5 day intervals, cells were washed, trypsinized, recovered, cell number determined using a hemocytometer, and re-plated at 100 cells/cm^2. Long-term proliferation rates were determined using the population doubling equation. **A-E)** Individual population doubling. **F)** Scatter-plot for all 15 cMSC preparations (mean ± SD) at Passage 1 and 5. Each data point represents the population-doubling rate for an individual cMSC preparation (bar=mean population doubling rate across the 5 donors).

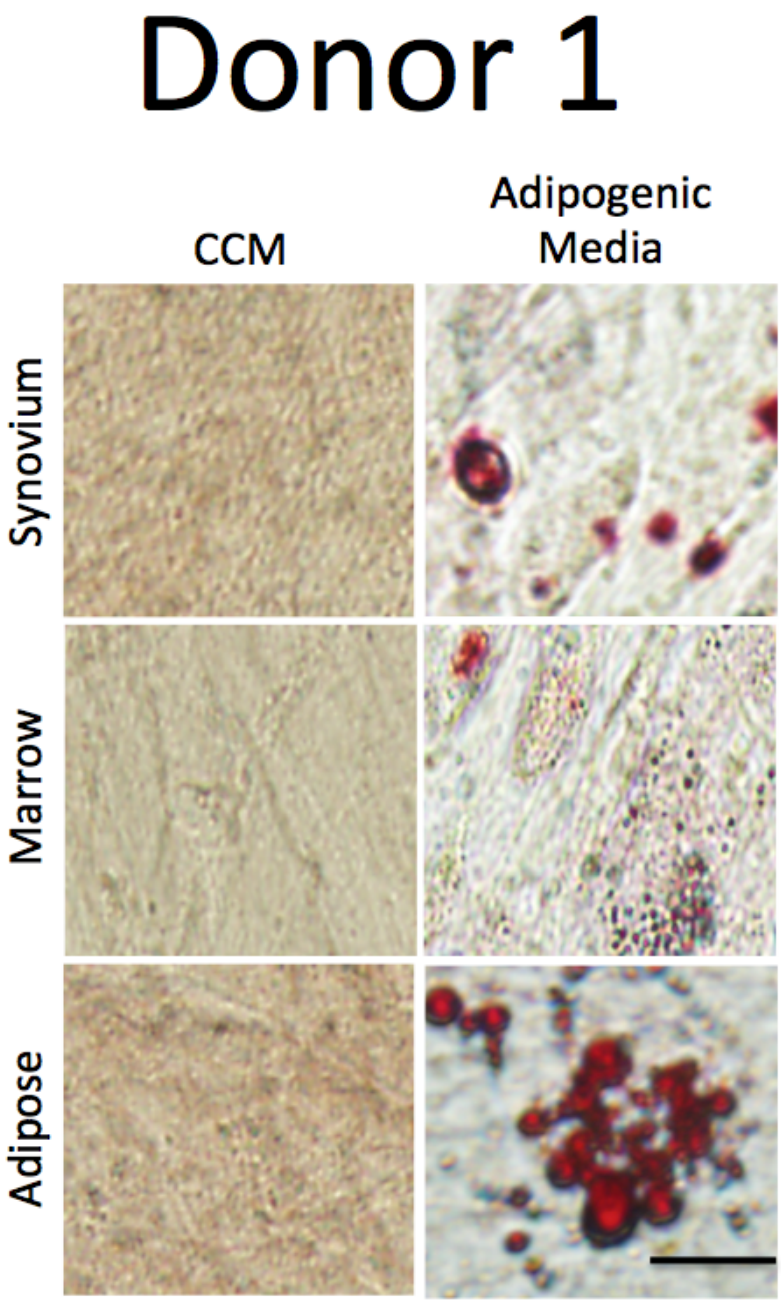

Appendix 1.7. *Adipogenesis of synovium, marrow, and adipose of an individual cMSC donor.* Passage 2 cMSCs were cultured in quadruplicate wells in CCM or modified adipogenic media with media exchange twice weekly. At 21 days, cells were formalin fixed and evaluated for lipid accumulation with Oil Red O (bar=25µm).

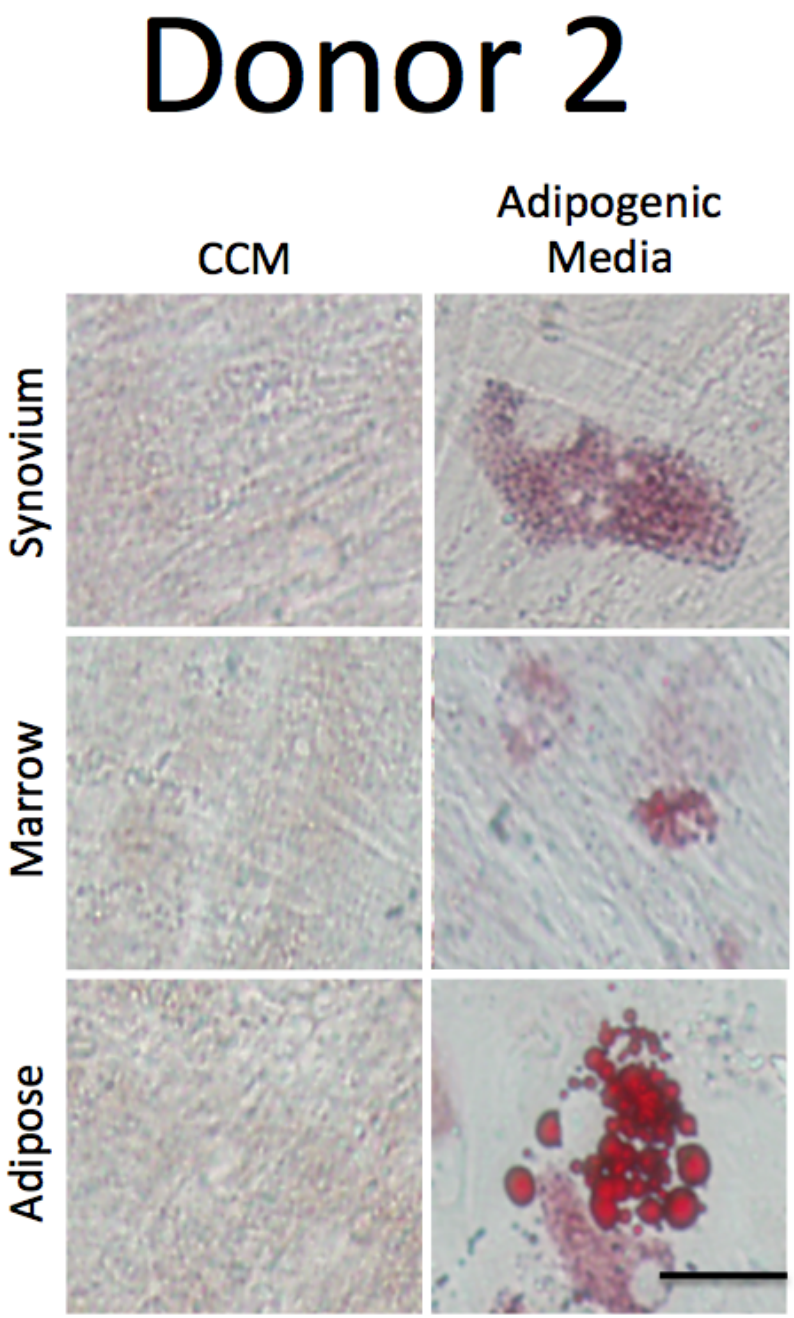

Appendix 1.8. *Adipogenesis of synovium, marrow, and adipose of an individual cMSC donor.* Passage 2 cMSCs were cultured in quadruplicate wells in CCM or modified adipogenic media with media exchange twice weekly. At 21 days, cells were formalin fixed and evaluated for lipid accumulation with Oil Red O (bar=25µm).

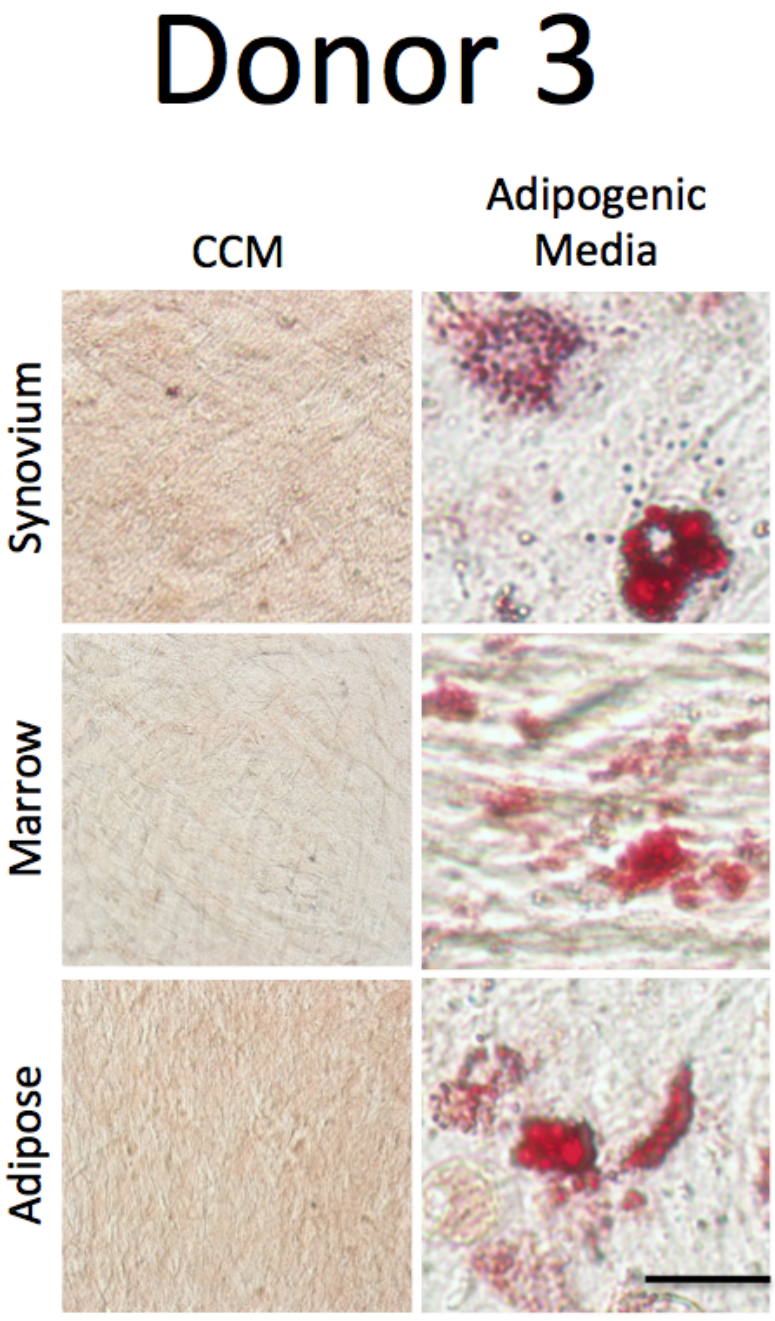

Appendix 1.9. *Adipogenesis of synovium, marrow, and adipose of an individual cMSC donor.* Passage 2 cMSCs were cultured in quadruplicate wells in CCM or modified adipogenic media with media exchange twice weekly. At 21 days, cells were formalin fixed and evaluated for lipid accumulation with Oil Red O (bar=25µm).

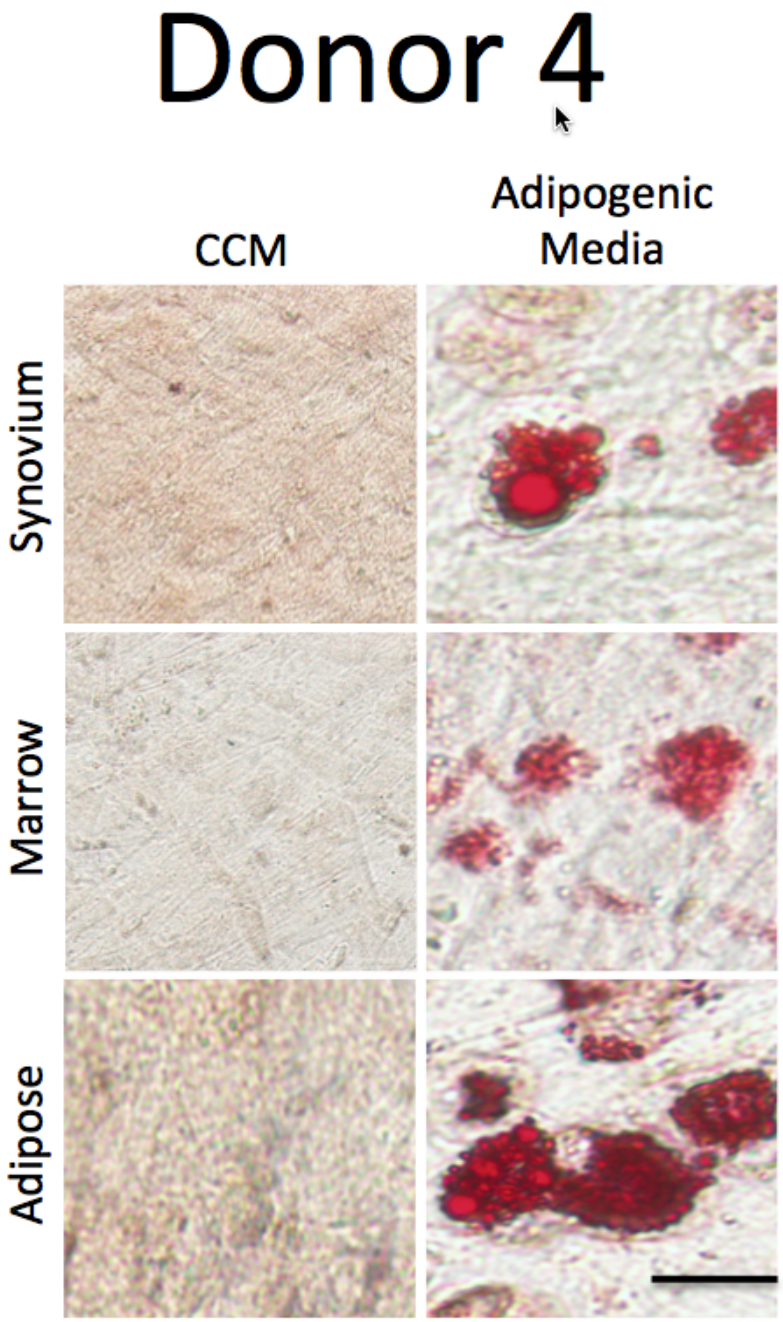

Appendix 1.10. *Adipogenesis of synovium, marrow, and adipose of an individual cMSC donor.* Passage 2 cMSCs were cultured in quadruplicate wells in CCM or modified adipogenic media with media exchange twice weekly. At 21 days, cells were formalin fixed and evaluated for lipid accumulation with Oil Red O (bar=25µm).

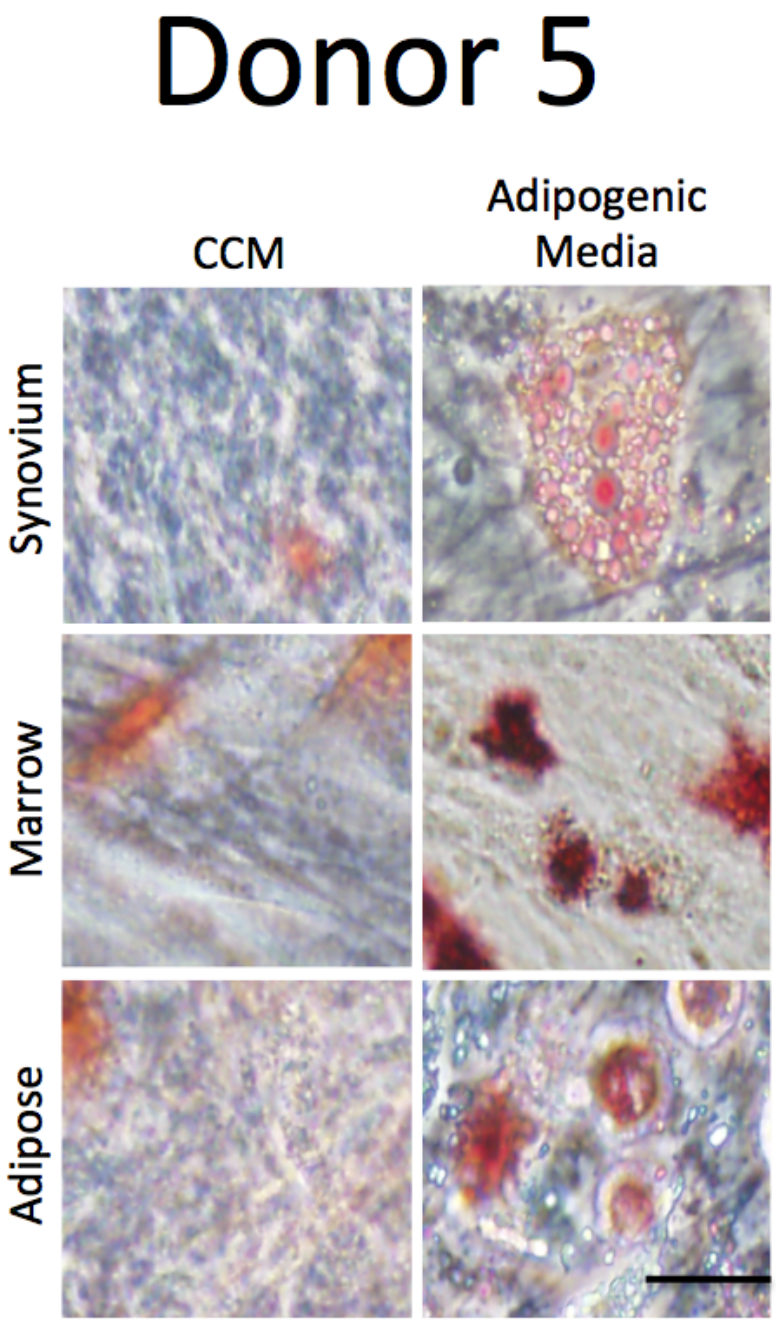

Appendix 1.11. *Adipogenesis of synovium, marrow, and adipose of an individual cMSC donor.* Passage 2 cMSCs were cultured in quadruplicate wells in CCM or modified adipogenic media with media exchange twice weekly. At 21 days, cells were formalin fixed and evaluated for lipid accumulation with Oil Red O (bar=25µm).

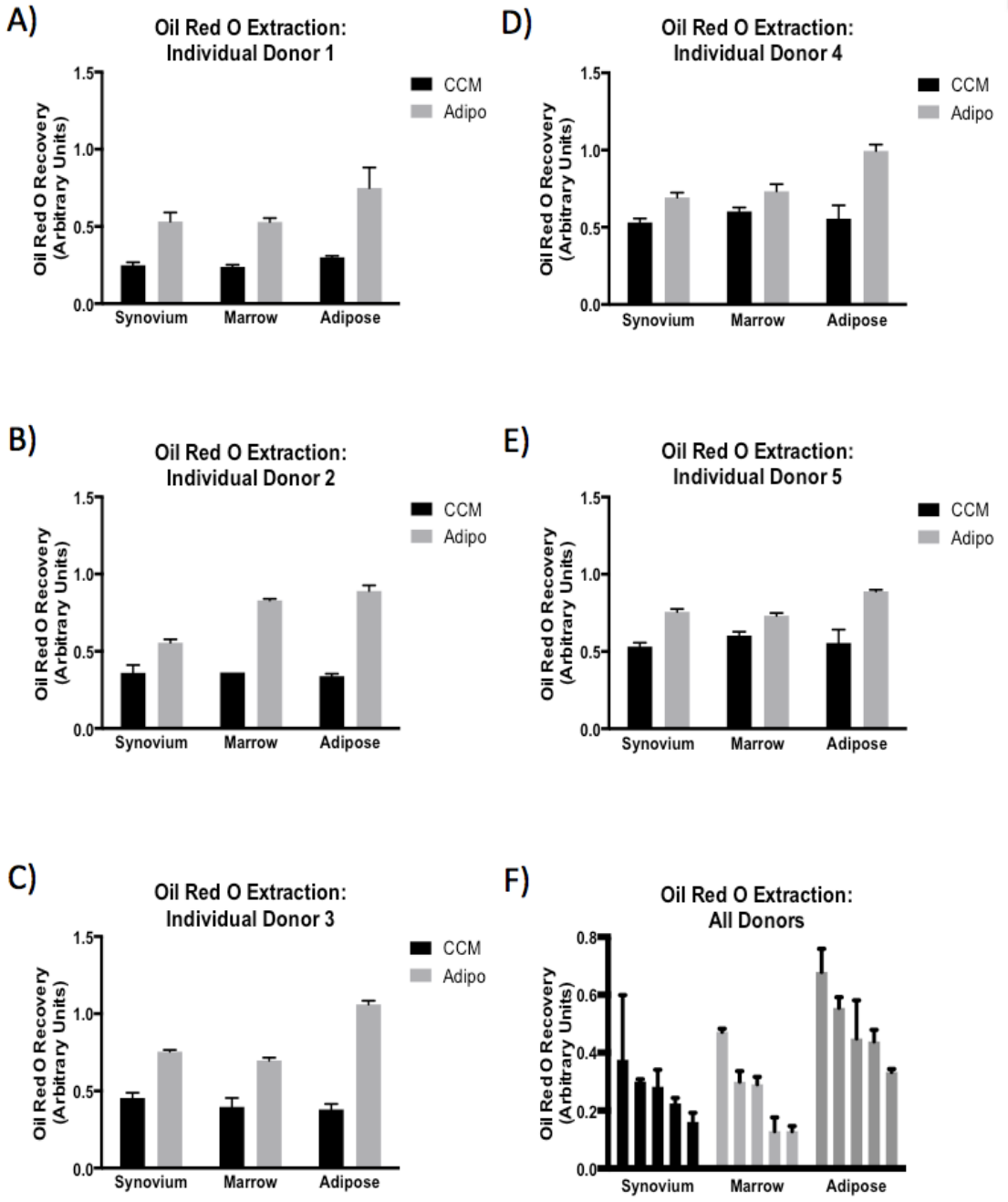

Appendix 1.12. *Oil Red O quantification of adipogenic synovium, bone marrow, and adipose cMSCs*. Passage 2 cMCs were cultured in quadruplicate wells and supplied with CCM or adipogenic media. At 21 days, cells were formalin fixed and evaluated for lipid accumulation with Oil Red O. **A-E)** Oil Red O quantification (mean ± SD) for five individual donors. **F)** Extraction values for adipogenic conditions for all 15 cell lines. CCM values have been subtracted from adipogenic values. Data are reported in descending order for each tissue.

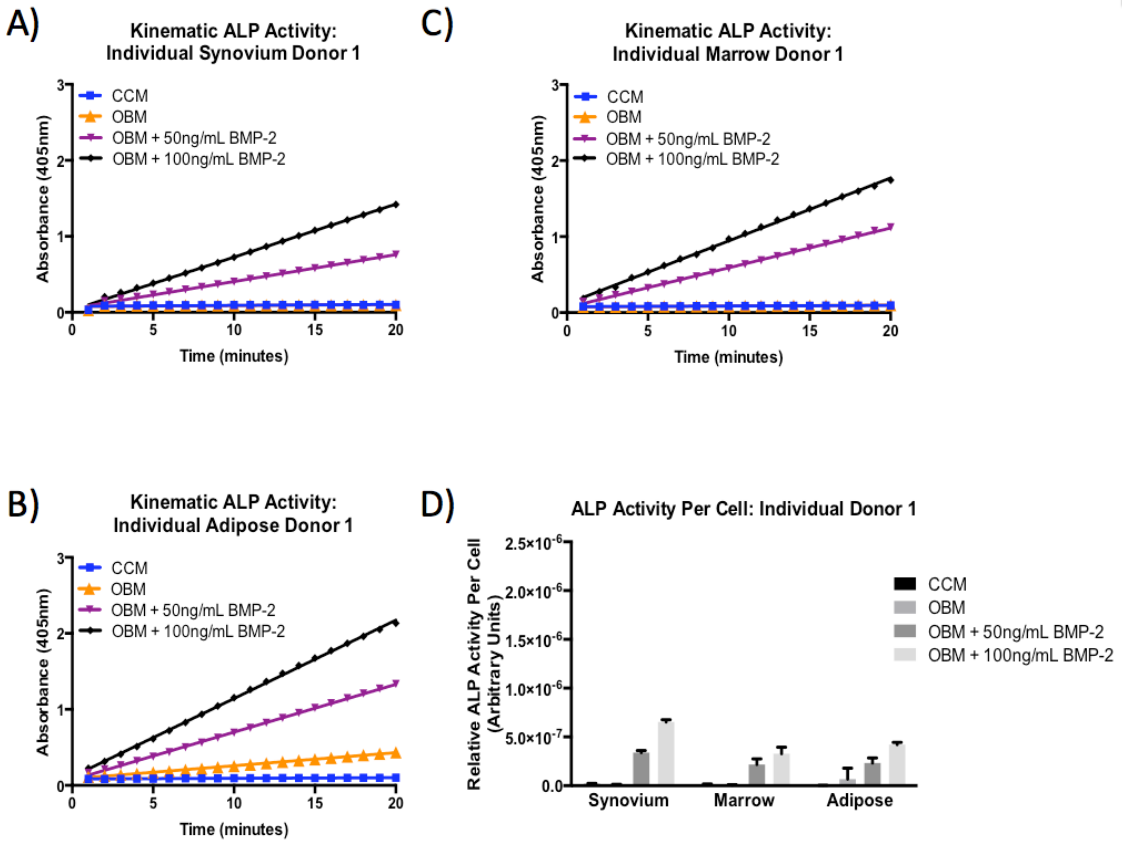

Appendix 1.13. *Short-term osteogenesis of synovium, marrow, and adipose cMSCs from an individual donor.* Short-term osteogenesis was determined using the alkaline phosphatase activity (ALP) assay. Passage 2 cMSCs were cultured in CCM, OBM, or OBM + rhBMP-2 for 7 days and evaluated for the ability to convert the colorless substrate PNPP to colorimetric PNP over time. ALP activity was determined by spectrophotometer (absorbance 405nM) over a 20-minute time course. **A-C)** Kinetic ALP activity results for synovium, bone marrow, and adipose cMSCs preparations from an individual donor are shown. **D)** ALP activity normalized to cell number by DNA quantification for synovium, bone marrow, and adipose from an individual donor are shown.

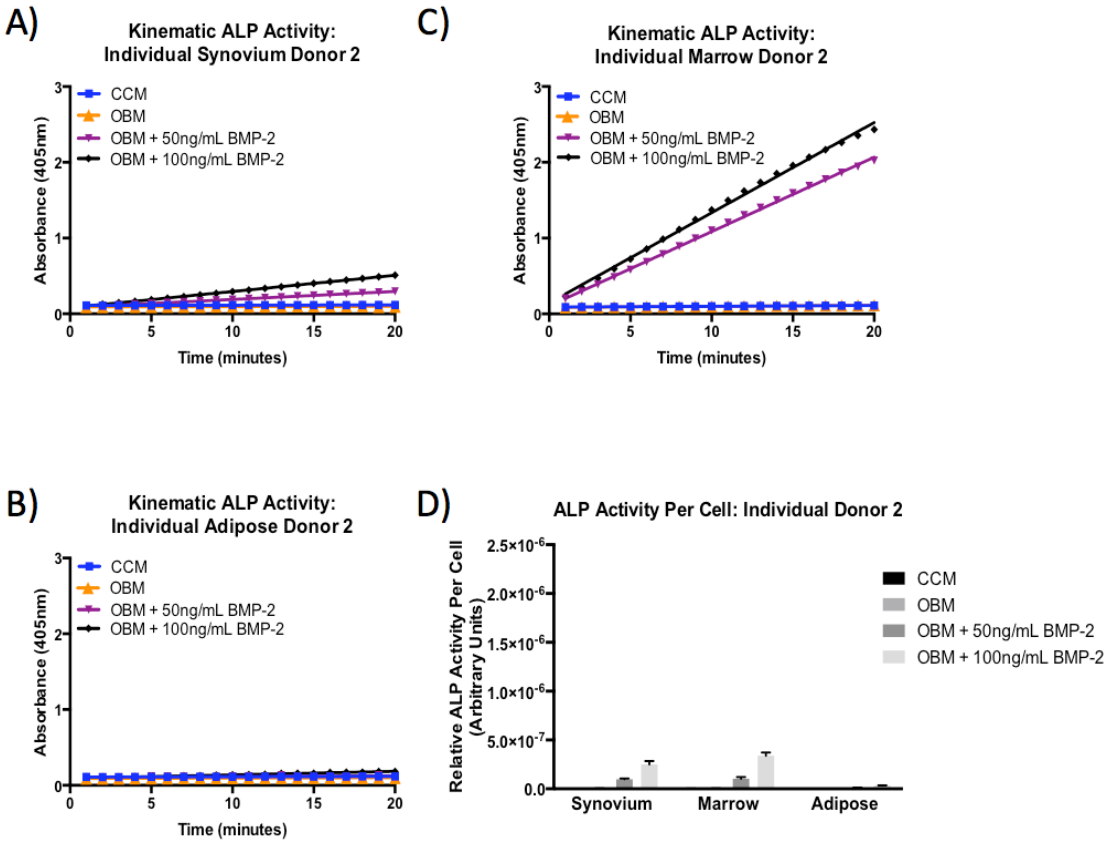

Appendix 1.14. *Short-term osteogenesis of synovium, marrow, and adipose cMSCs from an individual donor.* Short-term osteogenesis was determined using the alkaline phosphatase activity (ALP) assay. Passage 2 cMSCs were cultured in CCM, OBM, or OBM + rhBMP-2 for 7 days and evaluated for the ability to convert the colorless substrate PNPP to colorimetric PNP over time. ALP activity was determined by spectrophotometer (absorbance 405nM) over a 20-minute time course. **A-C)** Kinetic ALP activity results for synovium, bone marrow, and adipose cMSCs preparations from an individual donor are shown. **D)** ALP activity normalized to cell number by DNA quantification for synovium, bone marrow, and adipose from an individual donor are shown.

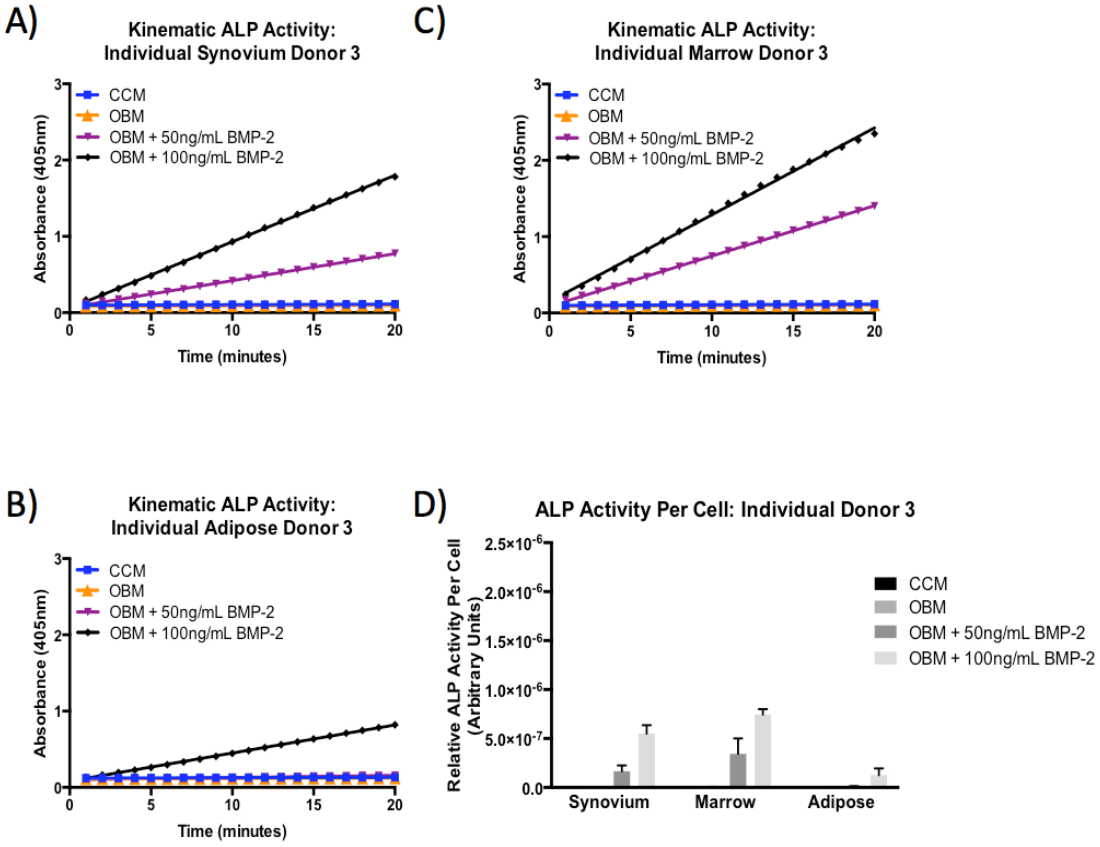

Appendix 1.15. *Short-term osteogenesis of synovium, marrow, and adipose cMSCs from an individual donor.* Short-term osteogenesis was determined using the alkaline phosphatase activity (ALP) assay. Passage 2 cMSCs were cultured in CCM, OBM, or OBM + rhBMP-2 for 7 days and evaluated for the ability to convert the colorless substrate PNPP to colorimetric PNP over time. ALP activity was determined by spectrophotometer (absorbance 405nM) over a 20-minute time course. **A-C)** Kinetic ALP activity results for synovium, bone marrow, and adipose cMSCs preparations from an individual donor are shown. **D)** ALP activity normalized to cell number by DNA quantification for synovium, bone marrow, and adipose from an individual donor are shown.

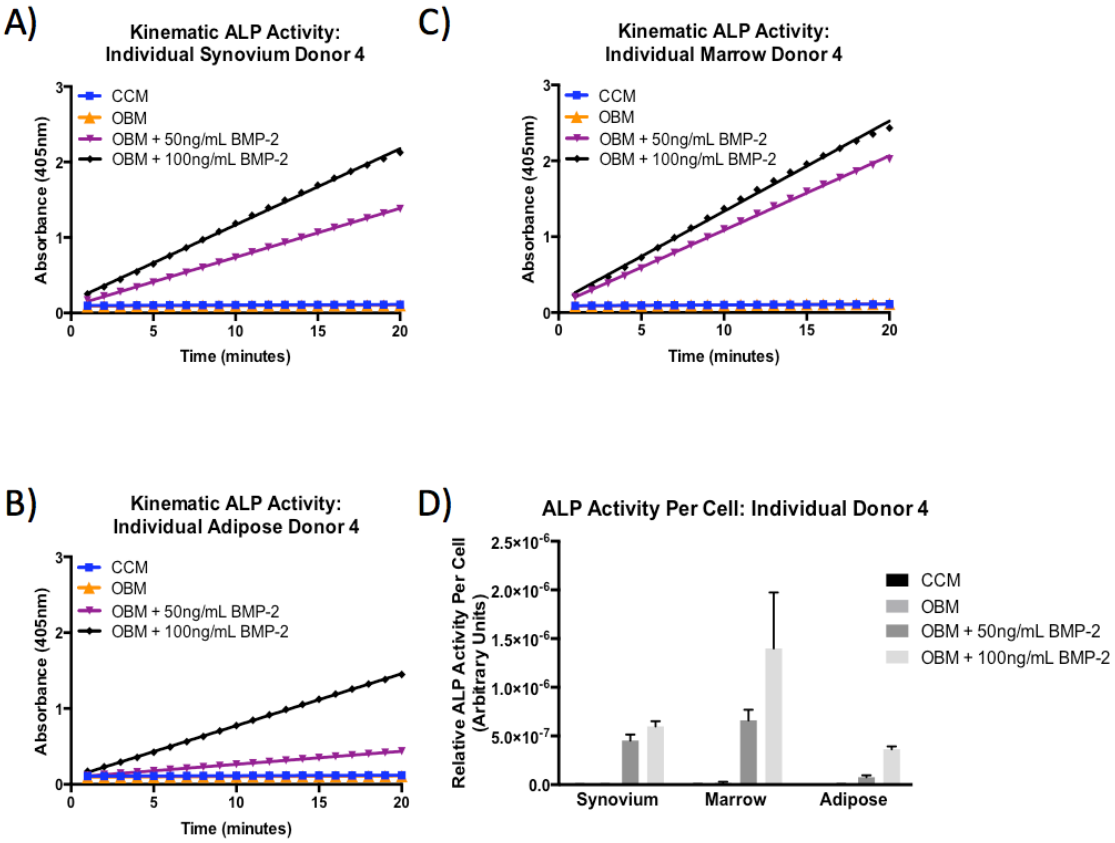

Appendix 1.16. *Short-term osteogenesis of synovium, marrow, and adipose cMSCs from an individual donor.* Short-term osteogenesis was determined using the alkaline phosphatase activity (ALP) assay. Passage 2 cMSCs were cultured in CCM, OBM, or OBM + rhBMP-2 for 7 days and evaluated for the ability to convert the colorless substrate PNPP to colorimetric PNP over time. ALP activity was determined by spectrophotometer (absorbance 405nM) over a 20-minute time course. **A-C)** Kinetic ALP activity results for synovium, bone marrow, and adipose cMSCs preparations from an individual donor are shown. **D)** ALP activity normalized to cell number by DNA quantification for synovium, bone marrow, and adipose from an individual donor are shown.

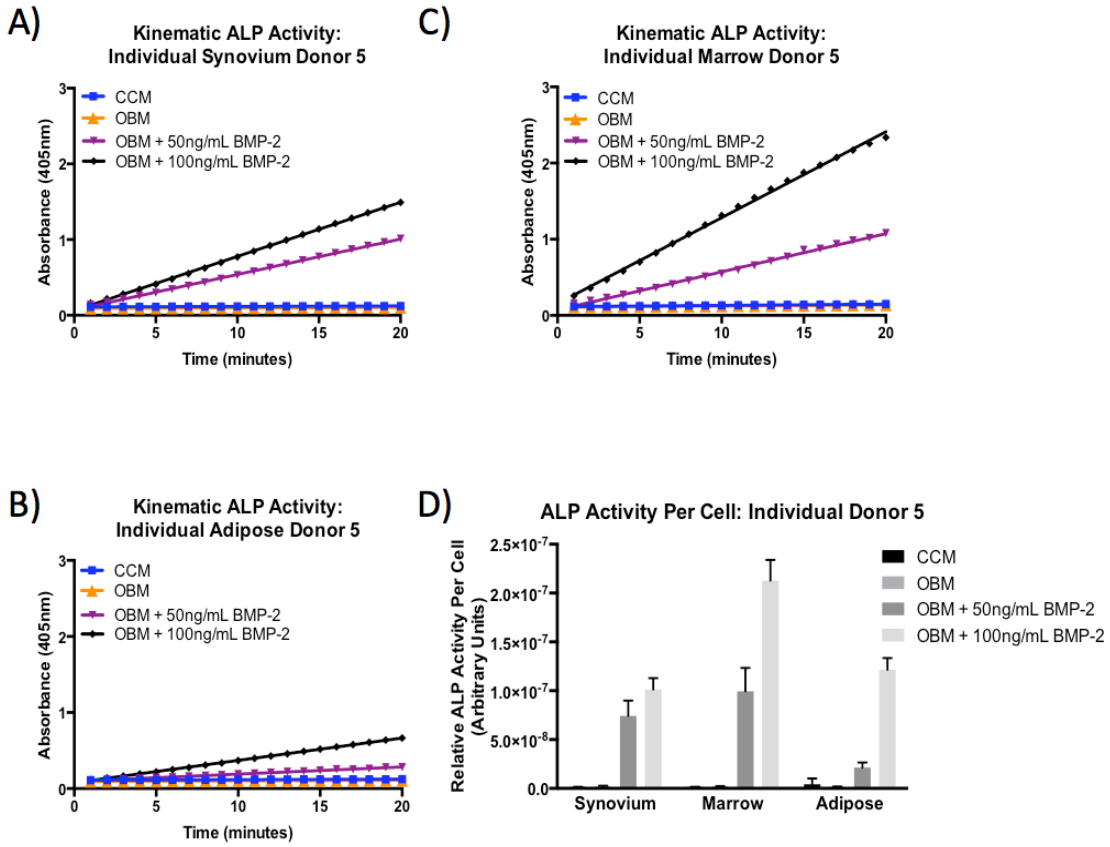

Appendix 1.17. *Short-term osteogenesis of synovium, marrow, and adipose cMSCs from an individual donor.* Short-term osteogenesis was determined using the alkaline phosphatase activity (ALP) assay. Passage 2 cMSCs were cultured in CCM, OBM, or OBM + rhBMP-2 for 7 days and evaluated for the ability to convert the colorless substrate PNPP to colorimetric PNP over time. ALP activity was determined by spectrophotometer (absorbance 405nM) over a 20-minute time course. **A-C)** Kinetic ALP activity results for synovium, bone marrow, and adipose cMSCs preparations from an individual donor are shown. **D)** ALP activity normalized to cell number by DNA quantification for synovium, bone marrow, and adipose from an individual donor are shown.

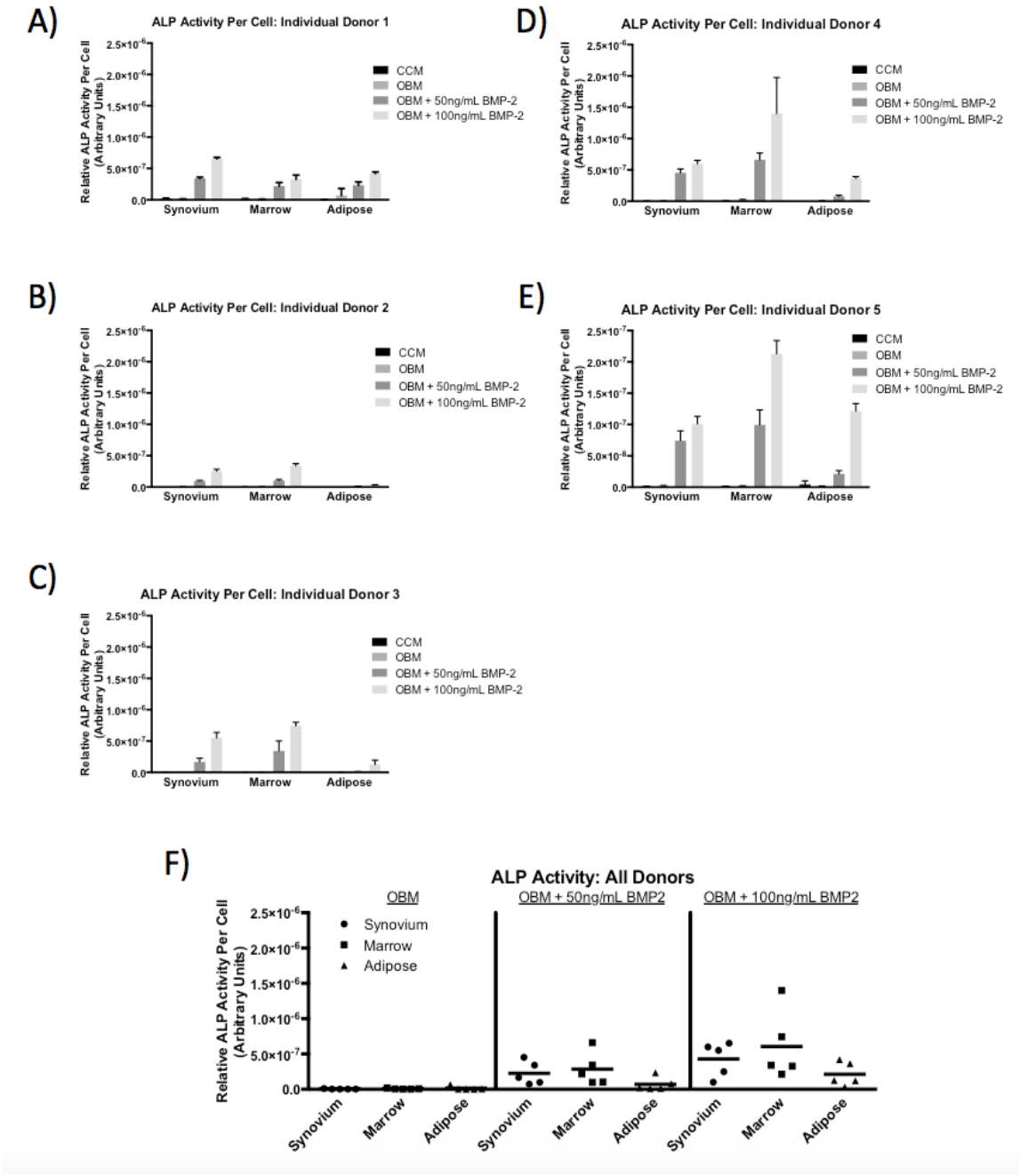

Appendix 1.18. *Short-term osteogenesis of synovium, marrow, and adipose cMSCs from an individual donor.* **A-E)** ALP activity normalized to cell number by DNA quantification from each individual donor as shown Supplemental figures 13-17. **F)** Scatter plots demonstrating ALP activity for all 15 cMSC preparations organized by tissue and media condition. Each data point represents the ALP activity per cell for an individual cMSC preparation and a given media condition (bar=mean across the 5 donors).

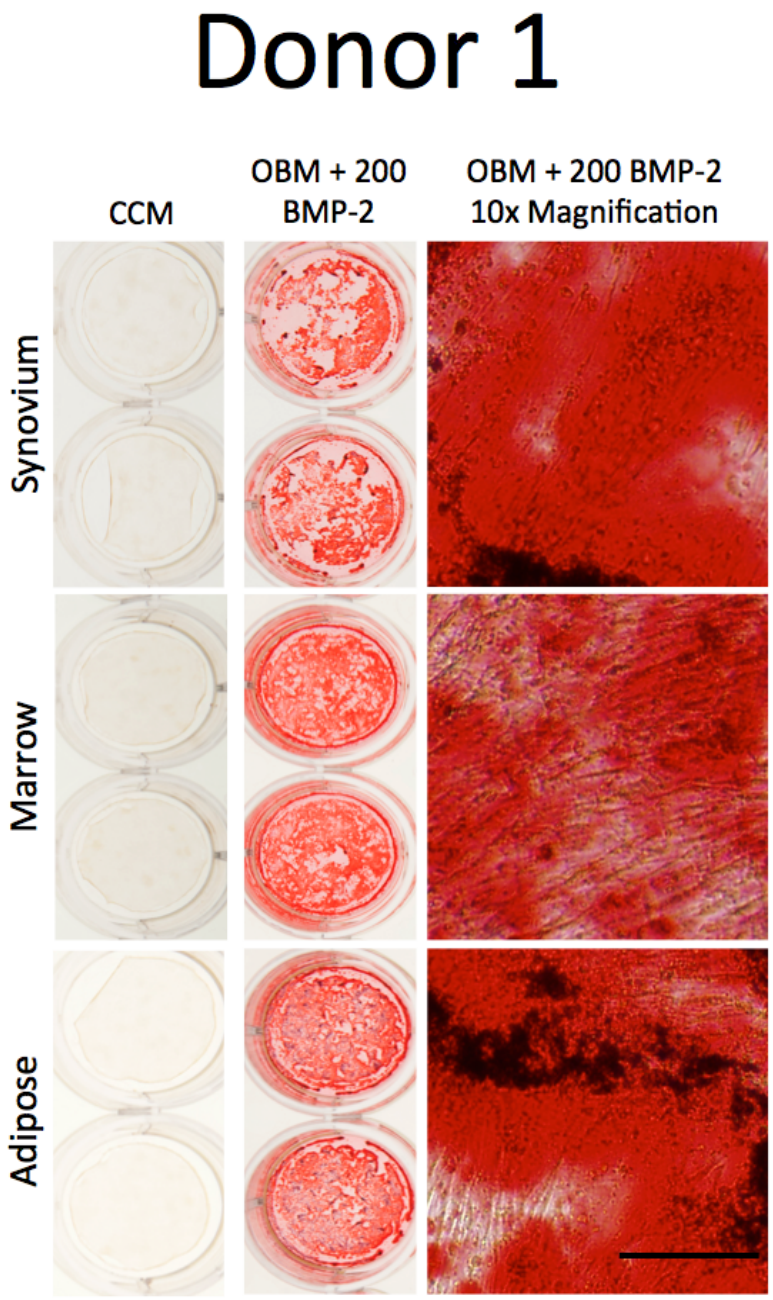

Appendix 1.19. *Long-term osteogenesis of synovium, marrow, and adipose of an individual cMSC donor.* Passage 2 cMSCs were cultured in triplicate wells in CCM or ODM with media exchange twice weekly. After 21 days of culture in CCM (left column) or ODM + 200ng/mL of rhBMP-2 (middle and right columns) monolayers were fixed in 10% formalin and stained with ARS. Plates were photographed (left and middle columns) and imaged with 10X objective light microscopy (right column) to document ARS accumulation (bar=125µm).

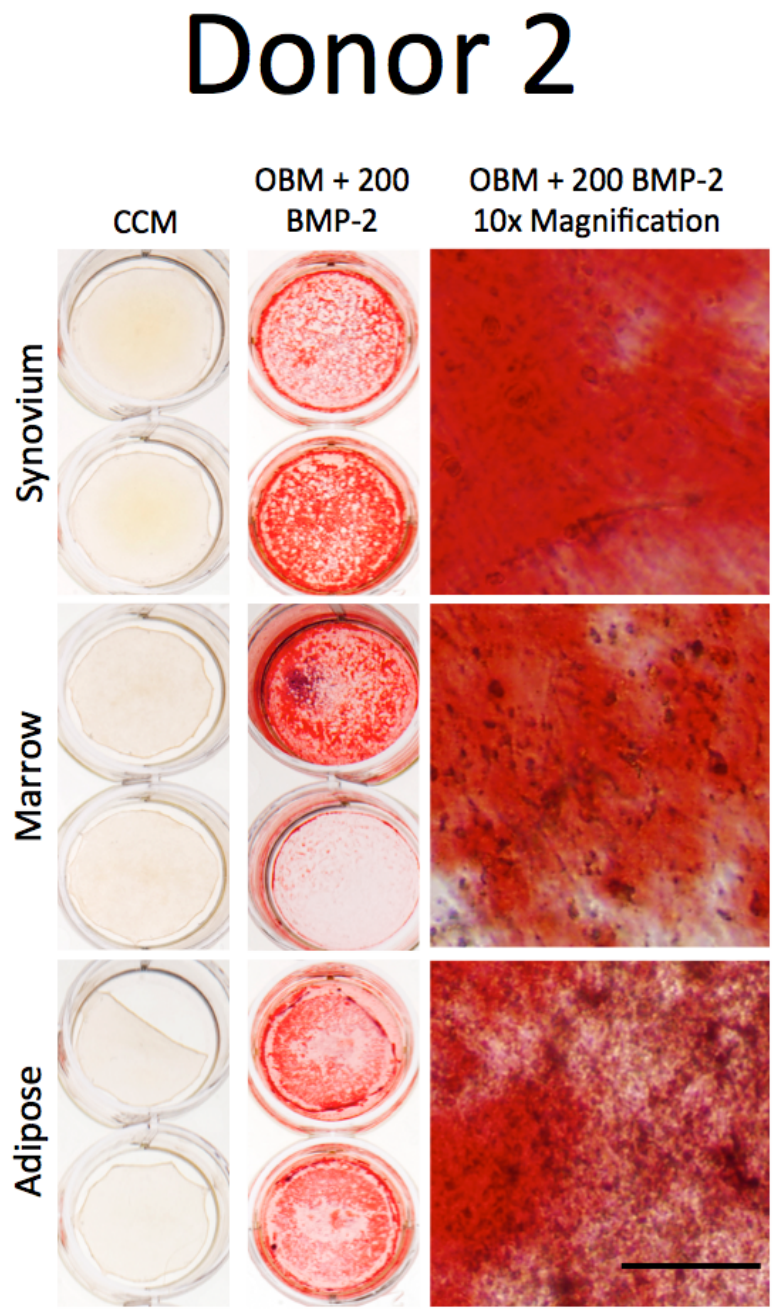

Appendix 1.20. *Long-term osteogenesis of synovium, marrow, and adipose of an individual cMSC donor.* Passage 2 cMSCs were cultured in triplicate wells in CCM or ODM with media exchange twice weekly. After 21 days of culture in CCM (left column) or ODM + 200ng/mL of rhBMP-2 (middle and right columns) monolayers were fixed in 10% formalin and stained with ARS. Plates were photographed (left and middle columns) and imaged with 10X objective light microscopy (right column) to document ARS accumulation (bar=125µm).

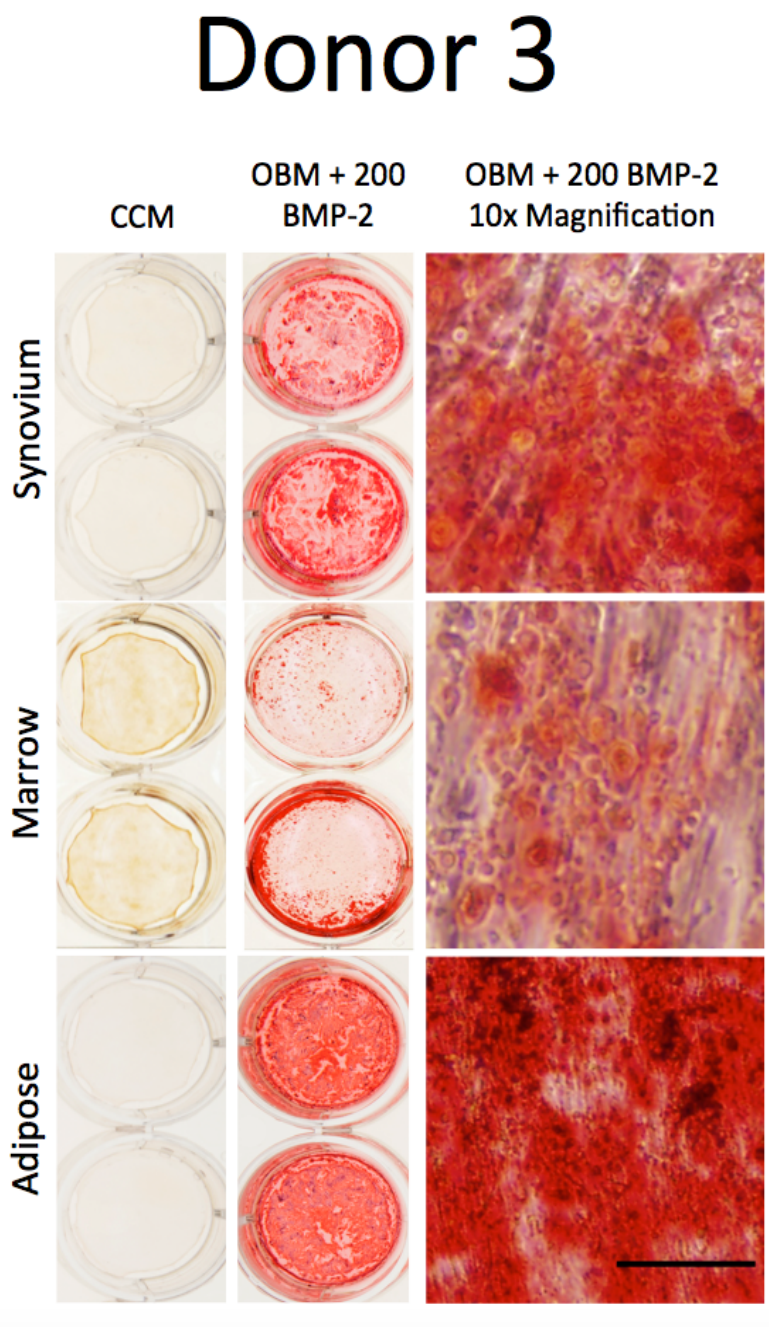

Appendix 1.21. *Long-term osteogenesis of synovium, marrow, and adipose of an individual cMSC donor.* Passage 2 cMSCs were cultured in triplicate wells in CCM or ODM with media exchange twice weekly. After 21 days of culture in CCM (left column) or ODM + 200ng/mL of rhBMP-2 (middle and right columns) monolayers were fixed in 10% formalin and stained with ARS. Plates were photographed (left and middle columns) and imaged with 10X objective light microscopy (right column) to document ARS accumulation (bar=125µm).

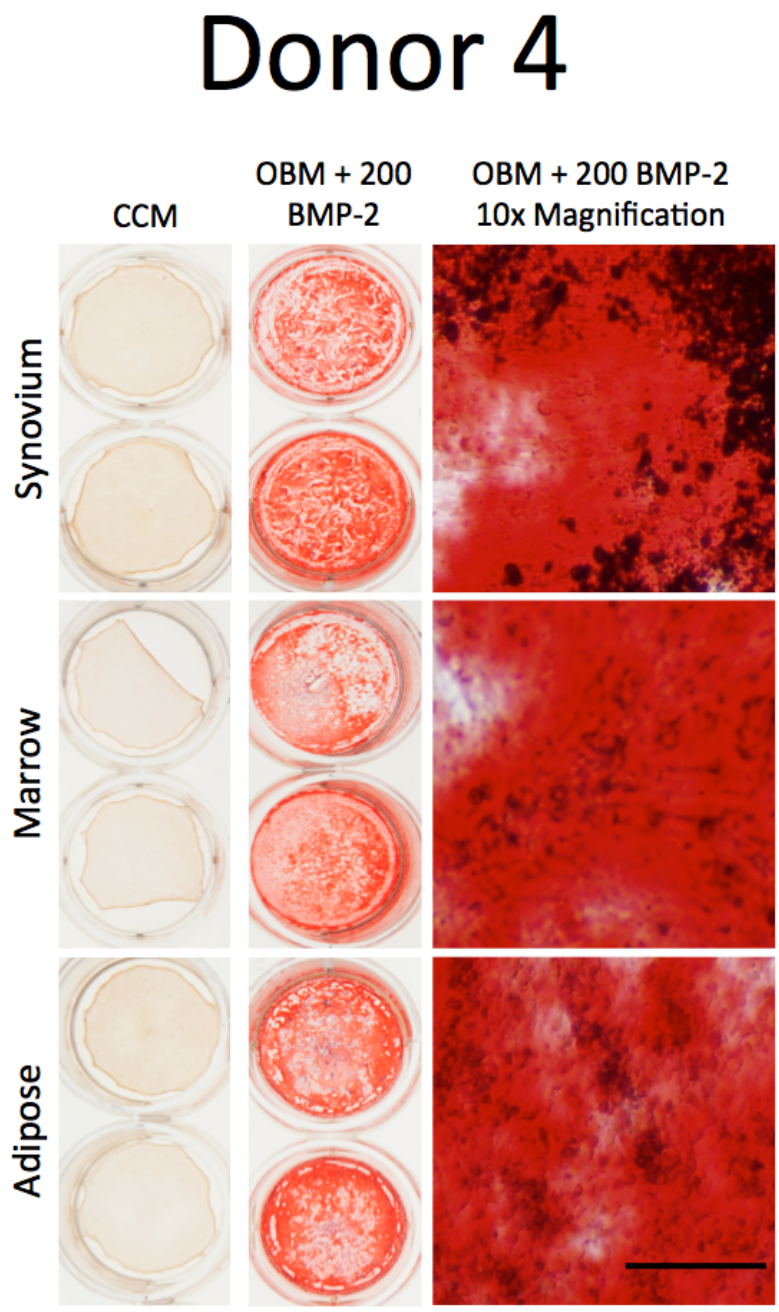

Appendix 1.22. *Long-term osteogenesis of synovium, marrow, and adipose of an individual cMSC donor.* Passage 2 cMSCs were cultured in triplicate wells in CCM or ODM with media exchange twice weekly. After 21 days of culture in CCM (left column) or ODM + 200ng/mL of rhBMP-2 (middle and right columns) monolayers were fixed in 10% formalin and stained with ARS. Plates were photographed (left and middle columns) and imaged with 10X objective light microscopy (right column) to document ARS accumulation (bar=125µm).

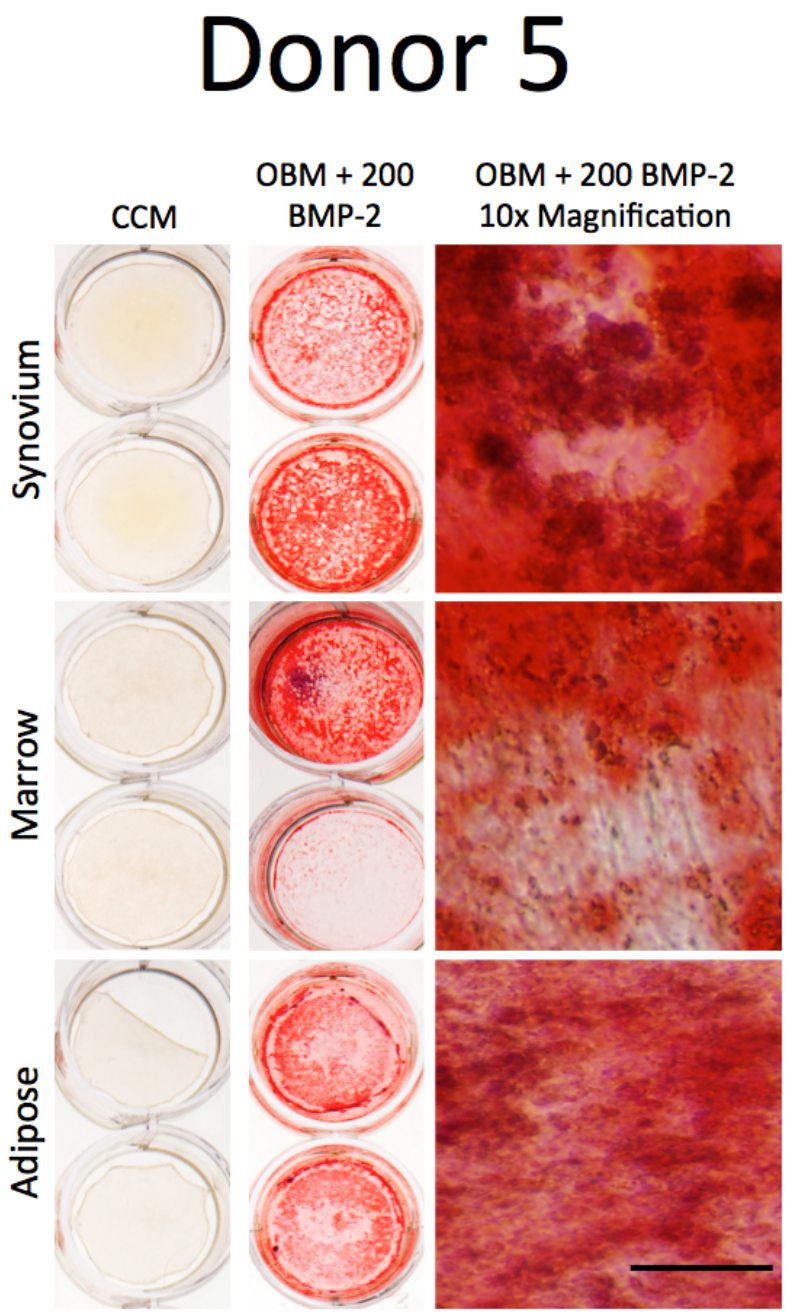

Appendix 1.23. *Long-term osteogenesis of synovium, marrow, and adipose of an individual cMSC donor.* Passage 2 cMSCs were cultured in triplicate wells in CCM or ODM with media exchange twice weekly. After 21 days of culture in CCM (left column) or ODM + 200ng/mL of rhBMP-2 (middle and right columns) monolayers were fixed in 10% formalin and stained with ARS. Plates were photographed (left and middle columns) and imaged with 10X objective light microscopy (right column) to document ARS accumulation (bar=125µm).

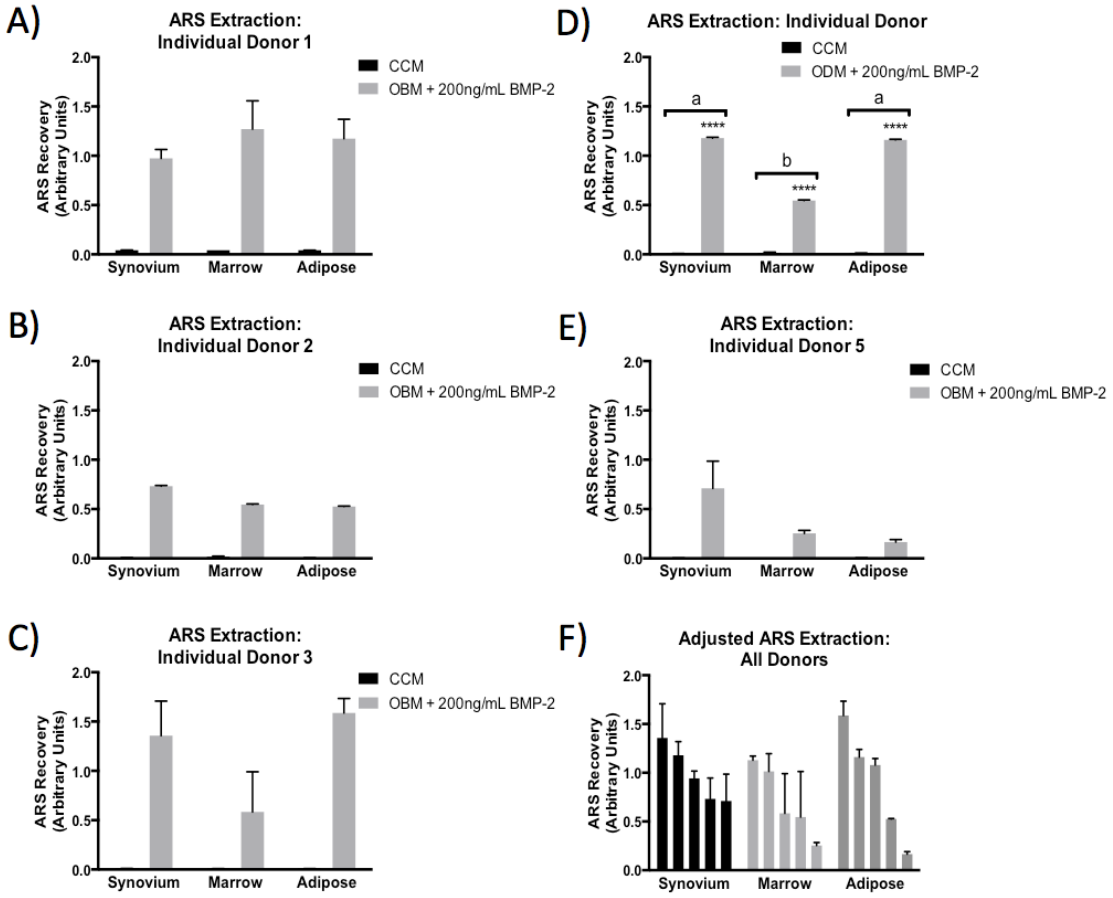

Appendix 1.24. *Long-term osteogenesis of synovium, marrow, and adipose cMSCs.* Passage 2 cMSCs were cultured in triplicate wells in CCM or ODM with media exchange twice weekly. After 21 days of culture in CCM or ODM + 200ng/mL of rhBMP-2 monolayers were fixed in 10% formalin and stained with ARS. **A-E)** ARS extraction (mean ± SD) for each individual donors. **F)** ARS extraction values (mean ± SD) for all 15 cMSC preparations. CCM values have been subtracted from osteogenic values to facilitate presentation of results. Data are reported in descending order for each tissue.

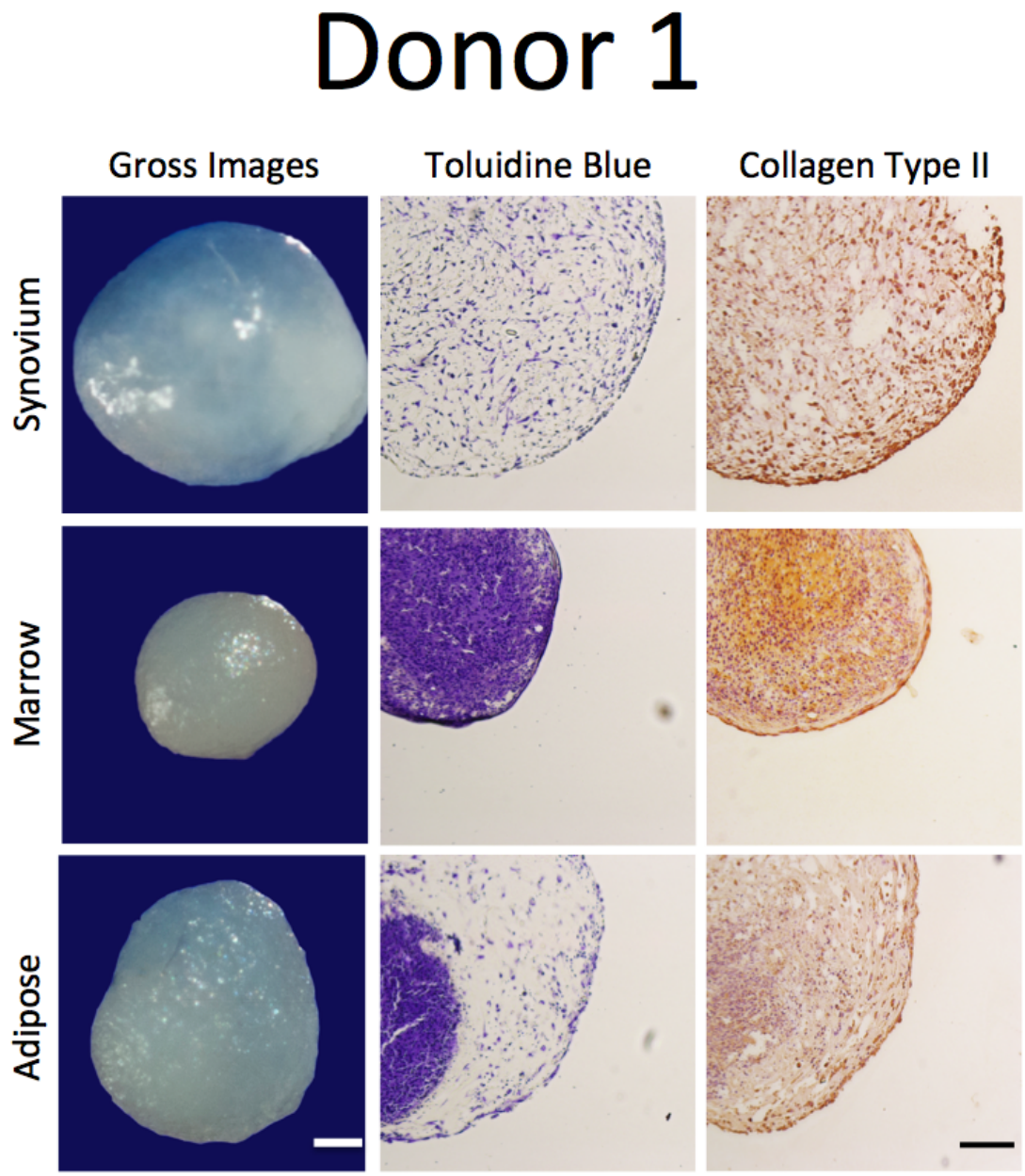

Appendix 1.25. *Chondrogenesis of synovium, marrow, and adipose of an individual cMSC donor.* Passage 2 cMSCs were evaluated for chondrogenesis using the micromass pellet technique. $5x10^7$ cells from each cMSC preparation were pelleted in triplicate and incubated for 21 days in chondrogenic medium with media exchange twice weekly. Pellets were photographed (gross images, bar=300µm), formalin fixed, and sectioned for histology. Pellets were positive for proteoglycan (toluidine blue) and collagen type II (10X objective, bar=150µm).

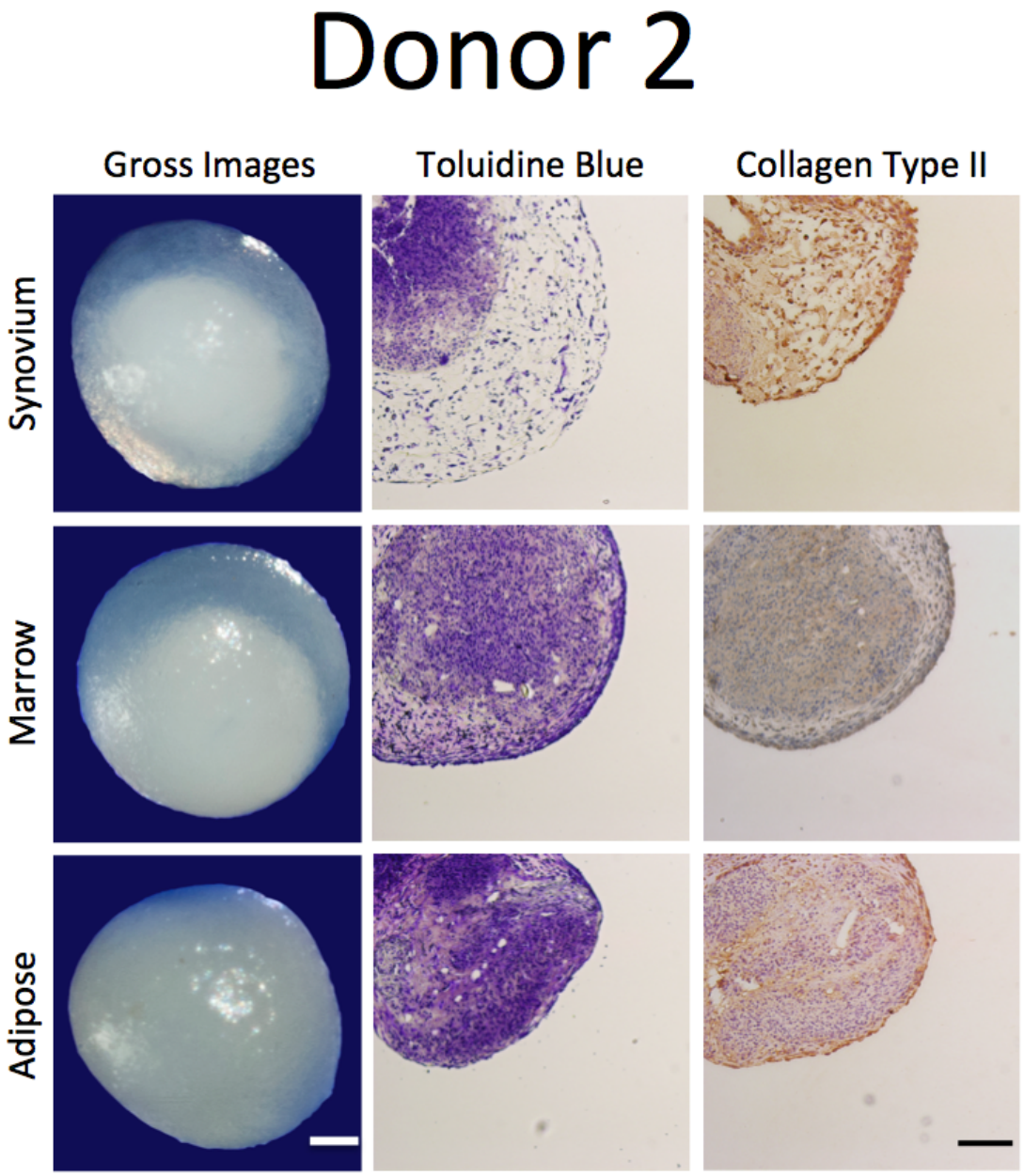

Appendix 1.26. *Chondrogenesis of synovium, marrow, and adipose of an individual cMSC donor.* Passage 2 cMSCs were evaluated for chondrogenesis using the micromass pellet technique. $5x10^7$ cells from each cMSC preparation were pelleted in triplicate and incubated for 21 days in chondrogenic medium with media exchange twice weekly. Pellets were photographed (gross images, bar=300µm), formalin fixed, and sectioned for histology. Pellets were positive for proteoglycan (toluidine blue) and collagen type II (10X objective, bar=150µm).

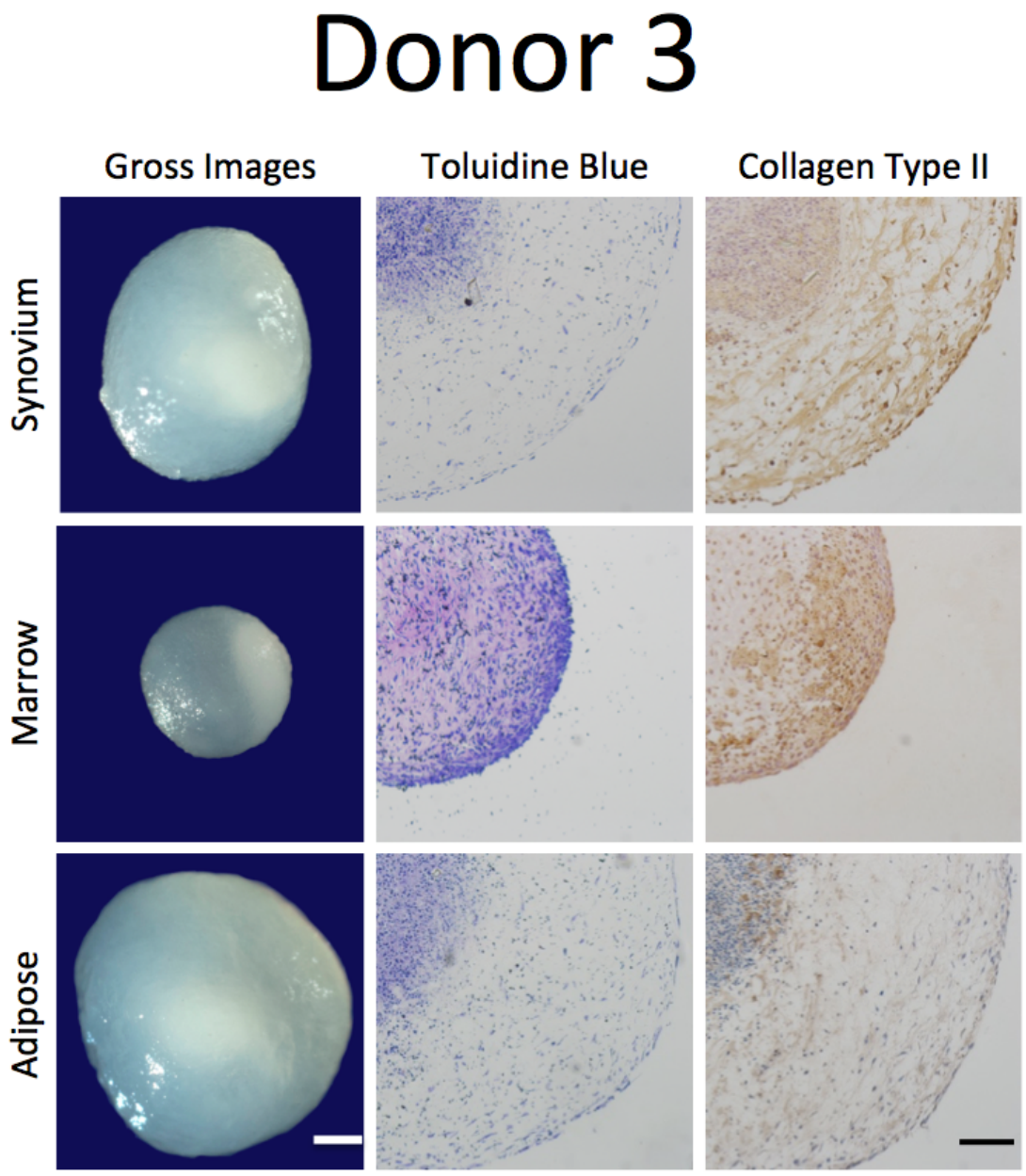

Appendix 1.27. *Chondrogenesis of synovium, marrow, and adipose of an individual cMSC donor.* Passage 2 cMSCs were evaluated for chondrogenesis using the micromass pellet technique. $5x10^7$ cells from each cMSC preparation were pelleted in triplicate and incubated for 21 days in chondrogenic medium with media exchange twice weekly. Pellets were photographed (gross images, bar=300µm), formalin fixed, and sectioned for histology. Pellets were positive for proteoglycan (toluidine blue) and collagen type II (10X objective, bar=150µm).

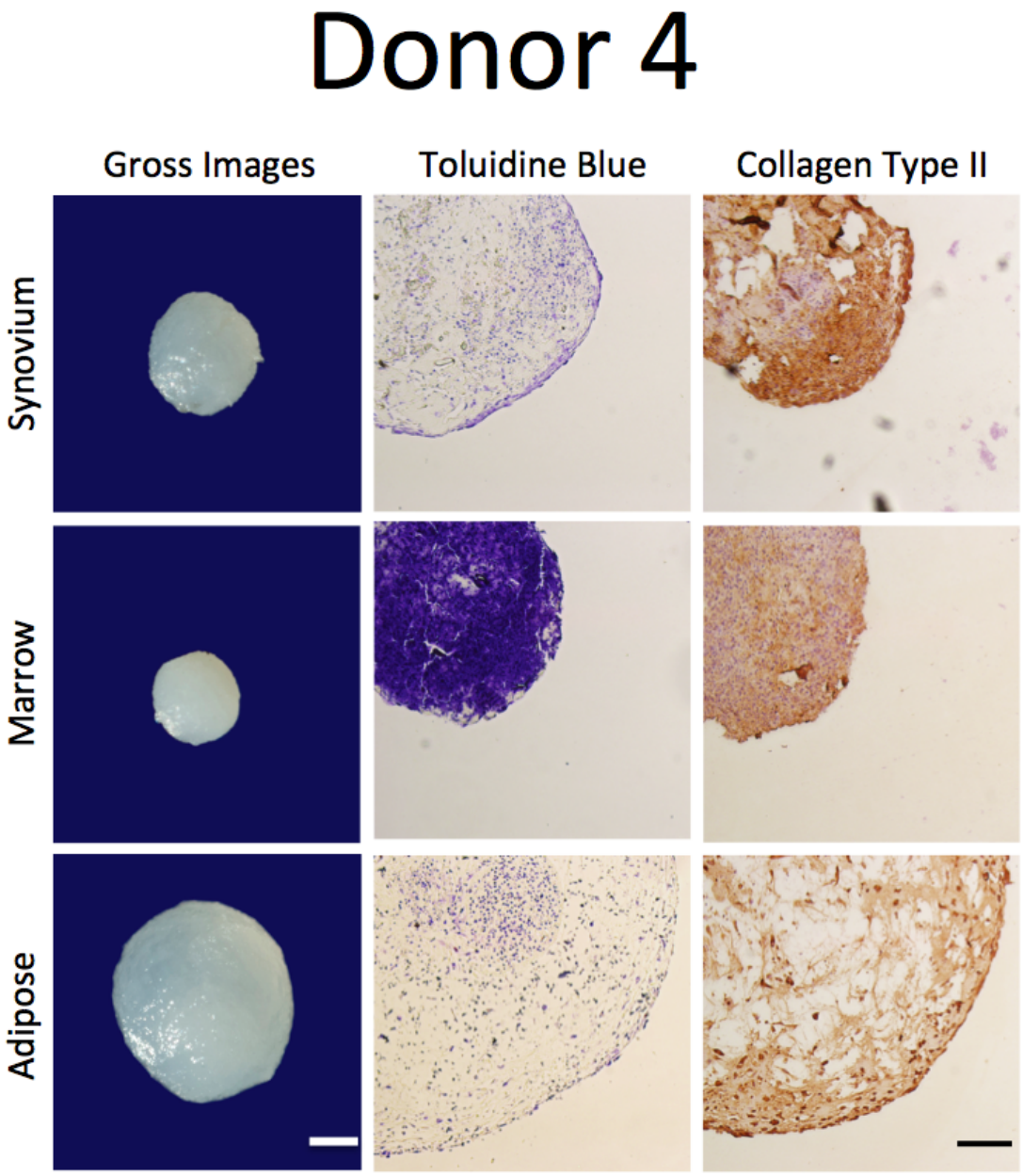

Appendix 1.28. *Chondrogenesis of synovium, marrow, and adipose of an individual cMSC donor.* Passage 2 cMSCs were evaluated for chondrogenesis using the micromass pellet technique. $5x10^7$ cells from each cMSC preparation were pelleted in triplicate and incubated for 21 days in chondrogenic medium with media exchange twice weekly. Pellets were photographed (gross images, bar=300µm), formalin fixed, and sectioned for histology. Pellets were positive for proteoglycan (toluidine blue) and collagen type II (10X objective, bar=150µm).

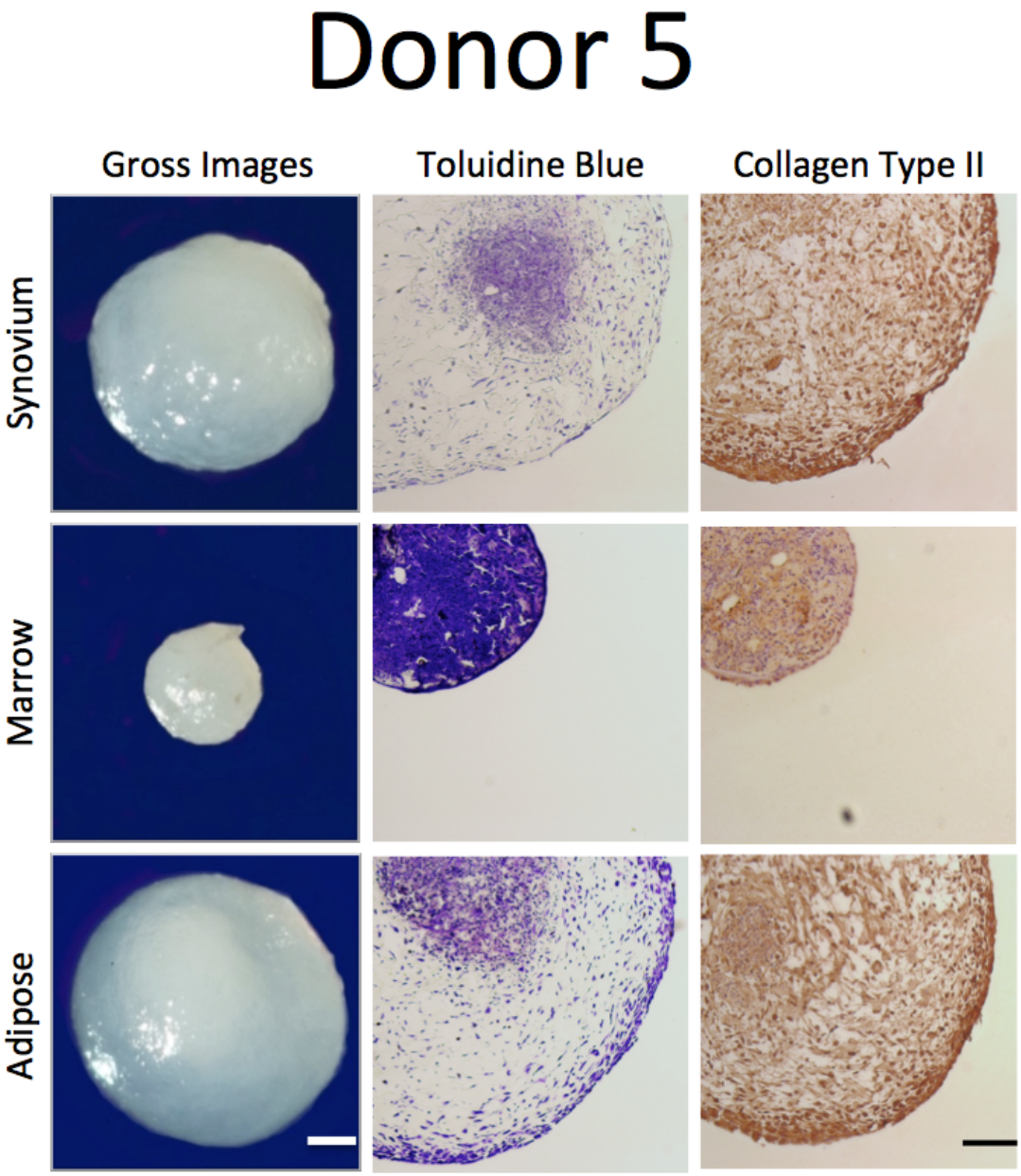

Appendix 1.29. *Chondrogenesis of synovium, marrow, and adipose of an individual cMSC donor.* Passage 2 cMSCs were evaluated for chondrogenesis using the micromass pellet technique. $5x10^7$ cells from each cMSC preparation were pelleted in triplicate and incubated for 21 days in chondrogenic medium with media exchange twice weekly. Pellets were photographed (gross images, bar=300µm), formalin fixed, and sectioned for histology. Pellets were positive for proteoglycan (toluidine blue) and collagen type II (10X objective, bar=150µm).

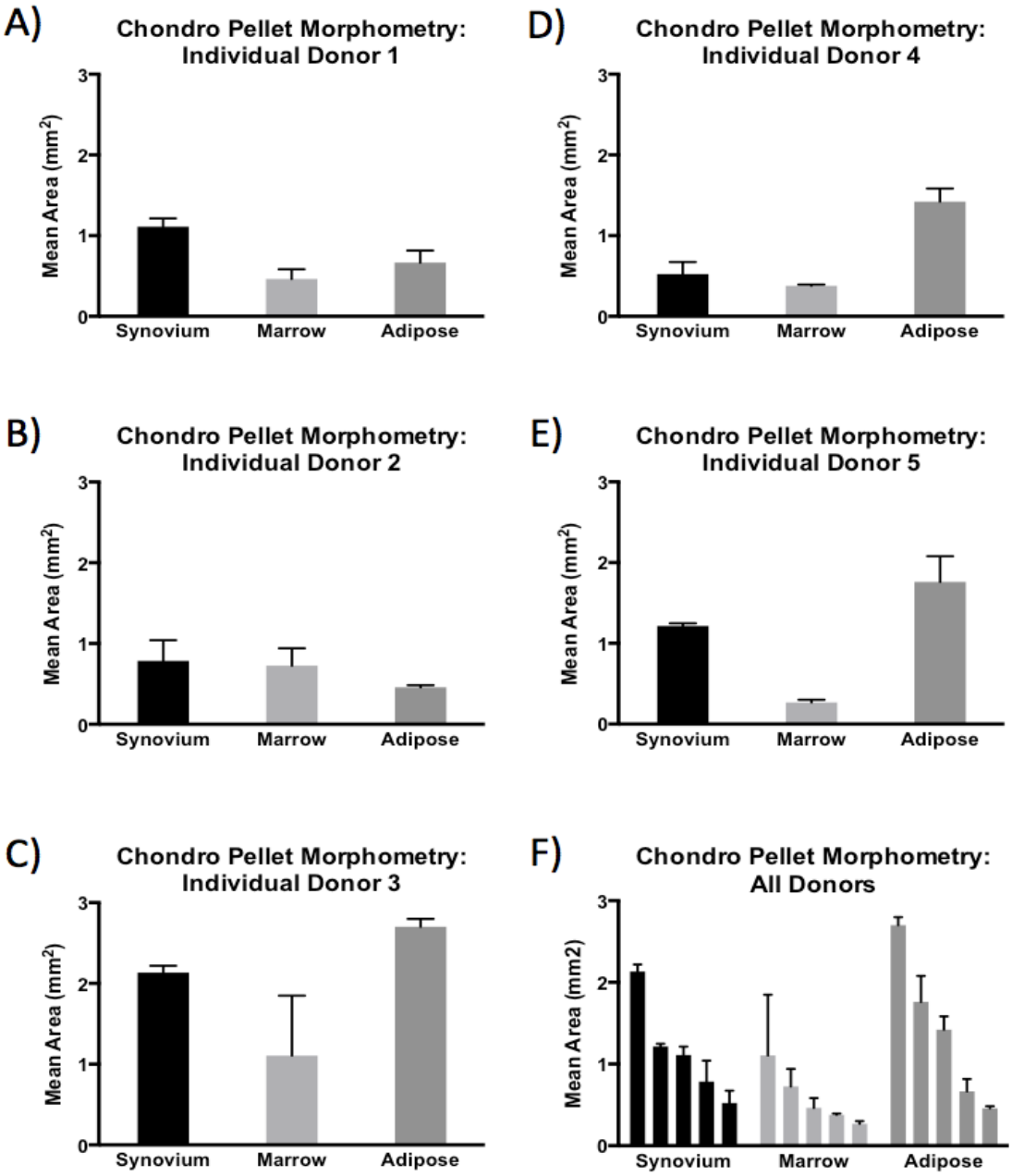

Appendix 1.30. *Chondrogenesis of synovium, marrow, and adipose of an individual cMSC donor.* Passage 2 cMSCs were evaluated for chondrogenesis using the micromass pellet technique. $5x10^7$ cells from each cMSC preparation were pelleted in triplicate and incubated for 21 days in chondrogenic medium with media exchange twice weekly. Pellets were photographed, formalin fixed, and sectioned for histology. **A-E)** Pellet morphometry for each individual donor (mean ± SD). **F)** Pellet area (mm^2) of chondrogenic pellets for all 15 cMSC preparations. Data are reported in descending order for each tissue.

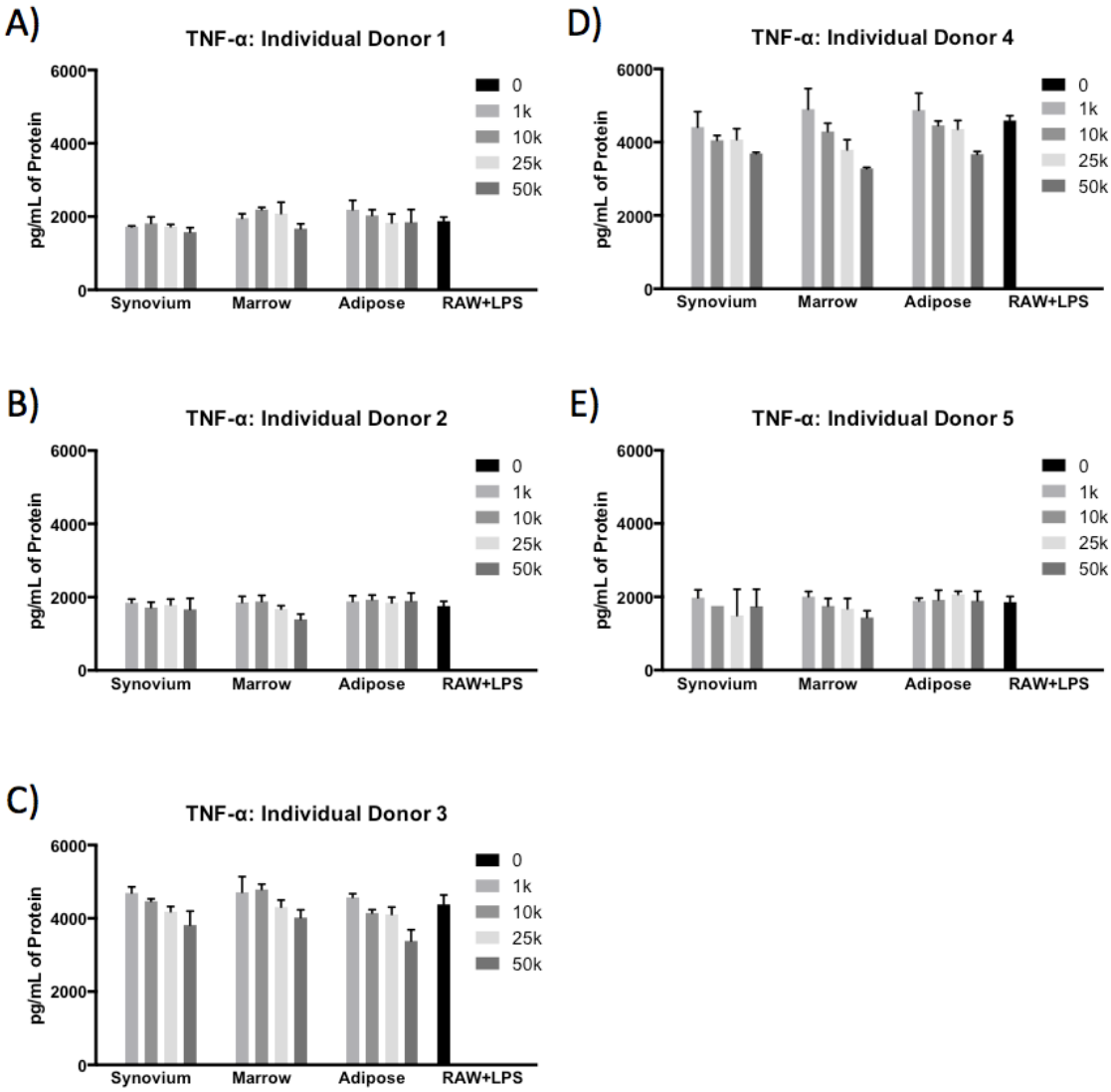

Appendix 1.31. *Immunomodulation of murine TNF-a by synovium, marrow, and adipose cMSCs.* Passage 2 cMSCs ($1x10^3$–$50x10^3$) were co-cultured with $1x10^4$ murine macrophage cells in 12 well plates in CCM (n=3 wells/condition). After 24hrs, LPS (0.5µg/mL) was added to co-cultures to activate macrophages and to assess cMSCs immunomodulation. After 18hrs, media were collected and ELISA performed to determine the concentration of secreted murine TNF-a. **A-E)** Murine TNF-a concentrations (mean ± SD) for all individual donors. RAW + LPS denotes TNF-a concentration from murine macrophages (RAW cells) in the absence of cMSCs (positive control).

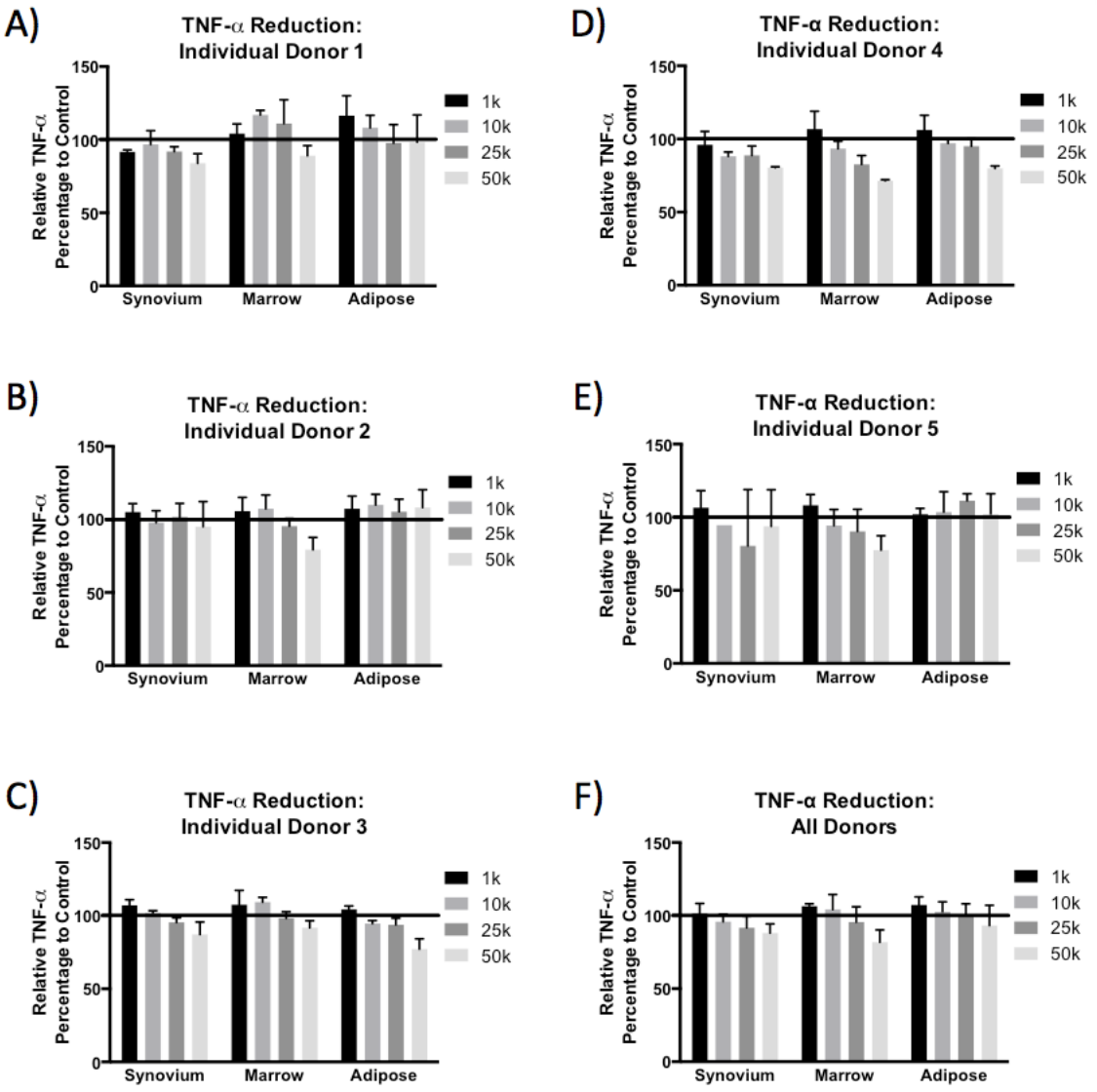

Appendix 1.32. *Immunomodulation of murine TNF-a by synovium, marrow, and adipose cMSCs.* Passage 2 cMSCs ($1x10^3$–$50x10^3$) were co-cultured with $1x10^4$ murine macrophage cells in 12-well plates in CCM (n=3 wells/condition). After 24hrs, LPS (0.5µg/mL) was added to co-cultures to activate macrophages and to assess cMSCs immunomodulation. After 18hrs, media were collected and ELISA performed to determine the concentration of secreted murine TNF-a. **A-E)** Data from each individual donor in Supplemental Figure 25 were transformed to reflect the percentage change in TNF-a relative to the RAW + LPS positive control. **F)** Comparative analysis across all 15 cMSC preparations reported as mean ± SD.

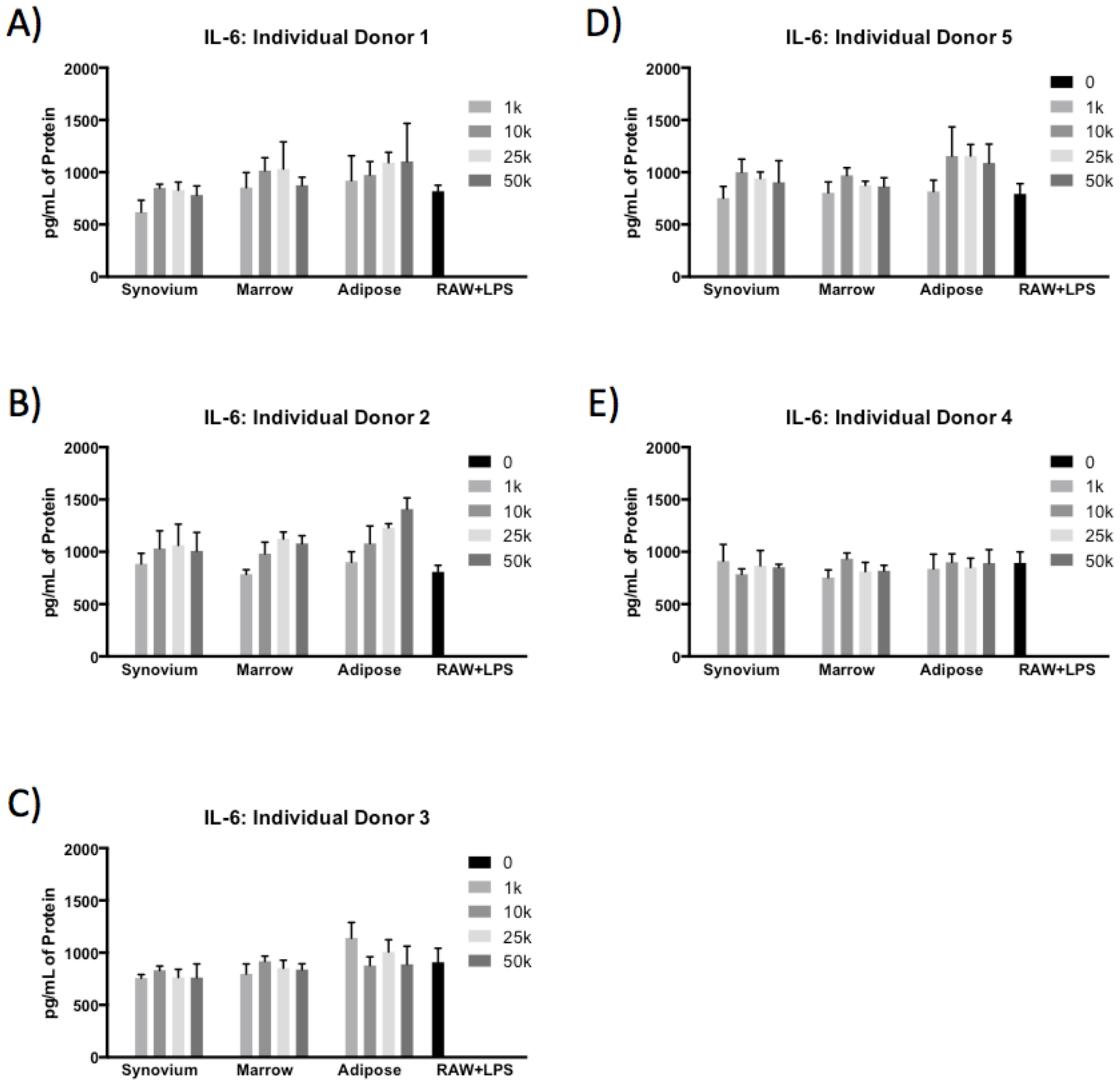

Appendix 1.33. *Immunomodulation of murine IL-6 by synovium, marrow, and adipose cMSCs.* Passage 2 cMSCs ($1x10^3$–$50x10^3$) were co-cultured with $1x10^4$ murine macrophage cells in in CCM (n=3 wells/condition). After 24hrs, LPS (0.5µg/mL) was added to co-cultures to activate macrophages and to assess cMSCs immunomodulation. After 18hrs in LPS stimulated co-culture, media were collected and ELISA performed to determine the concentration of secreted murine IL-6. **A-E)** Murine IL-6 concentrations (mean ± SD) for all individual donors. RAW + LPS denotes IL-6 concentration from murine macrophages (RAW cells) in the absence of cMSCs (positive control).

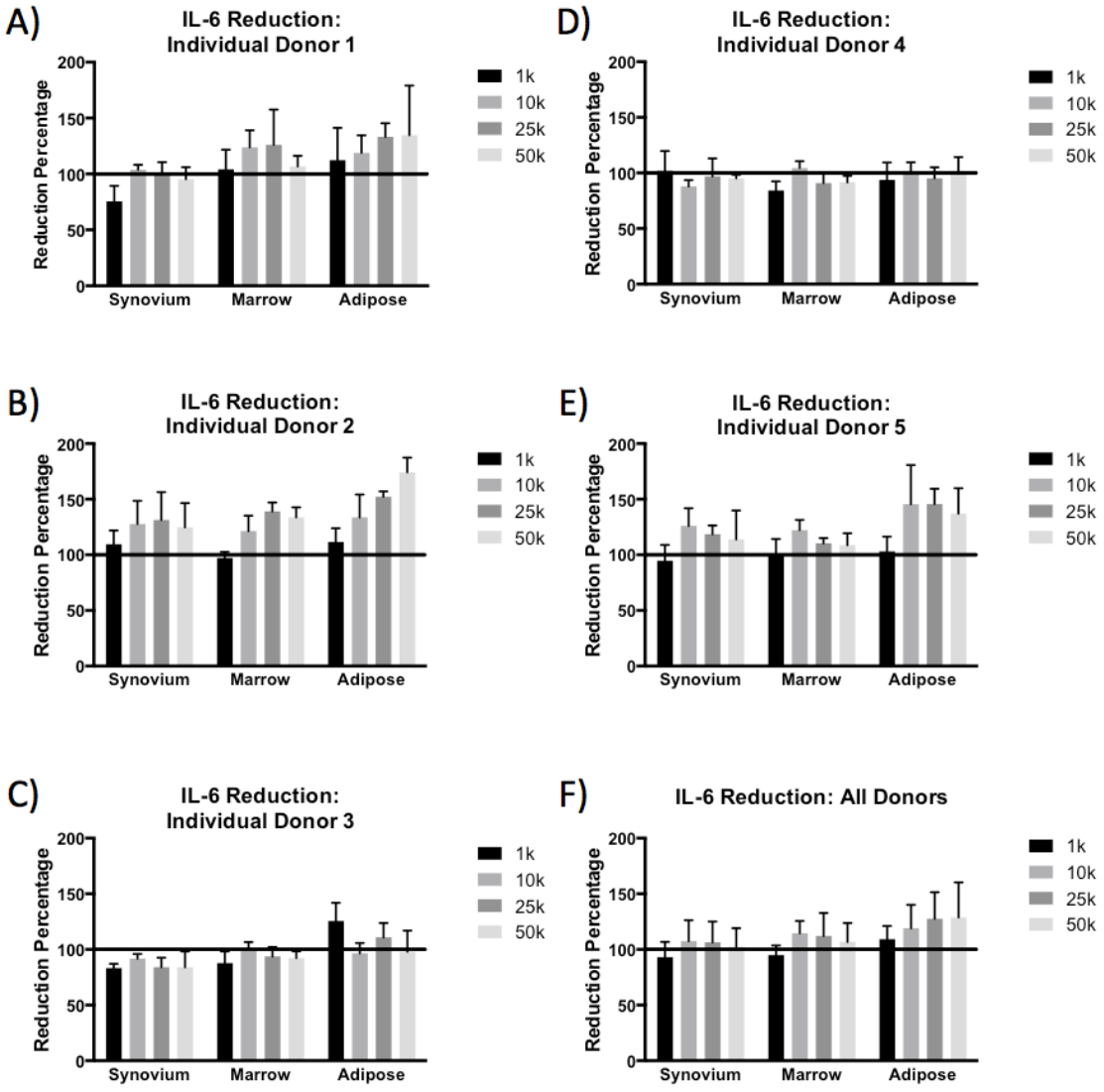

Appendix 1.34. *Immunomodulation of murine IL-6 by synovium, marrow, and adipose cMSCs.* Passage 2 cMSCs ($1x10^3$–$50x10^3$) were co-cultured with $1x10^4$ murine macrophage cells in 12-well plates in CCM (n=3 wells/condition). After 24hrs, LPS (0.5µg/mL) was added to co-cultures to activate macrophages and to assess cMSCs immunomodulation. After 18hrs in LPS stimulated co-culture, media were collected and ELISA performed to determine the concentration of secreted murine IL-6. **A-E)** Data from each individual donor in Supplemental Figure 27 were transformed to reflect the percentage change in IL-6 relative to the RAW + LPS positive control. **F)** Comparative analysis across all 15 cMSC reported as mean ± SD.